POLITECNICO DI MILANO

School of Civil, Environmental and Land Management Engineering

Master of Science in Civil Engineering for Risk Mitigation

Advanced two-dimensional river modelling. Hazard maps for the Guisa and Nirone rivers in the context of flood risk management planning

Supervisor: Dr. Alessio Radice

Co-supervisor: Dr. Daniele Ganora

Master Thesis of:

Damodar Maggetti – Matr. 968115

Gloria Faccenda – Matr. 970609

Academic Year 2021/2022

"The single raindrop never feels responsible for the flood."

~ Douglas Adams

Acknowledgements

Damodar and Gloria

Lecco, December 2022

Abstract (English version)

Nowadays, the frequency of flood events and the associated risk in urban areas are progressively increasing and stimulating major concern at a global scale. Indeed, such events can lead to significant short- and long-term economic, social and environmental negative consequences. Therefore, with the present predictions of worsening future scenarios, it is of paramount importance to pursue integrated flood risk management methods which encompass flood modelling. In Europe, after the publication of the EU Floods Directive (2007/60/EC), each Member State has to identify Areas of Potential Significant Flood Risk (APSFR) and, for each of them, prepare Flood Risk Management Plans (FRMPs), which must be also updated every 6 years.

In this context, this thesis contributes to producing flood hazard maps; these maps depict the spatial distribution of both the water depth and velocity for scenarios with prescribed probability, and are an important preliminary step in the preparation of a FRMP. This work is focused on two rivers included in the APSFR "North of Milan": the Guisa and Nirone, which are two small-medium sized watercourses characterized by a total length of, respectively, about 23 and 8 km and an average width of the riverbed of 4 m. The hazard maps have been produced employing unsteady, two-dimensional hydrodynamic modelling, with a spatial detail sufficient to resolve the flow distribution around individual buildings (that are numerous in the strongly urbanized area northern to Milan). The maps have been produced according to three different probabilities of occurrence, corresponding to return periods equal to 10, 100 and 500 years. Use has been made of geometric data (digital terrain model and a number of surveyed transverse sections), land cover data, building footprint, and hydrological data (available hydrographs and peak flow rates). The maps produced in this thesis represent a significant update of those released in 2019 by the Autorità di Bacino Distrettuale del fiume Po (AdBPo), which resulted from the application of one-dimensional and zero-dimensional approaches.

The hydrodynamic modelling has been performed using HEC-RAS. Therefore, a detailed analysis of some of the major critical aspects of the two-dimensional modelling with this software has been carried out. Specifically, careful consideration has been given to the sensitivity of the results due to the roughness parameterization, the computational time step for different sets of equations used, and the creation of the computational mesh. Based on the outcome of the sensitivity analysis, it has been possible to conclude that the methods used for the production of the updated hazard maps have been adequate for the purpose.

Abstract (Italian version)

Al giorno d'oggi, la frequenza degli eventi alluvionali e il conseguente rischio nelle aree urbane stanno progressivamente aumentando e stimolano una grande preoccupazione a livello globale. Infatti, tali eventi possono portare a significative conseguenze negative, sia a breve che a lungo termine, a livello economico, sociale e ambientale. Pertanto, viste anche le attuali previsioni di peggioramento degli scenari futuri, è di fondamentale importanza perseguire metodi integrati di gestione del rischio di alluvione che comprendano la modellazione delle esondazioni. In Europa, a seguito della pubblicazione della Direttiva Alluvioni UE (2007/60/CE), ogni Stato membro deve identificare le aree a potenziale rischio significativo di alluvione (Areas of Potential Significant Flood Risk - APSFR) e, per ognuna di esse, preparare i piani di gestione del rischio di alluvione (Flood Risk Management Plans - FRMP), che devono essere aggiornati ogni 6 anni.

A tale proposito, questa tesi contribuisce alla produzione di mappe di pericolosità da alluvione; queste mappe raffigurano la distribuzione spaziale sia della profondità che della velocità dell'acqua per scenari con prestabilite probabilità, e sono un importante passo preliminare nella preparazione di un FRMP. Questo lavoro è focalizzato su due fiumi inclusi nell'APSFR "Nord di Milano": il Guisa e il Nirone, che sono due corsi d'acqua di dimensioni medio-piccole caratterizzati da una lunghezza totale, rispettivamente, di circa 23 e 8 km e da una larghezza media dell'alveo di 4 m. Le mappe di pericolosità sono state prodotte utilizzando una modellazione idrodinamica a moto vario bidimensionale, con un dettaglio spaziale sufficiente a risolvere la distribuzione del flusso intorno ai singoli edifici (che sono numerosi nell'area fortemente urbanizzata a nord di Milano). Le mappe sono state prodotte secondo tre diverse probabilità di accadimento, corrispondenti a tempi di ritorno pari a 10, 100 e 500 anni. Sono stati utilizzati dati geometrici (modello digitale del terreno e un certo numero di sezioni trasversali rilevate), dati di copertura del suolo, impronta degli edifici e dati idrologici (idrogrammi disponibili e portate di picco). Le mappe prodotte in questa tesi rappresentano un significativo aggiornamento di quelle rilasciate nel 2019 dall'Autorità di Bacino Distrettuale del fiume Po (AdBPo), che derivavano dall'applicazione di approcci monodimensionali e zero-dimensionali.

La modellazione idrodinamica è stata eseguita utilizzando HEC-RAS. Pertanto, è stata condotta un'analisi dettagliata di alcuni dei principali aspetti critici della modellazione bidimensionale con questo software. In particolare, è stata presa in considerazione la sensibilità dei risultati dovuta alla parametrizzazione della scabrezza, al passo temporale di calcolo per i diversi insiemi di equazioni utilizzati e alla creazione della maglia di calcolo. Sulla base dei risultati dell'analisi di sensibilità, è stato possibile concludere che i metodi utilizzati per la produzione delle mappe di pericolosità aggiornate sono stati adeguati allo scopo.

Contents

List of figures

List of tables

1. Introduction and objectives

1.1. Relevance of flood modelling

A flood is an overflow of water that covers the surrounding land where there is normally no water. Floods are often caused by heavy rainfall, rapid snowmelt, or storm [1]. Generally, the consequences, both positives and negatives, of floods depend on the depth of water, the velocity, the speed, and the duration [2]. When considering negatives impacts, the resulting damages from floods can be direct, due to the physical presence of water; indirect, when they are characterized by a time lag or when they are outside the inundated area; tangible, if the damage to assets can be monetized with a market price and intangible, if instead the damaged assets it cannot be measured in economic terms [3]. The damages can cause both short-term (e.g.: temporary closure of a road due to the presence of water) and long-term problems. The latter can usually lead to more catastrophic social, economic, and environmental consequences, both to individuals and communities [2]. One of the most critical potential consequences of floods is the so-called Natech ("Natural Hazards Triggering Technological Accidents"), which can occur when a flood impacts industrial sites and, consequently, hazardous substances are released into the environment [4].

All over the world, between the years 1998 and 2017, there were 3'148 flood events, that caused economic losses for 656 billion of US\$, affected almost 2 billion people and killed 142'088 of them [5]. Figure 1.1, considering always the aforementioned interval of years, shows how flood events are divided for each continent. In addition, Figure 1.2 provides information about the number of events divided by the surface of the continents (in $km^2/10^6$) [6].
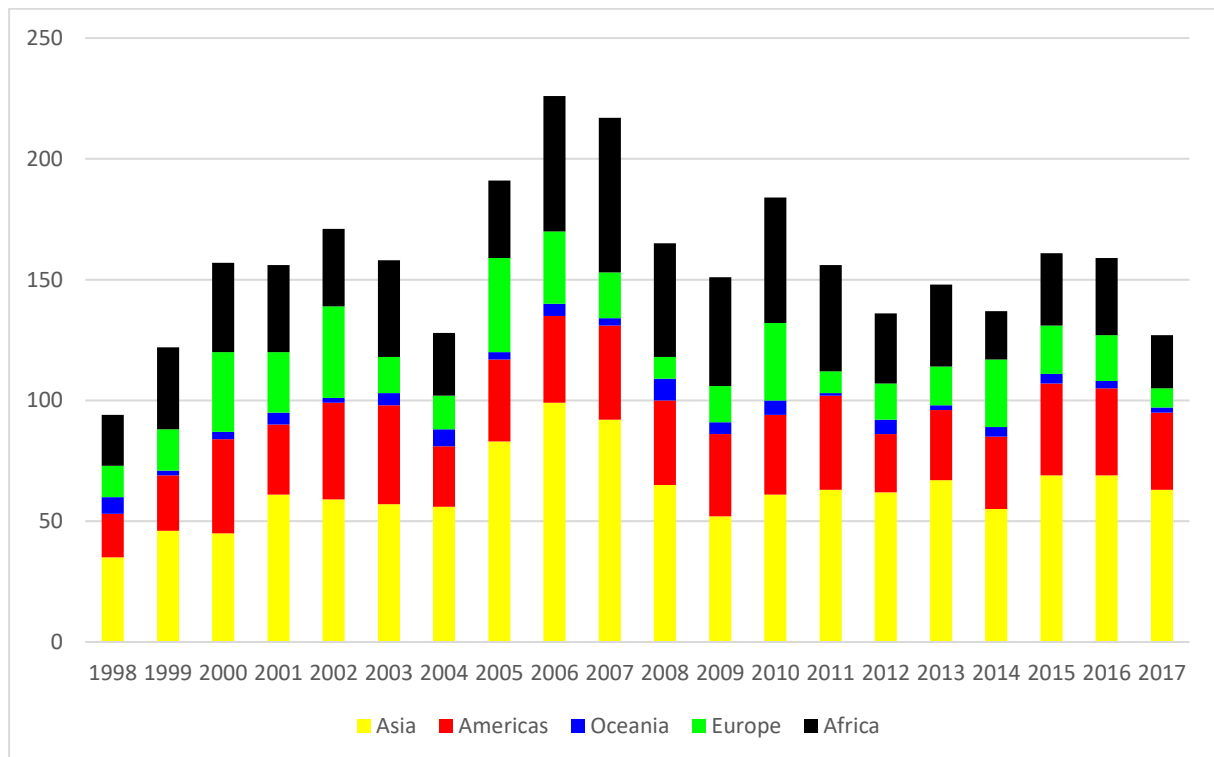
Figure 1.1: Number of flood events for each continent
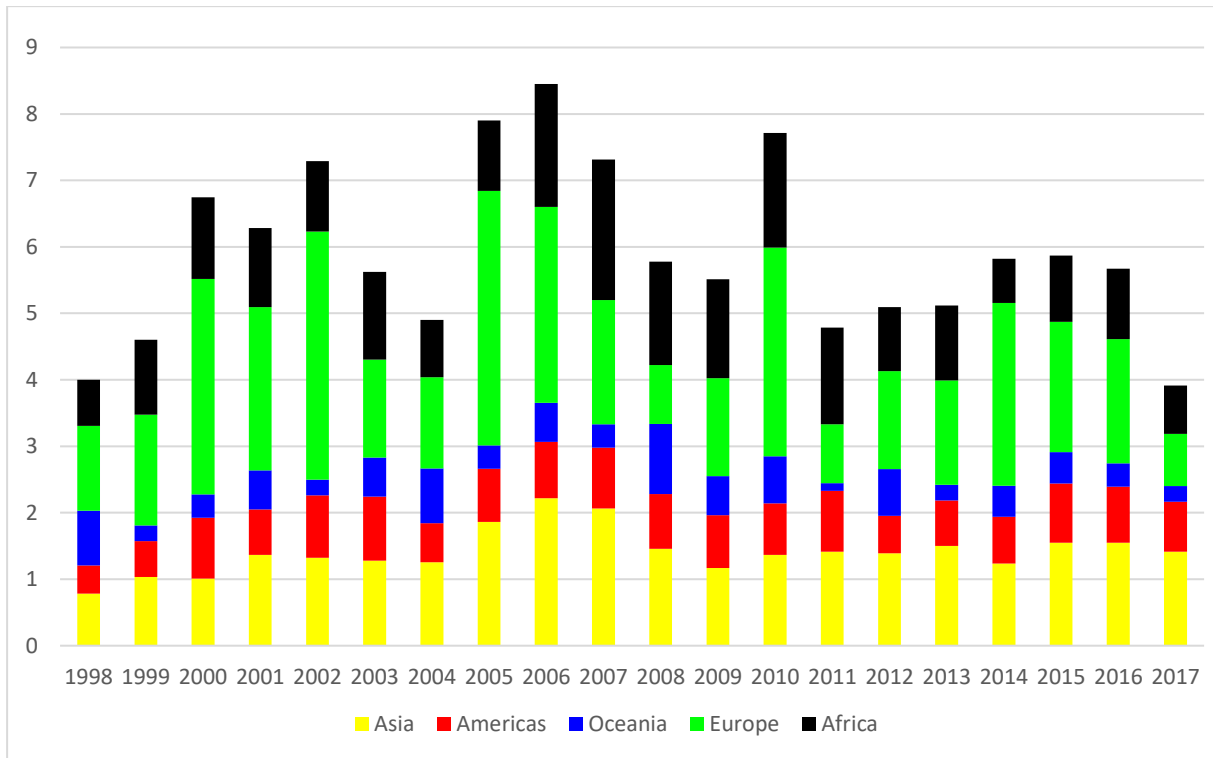
Figure 1.2: Number of flood events with respect to the area of the continent

From Figure 1.1 and Figure 1.2 it can be noticed that Europe is probably the most affected continent. For this reason, and also because Europe is the continent in which the analyses made during this thesis were focused on, further investigations about this continent were made, taking advantage of data from the European Environmental Agency (EEA).

Specifically, the analysis conducted by the EEA takes into consideration a period of time including the years between 1980 and 2010, and the data collected are about the number of flood events and their characteristics [7]. Among all the characteristics, the most relevant one is the severity (Figure 1.3), which can be moderate, high or very high depending on the following classification [8]:

- Moderate severity: When an event caused significant damages to structures or agriculture and/or when it has a return period included between 10-20 years.
- High severity: When an event affected a large geographic region (larger than 5,000 km^2) and/or when its return period is bigger than 20 years but less than 100 years.
- Very high severity: When an event has a return period bigger than 100 years.
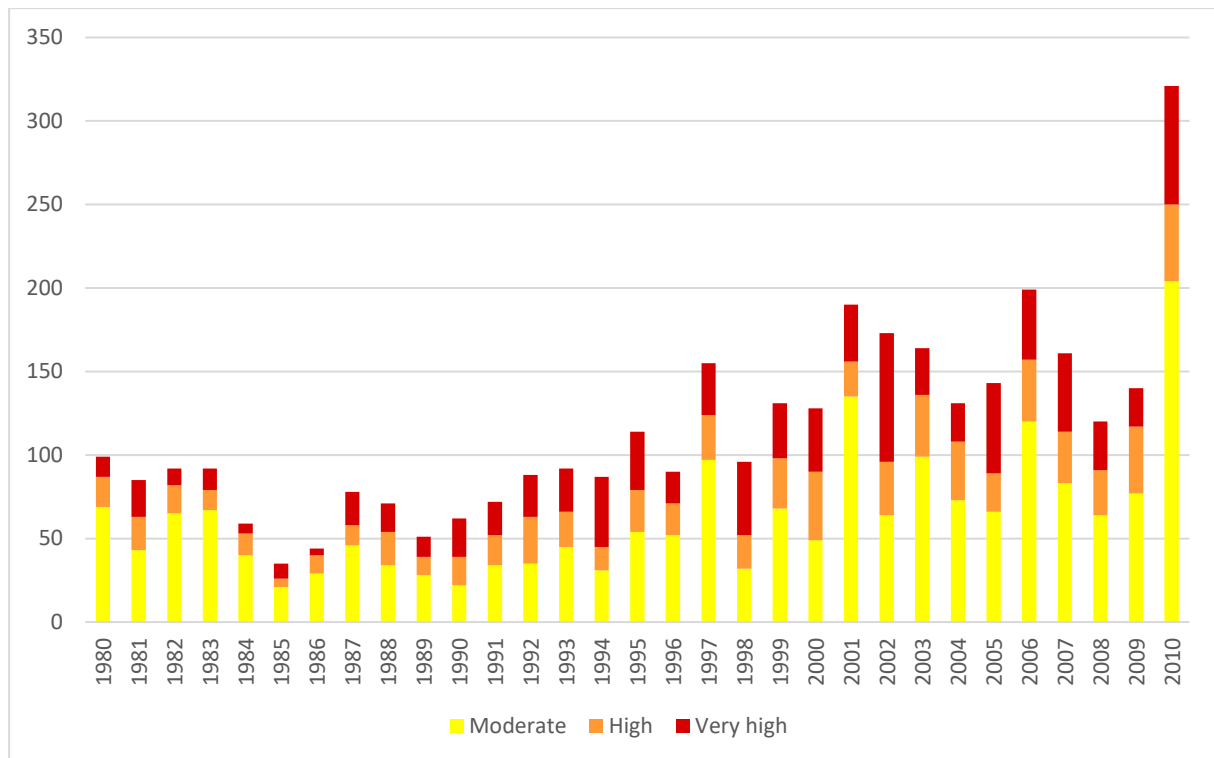
Figure 1.3: Number of flood events in Europe based on their severity

From Figure 1.3 it can be noticed that the total number of flood events is clearly increasing over the years, and the same is true for the number of high-severity events, which are the most dangerous for people and goods. Indeed, it is expected that in Europe the annual flood losses will increase by 5 times by 2050 and by 17 times by 2080 (with respect to the current ones) [3]. Therefore, correctly modelling flood events (or, in other words, accurately predicting the extension of the flooded area and the distribution of water depth and velocity for an event) is of paramount importance to produce hazard maps which can be very useful to better study the problem. Indeed, hazard maps are the basis for producing risk maps, which describe the potential consequences (i.e.: expected damages) considering also aspects related to the exposure and the vulnerability of an area. These maps are fundamental for the implementation of some mitigation strategies, which can be either structural (e.g.: detention basins, check dams, artificial levees, etc.) or non-structural (e.g.: spatial planning, communication, etc.), and that have the aim of reducing what would be the real impact of potential events.

Therefore, to face the problem of flood events, the European Commission published in 2007 the Floods Directive [9] which has the aim of managing the risk related to flood events and reducing the adverse consequences for human health, the environment, cultural heritage, and economic activities. According to this directive, each Member State has to prepare Flood Risk Management Plans (FRMPs), which require to be updated every 6 years. The FRMPs are obtained after a preliminary flood risk assessment and the production of flood hazard maps and flood risk maps. The plans are defined according to different probabilities of occurrence (low, medium, and high), which are related to the severity of the flood event.

The Directive also requires that each Member State of the European Union identify the areas prone to flood risk, the so-called Areas of Potential Significant Flood Risk (APSFR). In Italy, the APSFR are defined by five hydrographic districts (Po River, Eastern Alps, Northern

Apennines, Central Apennines and Southern Apennines) and by the Regions Sicily and Sardinia (Figure 1.4) [10], [11].

Figure 1.4: Administrative limits of the District Basin Authorities

1.2. Area of interest

The focus of this thesis is on a part of the Po River district (which is the one in red in Figure 1.4), which is the APSFR North of Milan (Figure 1.5). This APSFR has an extension of about 110 km^2 and includes the metropolitan city of Milan and the provinces of Monza-Brianza, Como, Lecco, Lodi, and Varese.

The main rivers included in this region are (Figure 1.5): Lambro, Olona, Seveso, Lura, Bozzente, and the group of rivers of the Groane park (Guisa, Nirone, Pudiga and Garbogera).
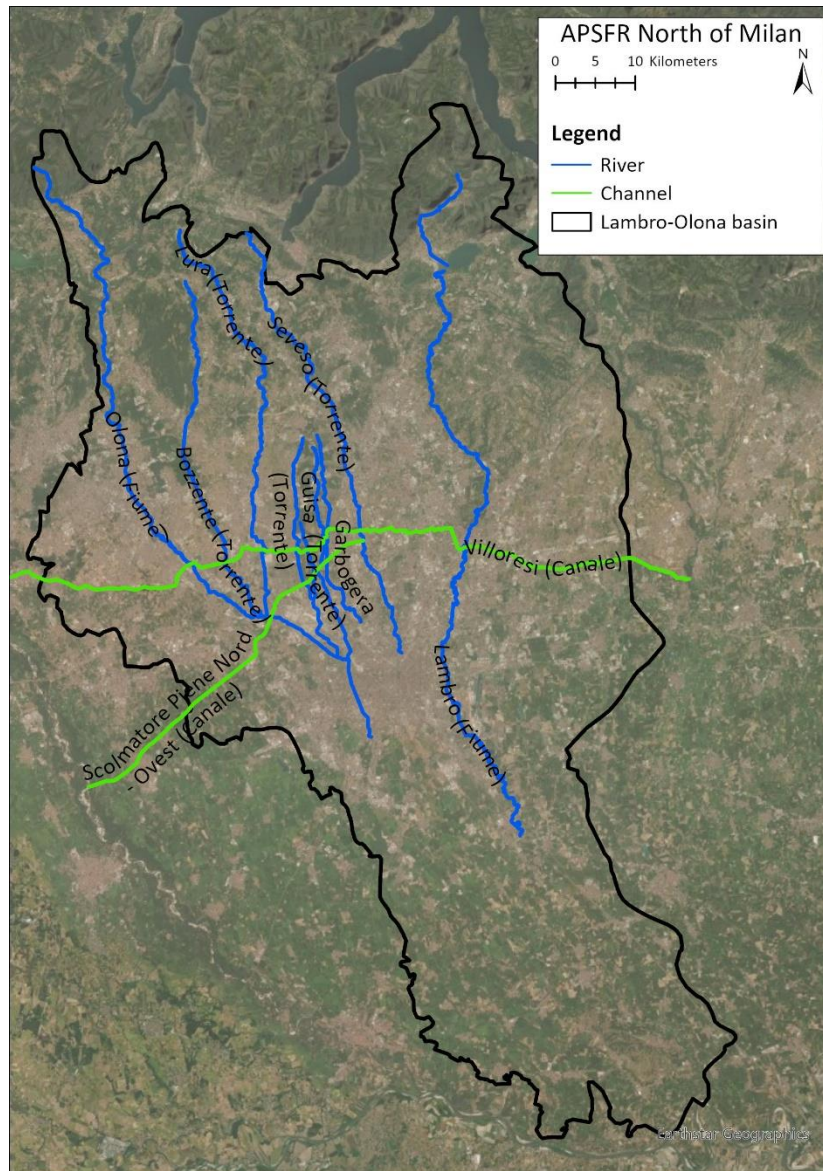
Figure 1.5: APSFR North of Milan

All the rivers included within the APSFR North of Milan are strongly interconnected since almost all of them are crossed by two channels: the Canale Scolmatore di Nord Ovest (CSNO) and the Canale Villoresi. The latter is an important irrigation channel, while the CSNO is designed to collect the overflowing water of the rivers, so that when strong events are occurring it can significantly reduce the amount of water that reaches the city of Milan. Additionally, the APSFR is characterized by the presence of several urbanized areas, industrial areas, infrastructures and productive and agricultural activities. Due to high urbanization, a significant portion of the watercourses is channelized in culverts and many bridges are present. Moreover, due to progressive urban development over the years, the sewage network is also becoming larger and larger, thus resulting in a rise of the discharge of water in the rivers. Mitigation measures are strongly necessary to reduce the effects of floods, which are also worsened by the increasing frequency of heavy storms due to climate change. Besides discharge diversion (already mentioned above), a structural intervention consists in building detention basins along the river; this measure has been applied or is under design for several watercourses of the APSFR.

This thesis is focused on two rivers of the Groane park, the Guisa and the Nirone that is a tributary of the former. Together, these two rivers cross 9 municipalities: Misinto, Cogliate, Ceriano Laghetto, Solaro, Cesate, Garbagnate Milanese, Arese, Bollate and Milano (Figure 1.6). The two streams cross urban and rural areas in the upper part, and densely urbanized areas with many industrial sites in the lower part. For this reason, in the lower part the rivers are channelized.
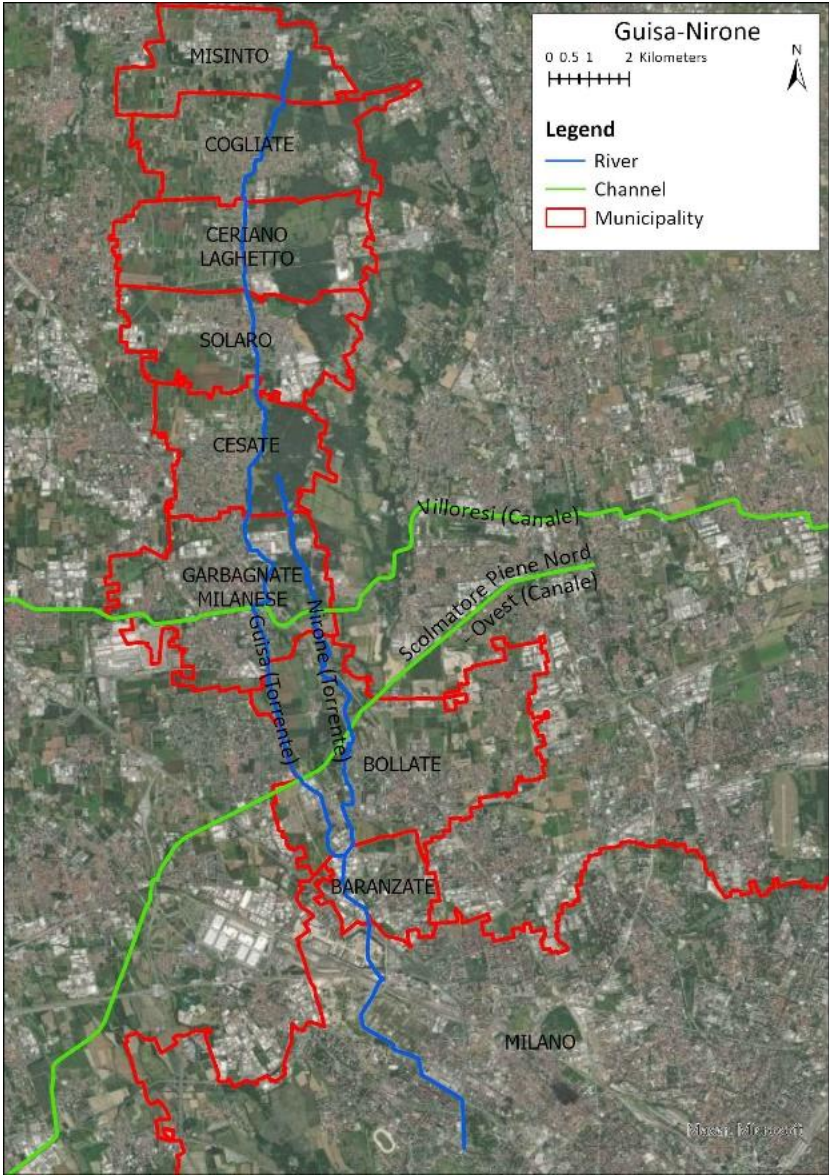
Figure 1.6: Guisa and Nirone rivers

The Guisa river starts from the municipality of Misinto and has a total length of about 23 km. The confluence with the Nirone river is reached after almost 16 km from the starting point. On the other hand, the Nirone river starts from the Cesate municipality and has a total length of about 8 km. Both riverbeds have an average width of 4 m. Along the rivers, many bridges and culverts are present (30 bridges and 11 culverts for the Guisa, while 7 bridges and 3 culverts for the Nirone).

The discharge of the Guisa river is influenced by the presence of four detention ponds and four major concentrated lateral inlets, which are due to urban drains and urban sewage systems. Their locations can be seen in Figure 1.7.
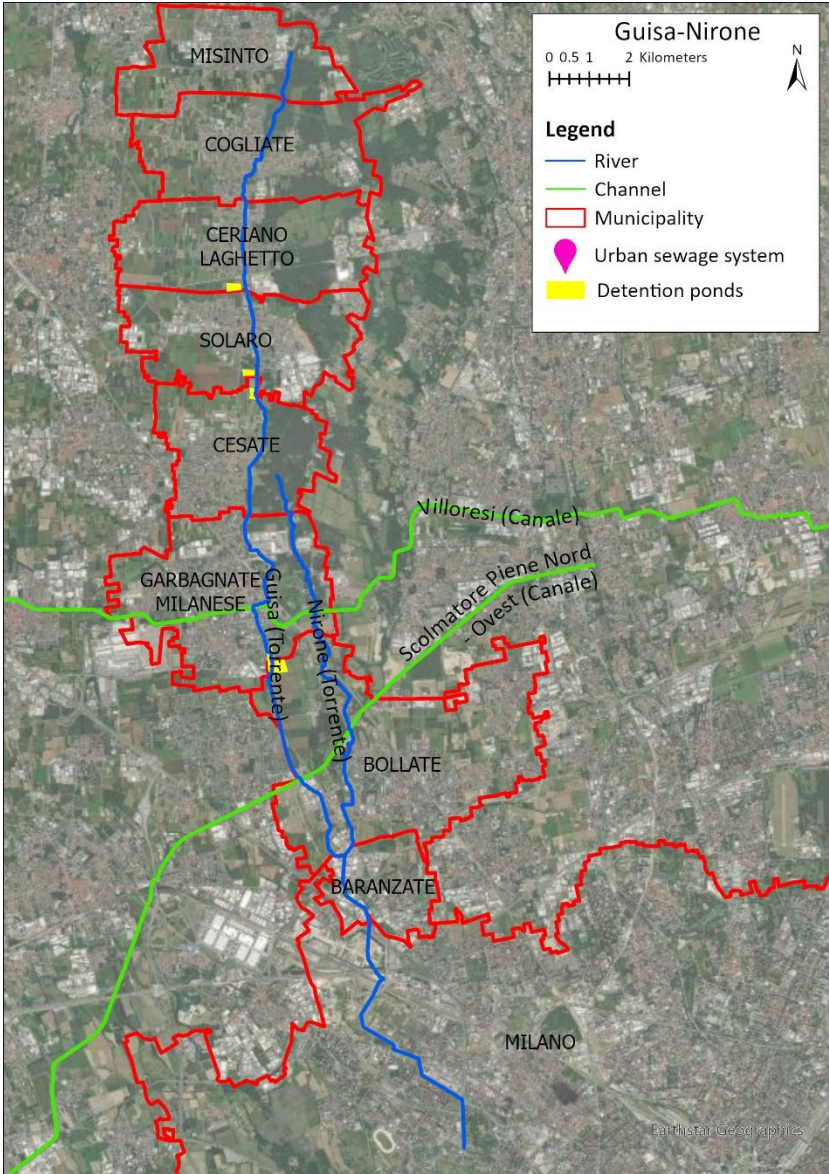
Figure 1.7: Guisa and Nirone rivers with the lateral inlets and the detention ponds

Some images representing the two rivers can be appreciated in Figure 1.8, Figure 1.9, Figure 1.10, Figure 1.11, Figure 1.12 and Figure 1.13.

Figure 1.8: Guisa river - Example 1

Figure 1.9: Guisa river - Example 2

Figure 1.10: Guisa river - Example 3

Figure 1.11: Guisa river - Example 4 (CSNO)

Figure 1.12: Guisa river - Example 5
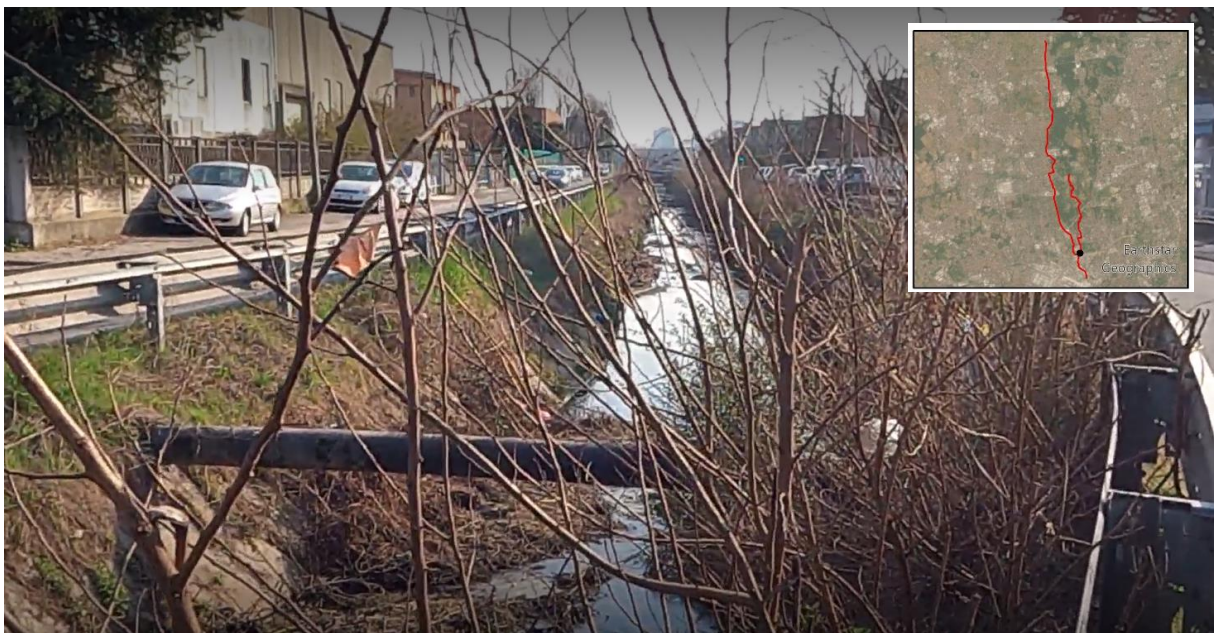
Figure 1.13: Guisa river - Example 6

1.3. Available data

1.3.1. Previous maps

The hazard maps for the previous version of the FRMP were obtained from the results of one-dimensional (1D) unsteady flow modelling [12]. The contour of the flooded area was determined by expert judgement considering the locations where the 1D model predicted water elevations exceeding the banks (and these contours were already present in the 2015 version of the FRMP). Furthermore, the water elevations computed at each cross-section were used for a spatial interpolation, determining a two-dimensional (2D) water surface whose extent was clipped at the boundary of the flooded area delimited as mentioned before. Since the

information about the water elevation was obtained by an interpolation and no hydraulic conditions were calculated, it could be said that actually a zero-dimensional (0D) method was used to determine the height of water in the floodplains (see, for details, [13]). This method is also called subjacency method since it evaluates the depth of water as the difference between the elevation of the free surface and that of the terrain. These maps were commissioned by the Autorità di Bacino Distrettuale del fiume Po (AdBPo) and were produced for all the rivers of the APSFR North of Milan in 2019 [14]. The above-described model was not applied over the entire length of the rivers, since the starting point was chosen depending on the first surveyed cross-section available. In detail, the Guisa river was analysed only from the municipality of Ceriano Laghetto, while the Nirone river was analysed only downstream of the Canale Villoresi. Therefore, in this context, the Guisa river has a length of about 13 km until the confluence with the Nirone river, and then it proceeds for almost 2.5 km, while the Nirone river has a length of about 5.5 km [12].

The analysis was made considering three return periods (i.e.: three different scenarios): 10 years, which corresponds to a high probability of occurrence (H); 100 years, which corresponds to a medium probability of occurrence (M); and 500 years, which corresponds to a low probability of occurrence (L). The obtained results of the aforementioned analysis can be seen in Figure 1.14, Figure 1.15 and Figure 1.16. It is important to highlight that these maps may be affected by some errors due to interpolation problems for both the water surface elevation (WSE) and the terrain (the bathymetry of the river channels was reconstructed through a two-dimensional interpolation following a linear interpolation of the section thalweg points). For these reasons, in some points, negative values of water depth are present (i.e.: elevation of the terrain wrongly above the WSE).

For the Guisa river are also provided the 1D model developed in HEC-RAS, as well as further information included in the document "*Attività per la definizione di soglie di attenzione - allerta - allarme pluviometriche e idrometriche lungo l'asta del torrente Guisa*" of Majone Studio [15]).
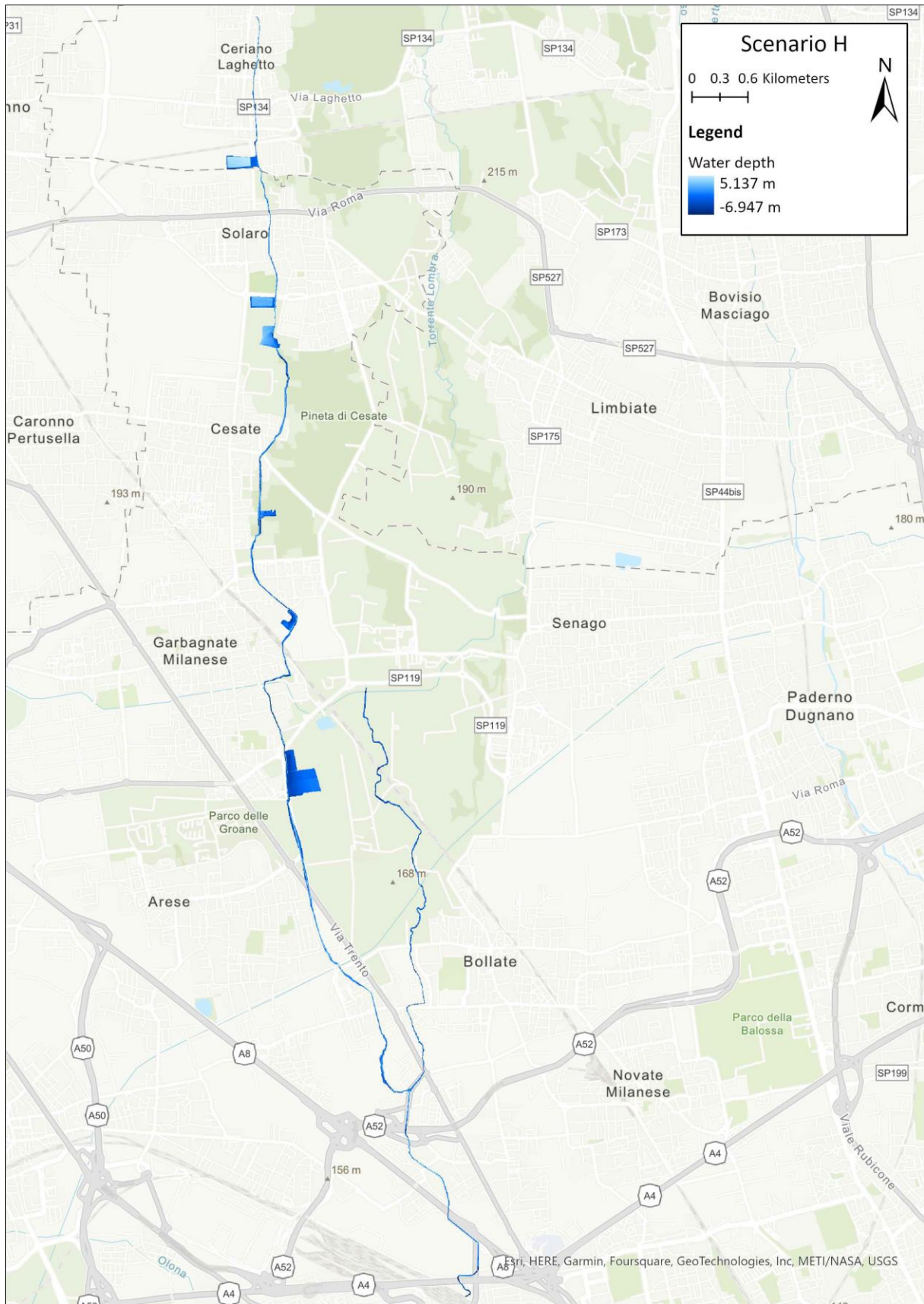
Figure 1.14: Guisa and Nirone, scenario H
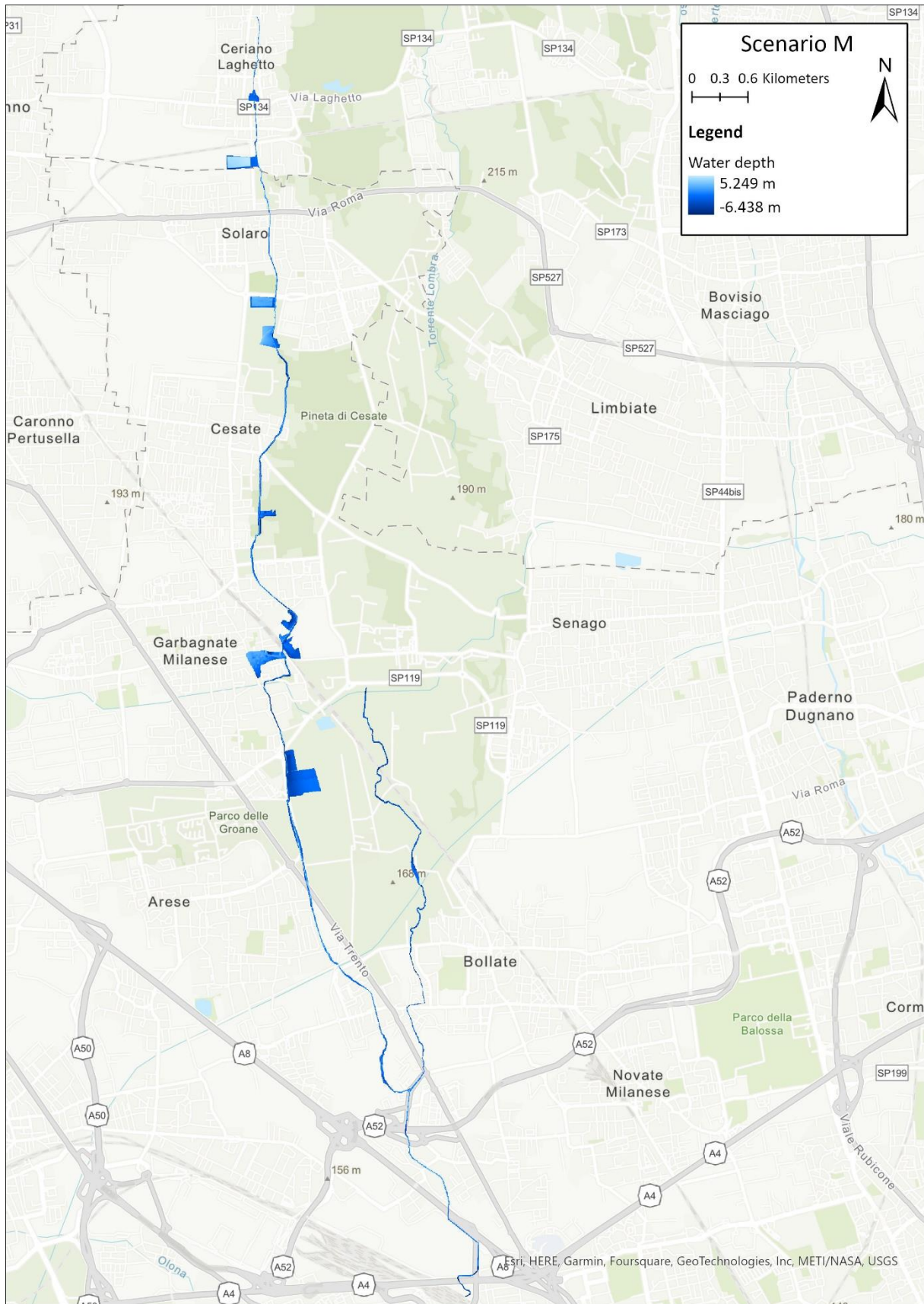
Figure 1.15: Guisa and Nirone, scenario M
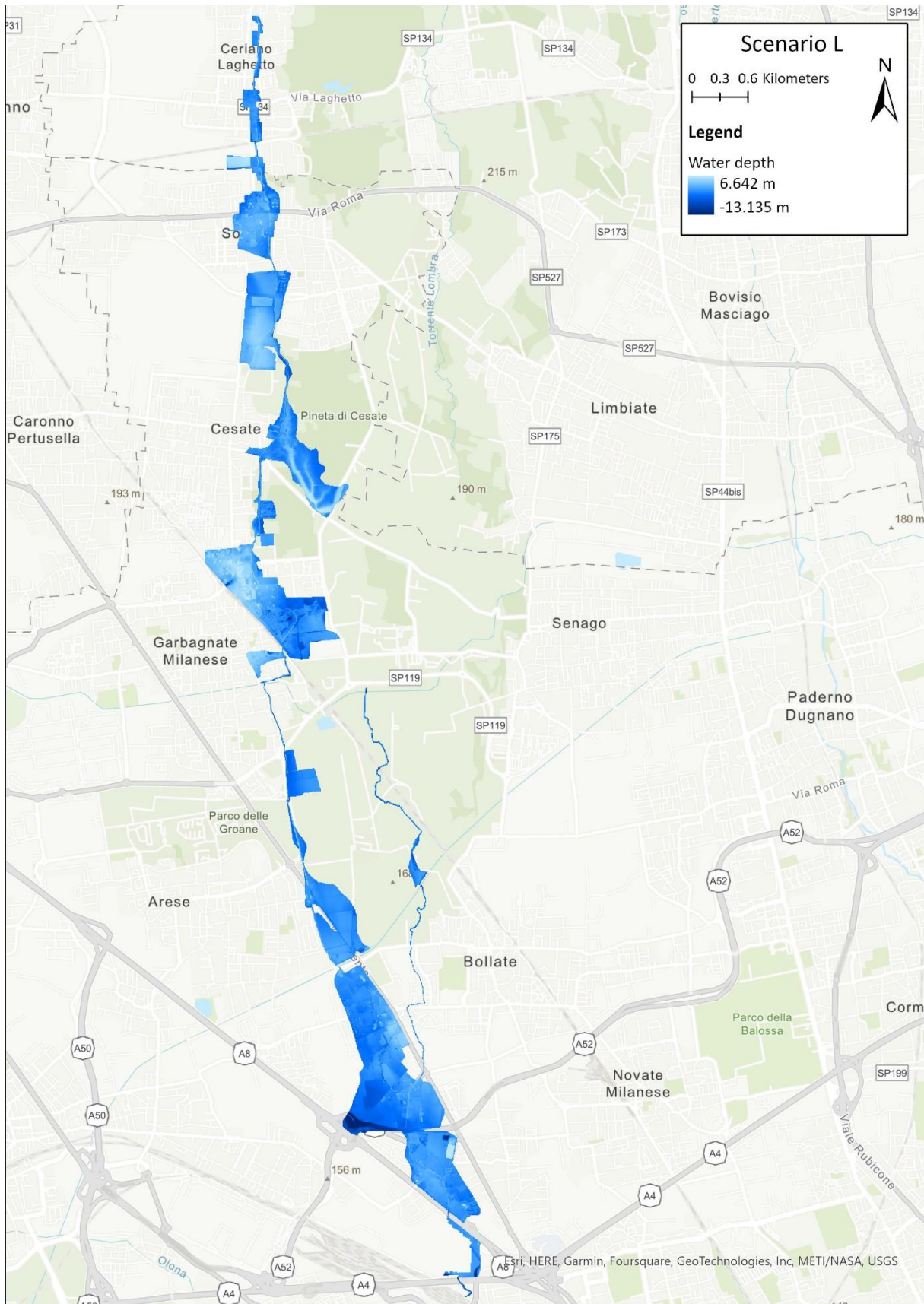
Figure 1.16: Guisa and Nirone, scenario L

1.3.2. Sections and terrain

Several cross-sections along the rivers are available; most of them are near structures, such as bridges and culverts, or critical areas, such as those close to hydrometers. Furthermore, sections are recorded as perpendicularly as possible to the riverbed. These sections were detected, commissioned by AdBPo, between the years 2002 and 2003. Georeferencing is available with reference to the system European Datum 1950 (ED50).

Furthermore, Digital Terrain Models (DTM) are available. The most detailed one was provided by the Ministero dell'Ambiente e la Tutela del Territorio e del Mare (MATTM). This DTM has a high resolution equal to 1 m and it was obtained through a LiDAR sensor [16]. Since the survey of the DTM was made between 2008 and 2009, it is important to acknowledge that it could have some discrepancies with respect to the current situation. A more recent DTM is that provided by Regione Lombardia in 2015, but it has a much lower resolution than the former, its raster cell being equal to 5 m. None of the DTMs available include the water detention ponds that were built recently along the river, which instead are described in the document "*Servizio di aggiornamento analisi idrologico-idrauliche del torrente Guisa*" of 2017 of Studio Paoletti [17].

Finally, information about the footprint of the buildings is available from the "*Geoportale della Regione Lombardia*" [18]. This data is important since it is necessary to take into consideration the presence of the buildings as obstacles to the flux of water.

1.3.3. Roughness

In general, many different sources provide an estimation of the roughness of different types of surfaces. Particularly relevant for the analysis carried out has been the information about the Manning's coefficient of the riverbed contained in the "*Studio di fattibilità della sistemazione idraulica dei corsi d'acqua naturali e artificiali all'interno dell'ambito idrografico di pianura Lambro - Olona*" (SdF) of 2003 [12]. In this document, the recommended value of the roughness depends on the type of the riverbed (e.g.: for natural channels it is suggested to use a Manning's coefficient between 0.025 and 0.035 $s/m^{1/3}$).

Instead, as far as the areas around the riverbed are concerned, the values of the Manning's coefficient can be defined using the land use information, that is provided for public use by Regione Lombardia [19]. For each type of land use is also provided a detailed description which can be used to properly assign a Manning's coefficient based on tables present in the HEC-RAS Manual [20], [21].

1.3.4. Discharge

Information about river discharge for some return periods comes from the SdF document of 2003 [12] and from the document provided by Studio Paoletti of 2017 [17].

The first study (SdF) defines the discharge using the MIKE 11 model by the Danish Hydraulic Institute (DHI). This model solves the hydrodynamic problem with an efficient numerical solution that has a limited computational time. The model can be used with three different approaches (which can be applied in branched water systems and in hydraulic nets with closed meshes): kinematic wave, diffusive wave and dynamic wave. In the SdF the dynamic wave approach was used, considering a complete motion equation to model fast transients [12].

The Paoletti Studio also used the MIKE 11 model, but considering that most of the area of the basin is urbanized. As a consequence, a "NAM-URBANO" approach was used, which is characterized by a greater detail of hydrologic-hydraulic modelling [17]. The resulting discharge values are different from those obtained in the study of 2003. This is true not only because two different modelling approaches were used, but also because in that time frame some detention basins were added along the rivers.

1.4. Aim of the work

The most important aim of the present work is to update the hazard maps produced in the year 2019 for the Guisa and Nirone rivers, using a 2D modelling approach. To this aim, the HEC-RAS software [22], which is released by the U.S. Army Corps of Engineers Hydrologic Engineering Center, is used. Among the many advantages of this numerical solver, particularly relevant is the fact that bridges and culverts can be very easily modelled in a 2D unsteady flow calculation, with the software that also automatically computes their resulting energy losses.

The technical objective is accompanied by methodological ones. The thesis will also propose an approach for the production of hazard maps, as well as investigate with care the response of the used tool to the intervention of the user. For the former, key aspect are related to the creation of a model geometry, to modelling singularities and to merging the results from different model runs for consecutive computational reaches. For the latter, the sensitivity of the results returned by the model due to the parameterization of roughness, also based on the description of buildings (impervious blocks or roughness tuning), to the relationship between geometry and mesh size and to the effect of the chosen mathematical formulation and computational time step will be documented. It is envisaged that the methodology proposed in the present thesis can be suitable for other river studies.

2. Flood mapping with a 2D modelling approach

This chapter aims to present the mathematical formulations that can be used to describe flood propagation, focusing more on the 2D urban flood modelling and on the numerical software which has been used in this thesis, which is HEC-RAS.

2.1. Two-dimensional flow modelling

2.1.1. Mathematical background

From a mathematical point of view, the propagation of floods over the Earth's surface is a three-dimensional (3D) time-dependent and incompressible fluid dynamics problem [23]. The equations which describe the flow propagation, considering just the water and neglecting the sediment transport processes, are the so-called Navier-Stokes (NS) equations. These equations consist of three momentum equations (one for each direction of the Cartesian coordinates x, y and z), which reflect the equilibrium of the forces involved, and one continuity equation, which reflects the conservation of the mass principle. However, in general, it is practically impossible to solve them for turbulent flows in a relatively long river reach. Therefore, in order to overcome the problem of turbulence, the NS equations can be simplified by averaging them in time [24], obtaining the Reynolds-Averaged Navier-Stokes (RANS) equations. The RANS equations are widely used in industrial aerodynamics and fluid mechanics, but, usually, they are still too complex and computationally demanding to describe flood problems in urban areas [23].

In order to simplify the mathematical description, it is possible to reduce the dimensionality of the model. In some cases, 1D approaches can be used. In this context, the equations that describe the flow propagation are the so-called Saint-Venant Equations (SVE), which are composed of one momentum equation (in the streamwise direction) and one continuity equation. Also in this context some further simplifications can be applied. Indeed, the experience coming from the monitoring of rivers during floods highlights the fact that typically, in many cases, the acceleration terms are smaller than the others and, therefore, they can be neglected. This simplification leads to the definition of two possible simplified models for describing flood wave propagation: the parabolic model and the kinematic model (in which also the term related to the pressure is neglected). Nevertheless, in some situations 1D modelling has some limitations that can also prevent it from being representative of a process to be modelled. Some examples of these critical situations are:

- 1D models are based on the hypothesis of having a single bulk value of velocity for each section (with a direction perpendicular to the section itself), which however is not true in reality, since the sections are characterized by some velocity distributions (since the velocity is zero at the interface between the water and the boundaries and then it increases going farther from the walls). In addition, this assumption leads to inconsistencies in the case of complex section shapes (e.g.: compound sections), in which it is usually accepted to have different velocities in the parts of the section.
- The above-mentioned hypothesis can also result in the impossibility to account for complex flow distributions, that may instead be relevant for some purposes (e.g.: impact on structures, pollutant transport, eco-hydraulics, recirculation, etc.).
- The 1D framework considers the flow direction as given. Nevertheless, this direction can also vary in peak conditions or over time, thus creating problems since the cross-sections should be as perpendicular as possible to the streamwise direction.

Therefore, since 3D models are usually too complex and computationally demanding while 1D models are affected by many limitations, frequently the best trade-off is represented by 2D models. In fact, "a model should be composed as simply as possible but as complex as necessary" [25]. In general, the formulation behind the 2D models can be obtained by imposing a force balance for a specific control volume appropriately chosen (typically a prism of water with vertical walls extending from the ground to the water surface), or by reducing the dimension of the NS equations by a depth averaging procedure (based on the idea that a river domain is much more extended in planar dimensions rather than in the vertical one). The final product which is obtained is the so-called Shallow Water Equations (SWE), which are composed of two momentum equations in directions x and y of the Cartesian coordinates ((2.1) and (2.2)) and one continuity equation (2.3). It is important to acknowledge that the assumptions behind the SWE are:

- Water shallowness, meaning that the river domain is much more extended in planar dimensions rather than in the vertical one (so that the river width and length are typically much larger than the water depth). Therefore, the model is able to represent the motion of water along the Cartesian direction x and y, while direction z is skipped (and therefore the vertical velocities are neglected).
- Hydrostatic pressure distribution.
- Incompressible fluid.
- The sinus of the angle can be approximated to the angle itself since the bottom slope of the river is assumed to be very small.
- Turbulent flow.
- Negligible Earth rotation effect.

The final representation of the SWE is reported below:

$$\frac{\partial ud}{\partial t} + \frac{\partial u^2 d}{\partial x} + \frac{\partial uvd}{\partial y} + gd\left(\frac{\partial d}{\partial x} - S_{0x}\right) = -gdS_{fx} + \frac{1}{\rho}\frac{\partial}{\partial x}(dT_{xx}) + \frac{1}{\rho}\frac{\partial}{\partial y}(dT_{xy}) \qquad (2.1)$$

$$\frac{\partial vd}{\partial t} + \frac{\partial uvd}{\partial x} + \frac{\partial v^2 d}{\partial y} + gd\left(\frac{\partial d}{\partial y} - S_{0y}\right) = -gdS_{fy} + \frac{1}{\rho}\frac{\partial}{\partial x}(dT_{yx}) + \frac{1}{\rho}\frac{\partial}{\partial y}(dT_{yy}) \qquad (2.2)$$

$$\frac{\partial ud}{\partial x} + \frac{\partial vd}{\partial y} + \frac{\partial d}{\partial t} = 0 \qquad (2.3)$$

Where:

- d   water depth
- u   velocity along direction x
- v   velocity along direction y
- g   gravitational acceleration
- S_{0i} longitudinal (bed) slope in the i-th direction
- S_{fi} friction slope in the i-th direction
- ρ   water density
- T_{ij} turbulent stress (or lateral stress)

To better interpret the SWE, Figure 2.1 shows the meaning of the different terms.

Figure 2.1: Components of the SWE

The SWE contain some additional unknowns that can be computed only with the help of closure equations. While for 1D models only one closure equation is needed (to determine the friction slope), 2D models require also an additional closure equation to determine the turbulent (lateral) stress. To evaluate the friction slopes, usually the equations (2.4) and (2.5), which are a function of the Manning's coefficient n, are used.

$$S_{fx} = \frac{n^2 u \sqrt{u^2 + v^2}}{d^{\frac{4}{3}}} \tag{2.4}$$

$$S_{fy} = \frac{n^2 v \sqrt{u^2 + v^2}}{d^{\frac{4}{3}}} \tag{2.5}$$

Furthermore, the evaluation of the lateral stress is usually achieved through the usage of a turbulence model, which may be represented by the so-called Eddy-viscosity model. The resulting equation (2.6) is the following (where v_t is the turbulent viscosity):

$$T_{ij} = \rho v_t \left(\frac{\partial u_i}{\partial x_j} + \frac{\partial u_j}{\partial x_i} \right) \tag{2.6}$$

Finally, also the 2D flood models can be simplified. Specifically, one possible approximation can be derived by considering only the forces related to gravity (weight), bed friction and pressure (and therefore the terms related to acceleration and lateral stresses are neglected), obtaining the so-called Diffusion Wave Equations (DWE). Of course, being the latter equations a simplification, there are some situations in which the complete SWE should be used, for example [26]:

- Highly dynamic flood waves: In this case (e.g.: when simulating a dam breaching or a flash flood), the flood wave will evolve very quickly. Therefore, since the change in acceleration, both in space and in time, will be dramatic, those terms (local and convective accelerations) should be present in the set of equations used to simulate the phenomenon.
- Abrupt contractions and expansions: In this context, SWE can capture more accurately the forces associated with these processes (in particular, it is important to include the convective acceleration term).
- Flat sloping river systems: For very flat rivers gravity and bed friction might not be the dominant forces. Therefore, the forces associated with acceleration terms should be included.
- Tidally influenced conditions: When modelling a bay, an estuary, or a river which is tidally influenced, in order to better model the propagation of wave, the full momentum equation set should be used.

- General wave propagation modelling: It is better to use SWE to model wave propagation (that may be due to activation of gated structures, or wave run-up around general structures).
- Super elevation around bends: The complete set of equations should be used if one wants to detect any super elevation of water externally of tight bends.
- Detailed velocities and water surface elevations at structures: Of course, the full momentum equation set should be used in order to obtain more detailed velocity distribution or water depth at or near to hydraulic structures (such as bridges, culverts, gates, etc.).
- Mixed flow regime: SWE should be used to better model changes in the flow regime (from supercritical to subcritical or vice versa).

2.1.2.   Geometry

As far as the geometry is concerned, while in 1D models its definition is made through cross-sections, in 2D models it can be defined in two ways: through a georeferenced point cloud or a DTM.

2.1.3.   Spatial discretization

The spatial discretization must always be defined in compliance with the model which is used. Once a description of the ground surface is available, a computational domain must be defined. This should include the whole area of interest and is composed by computational cells whose size and shape can vary a lot depending also on different numerical modelling approaches.

2.1.4.   Boundary conditions

The SWE are a system of three partial differential equations ((2.1), (2.2) and (2.3)) with three unknown variables: the water depth (d) and the two velocity components (u and v). Therefore, in order to solve the problem, three boundary conditions (BCs) are needed. In general, one needs to define three upstream BCs for supercritical flows (characterized by a Froude number Fr larger than 1) or two upstream BCs and one downstream BC for subcritical flows (characterized by Fr smaller than 1).

Flow	BCs upstream	BCs downstream
Supercritical (Fr > 1)	3	0
Subcritical (Fr < 1)	2	1

Table 2.1: BCs in 2D models depending on the flow regime

As it can be noticed also from Table 2.1, independently on the type of flow, there are always two upstream BCs, which typically are given by the velocity components in directions x and y. Therefore, the type of flow affects only the position of the last BC, that is the water depth, which must be defined upstream in case of supercritical flow and downstream if the flow is subcritical. However, the location of upstream and downstream BCs, differently from 1D models, in 2D models is not so straightforward to be defined. Indeed, in general in 2D models what is defined, through an additional effort to identify them, are an inflow region and an outflow region along the global perimeter of the computational domain (Figure 2.2).
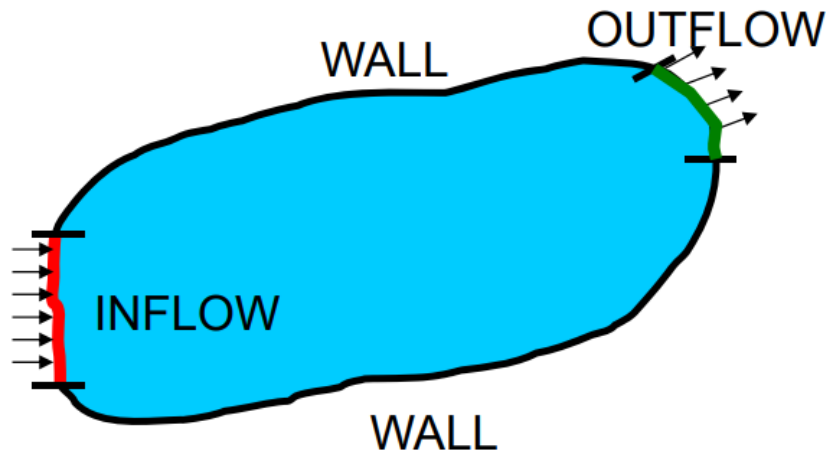
Figure 2.2: General structure of the outer perimeter of the computational domain

Therefore, in principle both the velocity components and the water depth should not be defined just in a single point, but for each cell which intersects the computational domain in the inflow and outflow regions. Nevertheless, since all this information is usually not available, typically some drastic simplifications are introduced:

- Same water elevation for all the cells embedded either in the inflow region or in the outflow region (depending on the type of flow), so that the profile of the free surface along the boundary line will be horizontal.
- In the upstream region, instead of providing the two velocity components (u and v), just a value of the flow rate (Q) is defined. Then, typically the solver used will redistribute the flow rate by assigning a zero value to the transversal velocity component and redistributing the horizontal component based on the local water depth.

In conclusion, also given the significant simplifications that usually are applied, it is important to highlight the fact that it is always suggested to put the BCs far from the area of interest (where the flood phenomenon is studied) so that their influence on the results is reduced.

2.2. Two-dimensional urban flood modelling

Several modelling strategies can be employed to simulate open-field flood propagation in urban environments. With regard to this, a very critical aspect is represented by the choice of how to represent the buildings in a numerical model. In general, depending on the available data and on the purpose of the simulation, it is possible to distinguish between three main possible methods to represent buildings.

The first method consists in incorporating buildings as impervious blocks, so excluding them from the computational space by raising walls along their perimeter (Figure 2.3). This choice is typically the most accurate that can be obtained from a SWE simulation [23], and it is quite easy to be implemented and thus recommended if a layer with all the buildings, represented as polygons, is already available on a GIS platform.
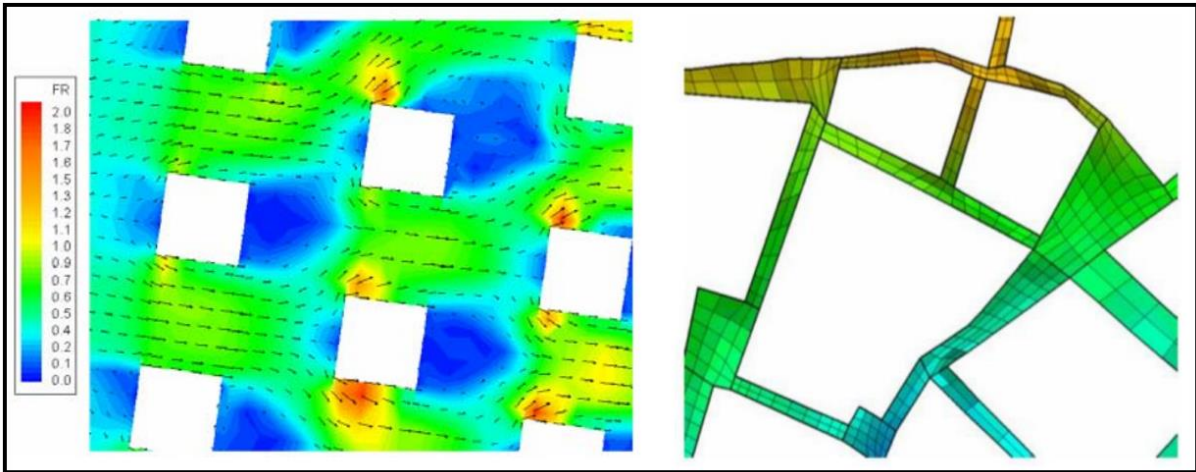
Figure 2.3: Examples of the visualization considering buildings as impervious blocks

Alternatively, buildings can be represented as ground elevation (Figure 2.4). This technique consists in rising the grid points that fall within a building area by a certain amount, which can be for example a pre-defined value or the rooftop elevation. The main problem of this method is that, even if buildings generally rise up vertically from the ground, the discrete slope is extremely steep and depends on the cell size. Specifically, with a coarse discretization (mesh size comparable with the building height) the slope is commonly of order 1, while in the case of very fine discretization (building elevation much greater than the mesh size), the slope can also reach several orders of magnitude [23]. Nevertheless, although this violates the mild slope assumption of the SWE, the model cannot be considered invalid because in this context buildings are acting as internal boundaries causing the stagnation of the fluid, and thus water around buildings can still be considered shallow [23].
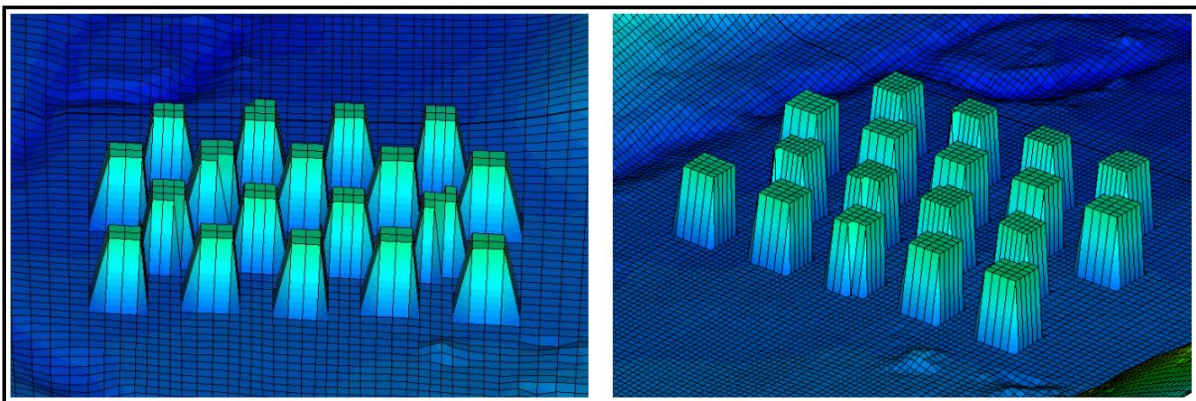
Figure 2.4: Examples of buildings representation when considered as ground elevation

The two above-mentioned methods can be considered very similar. Indeed, on the one hand, they both represent correctly the fact that in urban environment water moves in the free spaces (so it basically follows the streets), but, on the other hand, they set to zero the amount of water that can be stored in a flooded building (while, in general, if water enters into buildings the flood volume that proceeds downstream is reduced).

Finally, the last method consists in representing the buildings as areas with an increased roughness value, in order to better capture local flow effects (Figure 2.5, b)). Depending on the scale of the problem and the resolution needed, the last method can also be simplified so that

the whole urban area (or a group of close buildings) is considered as a unique region with an increased friction coefficient (Figure 2.5, a)). This approach better reflects the fact that if a building is flooded it will contain some water, but it returns wrong results in terms of velocities and directions.

Of course, the three possible methods will always lead to different results, which means that the spatial and temporal evolution of the water depth and the velocity at different places will depend, among other things, also on the method selected to represent the buildings.
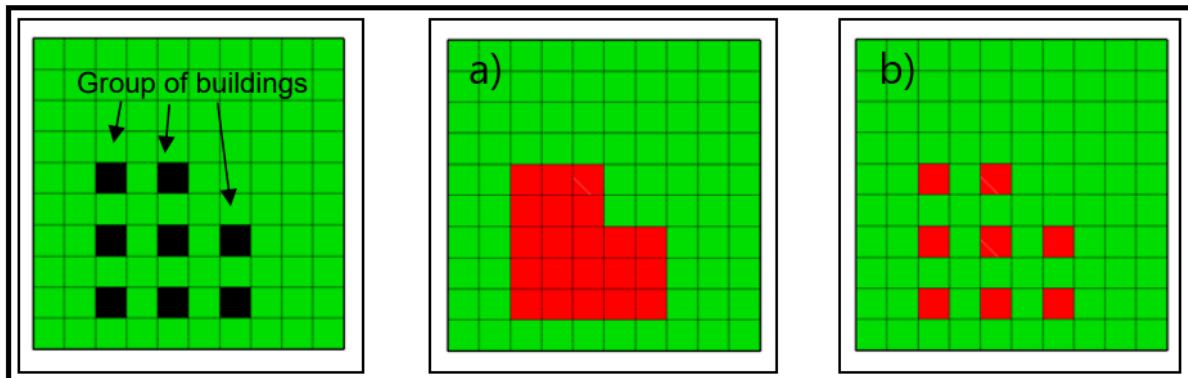
Figure 2.5: Example of a group of buildings in which friction is represented: a) As a full zone with increased friction; b) As localized spots of high friction

However, in an urban context, in addition to buildings, there are also many other kinds of obstacles which influence the roughness that should be used, such as streets, squares, and so on. Therefore, a comprehensive model should ideally include all these elements (by attributing to them different roughness values) to, at least from a theoretical point of view, reduce the gap between the results of numerical simulations and what could happen during a real flood event.

Nevertheless, there are some issues which usually prevent the user to be able to use such comprehensive models. First, an important difficulty stands in the determination of appropriate roughness coefficient values. Indeed, even if there are several tables which provide Manning's coefficient value according to different land cover units, the great heterogeneity and dynamism of urban settings make it very difficult the process of allocation of friction coefficients to all the elements. For example, in general, the friction of buildings depends on their density, the scale of the flooded area and the ratio between the flow depth and the height of the building considered [23]. Therefore, also different buildings may require slightly different Manning's coefficient values. Another example that can be mentioned is on how streets can be treated. In fact, usually streets are very smooth and flat and therefore a very small roughness value should be more appropriate. Nevertheless, on the roads there are some static or dynamic elements, such as road signs, dumpsters, sidewalks, cars, and so on, which, if considered, should increase the Manning's coefficient to be assigned. In addition, it is also important to point out that the determination of an appropriate friction coefficient is a problem which concerns not only urban settings, but also rural ones and the river itself. With respect to this last point, one can highlight that an average value of the Manning's coefficient is frequently assigned to the riverbed. However, the morphology of rivers, especially when they are very long, can also vary a lot in different sections and therefore also the friction along the river may change significantly. Second, there is an issue related to the dimension of the problem. Indeed, in the case of very limited areas, it could be reasonable to try to consider all the elements which are present within

the model, while if a large area has to be modelled some simplifications must be necessarily introduced.

To sum up, by merging together the above-mentioned issues, it is possible to understand that in the case of models which include a very limited area, the most challenging point is to assign proper roughness values to all the included elements; while for models which cover a very large area, the most difficult part lies in clustering together different elements and assigning to the resulting classes appropriate averaged values of the roughness. Of course, the roughness effects are not independent from the selected mesh size, since the latter plays an important role in how different objects, if visible, are represented in the model. In conclusion, it is possible to highlight the fact that, since every solver has limited capabilities and beyond them the model will crash, there is always a mismatch between the level of detail that the user would like to put in the model and the level of the detail that can be really put on that.

2.3. Two-dimensional numerical modelling with HEC-RAS

Nowadays many 2D numerical software packages are available on the market; some of them are free while others are subjected to charge. Of course, different solvers can lead to different numerical solutions (of the set of differential equations), generally depending on the discretization strategy, the mesh employed and the numerical scheme executed [23]. The software which was used in this thesis is HEC-RAS (Hydrologic Engineering Center's River Analysis System), which will be described in a bit more detail in the following, always referring to the information included in the official documentation [26].

2.3.1. Embedded equations

2D unsteady flow simulations in HEC-RAS can be performed using either the SWE or the DWE. Specifically, the user can select among three possible sets of equations: the original Shallow Water Equations (also called SWE/ELM: Shallow Water Equations, Eulerian-Lagrangian Method); new Shallow Water Equations solution which are more momentum conservative (also called SWE/EM: Shallow Water Equations, Eulerian Method); and the Diffusion Wave Equations (DWE). Using the SWE provides also the possibility for modelling turbulence and Coriolis effects but is obviously more computationally demanding than using the DWE.

2.3.2. Creation of the model computational mesh

Once a geometric description of the terrain in the area of interest is available and imported into HEC-RAS, the first step is to create the computational domain. This can be very easily performed in the RAS Mapper, simply by drawing the perimeter of the 2D flow area using the dedicated function. It is important to point out that the only limitation is that the computational domain must be drawn within the limits of the terrain model surface being used for the study. Then, the subsequent step is to create the computational mesh. With respect to this, in general, there are three main standard approaches to perform the spatial discretization of a numerical model: Finite Difference, Finite Volume and Finite Element methods [23]. HEC-RAS 2D modelling uses a Finite Volume solution scheme, which in general provides an increased stability and robustness compared to the other two possible techniques. In HEC-RAS the computational grid can be a mixture of 3-sided, 4-sided, etc. up to 8-sided computational cells, having the following three properties (look also at Figure 2.6):

- Cell Centre: This is the computational centre of the cell (which does not necessarily correspond to the exact cell centroid), and it is where the water surface elevation is computed for the cell.
- Cell Faces: These are the cell boundary faces, which generally are straight lines, but they can also be multi-point lines (such as the outer boundary of the 2D flow area).
- Cell Face Points: The cell Face Points (FP) represent the ends of the cell faces. The FP numbers for the outer boundary of the computational domain are used to attach the 2D flow area to a 1D elements and boundary conditions.
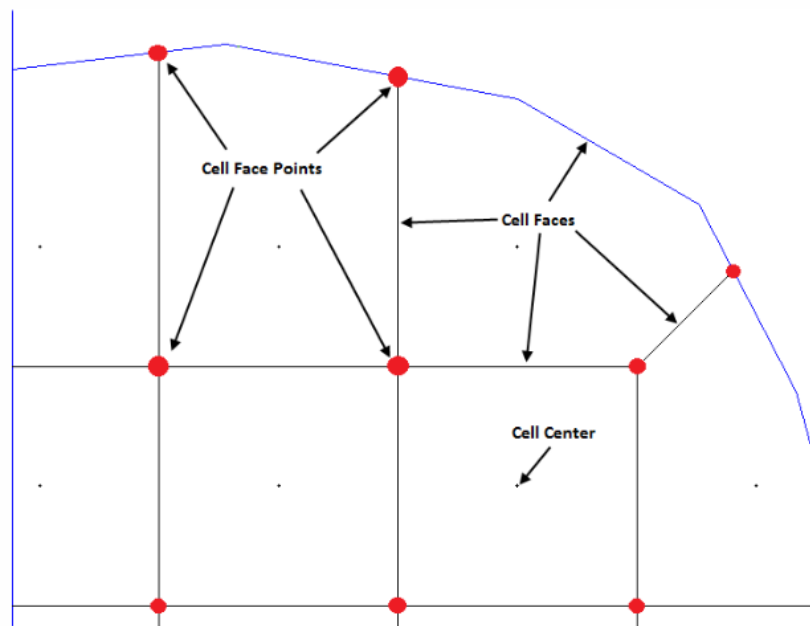
Figure 2.6: Computational mesh terminology in HEC-RAS 2D

Even if the computation cells may be manually introduced, typically they are automatically built by HEC-RAS (by following the Delaunay Triangulation technique and the construction of a Voronoï diagram) after the user has selected the desired nominal grid resolution to be used. The definition of the computation mesh is of paramount importance since this is what controls the movement of water in the 2D flow area. Specifically, when a simulation is running, at each time step one water surface elevation is computed for each cell centre and the cell faces control the flow movement between neighbouring cells. In addition, within HEC-RAS, the computational mesh and the underlying terrain are pre-processed to develop two main aspects: detailed elevation-volume relationships for each cell, and detailed hydraulic property curves for each cell face (relating the elevation to the wetted perimeter, area and roughness). All this information is also stored in dedicated hydraulic property tables, and the final effect is that the details of the underlying terrain are still examined in the water storage and conveyance, independently from the computational cell size. However, there are still some suggestions about the optimal cell size to be used, knowing that this depends on the slope of the water surface in a given area, as well as on the presence of barriers to flow within the terrain. Specifically, it is recommended to:

- Use larger grid cell sizes when the water surface slope is flat and not changing rapidly.
- Use smaller grid cell sizes in case of steeper slopes or when there are localized areas where the water surface elevation and slope change more rapidly.

In HEC-RAS the computational mesh can be edited either by using simple functions that allow for example to move, add or delete points or by using more complex tools, such as break lines and refinement regions. Some characteristics and functions of these two tools are reported below:

- Break lines: The user can add break lines at any time (also before the creation of the computational mesh). These lines force the computational cells to align along them, which is very important to be done for areas that are barriers to flow (e.g.: levees, roads, etc.) in order to properly detect ground elevation along the cell faces.
- Mesh refinement regions: This tool allows the user to refine or coarsen a zone of the mesh. Therefore, refinement regions can be used either to densify a region where more detailed results are desired (e.g.: due to quick changes in terrain or water surface elevation), or to simplify a peripheral region (e.g.: in cases in which the water surface elevation does not change a lot). In order to do that, a polygon needs to be created to define the boundaries of the refinement region area. This polygon is characterized by an external perimeter which acts as a break line and an interior part where a cell spacing must be defined (exactly as it was done for defining the computational mesh).

2.3.3. Roughness definition

Once the geometric description of the model has been defined, also the roughness needs to be introduced. In HEC-RAS the user can import multiple land use information in both raster and polygon (shapefile) formats. In addition, it is also possible to define a priority scale (the file at the top of the list has the highest priority, and so on), so that if in one area two layers are overlapping each other's, the one with a higher priority level will be accounted. Once all the desired layers are imported, the software creates a single land use coverage layer and stores it as a GeoTIFF file.

Finally, roughness values for 2D flow areas and 1D river reaches can be defined in the Land Cover layer by filling a table of Land Cover versus Manning's coefficient values. It is important to highlight that where the values are not defined, the software assigns a default value of the Manning's coefficient equal to 0.06 $s/m^{1/3}$. Additionally, when the user intends to use precipitation and infiltration features within HEC-RAS, it can also be defined a Percent Impervious for each Land Cover Classification type.

2.3.4. Available boundary conditions and initial conditions

As far as the BCs are concerned, HEC-RAS has a wide range of conditions that can be added to a model (using either the RAS Mapper or the Geometric Data editor and then the Unsteady Flow Data editor). A user can add both external and internal BCs. The former are applied along the perimeter of the computational mesh, and there are four types of them:

- Flow hydrograph: This type of BC consists in inputting a time series of discharges and is generally used to inject flow into the model. However, if negative flow values are inserted then flow will be withdrawn from the 2D area.
- Stage hydrograph: This consists in enter a time series of stages (i.e.: water surface elevations). Also this BC type can be used either to inject flow (if the stages are higher than the ground or the water surface in a 2D flow area) or to withdraw it (if the water surface elevation in the stage hydrograph is lower than the water surface in a 2D flow

area) of the model. Instead, the flow will not be created if a cell is dry and the stage BC is lower than the 2D flow area cell minimum elevation.

- Normal depth: This BC is based on the assumption that the river flows under normal flow (uniform flow) conditions at the downstream boundary of the model and therefore can be used only for downstream boundaries. The only input needed in this case is the friction slope for the outflow area.
- Rating curve: This consists in inputting a relation between stages and stream flows (i.e.: discharges). Also this BC can be used only in locations where the flow leaves the computational mesh.

The internal BCs can be used, for example, to model lateral inlets and they can be distinguished among two possible types:

- Flow hydrograph: This BC consists in entering exactly the same kind of information described in the case of external flow hydrographs.
- Precipitation: This BC can be directly applied to any model as a time series of rainfall excesses (rainfall minus losses caused by interception and/or infiltration).

In addition, HEC-RAS also gives the possibility to enter global BCs, which are conditions directly applied to the entire model (currently there are three types of them: precipitation, evapotranspiration and wind).

Finally, to complete the modelling part and be able to run a simulation, also the initial conditions (ICs) must be defined within the model. HEC-RAS provides several ways in which the user can set the ICs:

- Dry initial conditions: This is the default option.
- Single water surface elevation: In this case, all the cells having a lower terrain elevation than the user-established water surface will be wet, while the other cells will be dry.
- Restart file: This can be used to set ICs for an entire simulation, thanks to the information (water surface elevation for every cell in the model) of previously run simulations.
- Interpolation from previously computed results: In this case, the ICs are set by interpolating the results coming from an existing result file for a specific Plan, date and time.
- 2D flow area initial conditions ramp-up option: HEC-RAS provides always an option to run a model for a warm-up time, which allows the model to establish water surface elevations and flows which are consistent with the applied unsteady flow equations. In addition, for 2D modelling, there is an additional option called "Initial Condition Ramp Up Time", which must be turned on in case the model has external BCs or if it is linked to a 1D element (which exchanges flow with the 2D model) in order to establish ICs before the start of the simulation.
- Initial conditions points: This function consists in defining ICs points with a specified water surface.
- Flow per unit width computation procedure: This procedure to establish ICs can be used in the RAS Mapper and is based on several assumptions (such as that the normal depth is achievable given the chosen geometry and that a Manning equation is appropriate and that the wide-channel assumption is valid) to give a unit flow width equation. Then,

using this equation in an iterative procedure, HEC-RAS is able to compute a reasonable starting water surface for the 2D model.

2.3.5. Time step selection

Defining an appropriate computational time step is another fundamental element to obtaining a successful result in HEC-RAS. Indeed, it is very important that the chosen computational time step is neither too large, which can lead to very coarse results, nor too small, which increases a lot the computational effort, with simulations possibly lasting for very a long time. In addition, in the worst cases, the solver can crash when an unsuitable time step is selected.

In HEC-RAS there are three different approaches for selecting and controlling the computational time step:

- Fixed time step (basic method): This is the default method, in which the users simply select the wanted time step.
- Adjust time step based on Courant: This method is based on monitoring Courant numbers (or residence time within a cell).
- Adjust time step based on time series of divisors: This method allows the users to define a table of dates and time step divisors.

The last two methods are also called variable time step options, and in general, they can be used to improve the model stability and therefore to reduce the computational time (even if not all the models will be faster with the use of the variable time step options).

3. Hydraulic simulations towards updated flood hazard maps for the Guisa and Nirone

3.1. Data pre-processing

3.1.1. Terrain

To perform 2D simulations and correctly understand the behaviour of a river, the bed elevation in each cell is needed. In order to achieve that amount of information, use was made of a Digital Terrain Model (DTM) provided by the Ministero dell'Ambiente e la Tutela del Territorio e del Mare (MATTM). This DTM, which is characterized by a spatial resolution equal to 1 meter, resulted from a survey taken between the years 2008 and 2009. This DTM was produced following the law n°179/2002, which foresaw the allocation of funds for the implementation of an extraordinary high-precision remote sensing plan, aimed at the assessment and monitoring of areas characterized by high hydrogeological risk [16].

However, throughout the years, and especially before Expo 2015, the Guisa and Nirone rivers have been the object of many restorations works. Particularly relevant for the 2D modelling is the fact that four detention ponds were added along the Guisa river (Figure 3.1). Therefore, recent data about these ponds were used to manually correct, when necessary, through the help of the *Pixel editor* tool embedded in ArcGIS Pro software, the DTM.
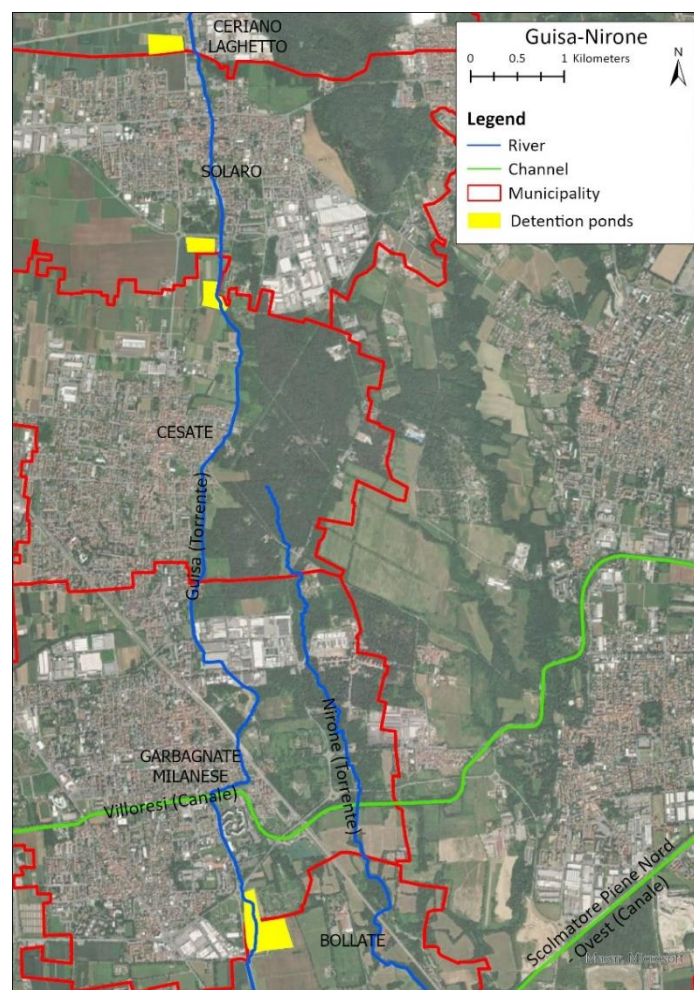
Figure 3.1: Zoom on the four detention ponds

Starting from the upstream, the first two ponds are connected to the mainstream through culverts (look also at Figure 3.29 and Figure 3.30). The DTM in this case was not modified since the area was naturally set up to host both detention basins. Instead, with the help of planimetric information and of some cross-sections [16], the DTM was manually modified in order to add the last two detention basins. Specifically, it has been necessary both to lower the ground elevation in the ponds and to introduce some walls (identifying the outer borders of the basins) in the DTM (Figure 3.2 and Figure 3.3). In addition, it is important to point out that the third detention pond can be filled through a spillway and can be emptied both through another spillway and a culvert connecting its lower part to the river (look also at Figure 3.31). The last detention basin is instead characterized by the presence of a secondary pond, which can be filled by water through a spillway connecting it to the main basin (look also at Figure 3.32).
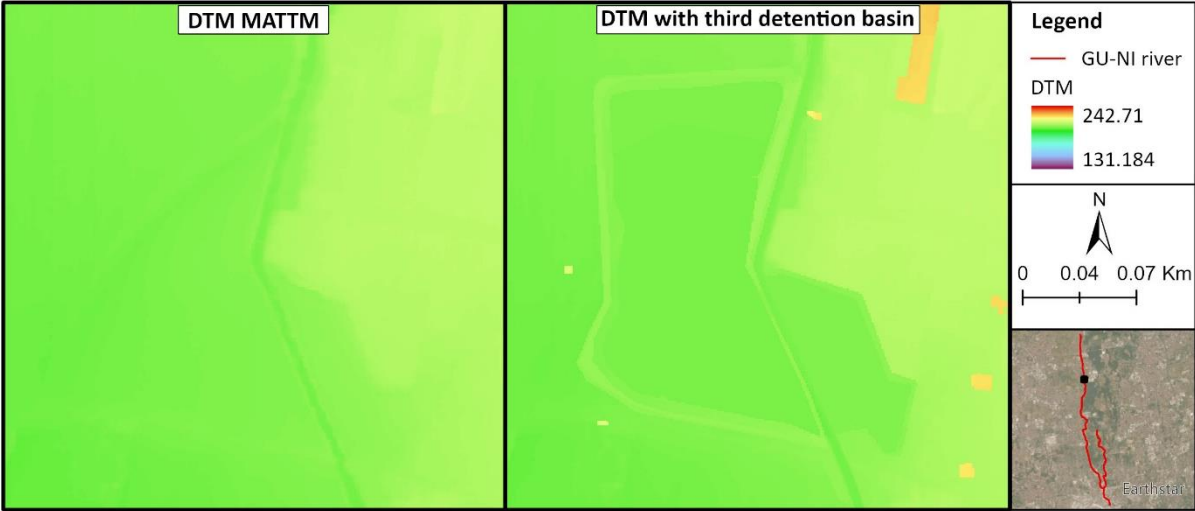
Figure 3.2: Correction of the third detention pond
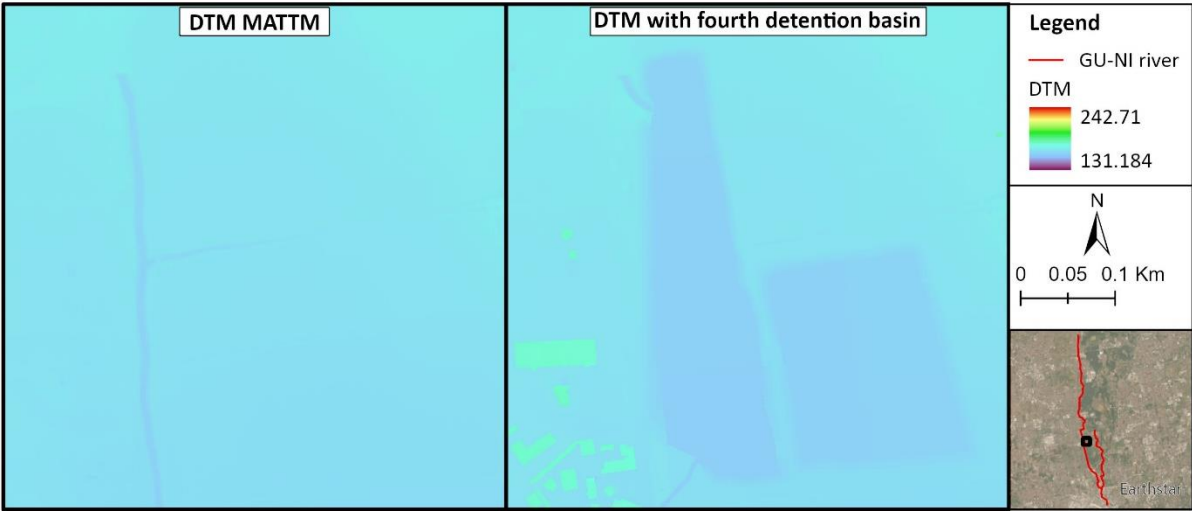
Figure 3.3: Correction of the fourth detention pond

Since the DTM was made with the Laser Scanning LiDAR (Light Detection and Ranging), which measures the distance between a target (e.g.: the water surface) and the sensor itself, the correct elevation of the riverbed is not detected. Therefore, some sections along the river are needed. Specifically, for the case study under investigation, 91 cross-sections are available for

the Guisa river and 47 for the Nirone river. These cross-sections were detected between the years 2002 and 2003 and they are provided both in GIS format (as shapefile) and in Excel format (an example is reported in Figure 3.4). In addition, further information is available, such as:

- Who commissioned the survey and who did it, as well as when and where the survey was made.
- Kilometric progressive.
- Coordinates of the vertices of the sections and their reference system, which is mainly ED50-UTM 32.
- Type of section (so if it corresponds to an artefact or land).
- How they were detected (mostly with GPS).
- Not only information about the riverbed, but also about its floodplains.

Rilievo		2002	Marzo	AdBPO	C.LOTTI
Corso d'acqua	10440020111	GUISA	GU		
Progressiva chilometrica	2.870	CTR 1:25.000			
Coord. Vertici Sezione (ED 50-UTM 32)	506429.94	5053939.03	506343.17	5053936.69	
Coord. Vertici Sezione (WGS 84-UTM 32)					
Coord. Intersezione Asse Fluviale (ED 50-UTM 32)	506384.66	5053937.81			
Coord. Intersezione Asse Fluviale (WGS 84-UTM 32)					
Caposaldi Sezione Nome	GU-73-S		GU-73-D		
Coord. Caposaldi Sezione (ED50-UTM 32)	506422.78	5053940.64	506362.46	5053938.68	
Coord. Caposaldi Sezione (WGS 84-UTM 32)					
Sistema Riferimento Rilievo Manufatto	ED 50	m.s.m.			
Strumentazione	GPS	STAZ. TOTALE	ECOSCAND.		
Toll. altimetrica punti (cm.)	± 30				
Larghezza impalcato (m) (profondità)	7.0				
Angolo rispetto direzione principale di deflusso (°)	32.0				
Larghezza plinto (m) (profondità)					
Forma plinto	RETTANGOLARE	CIRCOLARE	PRISMATICA	COMPOSTA	
Larghezza pila (m) (profondità)					
Forma pila	RETTANGOLARE	CIRCOLARE	PRISMATICA	COMPOSTA	
Altezza parapetto (m)	0.80				
Tipologia parapetto(TIPO 1 impermeabile,TIPO 2 permeabi	TIPO2				

| Dati Rilievo	Sezione	Sub	COD P	PROGR.	Q. TERRENO	COD P	PROGR.	Z1	COD P	PROGR.	Z2	COD P	PROGR.	Z3
	GU73		LOTS	0.00	223.00									
				0.00	221.97									
			LOCS	7.35	221.96									
				24.75	221.75									
			SPsx	43.05	221.60		43.05	221.20				SPsx	43.05	221.60
				43.05	219.35		43.05	219.35		43.05	221.20		45.30	221.62
			TH	45.30	219.37	TH	45.30	219.37		45.30	221.22			
				47.55	219.38		47.55	219.38		47.55	221.23	SPdx	47.55	221.63
			SPdx	47.55	221.63		47.55	221.23						
			LOCD	67.50	221.75									
				86.80	221.93									
			LOTD	86.80	223.00									

Figure 3.4: Example of information available for section GU73

In order to reconstruct the riverbed of the two rivers, a comparison between the cross-sections of 2003 and the corresponding sections extracted from the DTM has been performed. Since the two surveys were carried out in different years, the main problem detected has been that the two sources of information present many discrepancies. Indeed, frequently it turned out that the riverbed had different positions, widths, and shapes between the two surveys. Therefore, some geometric adjustments to the cross-sections, to better describe the riverbed, have been necessary. In order to do that, some characteristics of the riverbed were defined as follow:

- Width and position: They were defined mainly by using the base map (satellite imagery) available in ArcGIS Pro, since this is for sure the latest information available about the river path. This analysis highlighted the fact that usually, the position of the river in the base map was matching the one coming from the DTM of the MATTM, while usually the position of the cross-sections detected in the year 2003 was shifted by even several meters (Figure 3.5 and Figure 3.7).

- Shape: This aspect was defined mainly based on the cross-sections surveyed in the year 2003. This approach was followed since, as previously mentioned, the sections extracted from the DTM usually presented a wrong shape since the points represented either the water surface (e.g.: Figure 3.6) or a structure present across the riverbed (in this extreme case the riverbed is not recognizable at all, as it can be seen from Figure 3.8, which represents a section where a bridge is located).

Once the new cross-sections of the riverbed were defined (from Figure 3.5 to Figure 3.8 they are called "Section for MATLAB"), they were interpolated through a MATLAB code developed specifically for this purpose by students and professors of the Politecnico di Milano. This code, through data about the coordinates of the river axis and the endpoints of the sections, and data about the station and elevation of the riverbed points, allows the sections to be interpolated by a chosen distance. The results of the interpolation are two point clouds. The first one describes the contour of the riverbed and each point is described through the Cartesian coordinates x and y. In a second step, this point cloud was transformed into a polygon using the *Point to line* and then *Feature to polygon* commands embedded in ArcGIS Pro. The second one represents the riverbed and each point has its 3D coordinates, x, y and z. This point cloud was then transformed into a raster using the *Point to raster* command in the GIS software.

Subsequently, to get a complete description of the floodplains as well, the raster of the riverbed was overlaid with the DTM of the MATTM. Then, to check the correctness of the interpolation, the new data about the station and elevation of the cross-sections were extracted and then compared with the previous ones. From this analysis, as it can be seen from Figure 3.5 to Figure 3.8, it has been possible to conclude that the results obtained after the interpolation were coherent with the sections defined for the MATLAB code and the DTM defined by MATTM, therefore a final DTM (called "New DTM" from Figure 3.5 to Figure 3.8), which also includes the riverbed of the river, has been obtained.
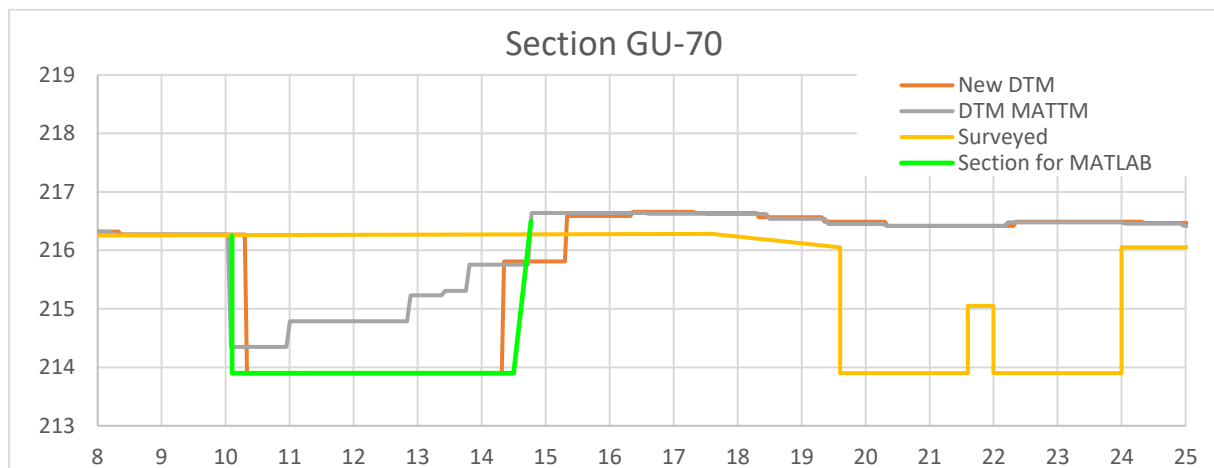

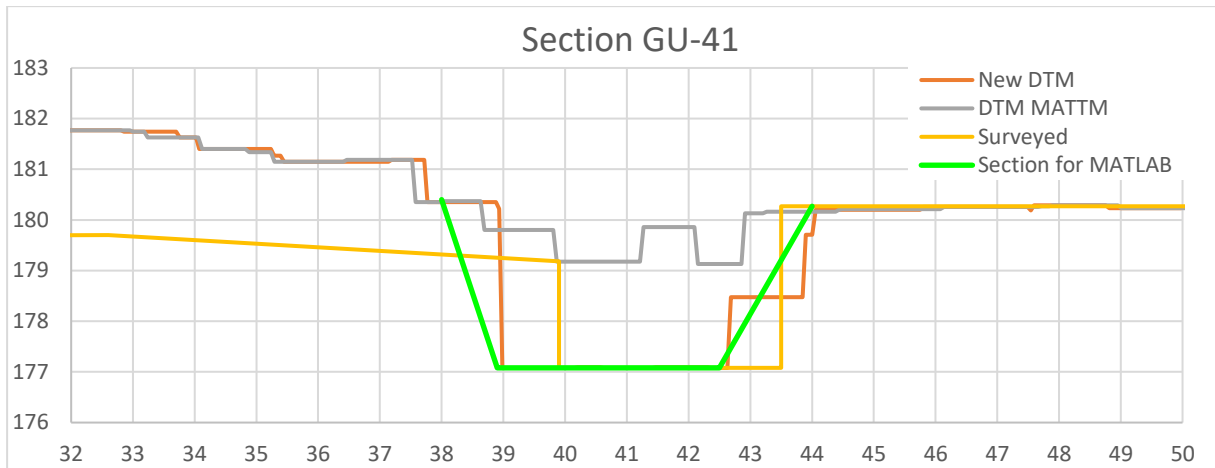*Figure 3.5: Example of the section moved on the right*

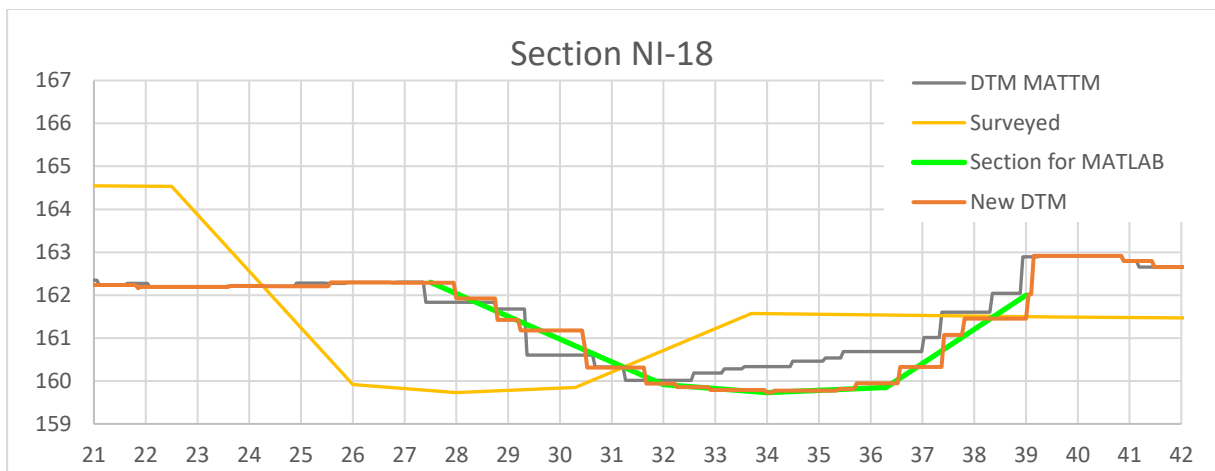*Figure 3.6: Example of the section where the riverbed changed the shape*

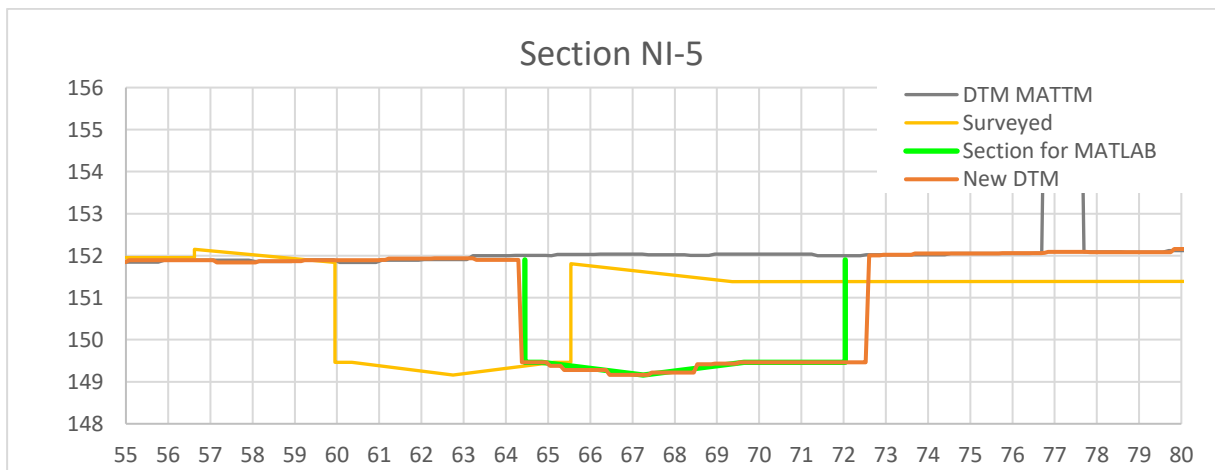*Figure 3.7: Example of section moved on the left*

Figure 3.8: Example of a bridge section

In Figure 3.9 it can be noticed how the DTM has changed after the application of all the aforementioned corrections. In the picture on the right, the riverbed is clearly visible while it was wrong in the original DTM.
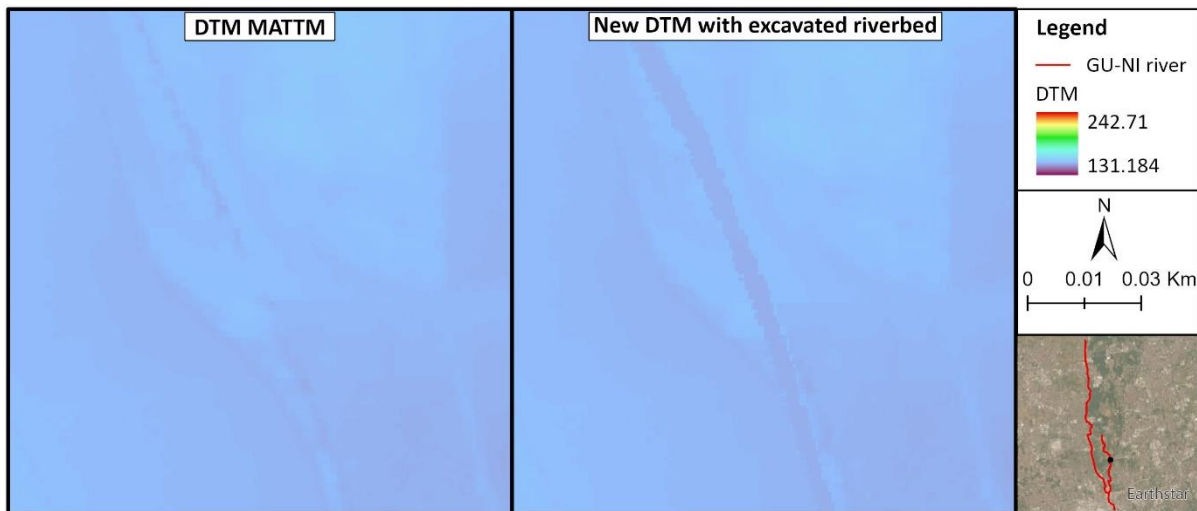
Figure 3.9: Example of the DTM correction to correctly represent the riverbed bathymetry

However, the fact of having excavated the riverbed also where culverts are located represents a problem that must be fixed. Indeed, coherently with the reality, in HEC-RAS it is required to have the elevation of the terrain in correspondence of the culverts. Therefore, in those locations, the original terrain elevation from DTM of the MATTM must be restored (Figure 3.10).
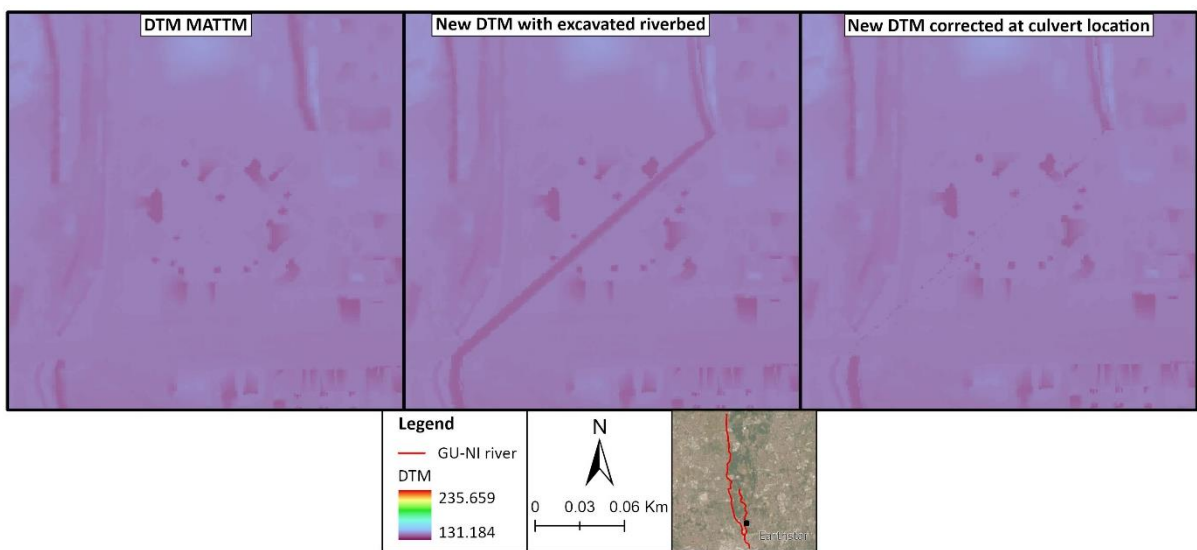

Figure 3.10: Example of the DTM correction to restore the original elevation at culverts

Finally, it has been necessary to modify the DTM also for taking into account the buildings, which in this case were considered as ground elevation. In order to do that, a shapefile of the footprint of the buildings, available from "*Geoportale della Regione Lombardia*" [18], was downloaded. Subsequently, the DTM was clipped where the buildings are present, and that portion was raised by 10 meters. Finally, this final raster file containing only the buildings and the previous DTM were overlapped, obtaining a final result that can be seen in Figure 3.11.
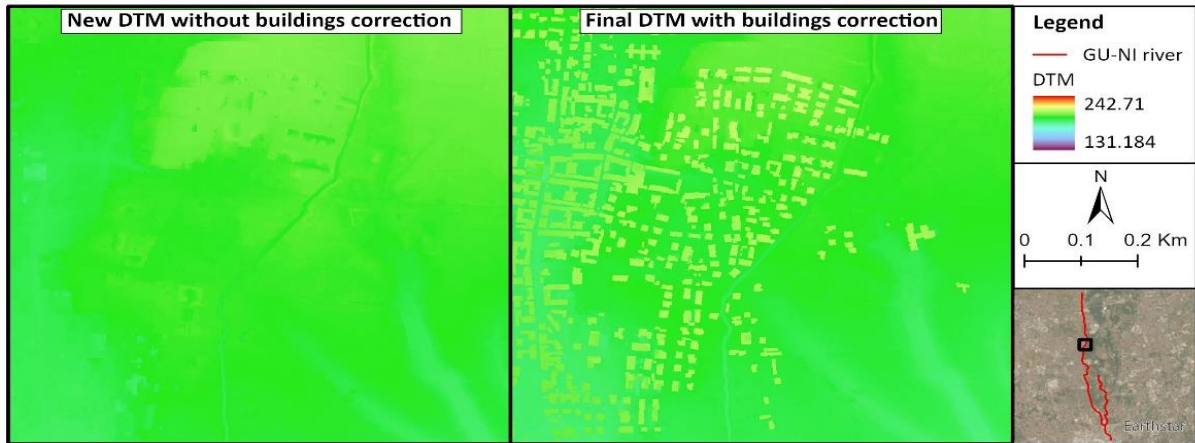
Figure 3.11: Example of adding the buildings to the DTM

After this modification, the final DTM to be used for the 2D modelling in HEC-RAS is obtained.

3.1.2.   Roughness

Over the whole modelling process, the roughness value is considered through the Manning's coefficient. Specifically, it has been decided to define just one value for the riverbed and a unique average value also for the remaining part of the model.

A value for river roughness was imposed within the polygon created from the point cloud describing the contour of the riverbed obtained from the MATLAB code. Then, the roughness value for the riverbed was defined considering the SdF document, where it was mentioned that for natural channels the coefficient can vary between 0.025 and 0.035 $s/m^{1/3}$; an average value equal to 0.03 $s/m^{1/3}$ was used [12].

As far as the remaining area is concerned, since the buildings were already considered as ground elevation with a height equal to 10 m above the underlying terrain, a uniform Manning's coefficient equal to 0.06 $s/m^{1/3}$ was used [20].

3.1.3.   Structures

To have a complete description of the river, the structures along it must be also added to the model. With respect to this, some information about the bridge spans and the culvert openings is available. As can be noticed from Table 3.1, which shows an example of the available data, for each structure the number of the cross-section where it is located is known, together with the type of structure (P stands for a bridge while T for a culvert), and the width and rise of its opening.

73P
4.5 x 1.85
72P
3.55 x 2.64
71P
5.62 x 2.15
70T
3.15 x 4.15

Table 3.1: Example of bridges and culverts data

In addition, also information about the bridges intrados and extrados is available [12].

35

3.1.4. Boundary conditions and lateral inlets

To run a 2D model, information about the boundary conditions (BCs) and the lateral inlets also needs to be provided. As said in Chapter 1.3.4, the main sources of information about the discharge, for all the return periods considered, have been the SdF document of 2003 [12] and the Paoletti study of 2017 [17].

The SdF document provided data about the shape of the hydrographs of the upstream BCs (detected at sections GU65 and NI27) and just upstream of the intersection with the CSNO (sections GU23 and NI12) for both the rivers, as shown from Figure 3.12 to Figure 3.15. This document also provides the rating curve defining the outflow region at the end of the Guisa river (Figure 3.16). These graphs have been successively digitized, and the hydrographs have been interpolated to get discharge information every 30 minutes since HEC-RAS requires equal time intervals data for successively run a simulation. In addition, also information about the peak discharges of the Nirone river after the CSNO (respectively equal to 2 m^3/s for T10, 3 m^3/s for T100 and 4 m^3/s for T500) and the peak flow rates coming from the lateral inlets (Table 3.2) are available in the SdF study. Since only information about the peak discharge is available for the lateral inlets, it is important to point out that it has been assumed that the shape of their hydrographs is the same as that corresponding to the upper BCs. Finally, the SdF document provided also a table putting in relation the discharge and the WSE in some cross-sections (Table 3.3). All the downstream BCs have been defined by interpolating the data contained in Table 3.3 (apart from the outflow region of the Guisa river, in which the rating curve is available).
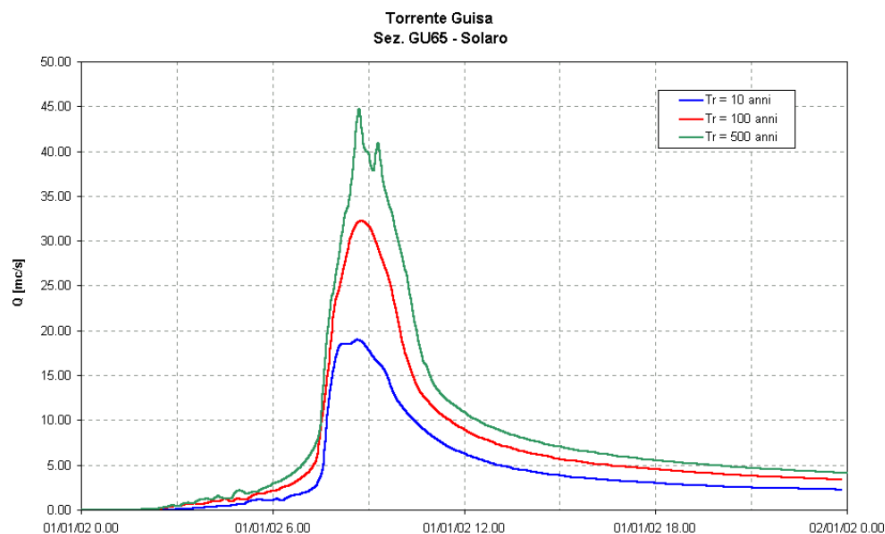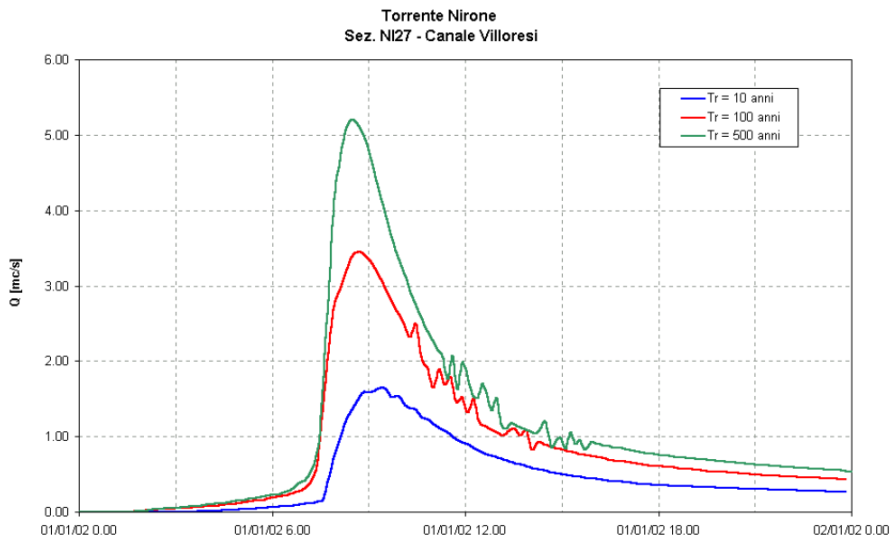

Figure 3.12: Hydrograph section GU65
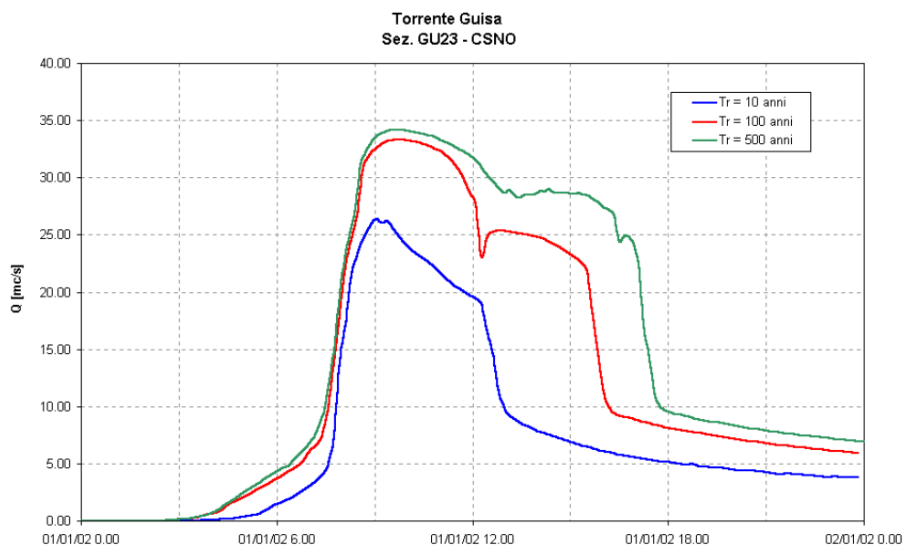
Figure 3.13: Hydrograph section NI27

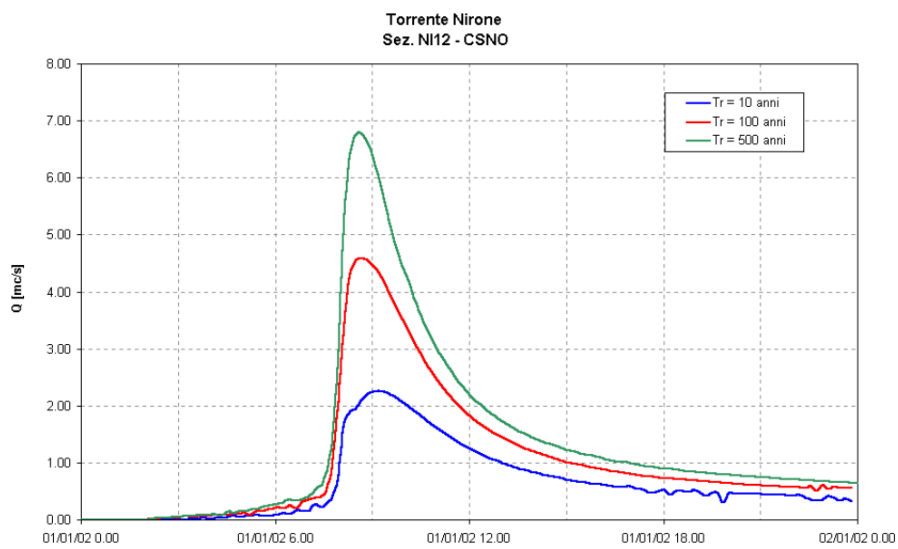*Figure 3.14: Hydrograph section GU23*

Figure 3.15: Hydrograph section NI12

37
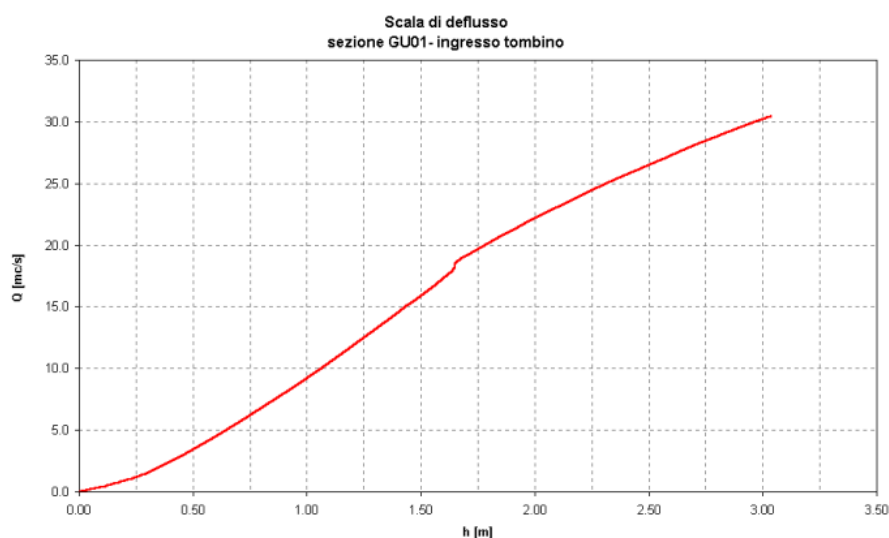
Figure 3.16: Rating curve section GU01

Nome bacino	AREA [KMQ]	Imm. conc.	Immissione distribuita	Q 10 [mc/s]	Q 100 [mc/s]	Q 500 [mc/s]
GU10	15.11	GU_73		14.91	25.38	38.33
GU09	3.72		GU_73 – GU_65	2.45	4.35	7.12
S1G - Solaro	2.00	GU_65		9.10	9.10	9.10
GU08	0.90		GU_65 – GU_60	1.03	2.10	2.93
GU07	2.43		GU_60 – GU_56	2.07	4.33	5.74
GU06	0.46		GU_56 – GU_49	0.30	0.57	0.90
S2G - Cesate	1.90	GU_49bis		9.50	9.50	9.50
GU05	1.44		GU_49 – GU_39	1.69	3.59	4.95
GU04	0.80		GU_39 – GU_32	1.46	2.47	3.95
S3G - Garbagnate	2.00	GU_35		12.35	12.35	12.35
GU03	2.02		GU_32 – GU_23	2.38	4.92	6.40
S4G - Garbagnate	1.70	GU_31		5.45	5.45	5.45
GU02	0.26		GU_23 – GU_15	0.56	1.08	1.68
GU01	1.78		GU_15 – GU_1	2.43	5.17	7.97
S5G - Bollate	2.50	GU_6		6.76	6.76	6.76
NI4	2.7	NI_27		1.61	3.16	4.86
S1N - Garbagnate	0.1	NI_27		1.00	1.00	1.00
NI3	1.05		NI_27 – NI_13-1	0.78	1.64	2.15
NI2	0.1		NI_13-1 – NI_06	0.13	0.27	0.39
S2N - Bollate	0.1	NI_06		1.00	1.00	1.00
NI1	0.001		NI_06 – NI_01	0.00	0.00	0.00

Table 3.2: Discharge information in SdF document of 2003

Sezione	Descrizione	T 10 Livello (m)	T 10 Portata (mc/s)	T 100 Livello (m)	T 100 Portata (mc/s)	T 500 Livello (m)	T 500 Portata (mc/s)
GU65	Solaro – P.te Via Varese	207.84	19.0	209.42	32.3	210.06	44.8
GU55	Cesate – P.te Via dei Martiri	196.47	16.1	196.55	20.2	196.63	28.2
GU38	Sifone Canale Villoresi	174.18	19.2	174.67	22.5	176.42	26.2
GU23	Sfioratore CSNO	157.42	26.4	157.52	33.3	157.55	34.2
GU01	Milano – Sottopasso FS Rho-MI	135.94	15.2	136.72	24.2	137.03	26.7
NI27	Sifone Canale Villoresi	171.27	1.6	171.54	3.4	171.76	5.2
NI12	Sfioratore CSNO	156.96	2.3	157.25	4.6	157.49	6.8
NI03	Bollate – P.te S.S. Varesina	146.19	2.5	147.01	4.6	147.07	5.3
CSNO-GUISA	Sfioratore CSNO	157.42	7.1	157.52	8.4	157.55	8.8
CSNO-NIRONE	Sfioratore CSNO	156.96	0.1	157.25	1.1	157.49	2.7

Table 3.3: Relation discharge-WSE

Instead, the Paoletti document of 2017 has been useful since it provides updated values, which consider also the presence of the detention ponds, of the peak discharge of the Guisa river both in correspondence of the upstream BCs and after the CSNO (Table 3.4).

Bacino	Corso d'acqua	Sezione Progr.(km)	Sezione Cod.	Sezione Denomin.	Superficie km²	Q10 m³/s	Q100 m³/s	Q500 m³/s
Lambro	Guisa	2.88	GU 73	Cogliate	15	8	10	14
Lambro	Guisa	5.042	GU 65	Solaro	21	8	10	13
Lambro	Guisa	7.576	GU 55	Cesate	26	9	11	15
Lambro	Guisa	10.784	GU 38	ponte canale Villoresi	35	11	14	16
Lambro	Guisa	13.787	GU 24	monte presa CSNO	40	9	11	14
Lambro	Guisa	14.223	GU 22	valle presa CSNO	40	3	3	3
Lambro	Guisa	18.346	GU 1	Milano (ingr. Tombinatura)	44	8	9	11

Table 3.4: Discharge information in Paoletti document of 2017

To sum up, all the available information, considering both the rivers, has been used as shown in Table 3.5:

		Guisa river	Nirone river
Upstream BCs	Hydrograph shape	SdF [12]	
	Peak discharge	Paoletti [17]	
Discharge after CSNO	Hydrograph shape	SdF [12]	SdF [12]
	Peak discharge	Paoletti [17]	
Downstream BCs		SdF [12]	
Lateral inlets			

Table 3.5: Usage of the available information for defining the BCs and the lateral inlets

3.2. Modelling in HEC-RAS

3.2.1. Model subdivision

Since the two considered rivers (in particular the Guisa river) are quite long, it was decided to apply two models for each river. Specifically, since the CSNO retains part of the discharge thus resulting in an important decrease of this value, it was decided to use its location as a breaking point between the two models for each river. This aspect can be better appreciated from Figure 3.17 and Figure 3.18, showing the progressive variation of the peak discharge computed by summing the values at the upstream end of a river and the lateral inflows (whose location is

also indicated). It is important to highlight that these graphs do not represent the actual discharge that will flow in the rivers since, in reality, the discharge peaks do not perfectly overlap due to the timing of the inflows and the dynamic propagation of flood waves.

It is important to highlight that the Nirone river has only one lateral inlet which, however, being located in correspondence of the inflow region of the model, has been directly included in the upstream BC.
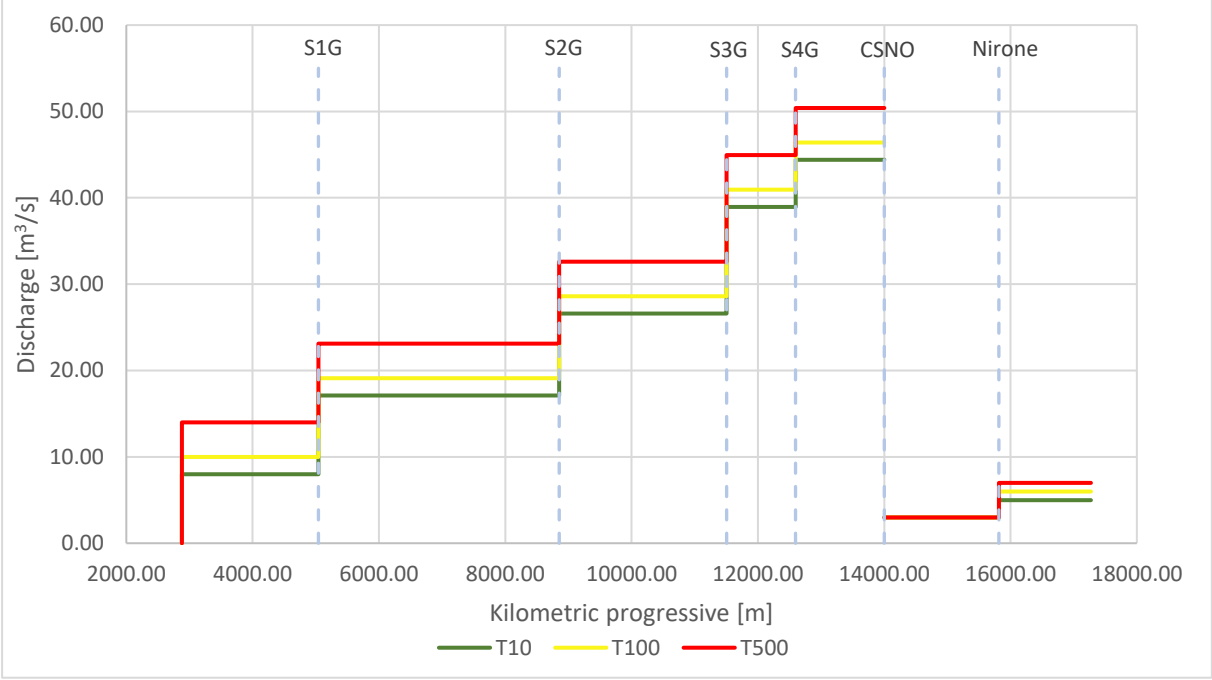

Figure 3.17: Peak discharge Guisa
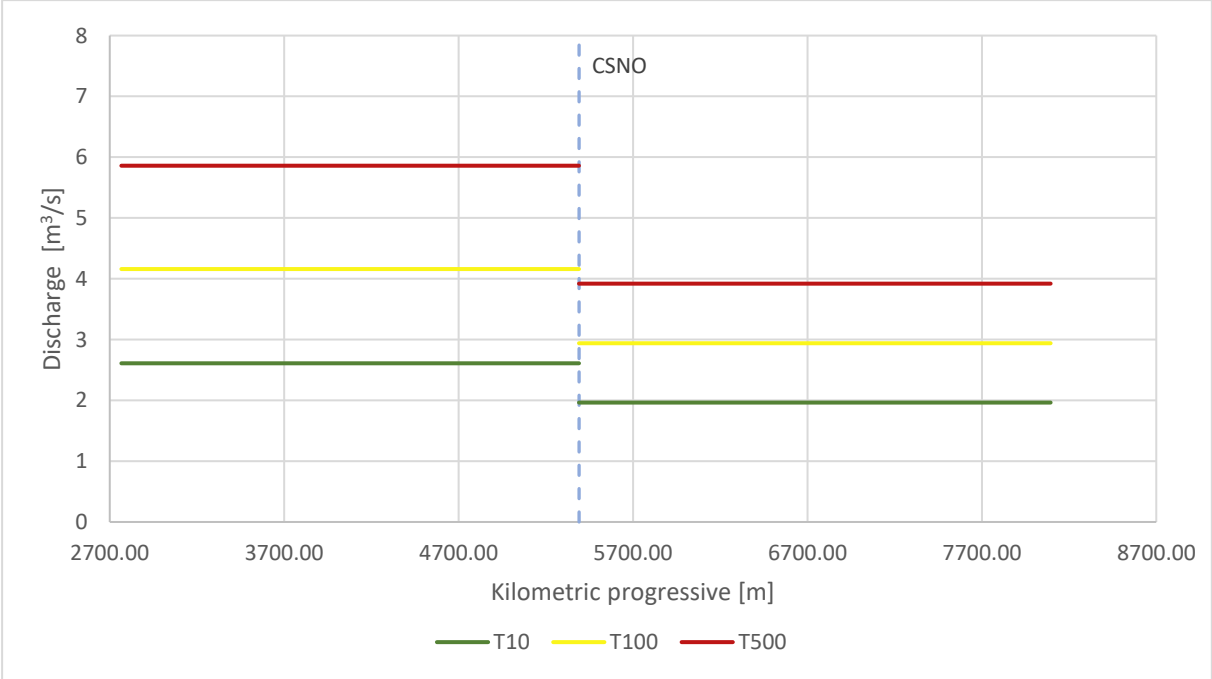
Figure 3.18: Peak discharge Nirone

Splitting the rivers into two parts for the numerical modelling also led to some advantages, such as the fact that the computational time can be reduced and/or a finer mesh can be defined, thus increasing the precision and the accuracy of the simulations. The final subdivision can be seen in Figure 3.19 and the four river reaches will henceforth be called "Guisa upstream", "Guisa downstream", "Nirone upstream" and "Nirone downstream". Table 3.6 reports the length of the four defined river reaches.
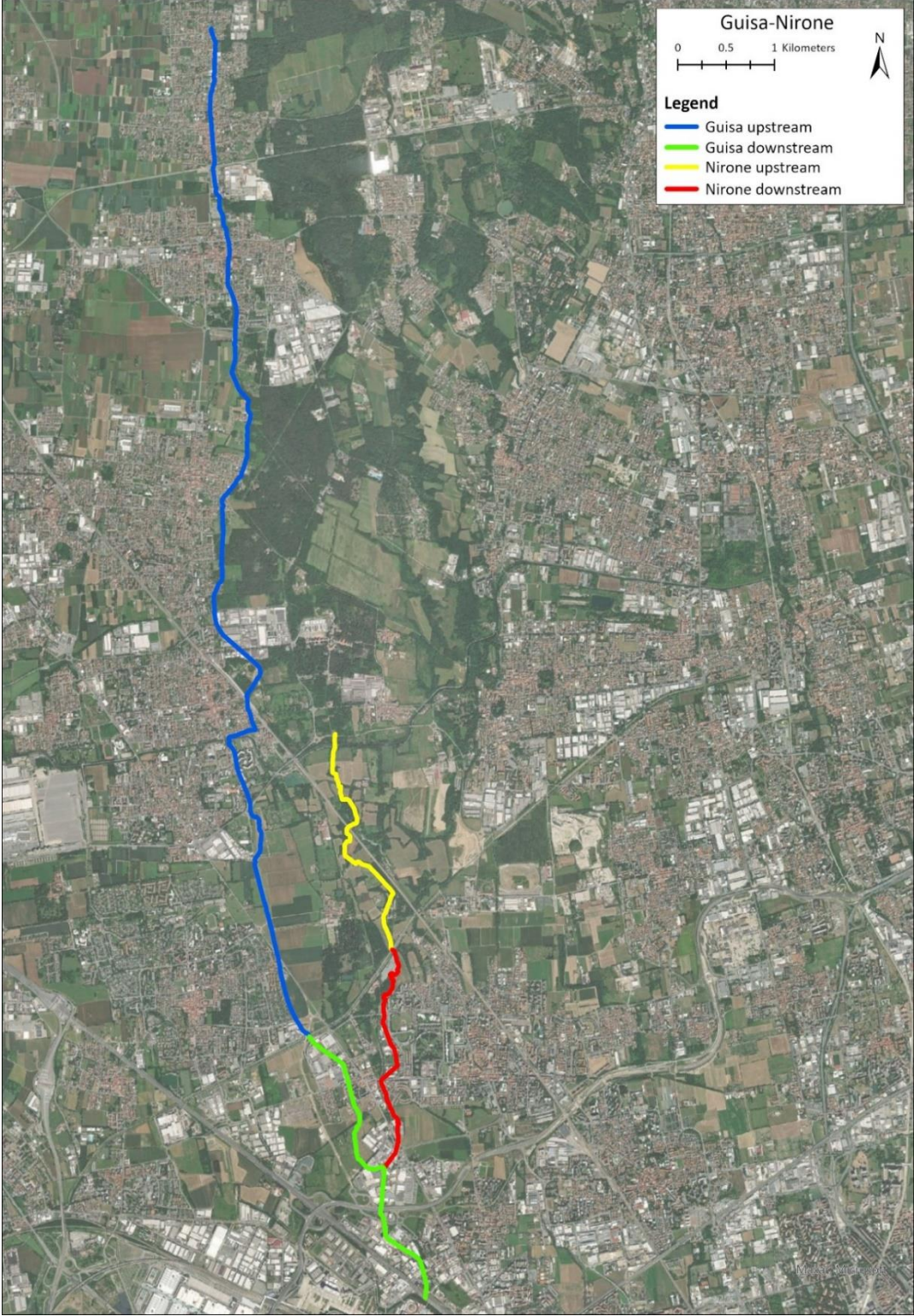
Figure 3.19: Model subdivision

It is important to point out that, since both the available cross-sections and the DTM were defined some years ago, the part of the Guisa river within the Expo area, which underwent many changes in the last few years (in particular between 2010 and 2015), is not analysed due to the absence of updated information.

	Guisa river		Nirone river	
	Upstream	Downstream	Upstream	Downstream
Length [km]	11.1	3.2	2.6	2.7

Table 3.6: Length of the parts

3.2.2. Model implementation

In this chapter all the steps that, taking advantage of all the data and actions mentioned in Chapter 3.1, have been made in HEC-RAS in order to run a 2D model will be presented.

First, the model of the terrain was added in the RAS Mapper and also the computational domain was defined. In addition, also a refinement region around the river was added, using the close polygon created from the point cloud describing the contour of the riverbed obtained from the MATLAB code, to better describe and model this critical zone. An example of how all these elements look in the software can be appreciated in Figure 3.20 and Figure 3.21.

Figure 3.20: Example of terrain and computational mesh representation (Guisa downstream)
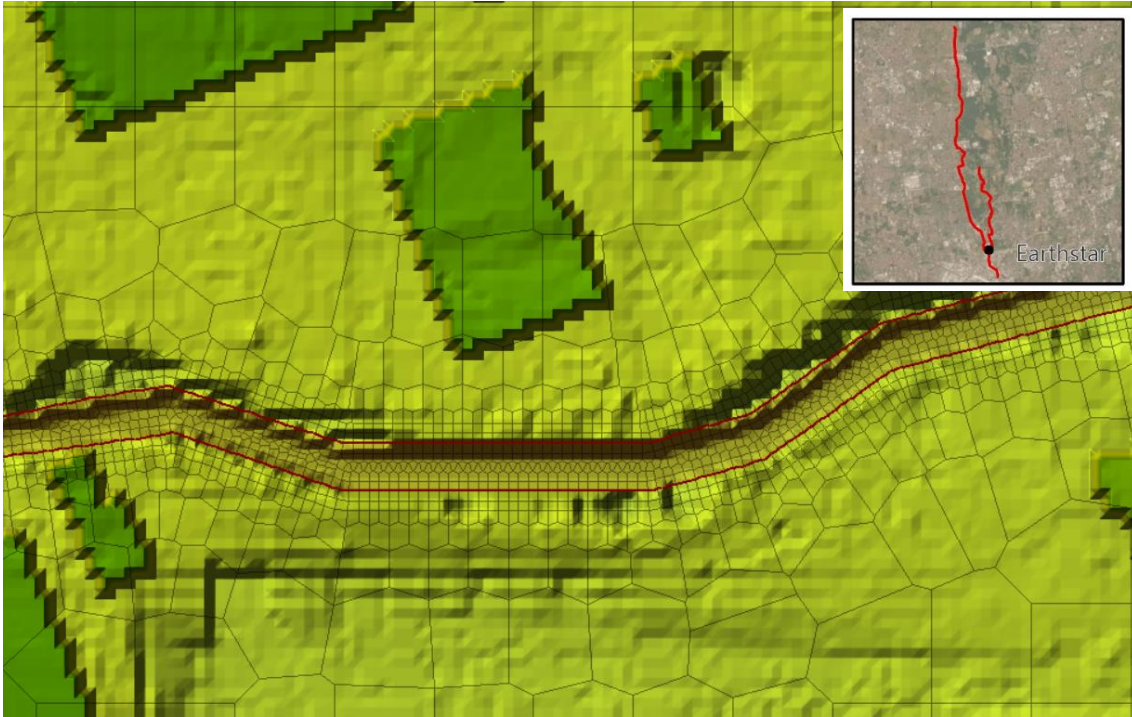
Figure 3.21: Example of refinement region representation (Guisa downstream)

The mesh and the refinement region sizes have not been defined in the same way in the four models. This choice was made based on the length of the different parts and on the quality of the results, which in some cases was still acceptable using coarser cell sizes. Table 3.7 summarizes all the different characteristics defined for the four river reaches.

	Guisa river		Nirone river	
	Upstream	Downstream	Upstream	Downstream
Mesh size [m]	10	10	5	10
Refinement region size [m]	3	1	3	1

Table 3.7: Mesh and refinement region size

A Manning's coefficient value of the entire model (equal to 0.06 s/m$^{1/3}$) was simply input by specifying it in the description of the computational mesh. Then, the roughness of the riverbed was specified by adding a Land Cover layer (Figure 3.22), which in this case was the same close polygon used to define the refinement region, and assigning to it the desired Manning's coefficient value (equal to 0.03 s/m$^{1/3}$).

Figure 3.22: Example of Land Cover layer (Guisa upstream)

The structures (i.e.: bridges and culverts) along the rivers are added like *SA/2D connection* tool. It is important to point out that the structures are always traced (in the RAS Mapper) from the hydrographic left to the hydrographic right. However, sometimes it was not possible to define the structures using the exact data available (see Chapter 3.1.3) since their height and/or width were not compatible with the geometry of the terrain. In these cases, both the width and the height of the structures were slightly changed to make them consistent with the terrain, but always trying to preserve the area of the openings. From Figure 3.23 to Figure 3.28 one can see some examples of the structures defined in HEC-RAS.

Figure 3.23: Bridge 72 - RAS Mapper
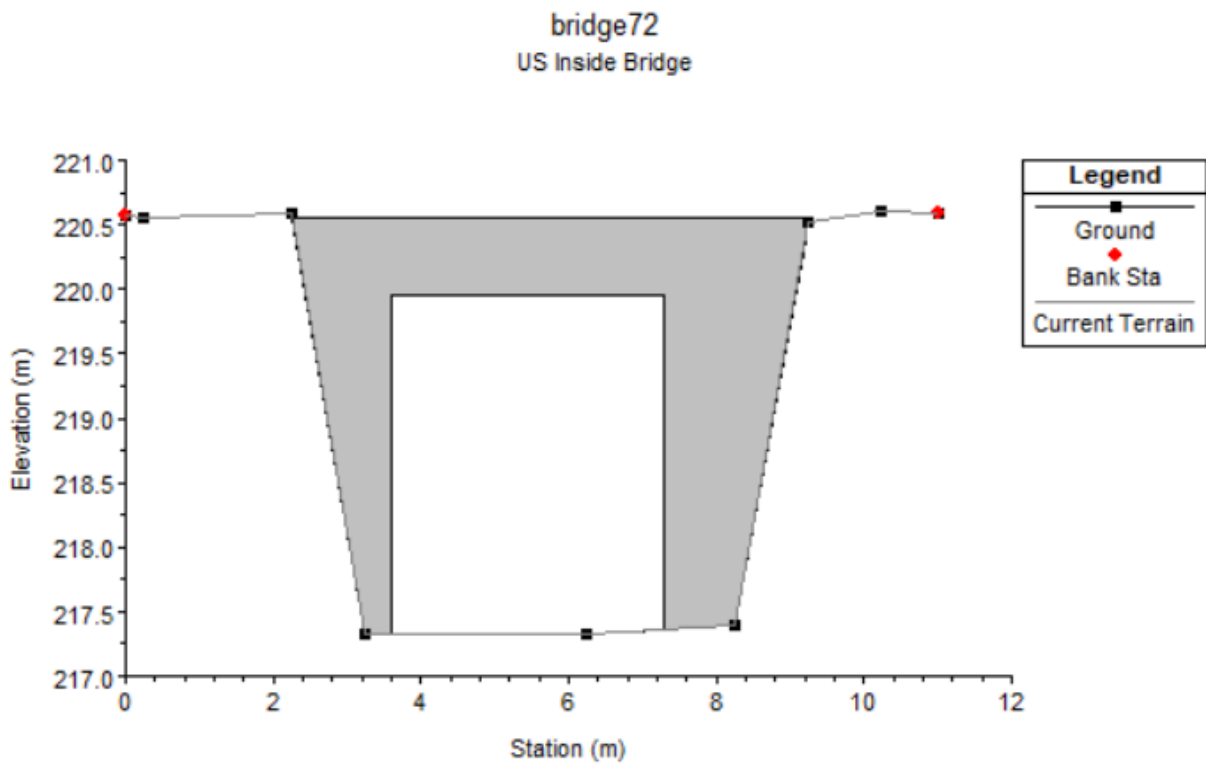
Figure 3.24: Bridge 72 - Geometry

Figure 3.25: Bridge 67 - RAS Mapper
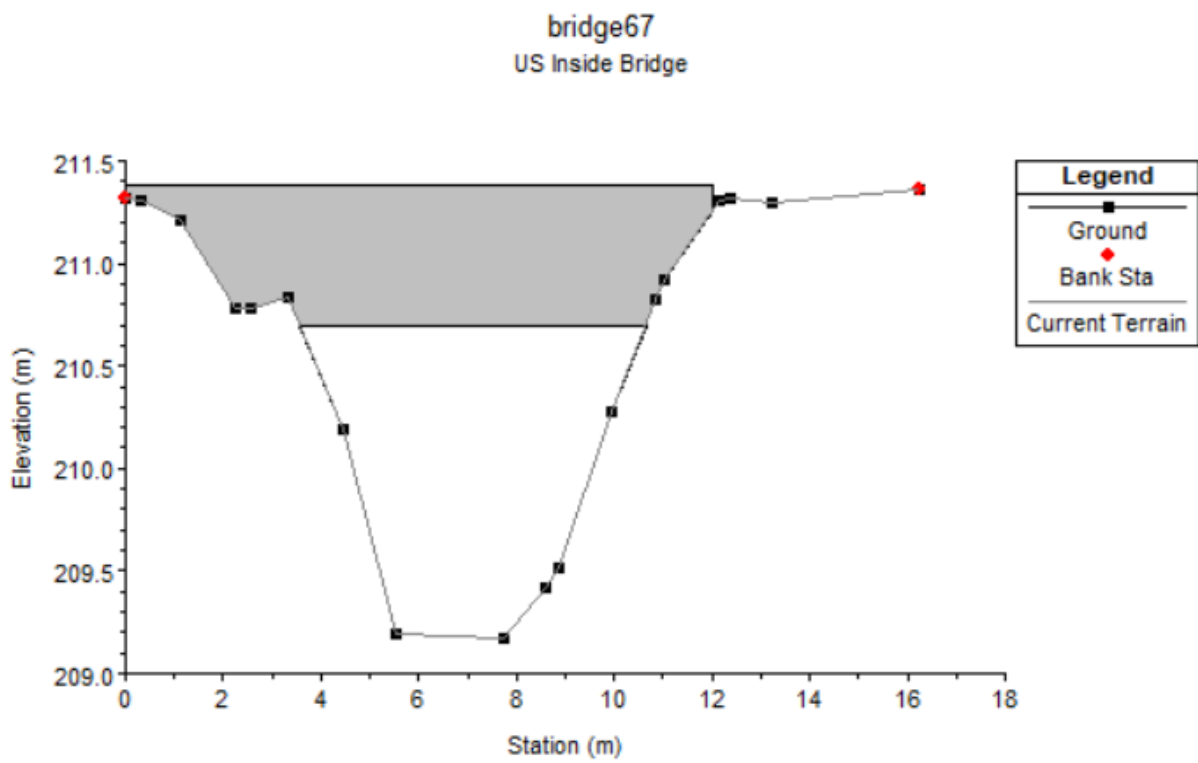
Figure 3.26: Bridge 67 - Geometry

Figure 3.27: Culvert 4 - RAS Mapper

culv4
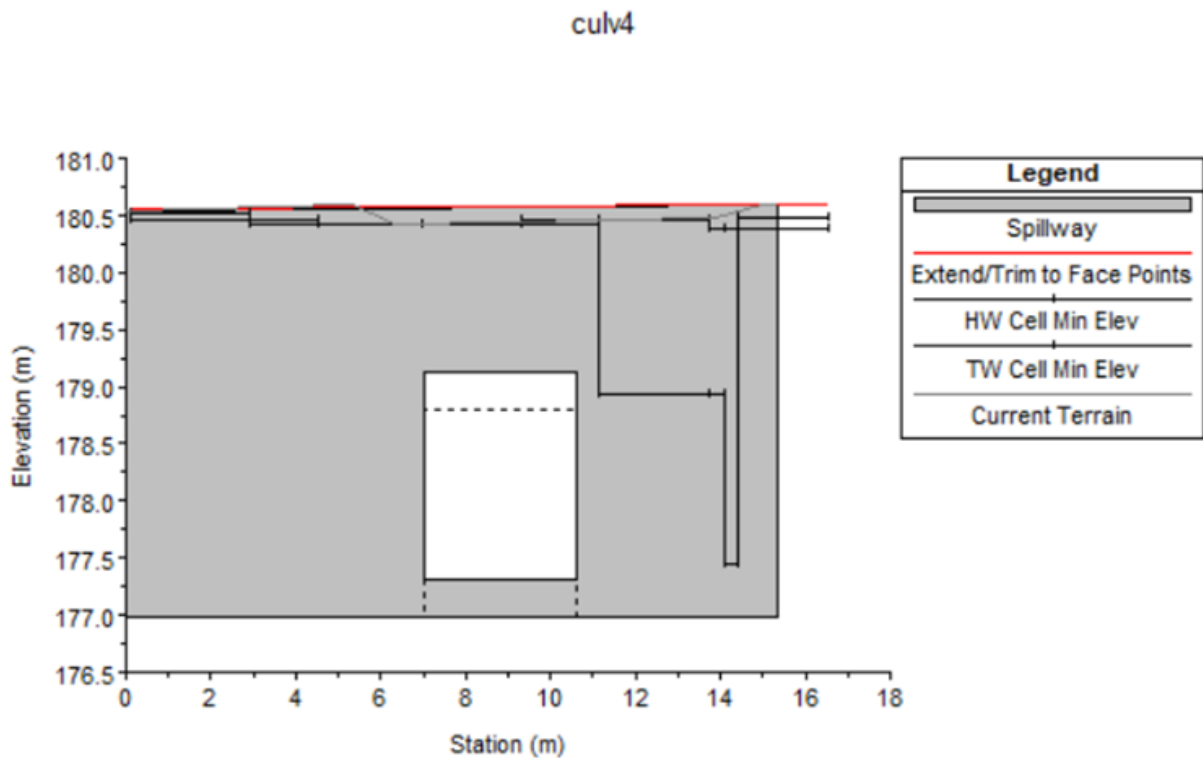
Figure 3.28: Culvert 4 - Geometry

In addition, there were added also culverts to connect the first two detention ponds to the Guisa river (Figure 3.29 and Figure 3.30), as well as one culvert to have the possibility to empty both the third detention pond and the secondary pond of the last basin within the mainstream (Figure 3.31 and Figure 3.32).
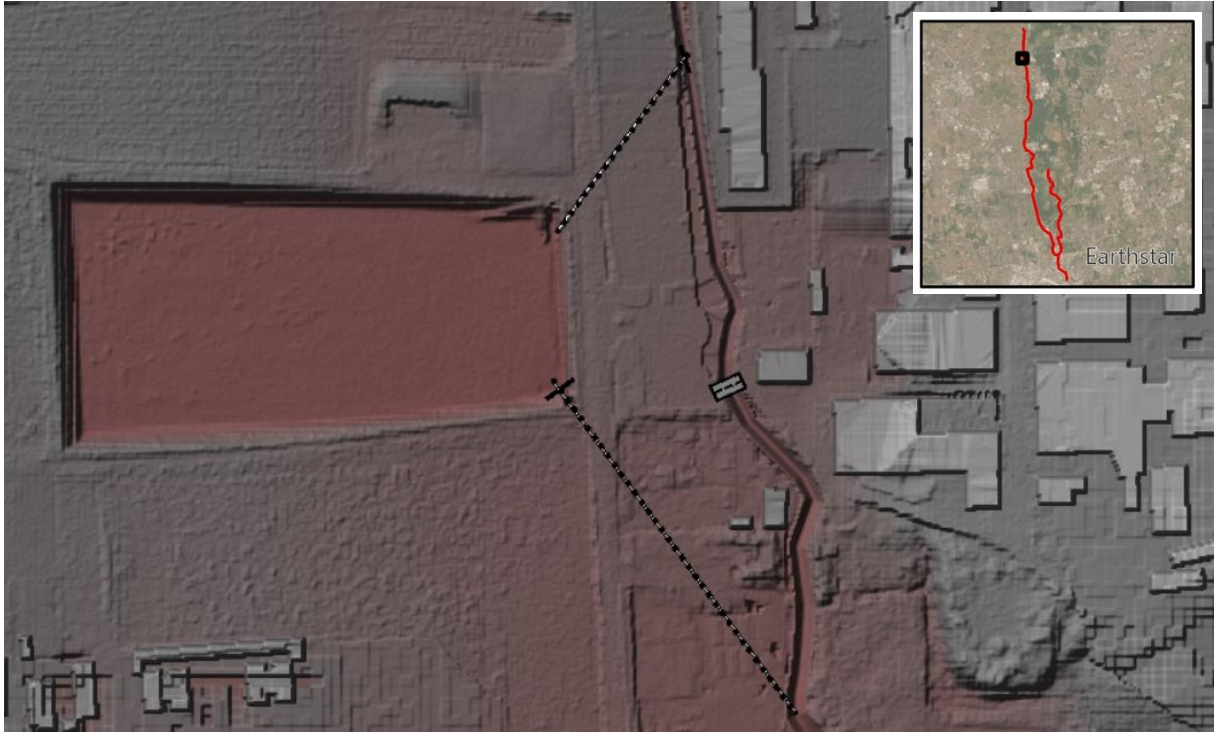
Figure 3.29: First detention pond in the RAS Mapper
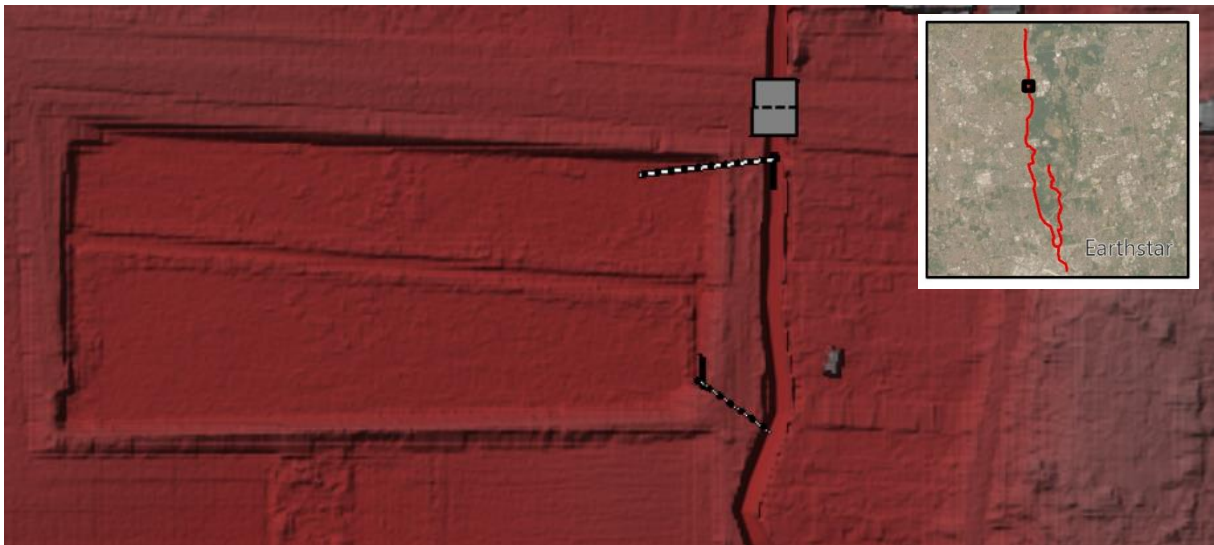
Figure 3.30: Second detention pond in the RAS Mapper
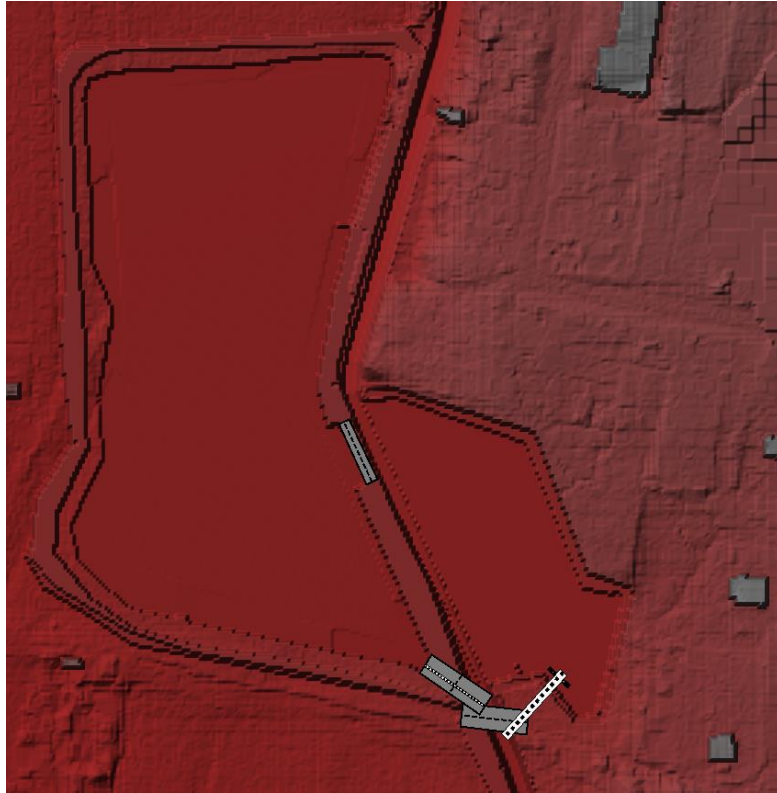
Figure 3.31: Third detention pond in the RAS Mapper

Figure 3.32: Fourth detention pond in the RAS Mapper

Table 3.8 summarizes all the structures which are present in the different river reaches.

	Guisa river		Nirone river	
	Upstream	Downstream	Upstream	Downstream
N° culverts	8	3	0	3
N° bridges	20	10	6	1
N° detention ponds	4	0	0	0

Table 3.8: Information about the number of structures

Concerning the boundary conditions, Figure 3.34 to Figure 3.41 report the BCs that have been obtained from the data available (see also Chapter 3.1.4), considering that some of them have also been digitalized and interpolated. For the Guisa upstream model, the hydrographs of the four lateral inlets are also reported (Figure 3.33); these are independent on the return period following Table 3.2.
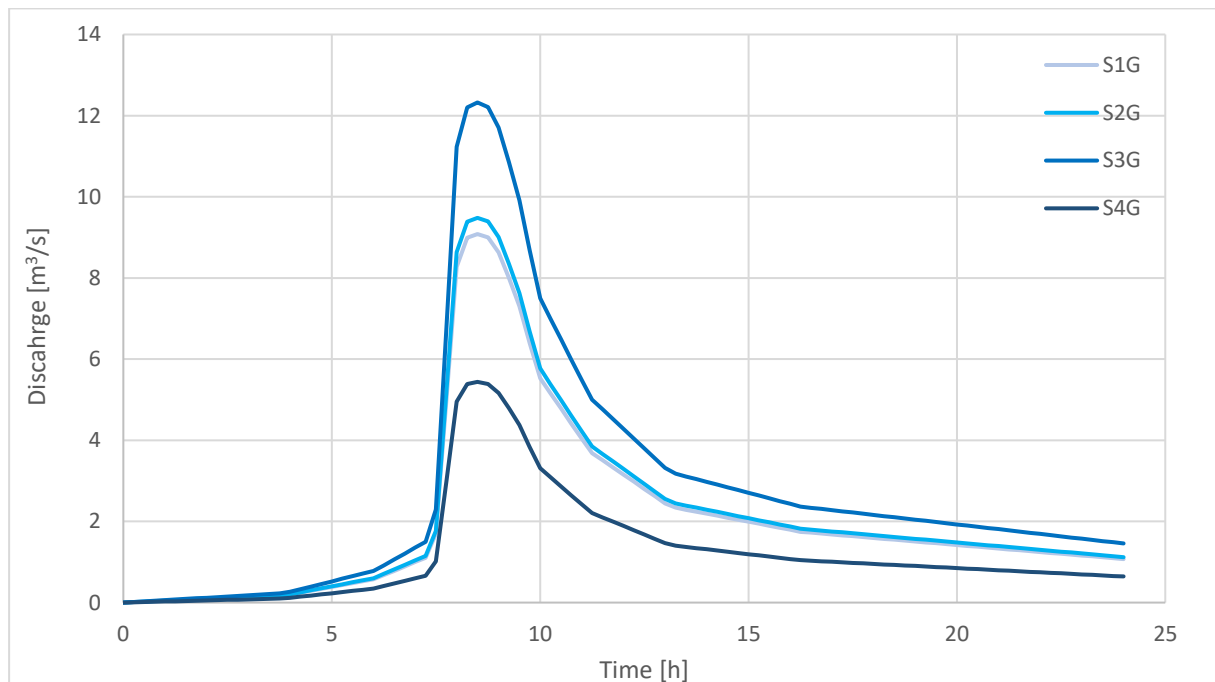
Figure 3.33: Guisa upstream - Lateral inlets
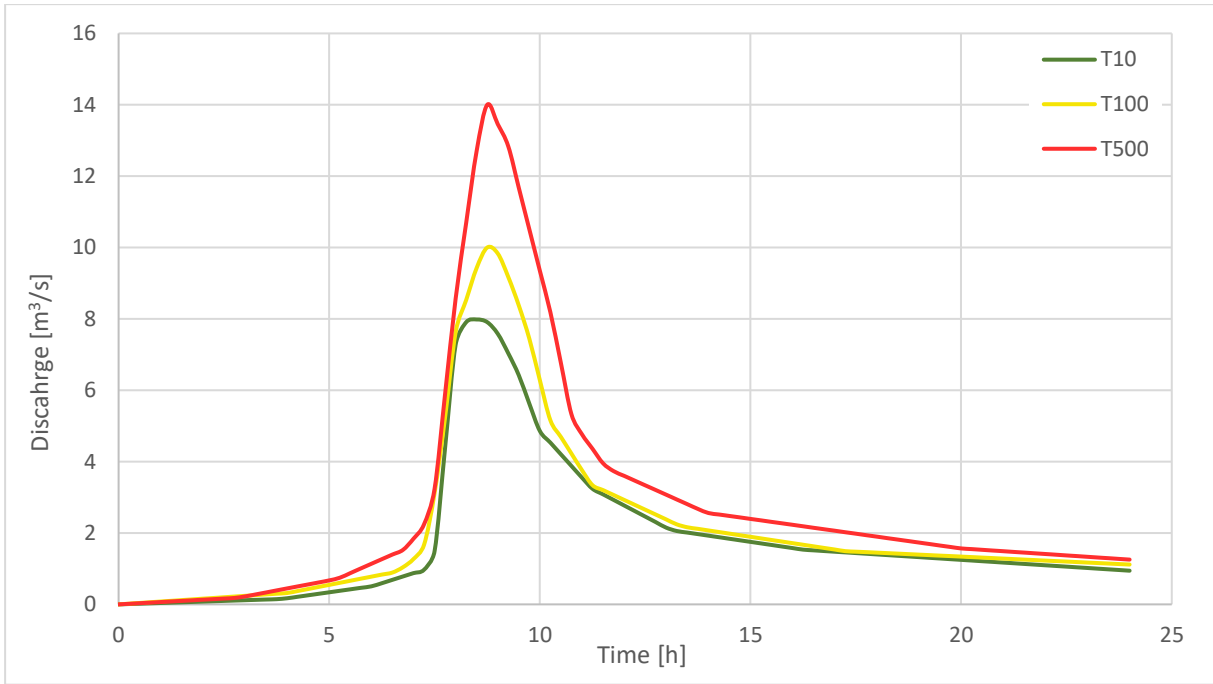
Figure 3.34: Guisa upstream - Upstream BCs
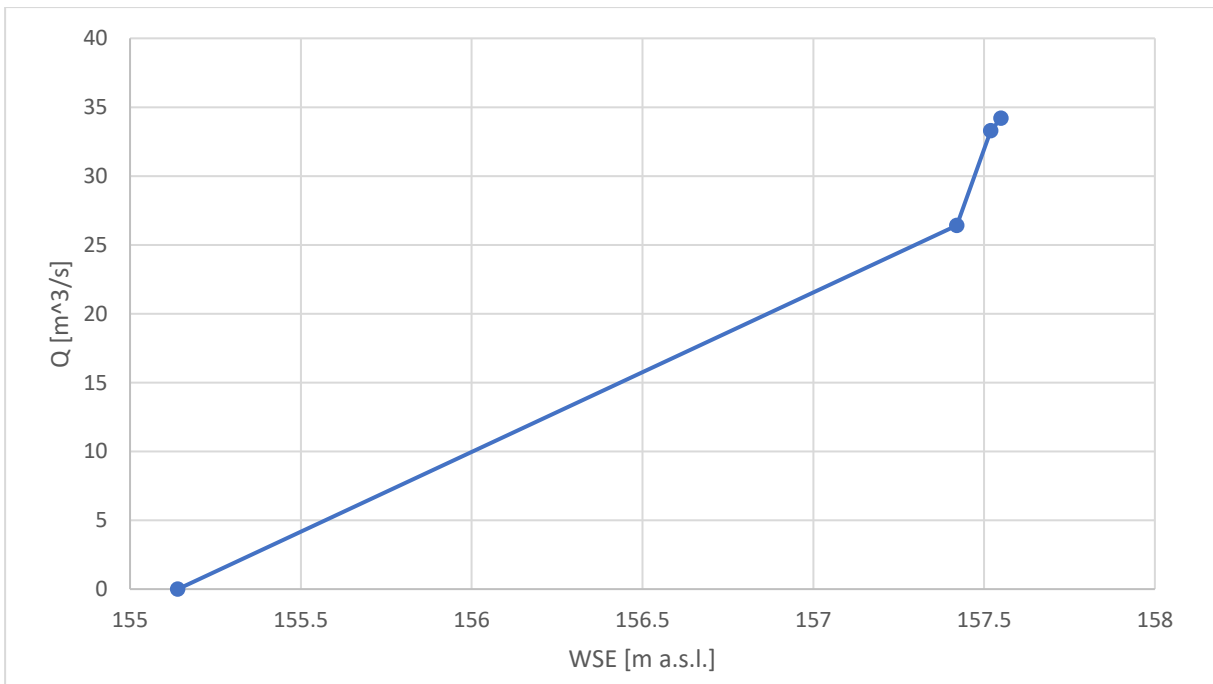
Figure 3.35: Guisa upstream - Downstream BC
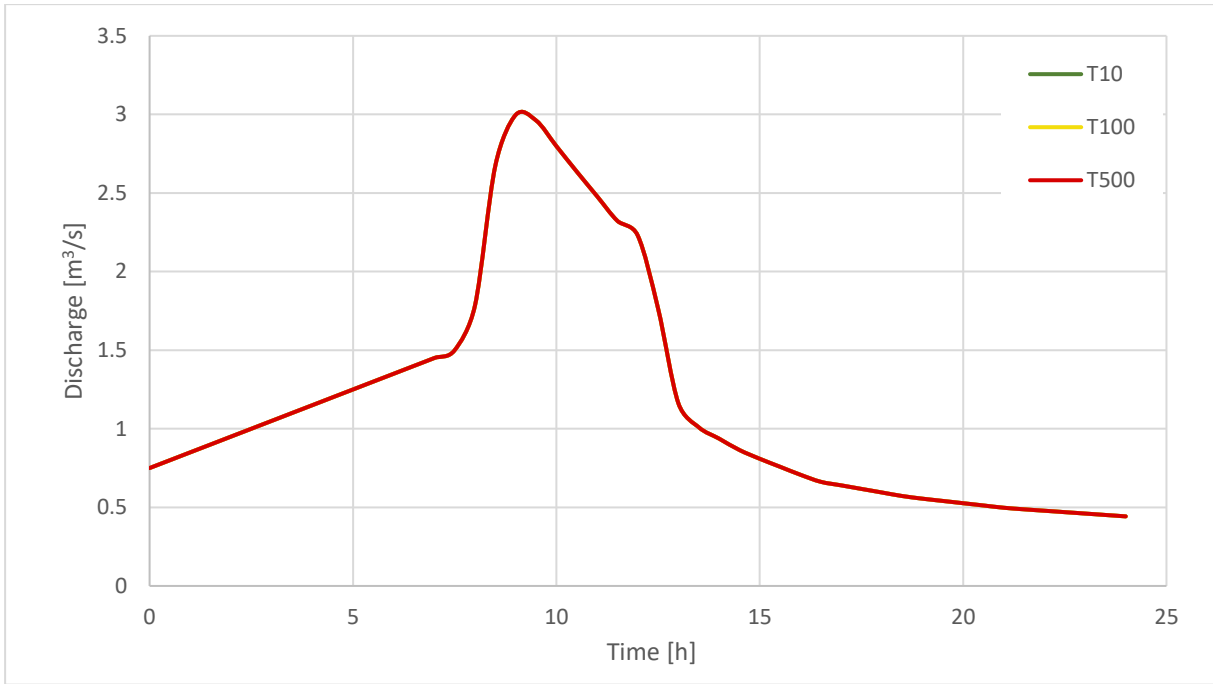
Figure 3.36: Guisa downstream - Upstream BCs
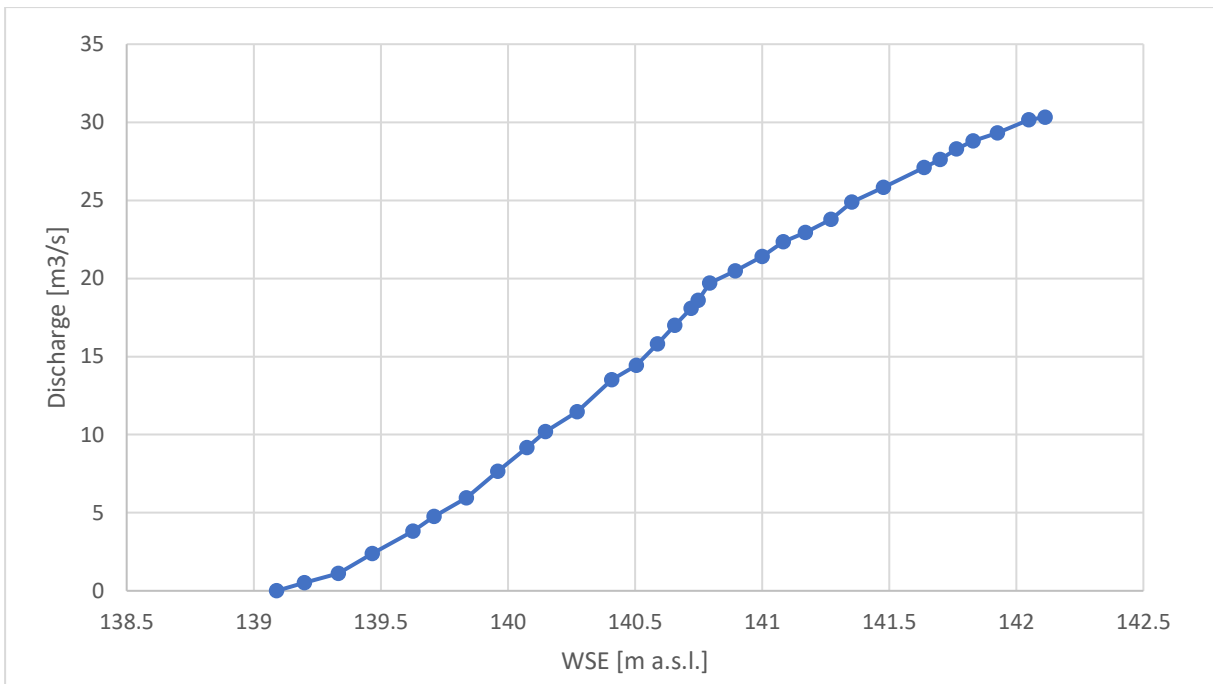
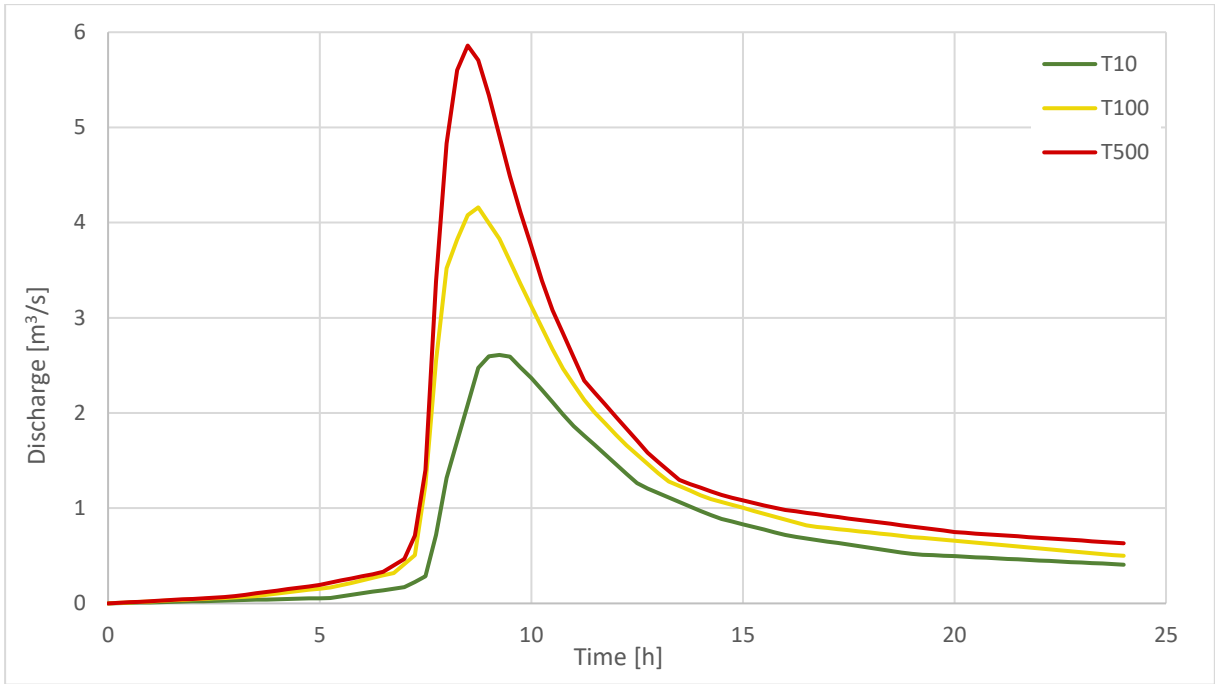*Figure 3.37: Guisa downstream - Downstream BC*

Figure 3.38: Nirone upstream - Upstream BCs
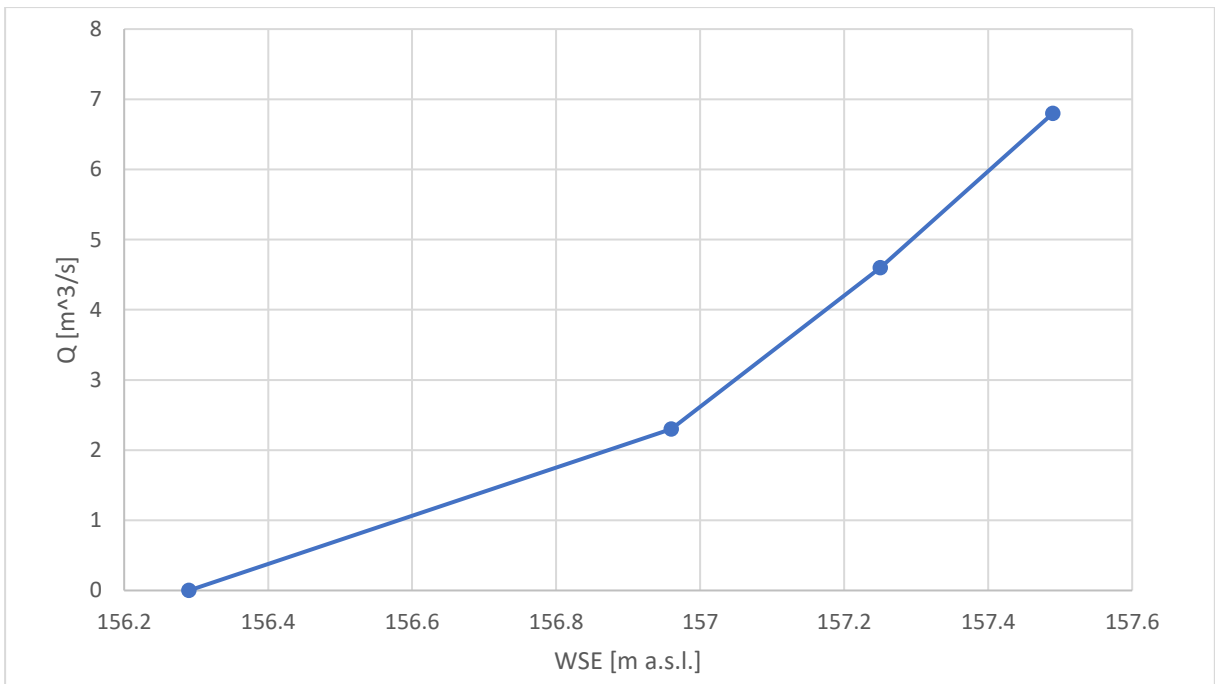

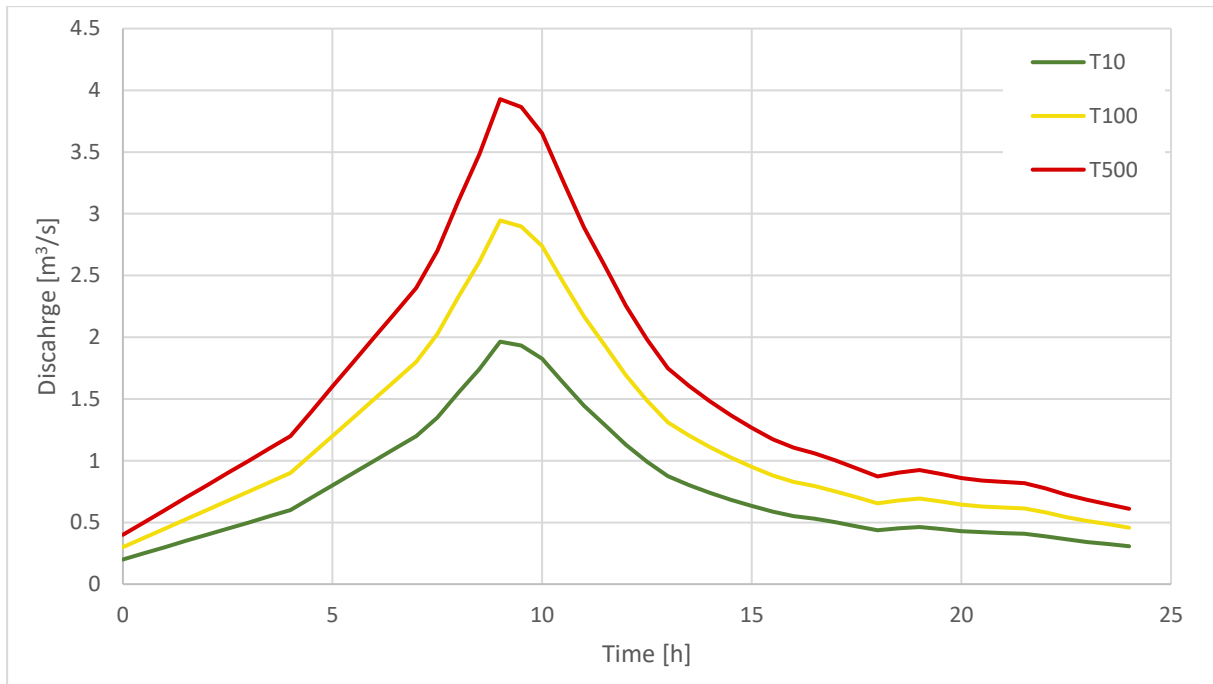*Figure 3.39: Nirone upstream - Downstream BC*
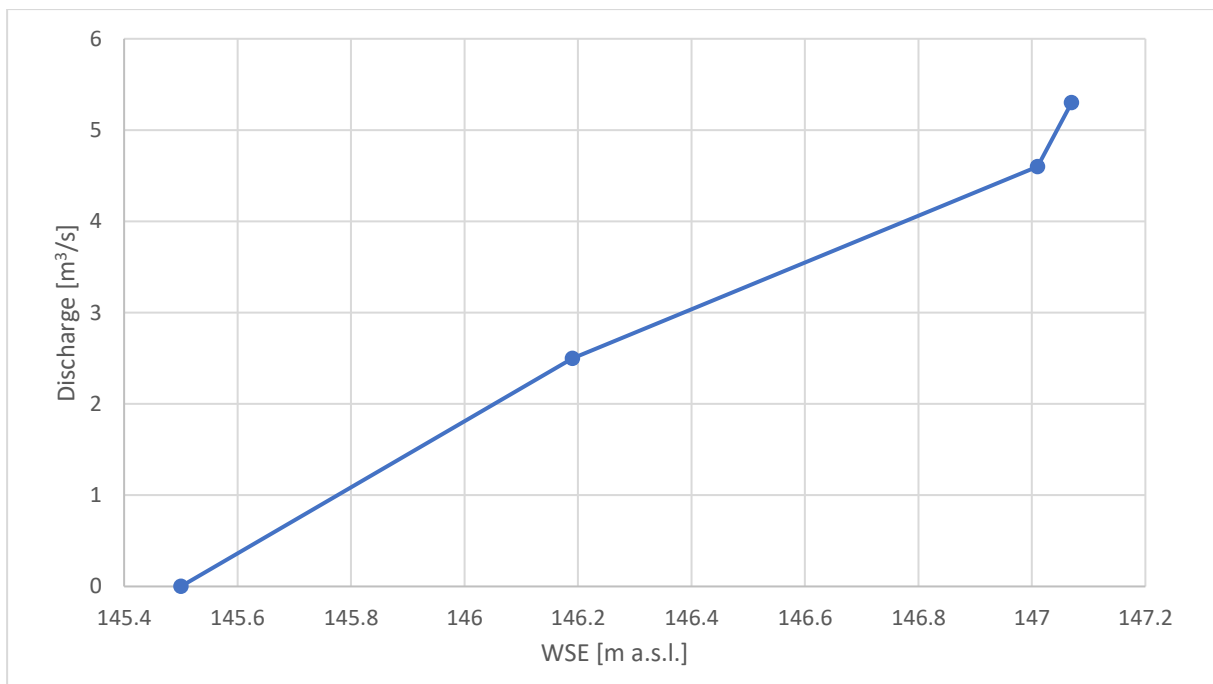
Figure 3.40: Nirone downstream - Upstream BCs

Figure 3.41: Nirone downstream - Downstream BC

Some important aspects characterizing the BCs are:

- In the Guisa downstream model, the three return periods have the same discharge due to the presence of the CSNO.
- In the Guisa downstream model, the rating curve has more points with respect to the others downstream BCs because it comes directly from a digitalization of the rating curve included in the SdF document [12]. Instead, the other rating curves have been obtained by interpolating the data about the discharge and the WSE (Table 3.3).

- The hydrographs of the Guisa downstream and Nirone downstream models have a flow rate that does not start from zero because, otherwise, the simulations were becoming unstable.
- In the Guisa downstream model, no hydrographs are available for the inflow of the Nirone. The inlet of the Nirone was modelled using the same hydrographs of the upstream BCs of the Nirone downstream model. This choice was considered reasonable since the latter model is quite short and, therefore, the hydrographs at the starting and ending point are similar (as was also checked after running the models).

Figure 3.42, Figure 3.43 and Figure 3.44 show some examples of how the BCs and the lateral inlets are inserted within the RAS Mapper. The inflow and outflow regions, just like the structures, must always be traced from the hydrographic left to the hydrographic right in the RAS Mapper.

Figure 3.42: Upstream BC - RAS Mapper (Guisa downstream)

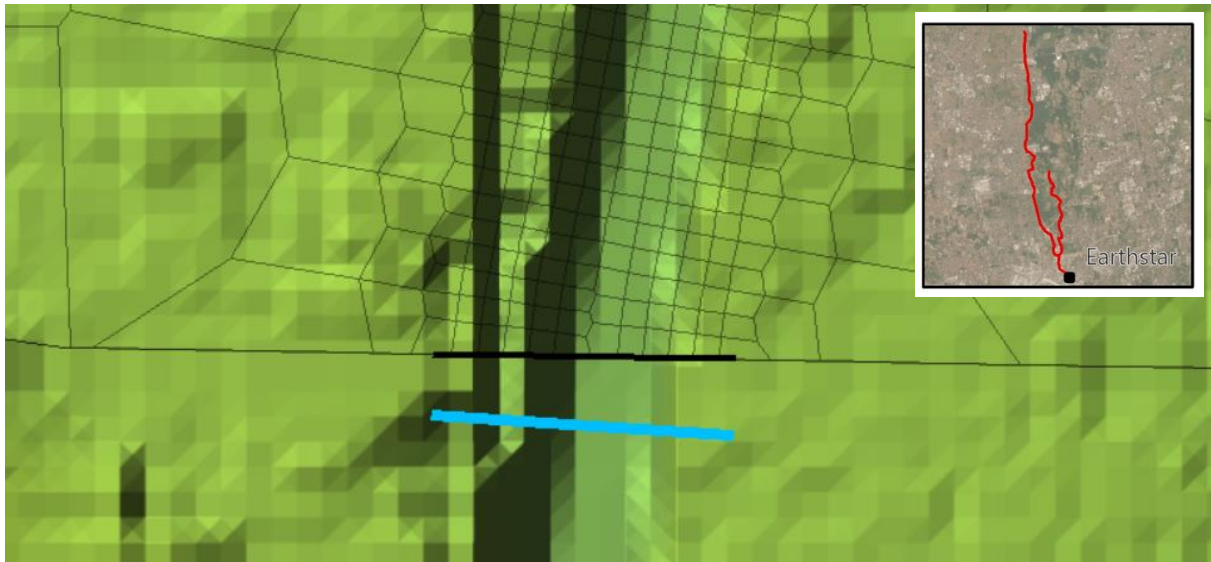*Figure 3.43: Lateral inlet - RAS Mapper (Guisa downstream)*

Figure 3.44: Downstream BC - RAS Mapper (Guisa downstream)

The last step to be done before running a simulation is to define the computational time step. With respect to this, a trial-and-error approach has been adopted, using more computational time steps for all the models and selecting the one which yielded the best trade-off between a satisfactorily small error and a reasonable running time. Table 3.9 shows the selected time steps for obtaining the final results of each model, with their corresponding running times and error percentages, which is an output value provided by HEC-RAS and gives a synthetic estimation of the error based on the mass conservation principle.

	Guisa river		Nirone river	
	Upstream	Downstream	Upstream	Downstream
Computational time step T10 [sec]	1	1	5	3
Running time T10 [hour:min:sec]	9:48:59	3:34:43	44:26	1:05:13
Error T10 [%]	6.91	0.327	0.06	7.074
Computational time step T100 [sec]	2	1	5	2
Running time T100 [hour:min:sec]	5:40:13	3:09:40	1:10:23	1:40:58
Error T100 [%]	6.51	1.103	0.06	6.728
Computational time step T500 [sec]	2	1	4	1
Running time T500 [hour:min:sec]	6:26:36	2:41:34	1:03:10	2:35:33
Error T500 [%]	5.426	0.226	0.04	2.338

Table 3.9: Computational time interval and error

For running the simulations, the Diffusion Wave Equations (DWE) have been used (which are also those set by default from HEC-RAS).

3.3. Results

In the following pages, the results obtained from the numerical simulations are reported, in terms of spatial distributions of both water depth and velocity (from Figure 3.45 to Figure 3.68), as listed in Table 3.10. In addition, also the perimeter of the flooded areas reported in the previous edition of the FRMP is visible on all of these maps.

		T10	T100	T500
Guisa upstream	Depth	Page 58	Page 59	Page 60
	Velocity	Page 61	Page 62	Page 63
Guisa downstream	Depth	Page 64	Page 65	Page 66
	Velocity	Page 67	Page 68	Page 69
Nirone upstream	Depth	Page 70	Page 71	Page 72
	Velocity	Page 73	Page 74	Page 75
Nirone downstream	Depth	Page 76	Page 77	Page 78
	Velocity	Page 79	Page 80	Page 81

Table 3.10: Organization of the representation of the results

At the end a map is presented showing a comparison between the three flooded areas (considering all the river reaches at the same time) obtained for the three different return periods (Figure 3.69).
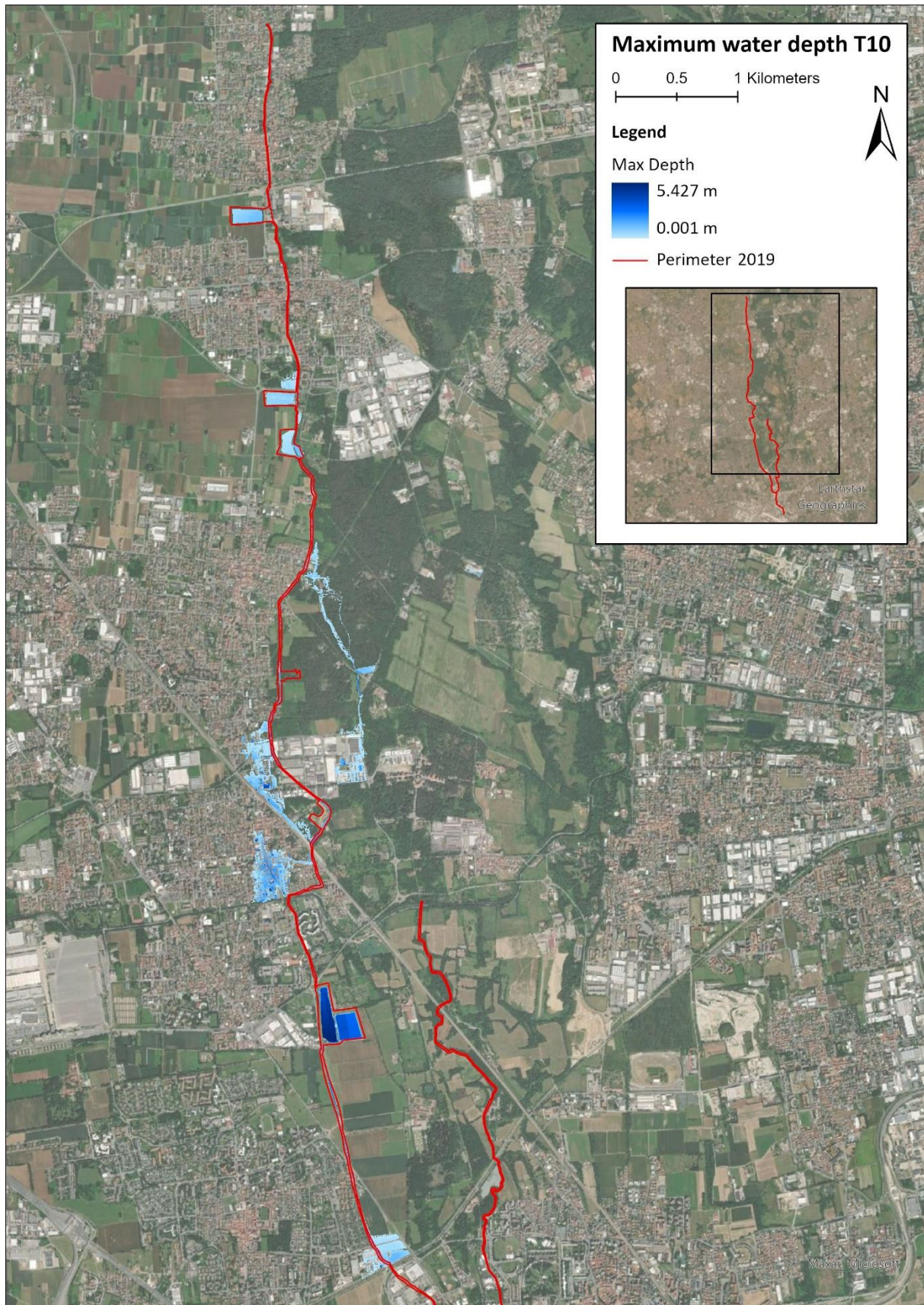
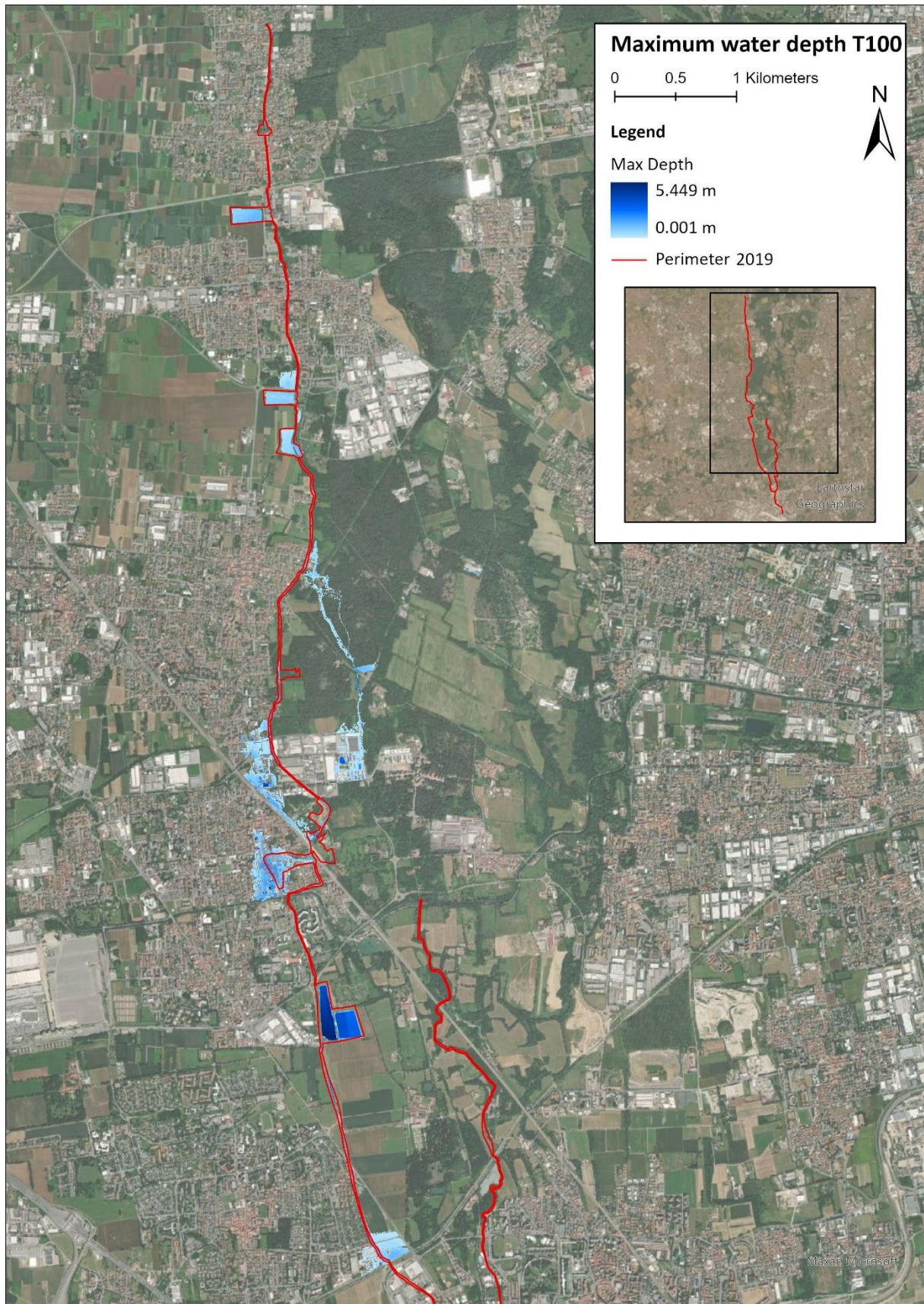*Figure 3.45: Guisa upstream - T10 - Depth*
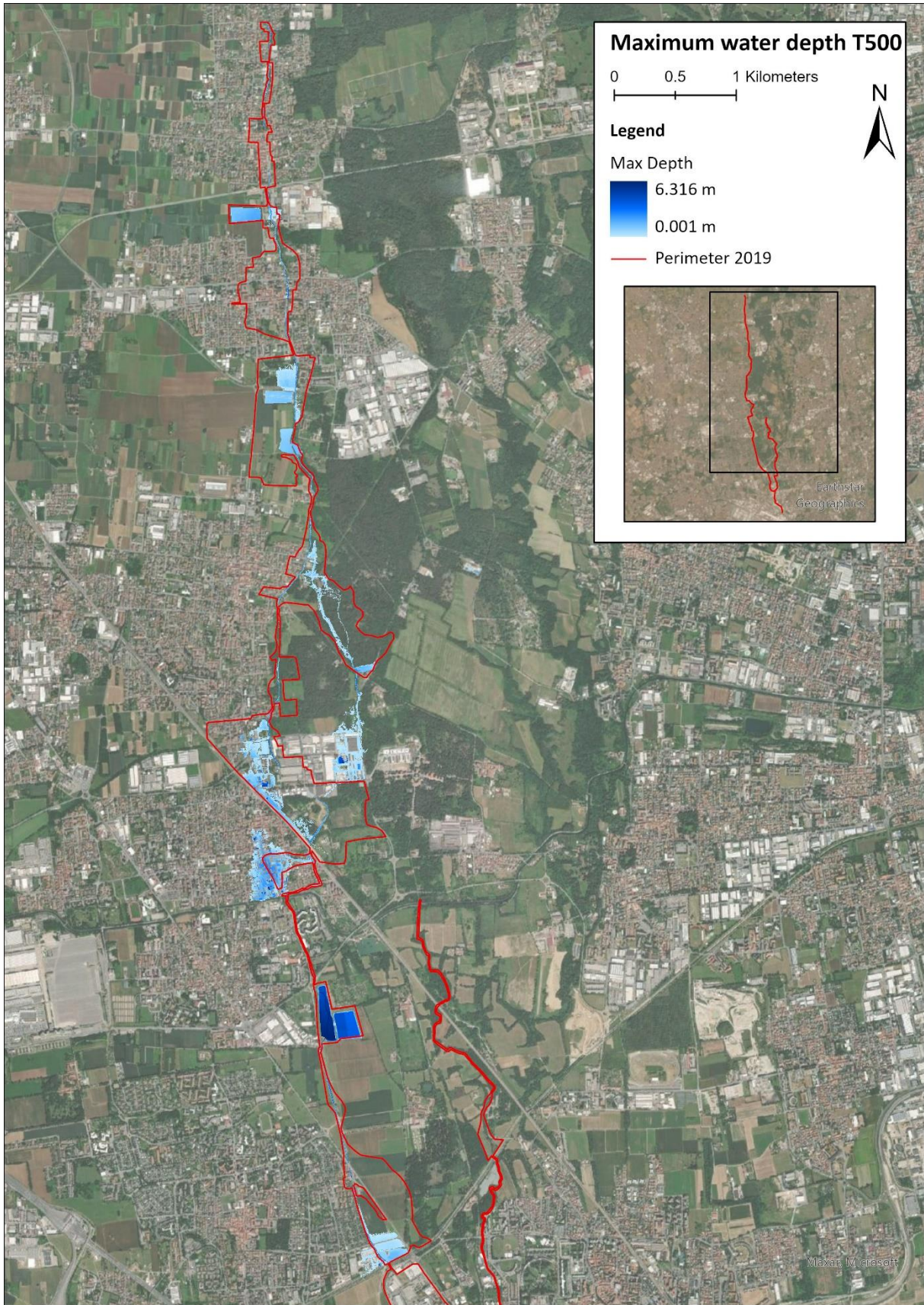
Figure 3.46: Guisa upstream - T100 - Depth

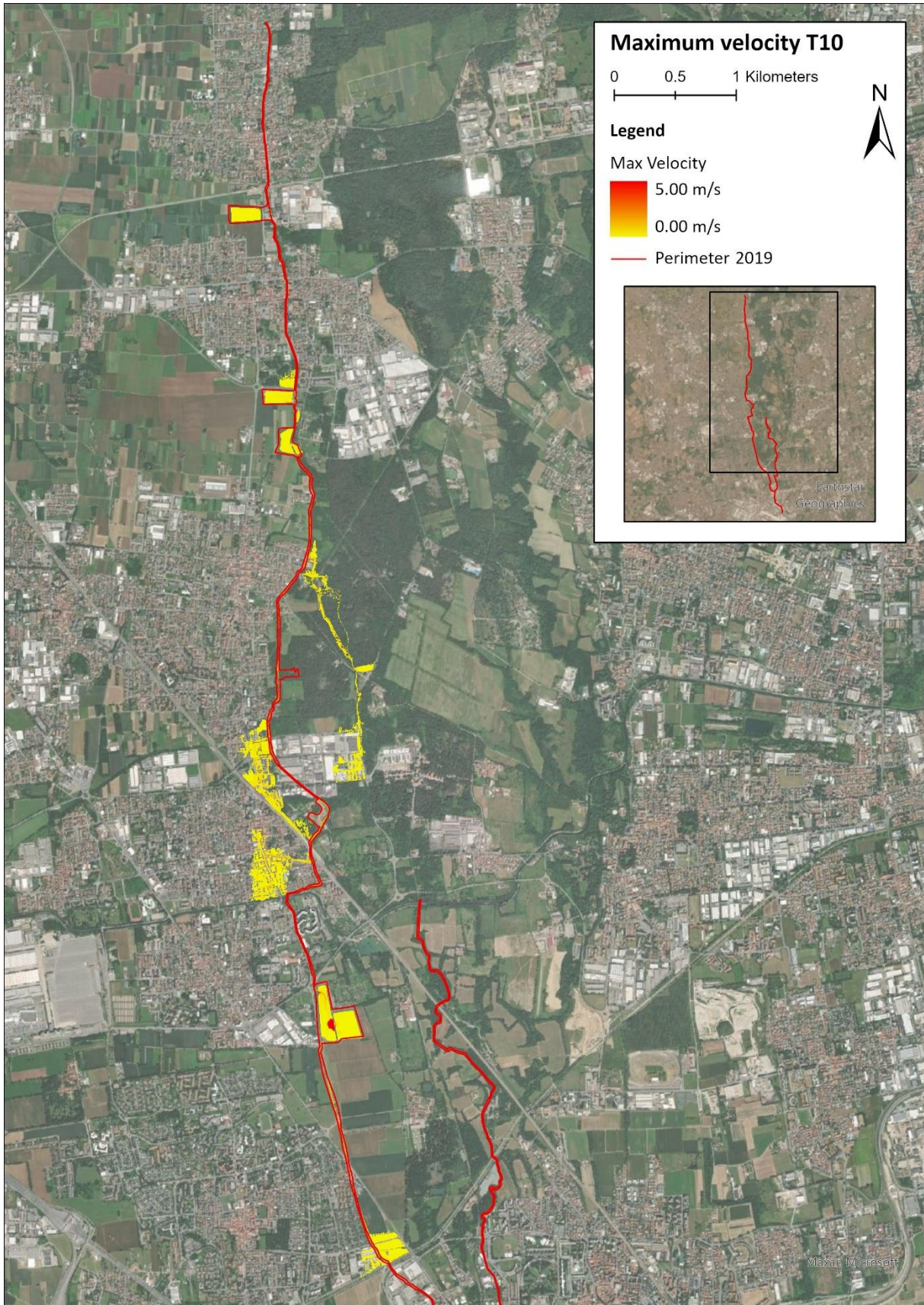*Figure 3.47: Guisa upstream - T500 - Depth*

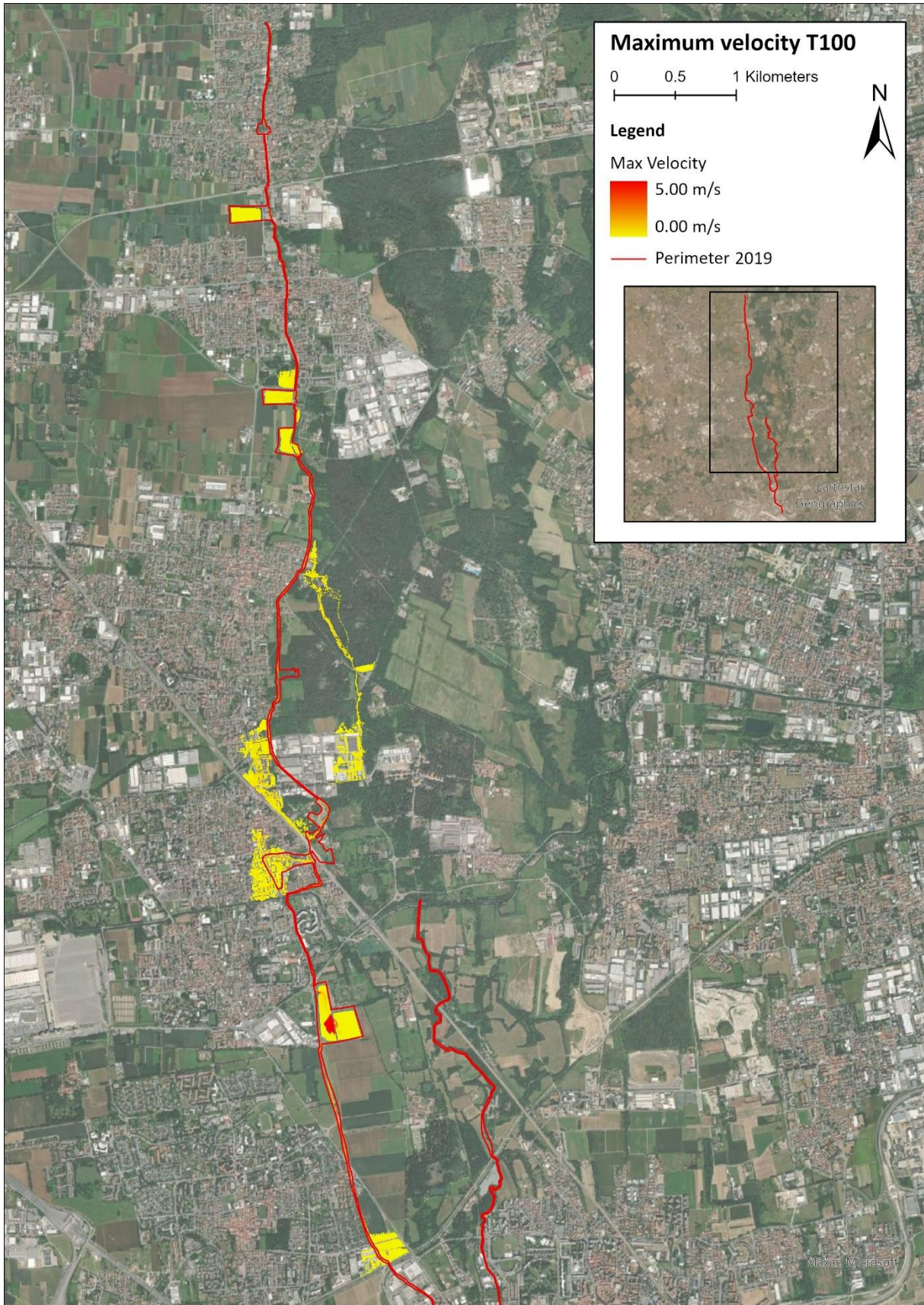*Figure 3.48: Guisa upstream - T10 - Velocity*

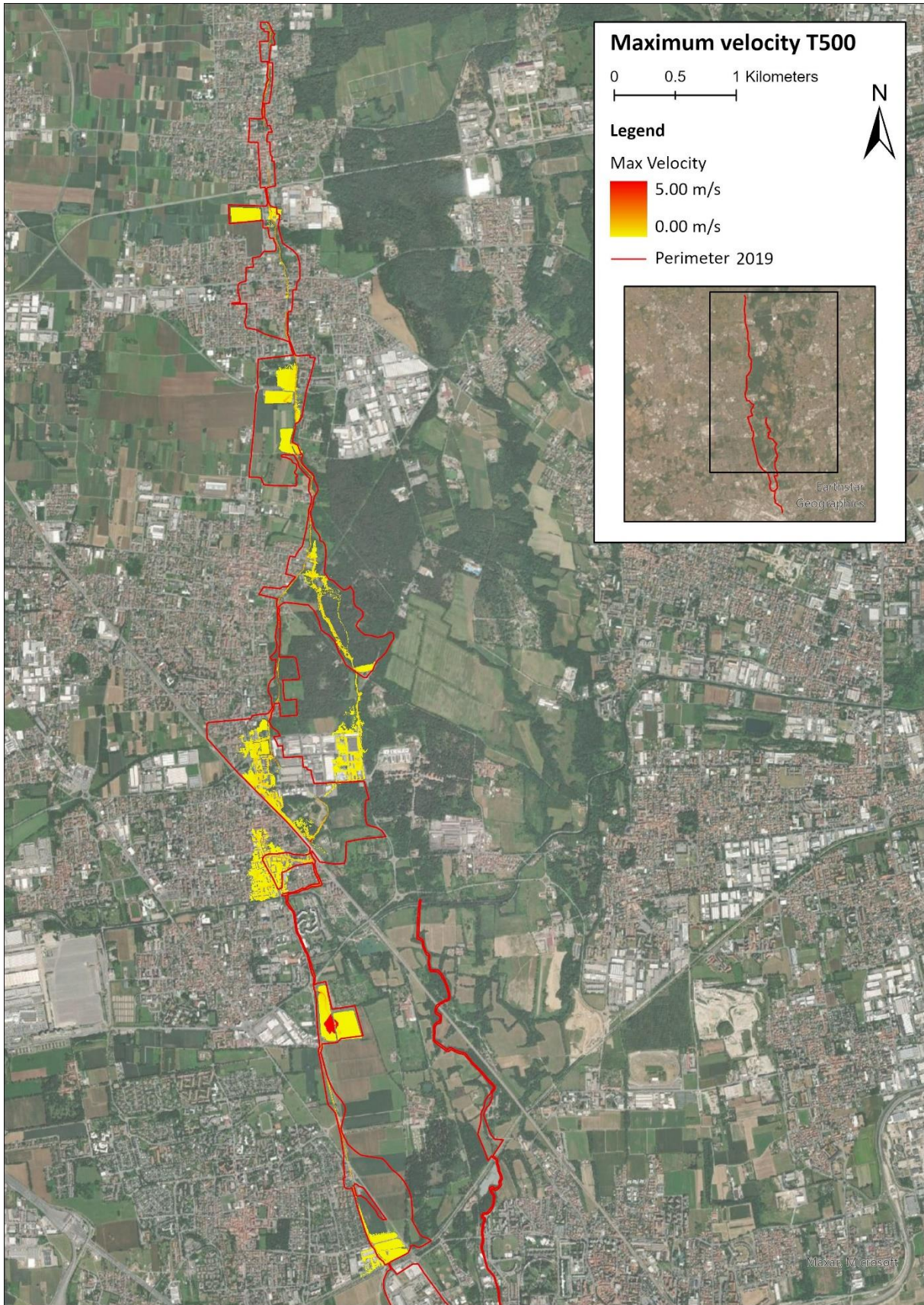*Figure 3.49: Guisa upstream - T100 - Velocity*
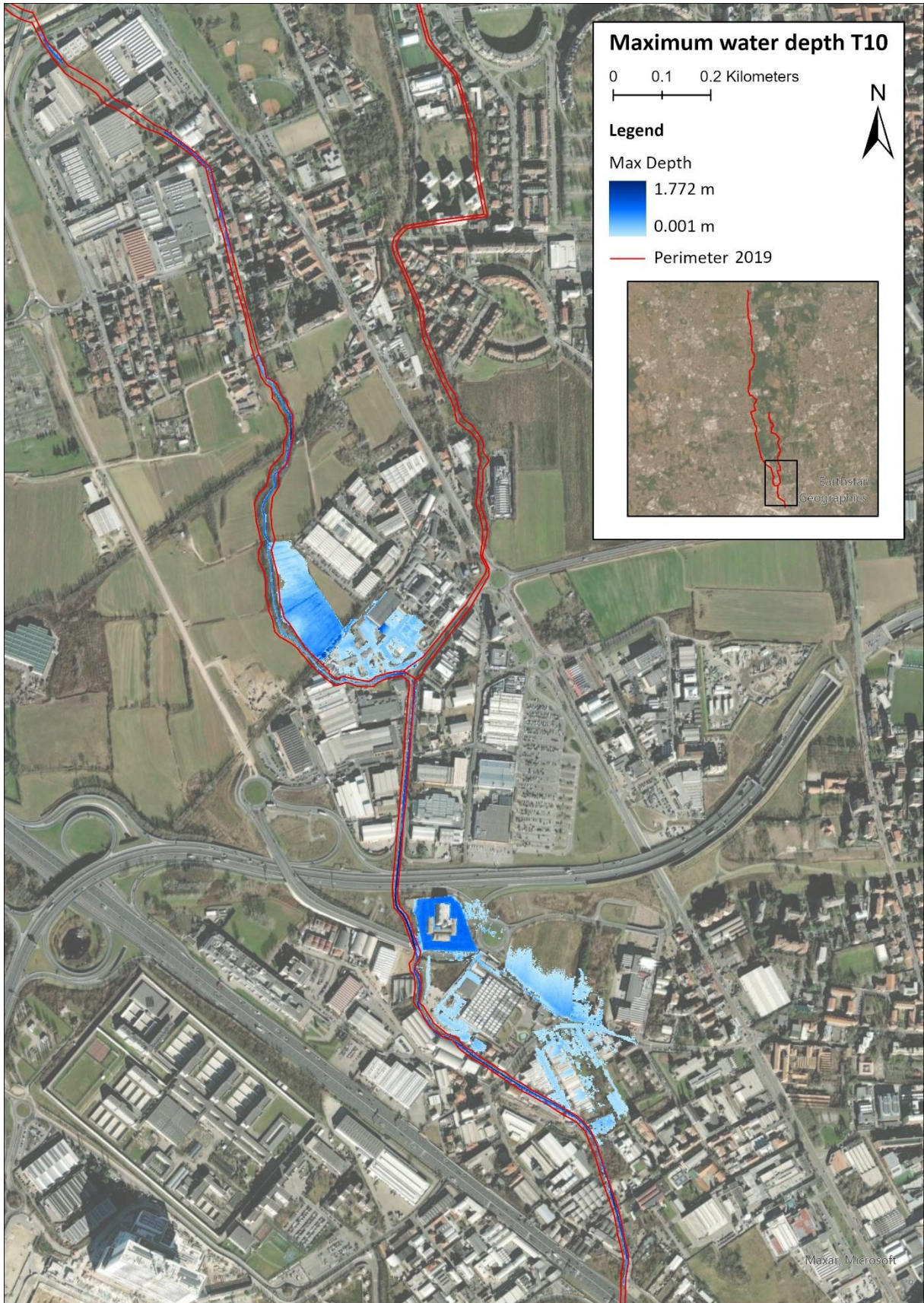
Figure 3.50: Guisa upstream - T500 - Velocity
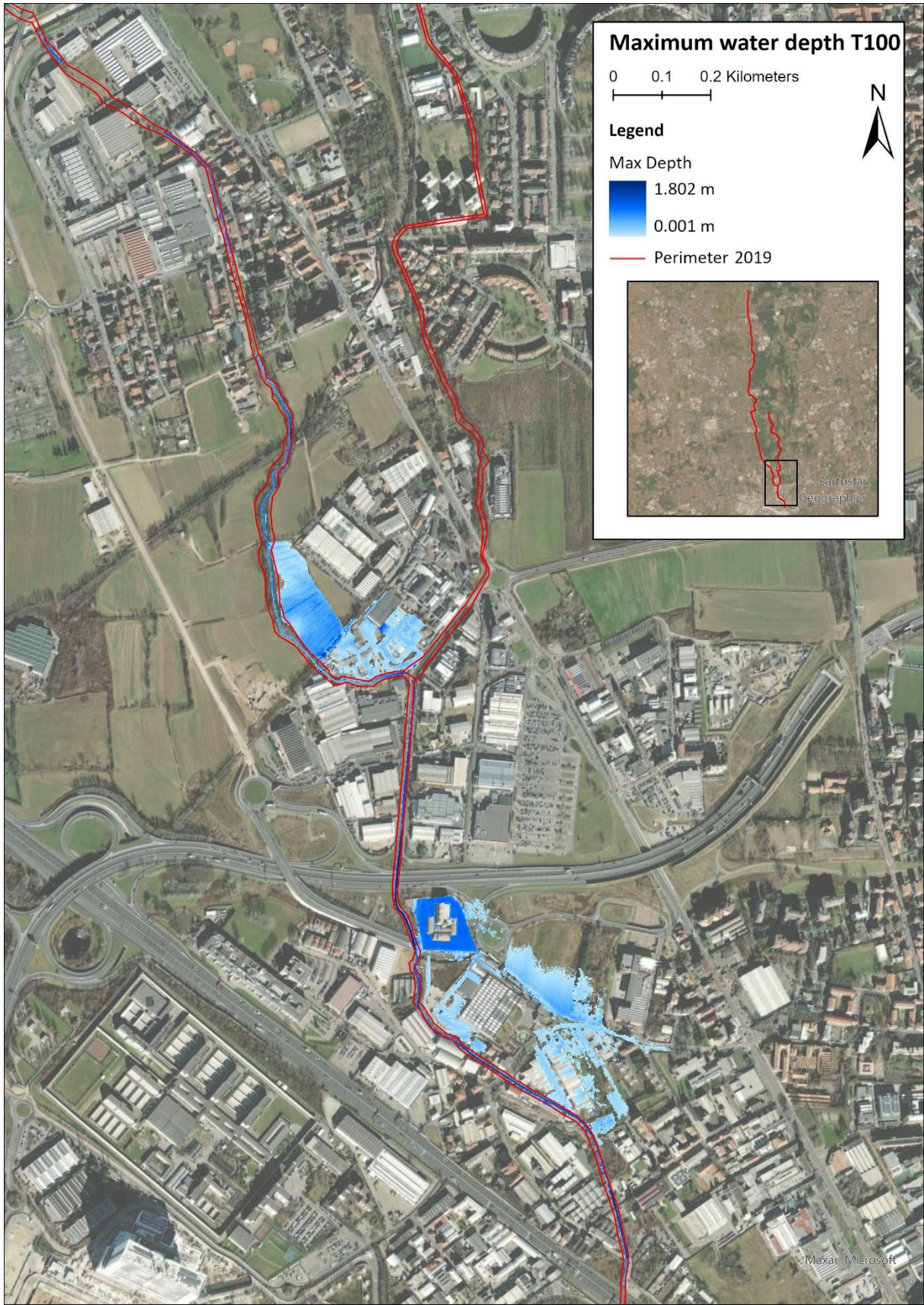
Figure 3.51: Guisa downstream - T10 - Depth

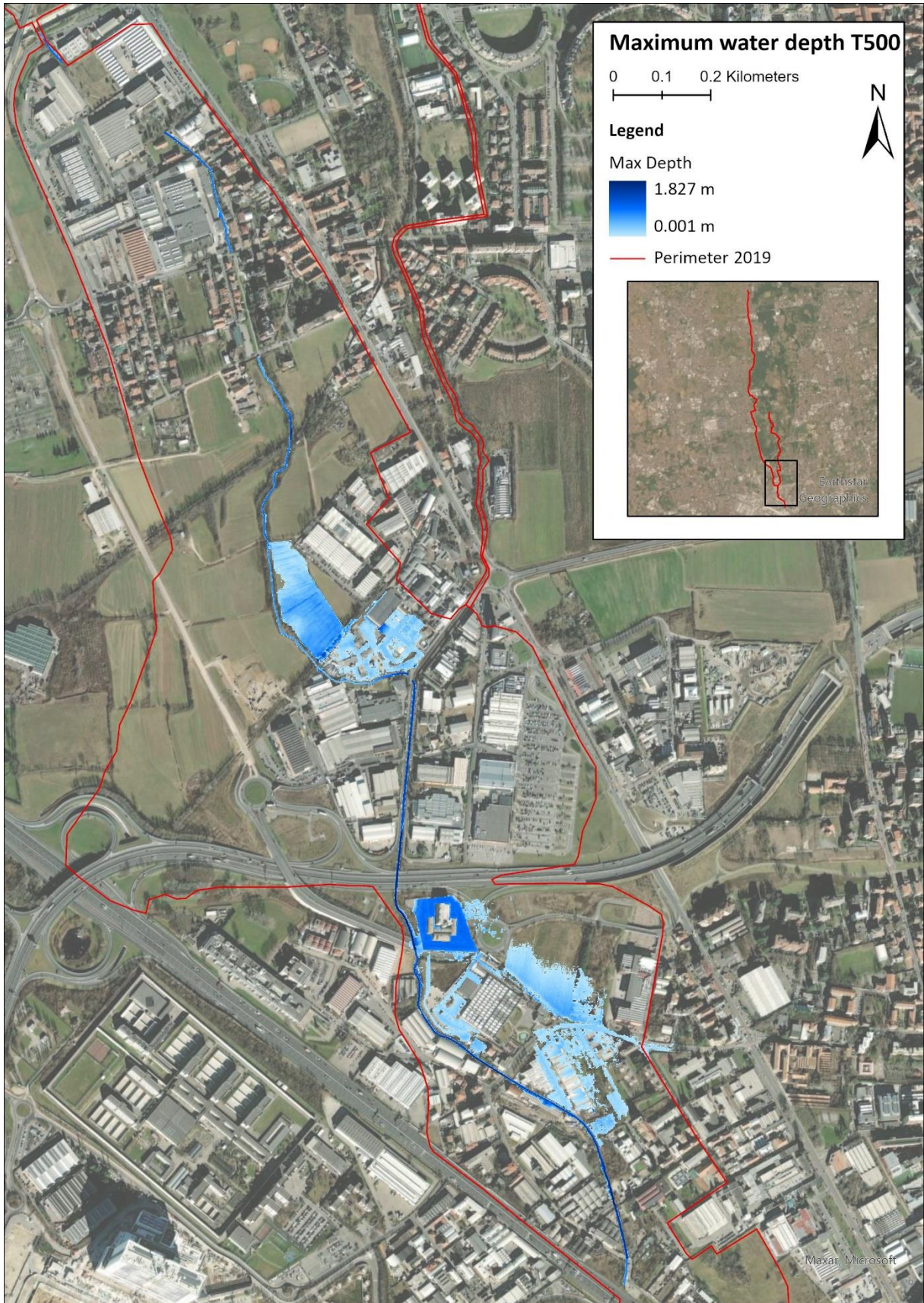*Figure 3.52: Guisa downstream - T100 - Depth*

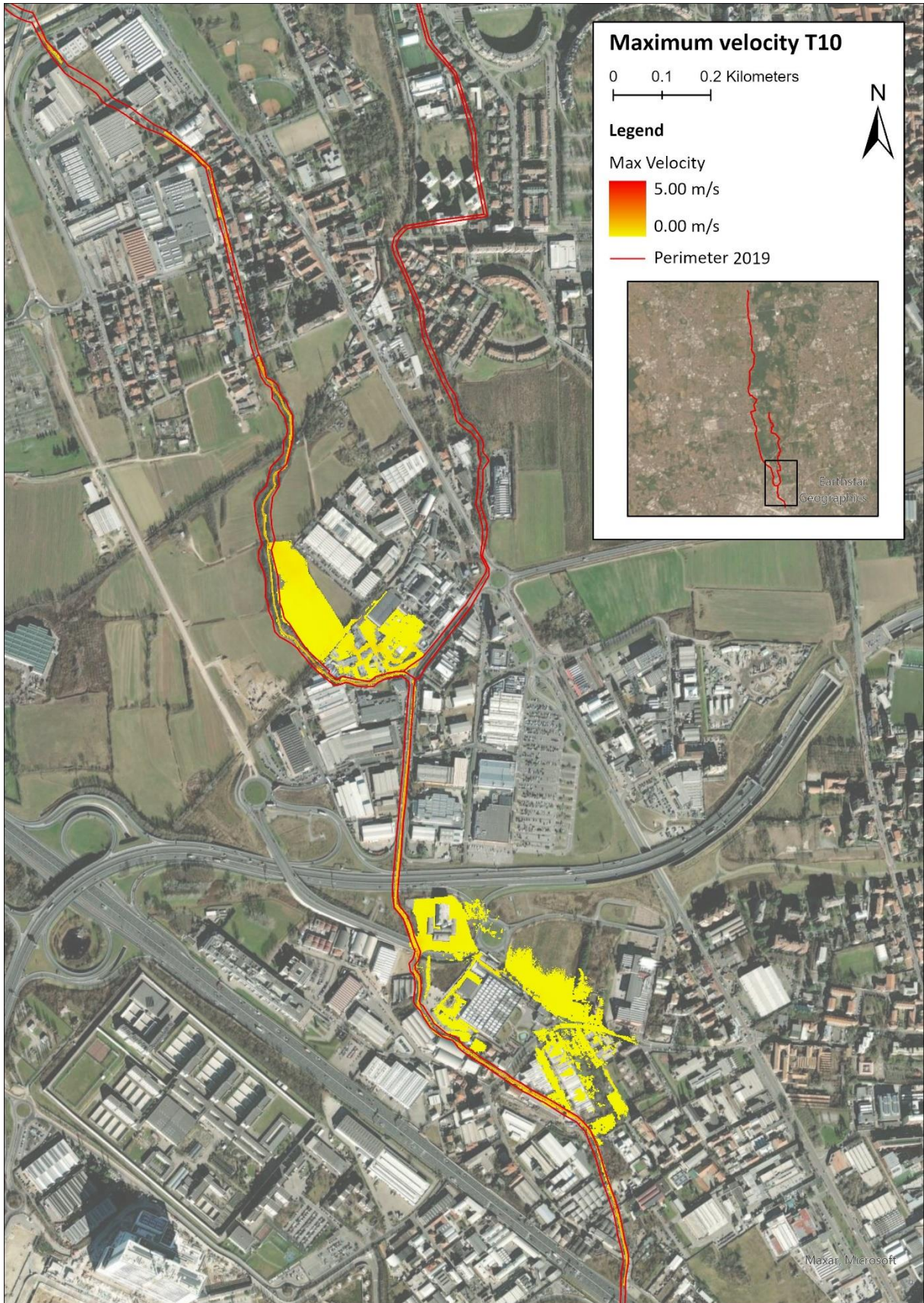*Figure 3.53: Guisa downstream - T500 - Depth*

Figure 3.54: Guisa downstream - T10 - Velocity
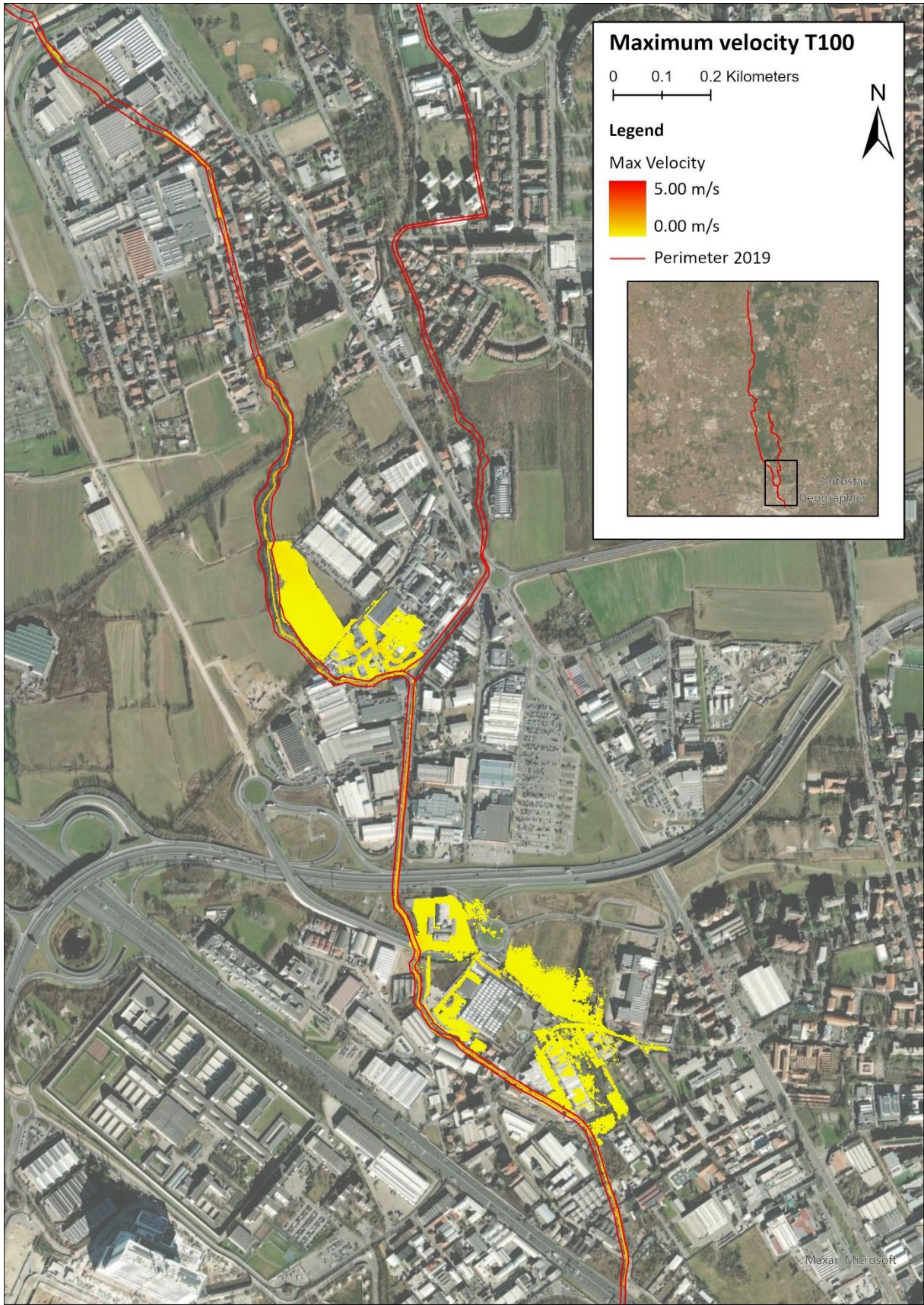
Figure 3.55: Guisa downstream - T100 - Velocity
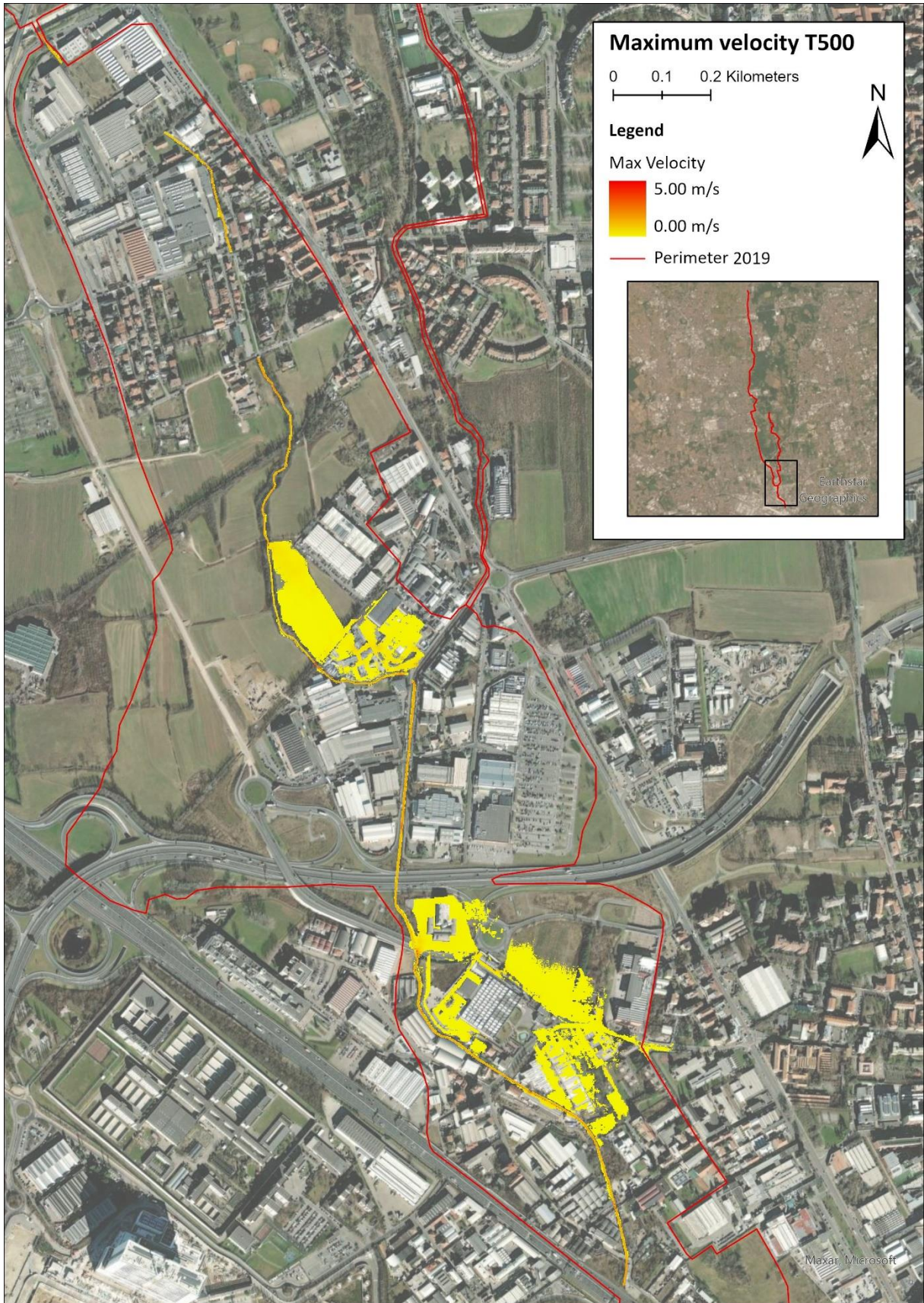
Figure 3.56: Guisa downstream - T500 - Velocity

Figure 3.57: Nirone upstream - T10 - Depth

Figure 3.58: Nirone upstream - T100 - Depth

Figure 3.59: Nirone upstream - T500 - Depth

Figure 3.60: Nirone upstream - T10 - Velocity

Figure 3.61: Nirone upstream - T100 - Velocity

Figure 3.62: Nirone upstream - T500 - Velocity

Figure 3.63: Nirone downstream - T10 - Depth

Figure 3.64: Nirone downstream - T100 - Depth

Figure 3.65: Nirone downstream - T500 - Depth

Figure 3.66: Nirone downstream - T10 - Velocity
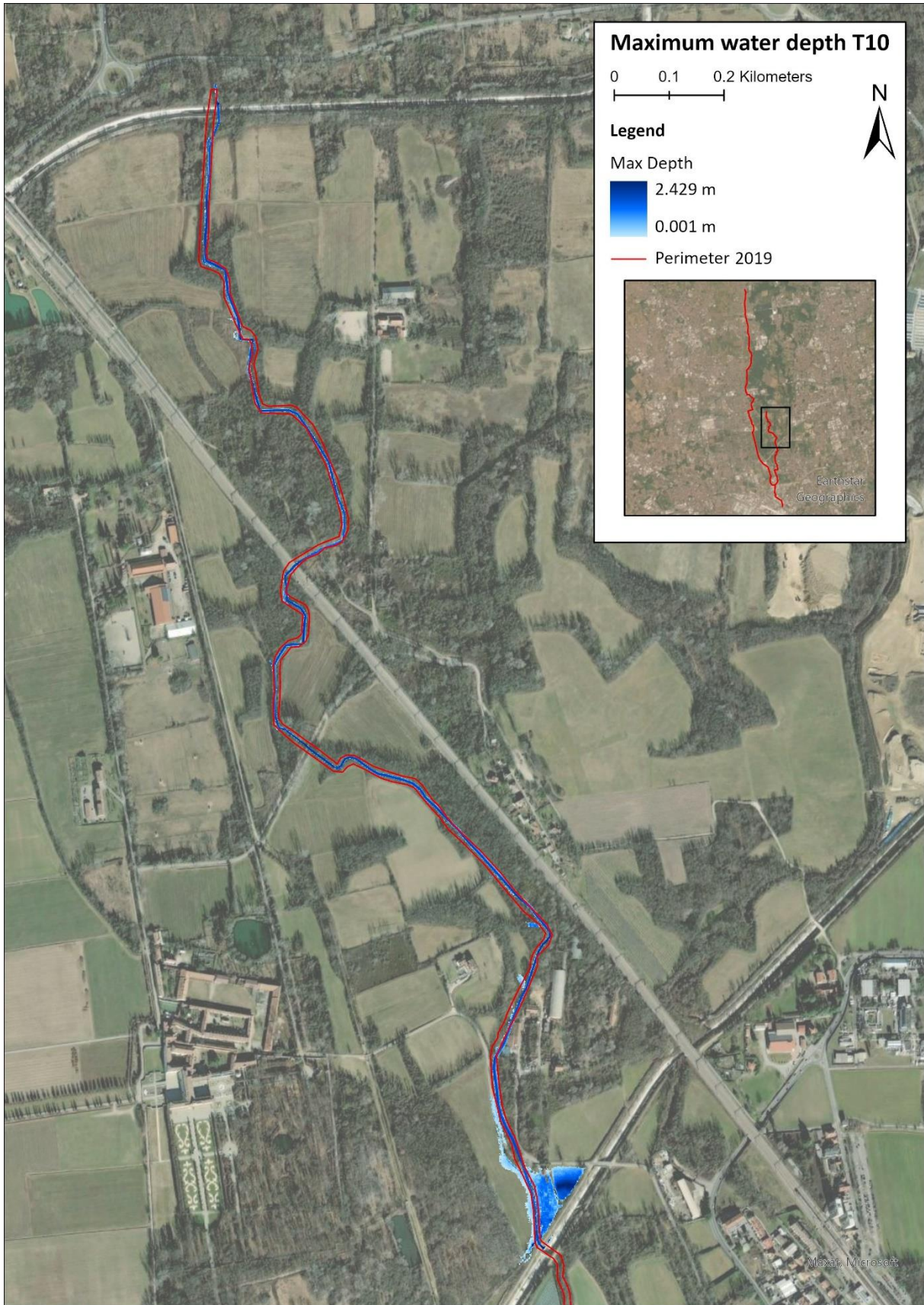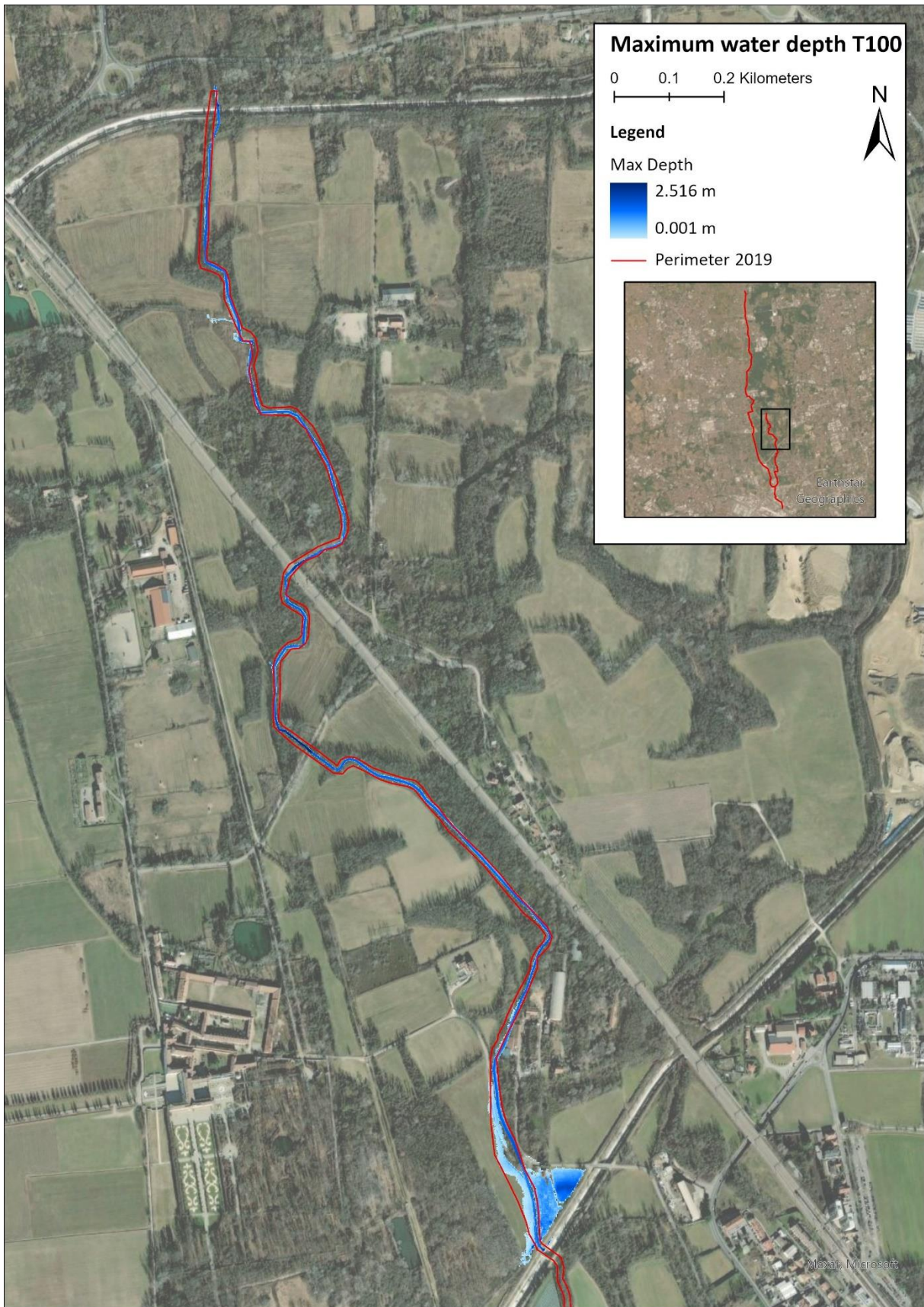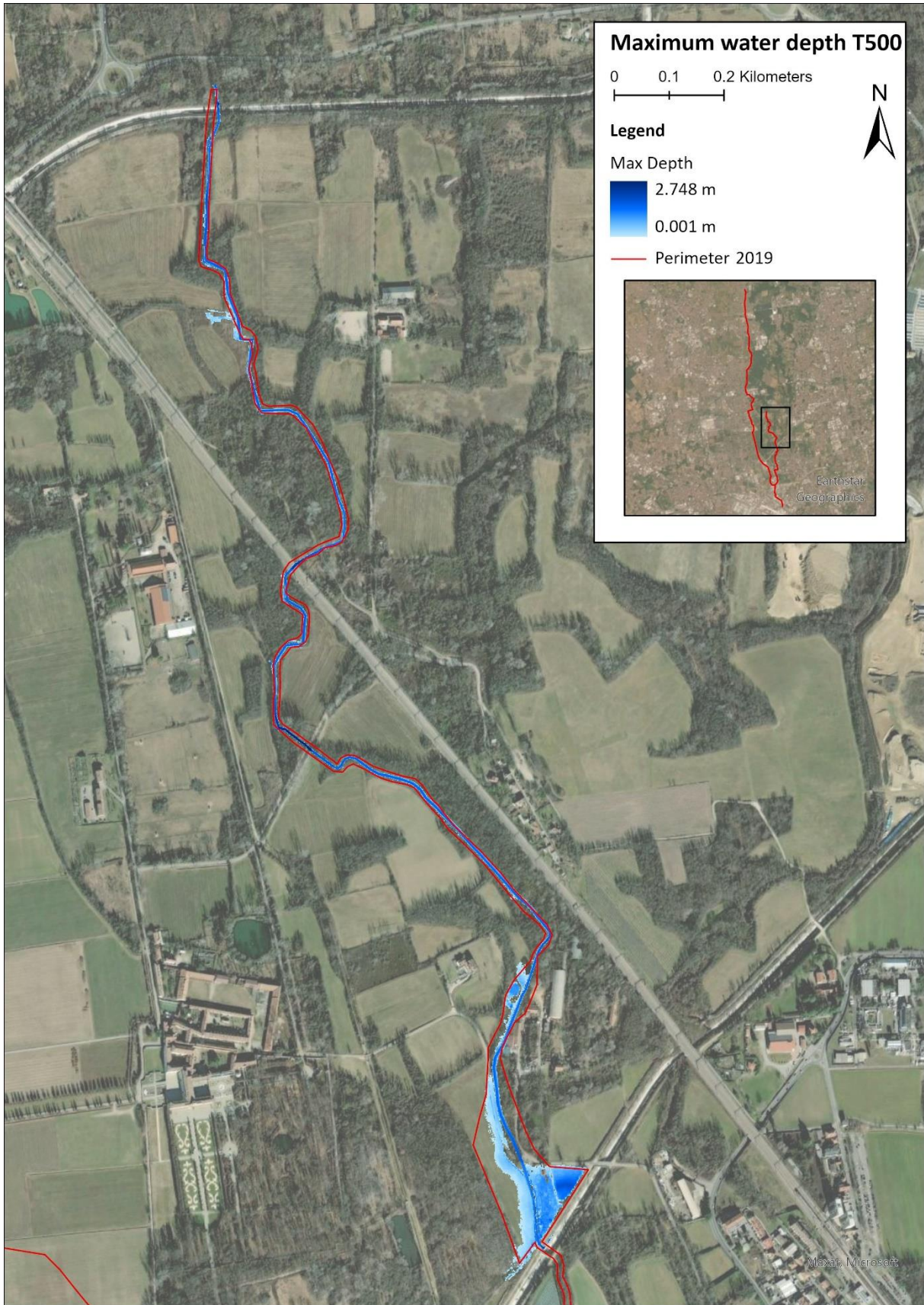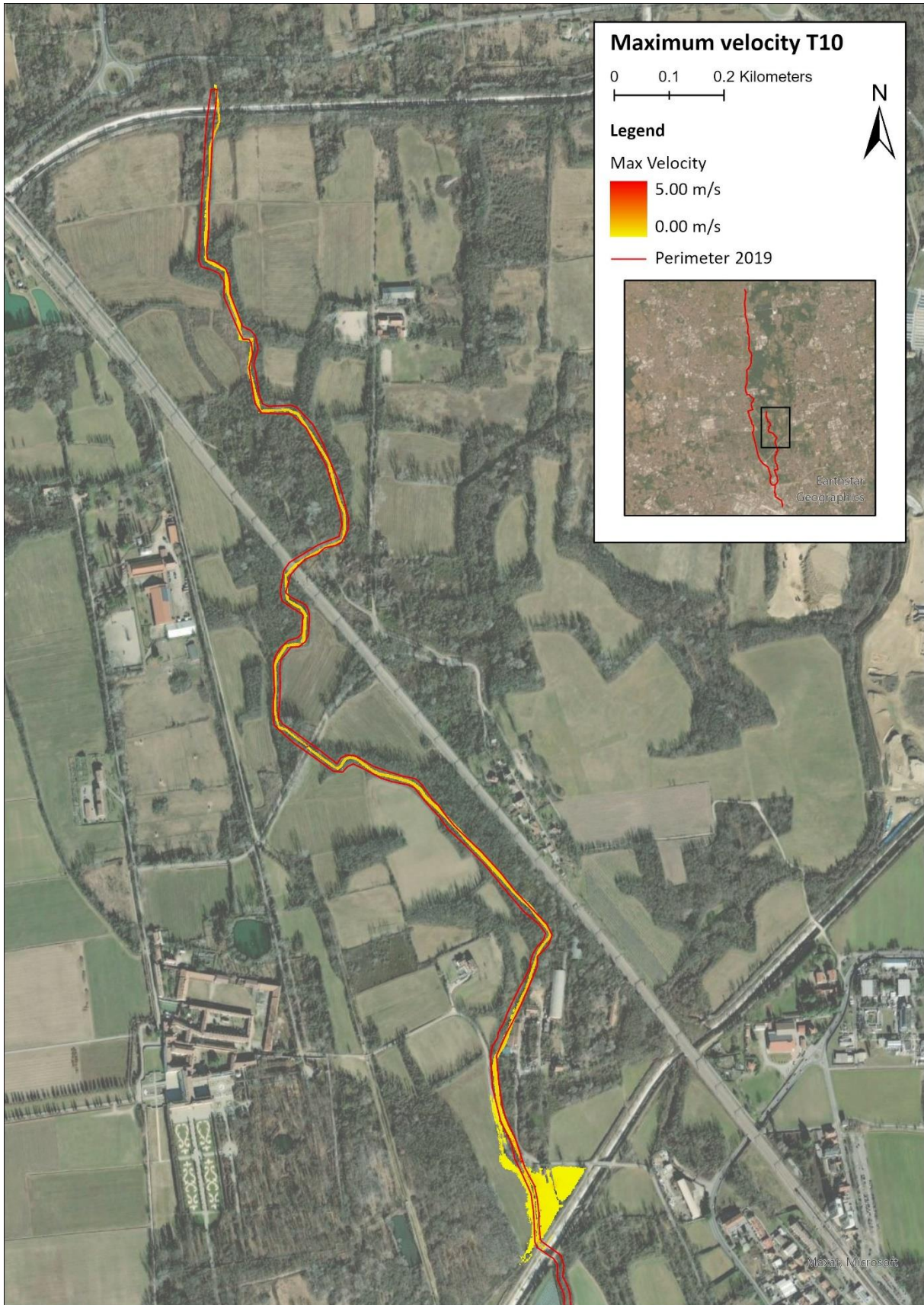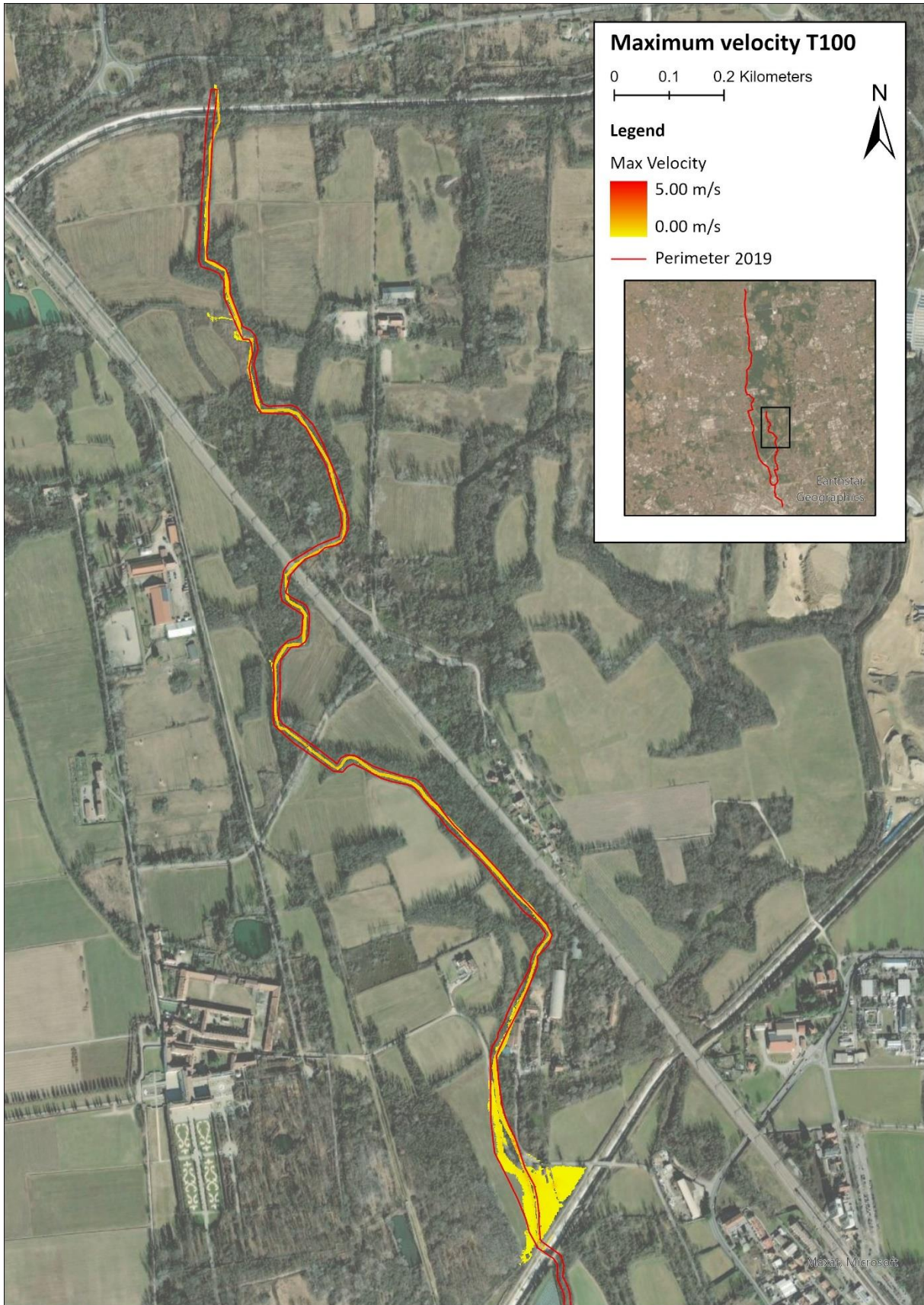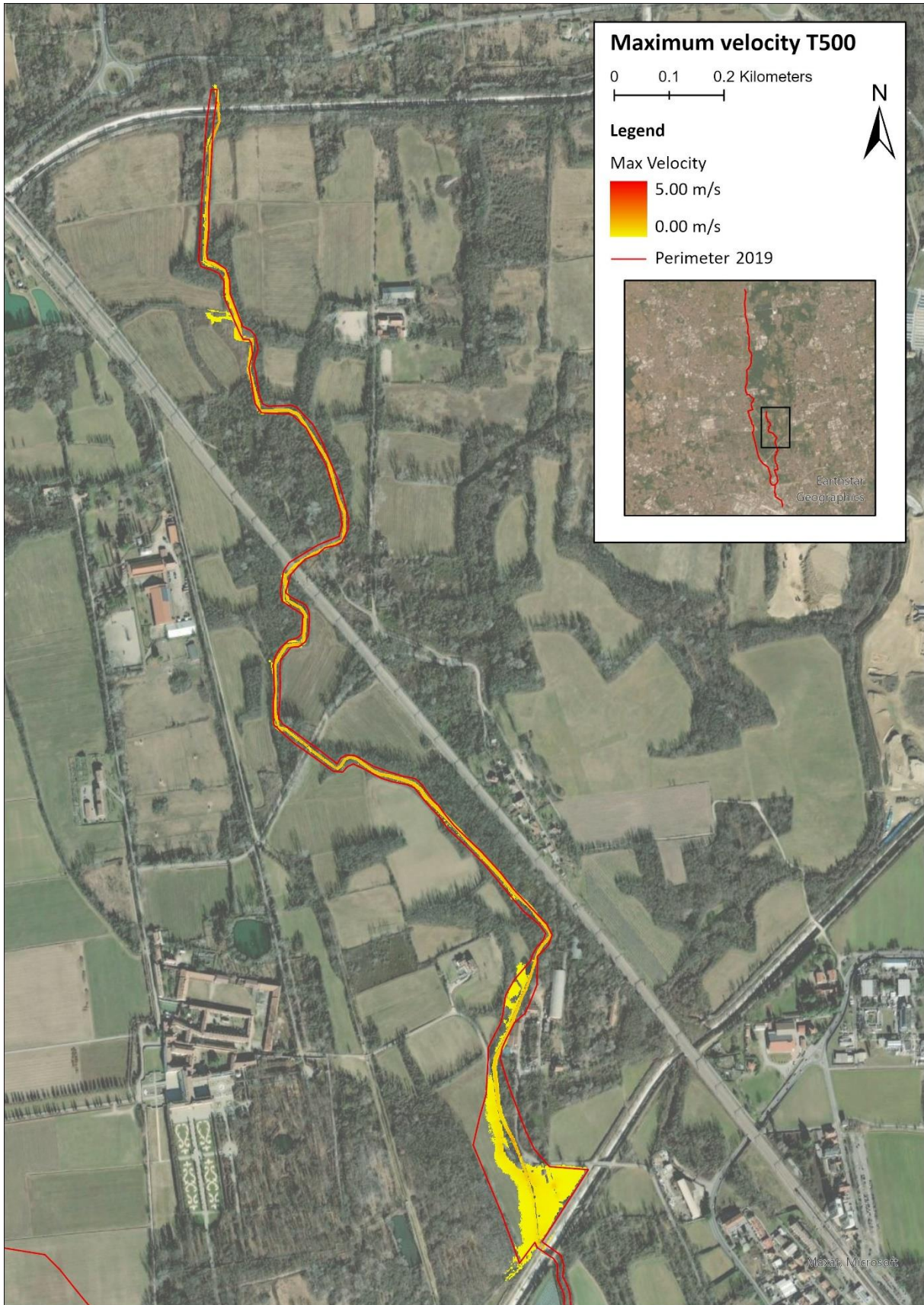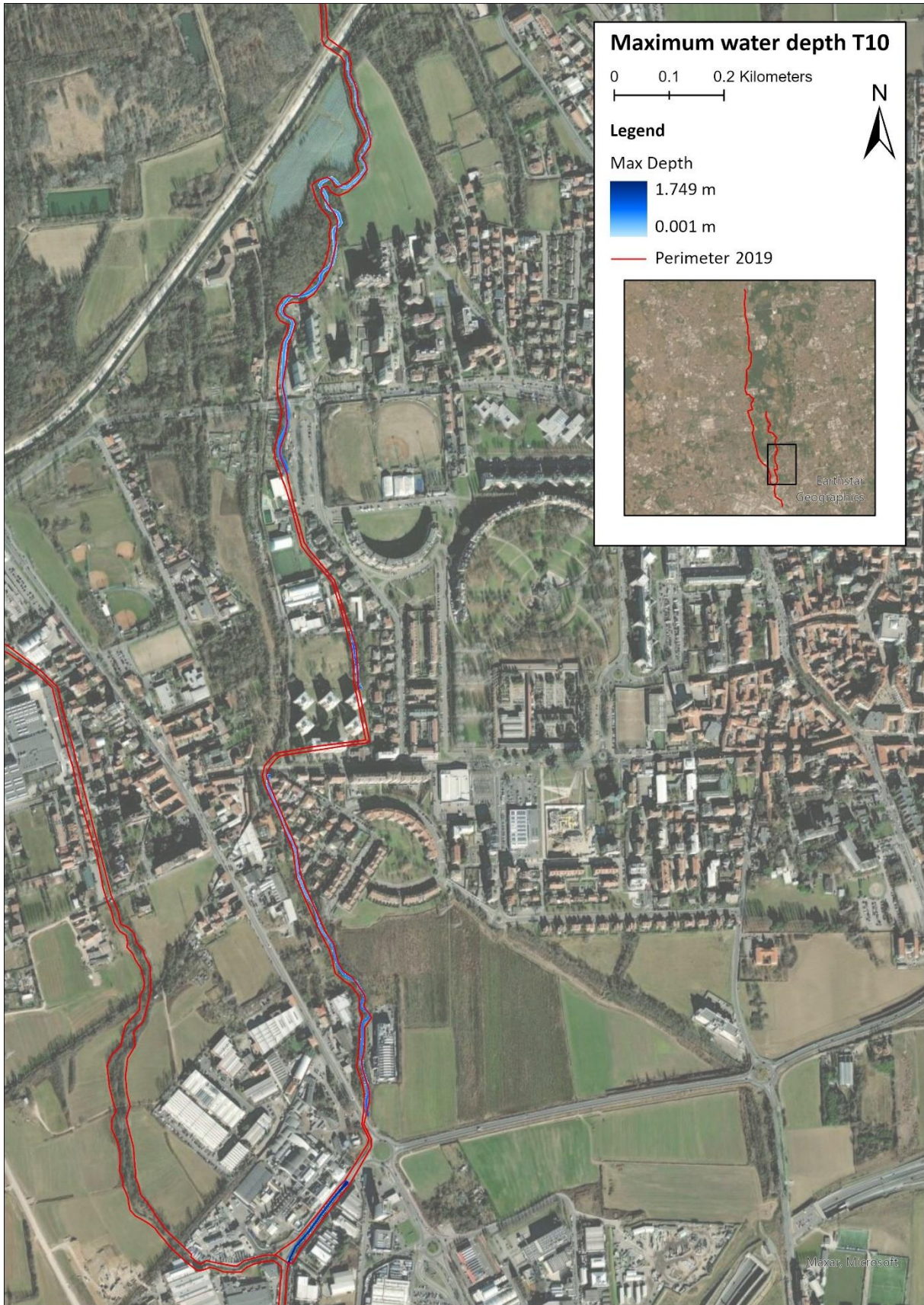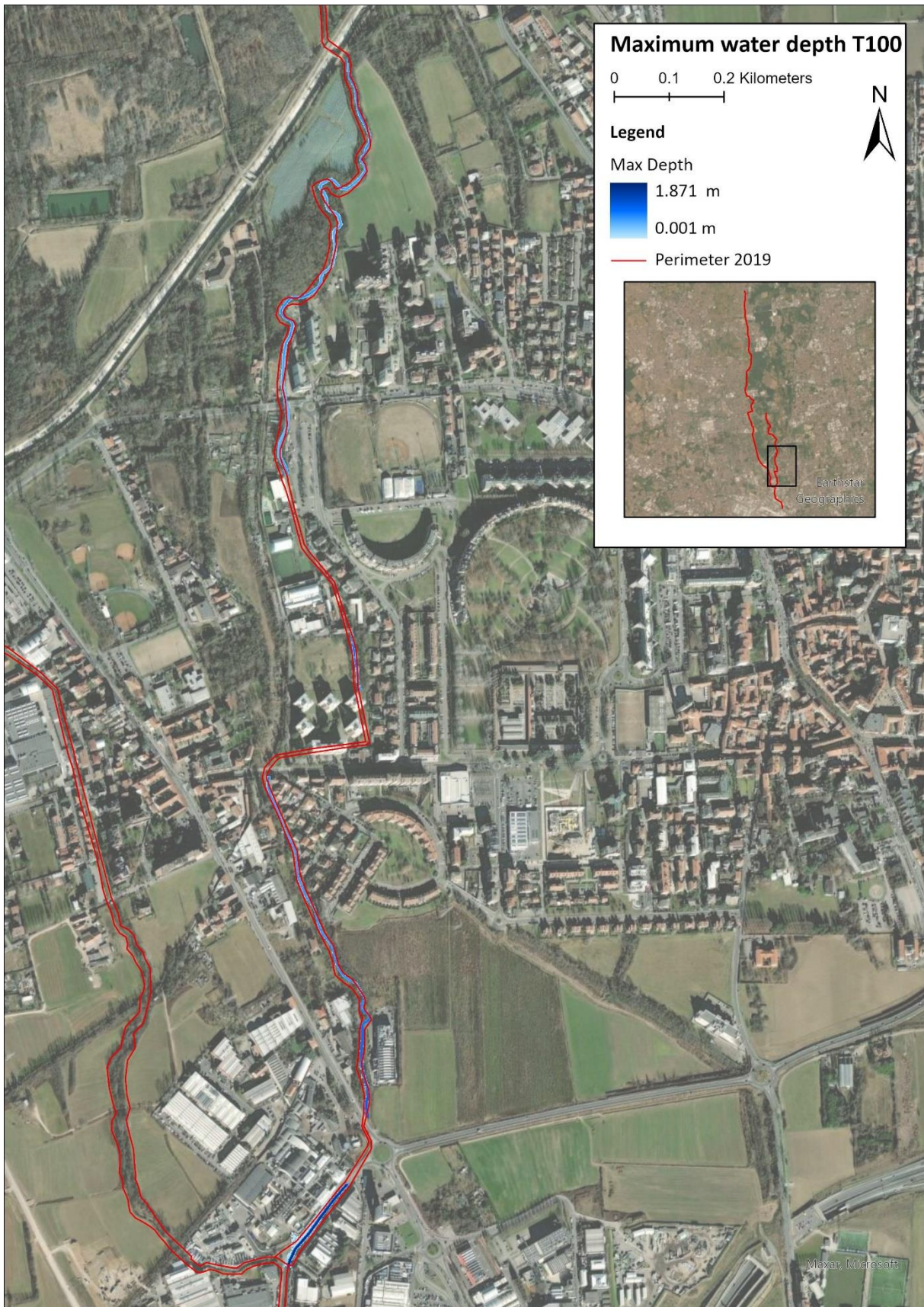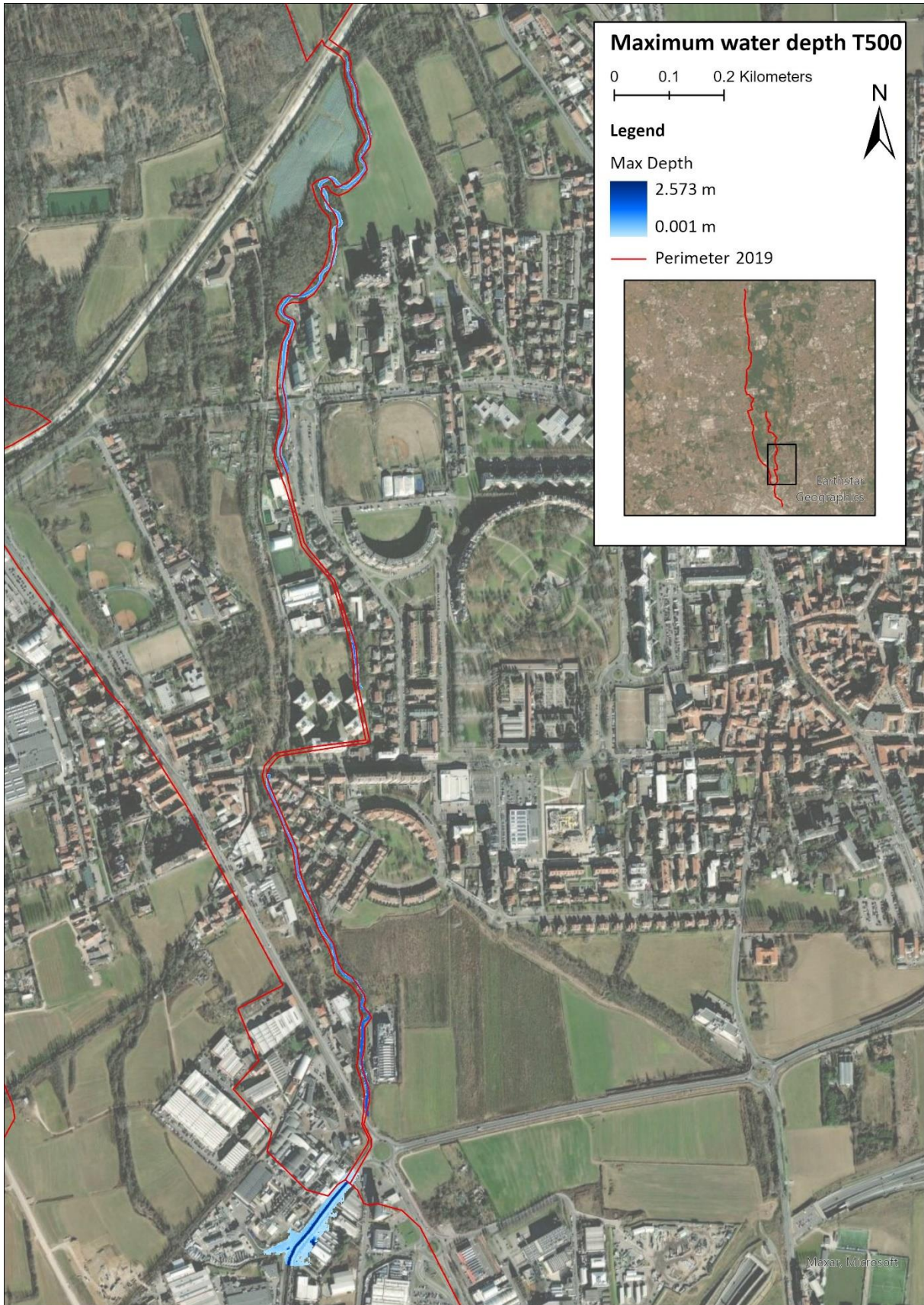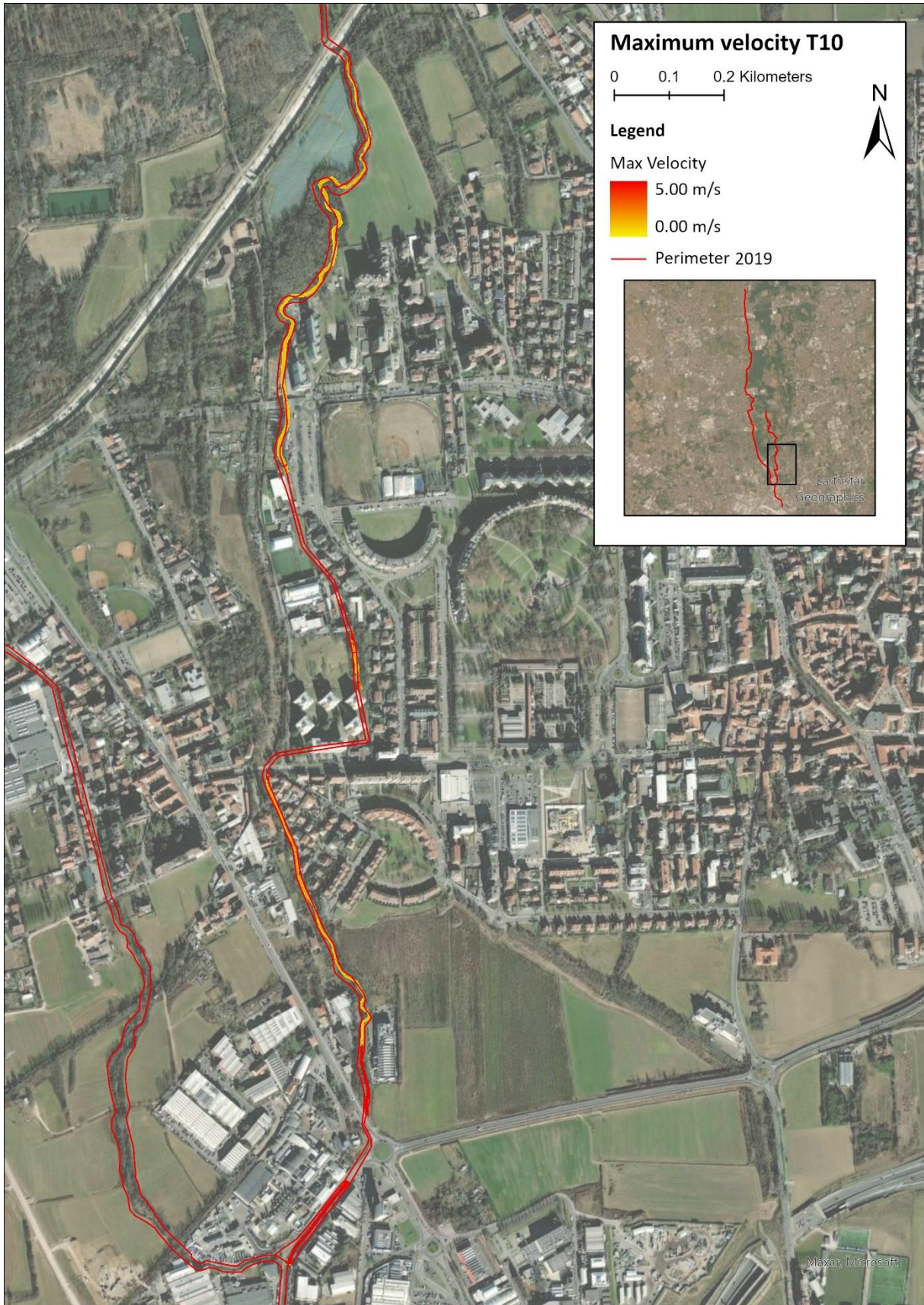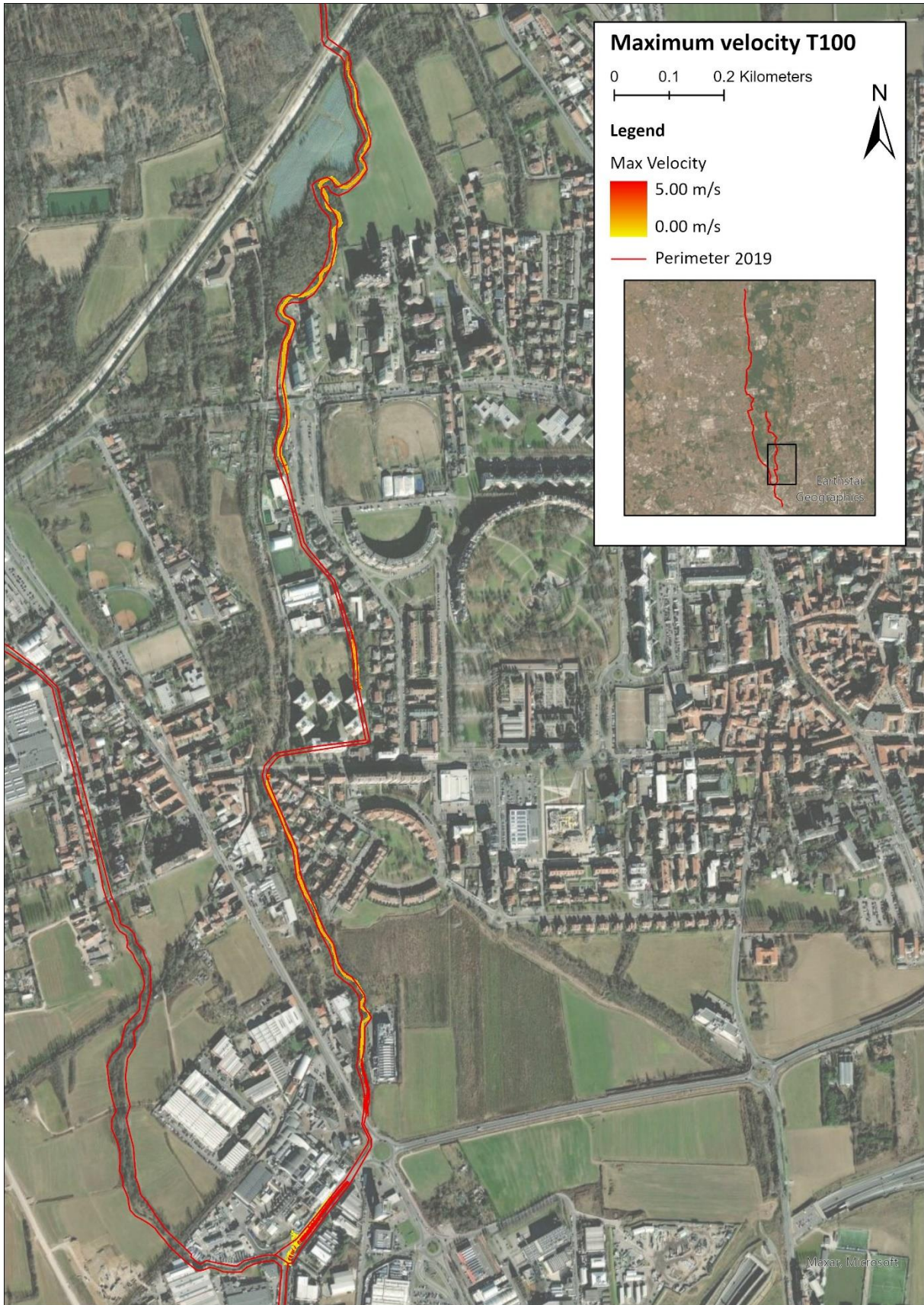
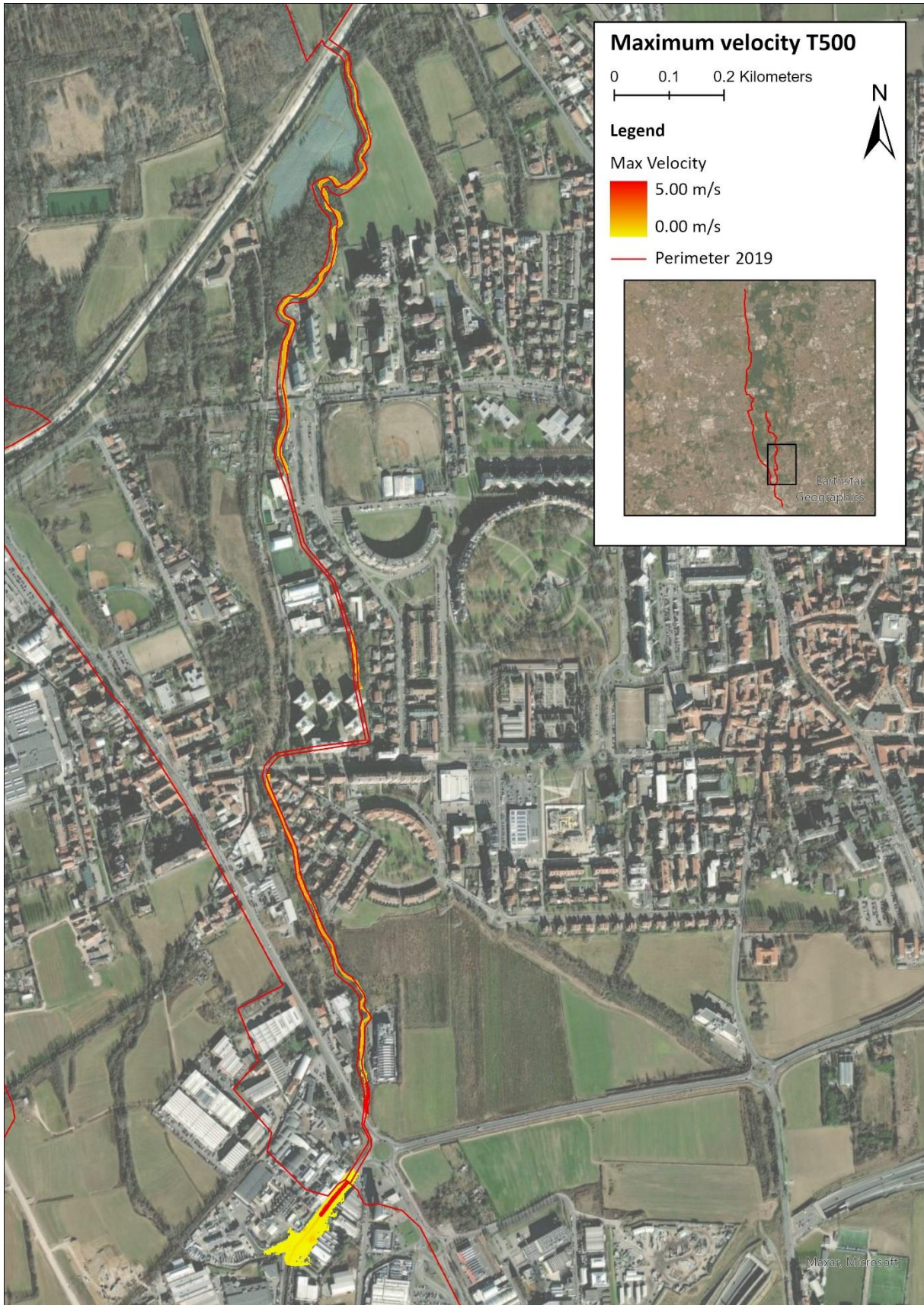*Figure 3.67: Nirone downstream - T100 - Velocity*

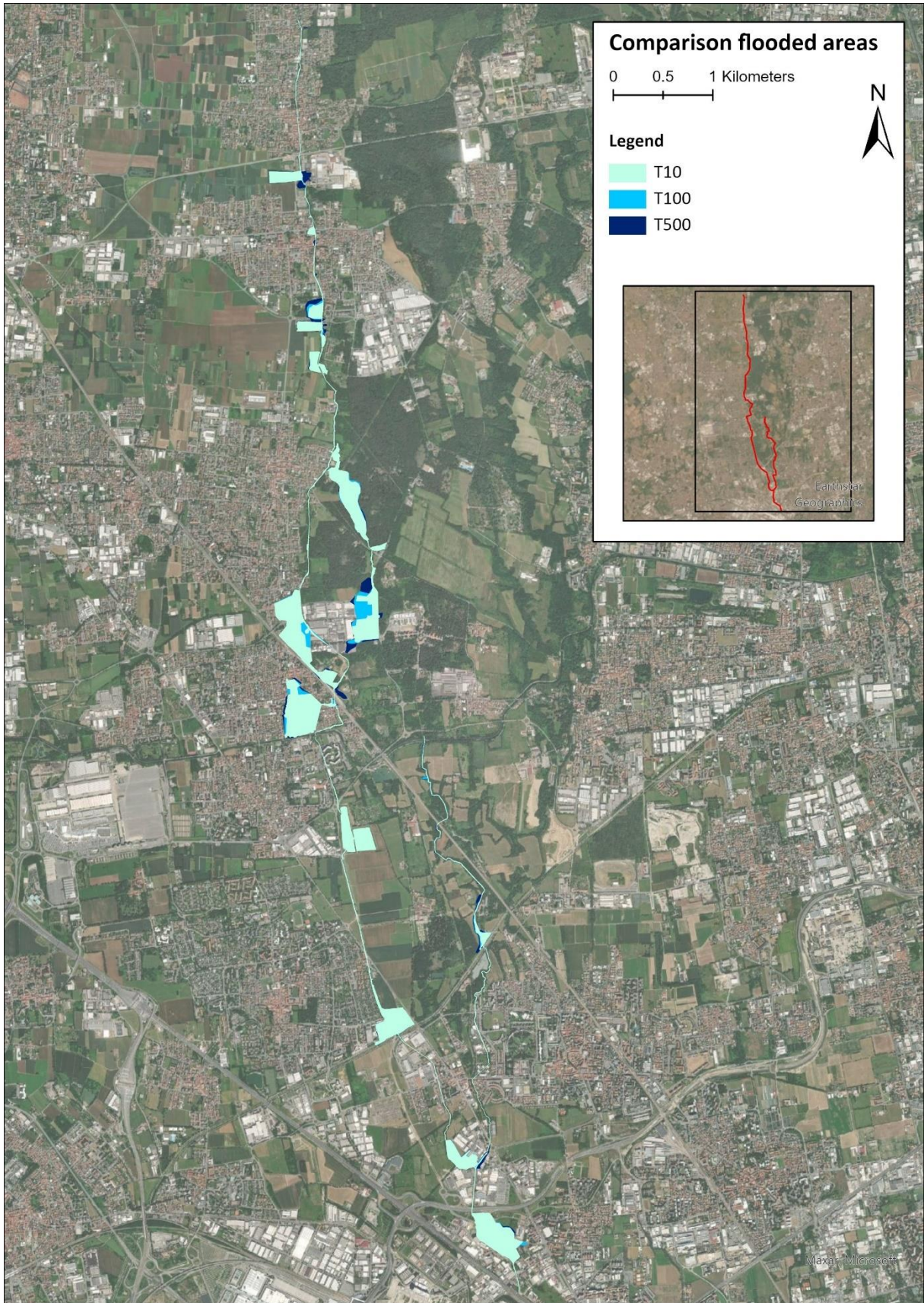*Figure 3.68: Nirone downstream - T500 - Velocity*

Figure 3.69: Comparison of flooded areas - T10 - T100 - T500

3.4. Critical discussion

From Figure 3.69 it can be noticed that the flooded areas do not change too much for the three different return periods. This can be explained through the following considerations:

- In the Guisa upstream model, the discharge is mostly influenced by the presence of the lateral inlets, whose flow rate is independent of the considered return period.
- In the Guisa downstream model, the upstream BCs are the same for the three different return periods. Therefore, the only difference is given by the inflow of the Nirone river, which however changes by only 1 m^3/s (considering the peak value) between two subsequent return periods considered (being 2 m^3/s for T10, 3 m^3/s for T100 and 4 m^3/s for T500).
- In the Nirone upstream and downstream models, the upstream BCs are similar between each other.

By a comparison of the results obtained with those produced in 2019 (with particular attention to the Guisa), it can be noticed that for T10 and T100 the flooded area is generally larger in the new maps. Instead, for T500 the opposite happens; this probably occurs because the previous study did not consider this return period and, therefore, the map of 2019 is traced based on older contours of the flooded area which were much more extended since not all the mitigation measures implemented were considered. The scenarios H, M, and L have different purposes. The H is the frequent one, something that a person may experience more than once in a life. The M is that on which the design of structural mitigation measures is based. Finally, the L is the one representing the residual risk for rare events. Smaller return periods may be more interesting than the very high ones since they correspond to higher probabilities of occurrence; therefore, in the following some considerations are proposed towards providing possible explanations for the discrepancies between the present results and the earlier ones that estimated lower hazard for the H and M scenarios. This analysis will be done only for the Guisa river (for which both the 1D model in HEC-RAS and further information provided by Majone Studio [15] are available), since the results obtained for the Nirone river are very similar to the previous ones and, moreover, no updated information is available for this river.

It is first important to highlight that the perimeter of 2019 also includes a fifth detention pond (located between the third and the fourth detention pond considered in this thesis) that was not considered in the present maps, because no information about it was made available and, in addition, it still has to be constructed.

Geometrical data are compared by analysing the different cross-sections (also in correspondence of the structures), since in 2018 some sections of the Guisa were surveyed again; these were not included in the present models of the Guisa because they are not georeferenced and they are available only in CAD format and through some pictures showing their approximate position along the river. Second, a comparison between the different discharges used in the two models is presented (for the 2019 analysis the discharges have been recovered from the 1D model in HEC-RAS).

The comparison between the cross-sections detected in the years 2018 and 2003 was made just for a few sections, namely those corresponding between each other (highlighted in red in Figure 3.70). In order to detect these cross-sections, it has been necessary to take the available pictures of the trace of the 2018 sections and georeference them through ArcGIS Pro.
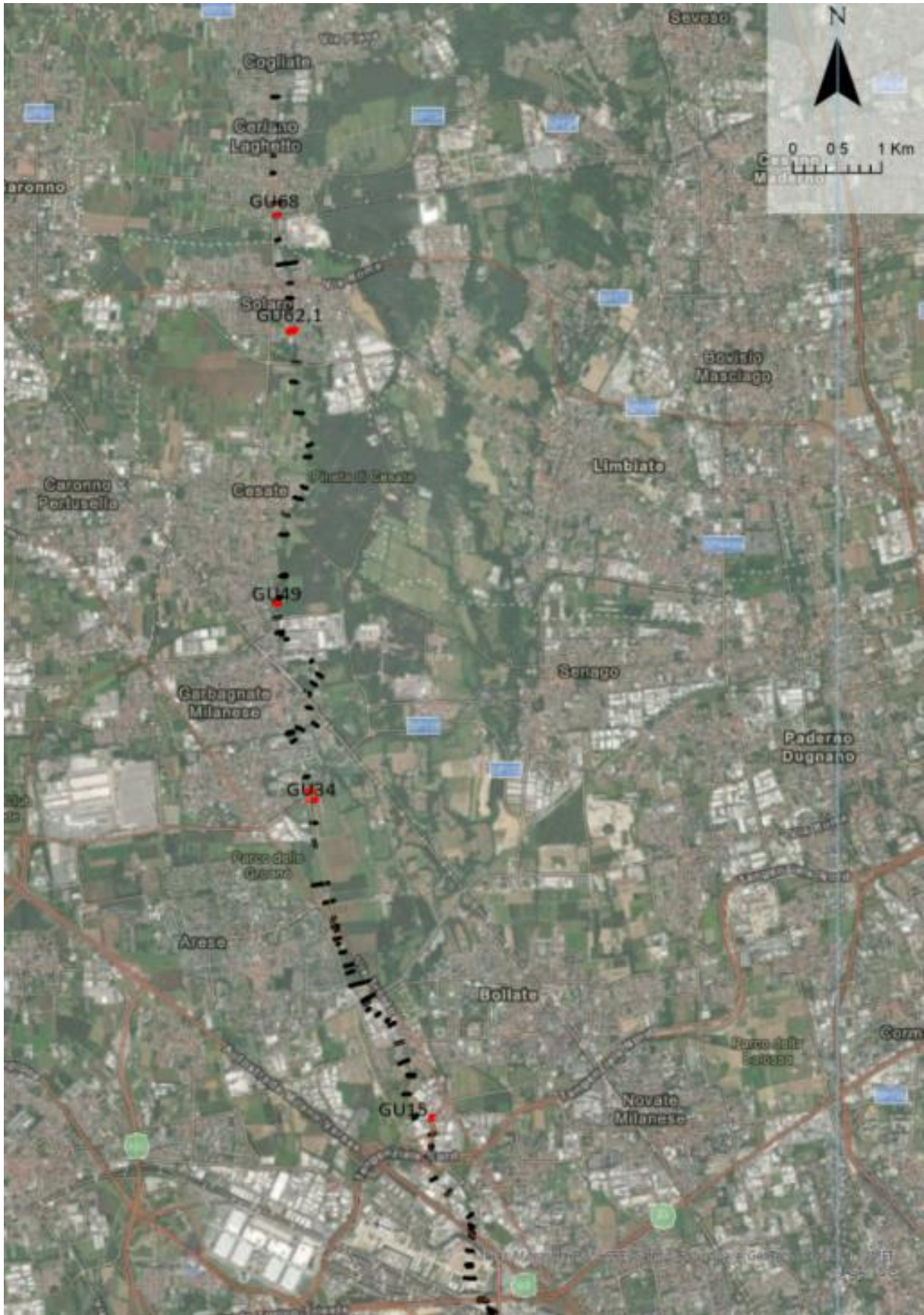
Figure 3.70: Compared cross sections (in red)

The obtained results from the comparison can be seen in Figure 3.71.
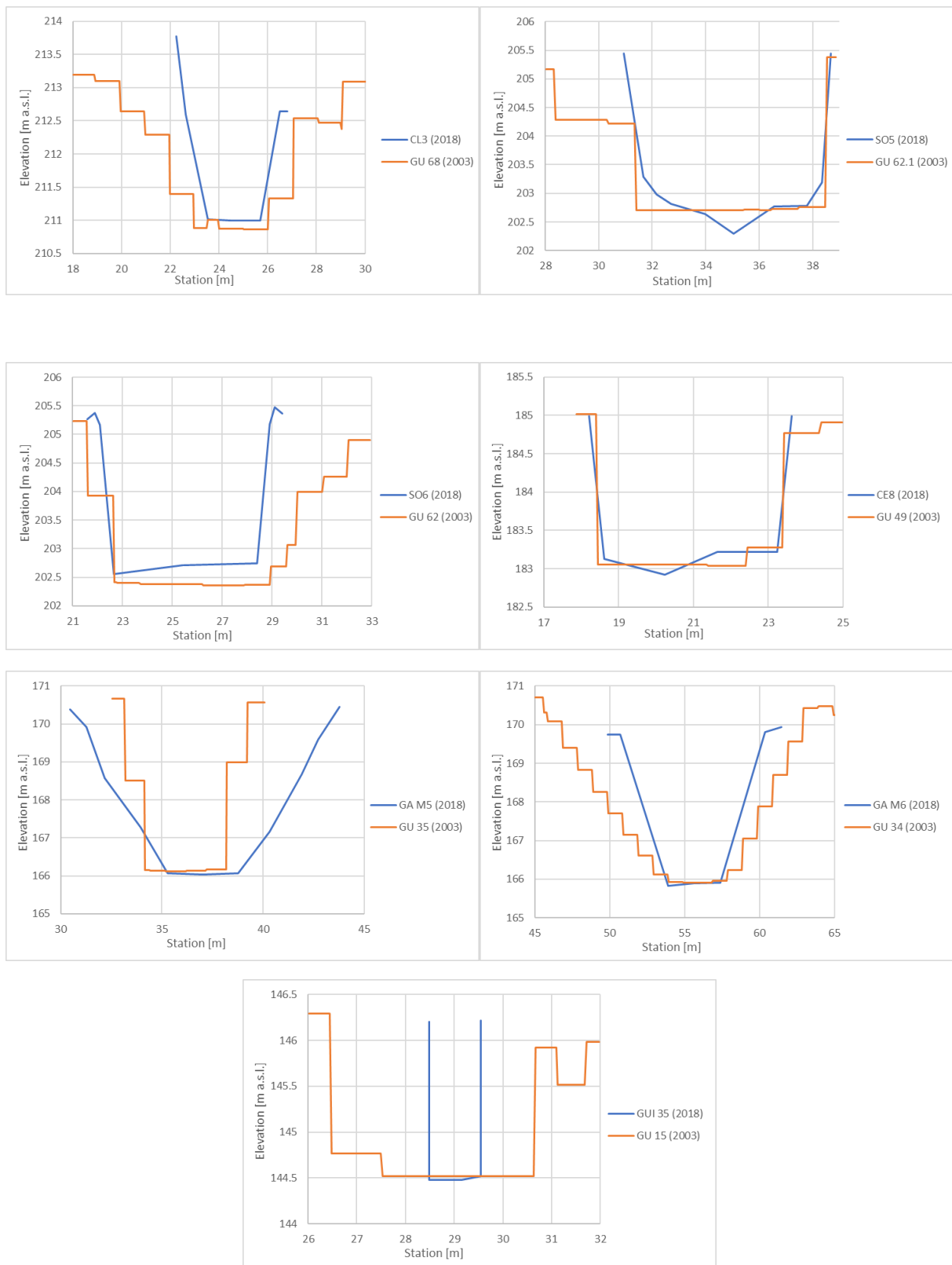
Figure 3.71: Comparison of cross-sections 2003-2018

For the sections considered, there are no substantial differences in the bottom elevation of the riverbed. On the other hand, the cross-sections from the survey of 2018 tend to be even narrower than those from 2003 and, in general, this could lead to less backwater in correspondence of contractions. This fact is particularly noticeable at sections where bridges are located, since in

the 2D modelling performed in this thesis they result in abrupt local contractions (considering the span of the bridge itself), while in the 1D model of 2019 this is not encountered, as seen for example in Figure 3.72 and Figure 3.73. This can explain the larger inundation area obtained in the present work, considering that the locations of outflows are indeed mostly upstream of narrow bridges.
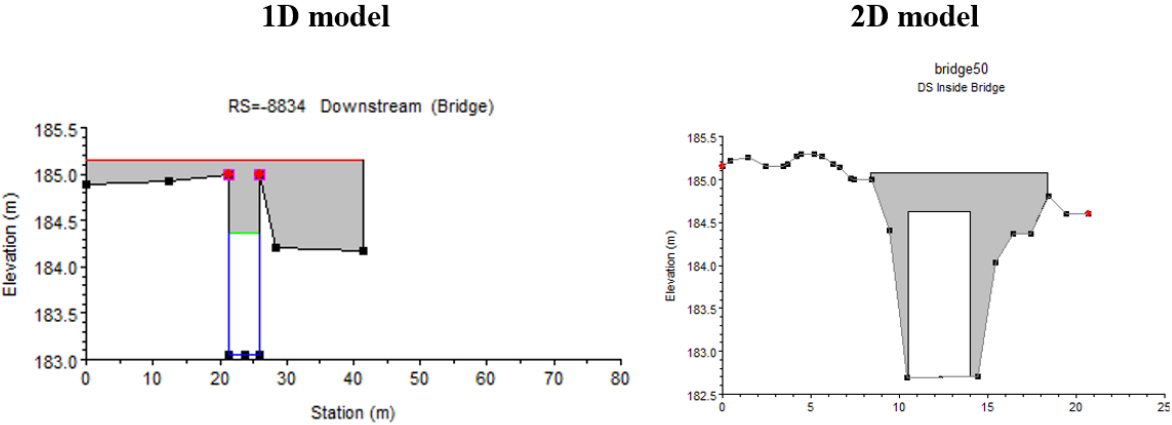
Figure 3.72: Comparison of a transversal cross-section where there is a bridge (1D vs 2D)
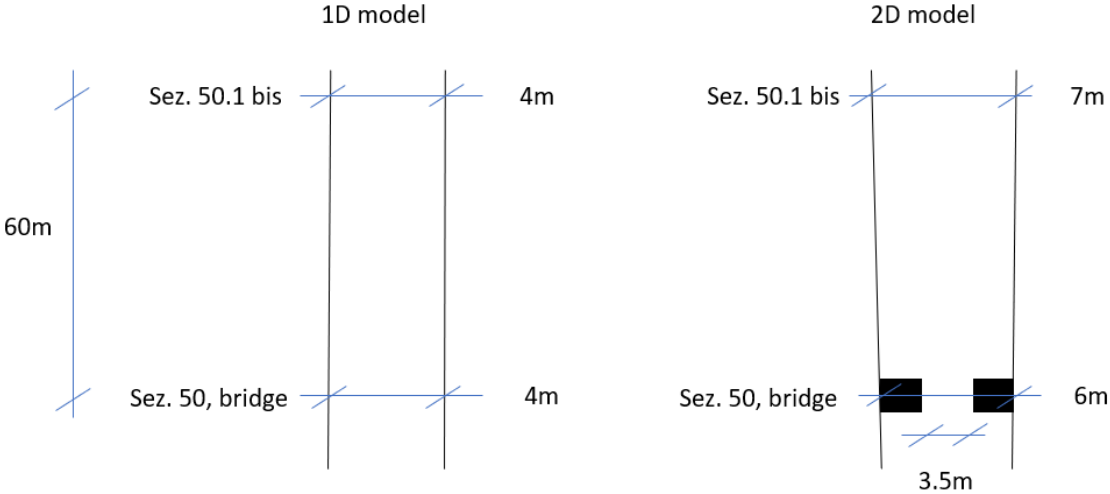
Figure 3.73: Comparison of a cross-section (seen from the top) where there is a bridge (1D vs 2D)

As said, a second comparison was related to flow rates. Figure 3.74 shows the cumulative curve of the peak discharges along the riverbeds. Two considerations are made in this respect. First, from the diagram it can be noticed that the location of the lateral inlets does not coincide in the two models, since they often differ also by several hundred meters. However, the longitudinal development of the curve is not very different until a bit later than the intersection with the Canale Villoresi (GU36.1) where instead a major difference is spotted. The 1D model was split into two parts in correspondence of this section (and not where the CSNO is located); furthermore, the upstream BC of the second model corresponded to the actual output discharge of the upstream model, which was much smaller than the one given by the sum of the peak flow rates. Therefore, the discharge of the 1D model downstream of section GU36.1 is quite low.
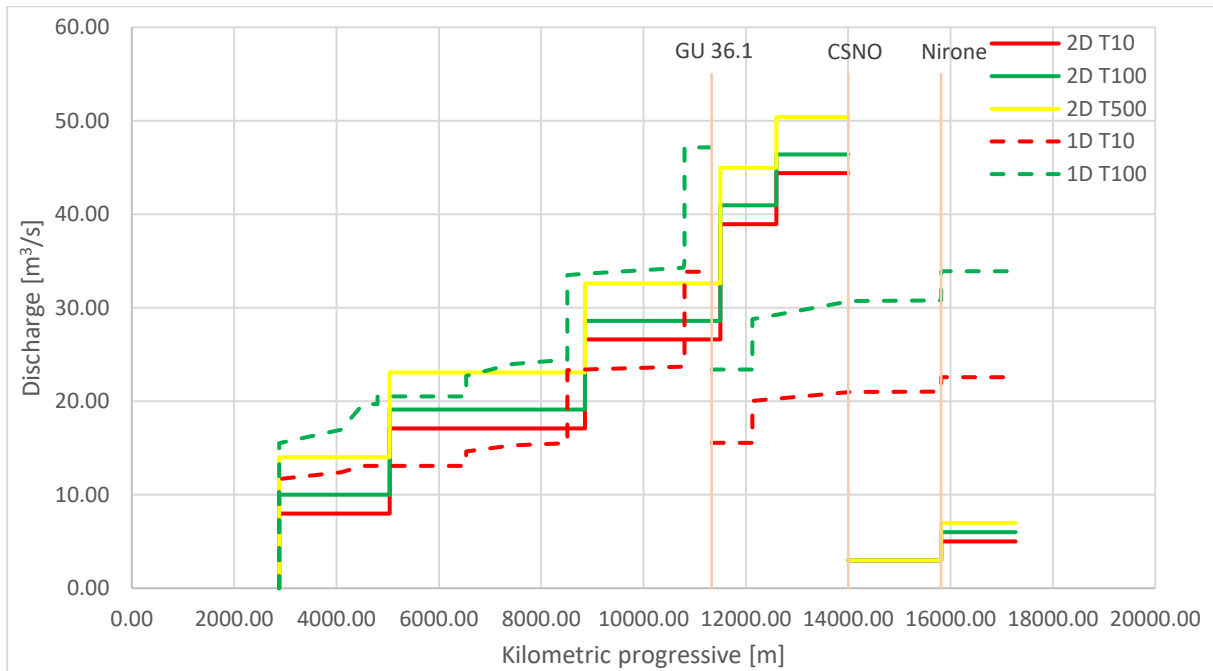
Figure 3.74: Peak flow rates comparison (1D vs 2D)

The second consideration is related to the timing of the hydrographs and to how the peak discharges of the lateral inflows contribute to the total one. While in the 2D modelling the shape of the hydrographs of the lateral inlets was obtained by scaling the upstream BC according to their peak flow rates, in the 1D modelling the hypotheses behind their shapes are not known. However, from the HEC-RAS model one notes that the peak time of the inflows is similar, so the peak discharges are not going to be added to one another for the river discharge.

Finally, also some hydraulic hydrographs returned by the two models in some cross-sections are presented. Specifically, this information was extracted only in correspondence of some sections located upstream of the flooded area detected in this document, as well as where the Canale Villoresi (GU38) and where the end of the 1D upstream model are located (Figure 3.75).
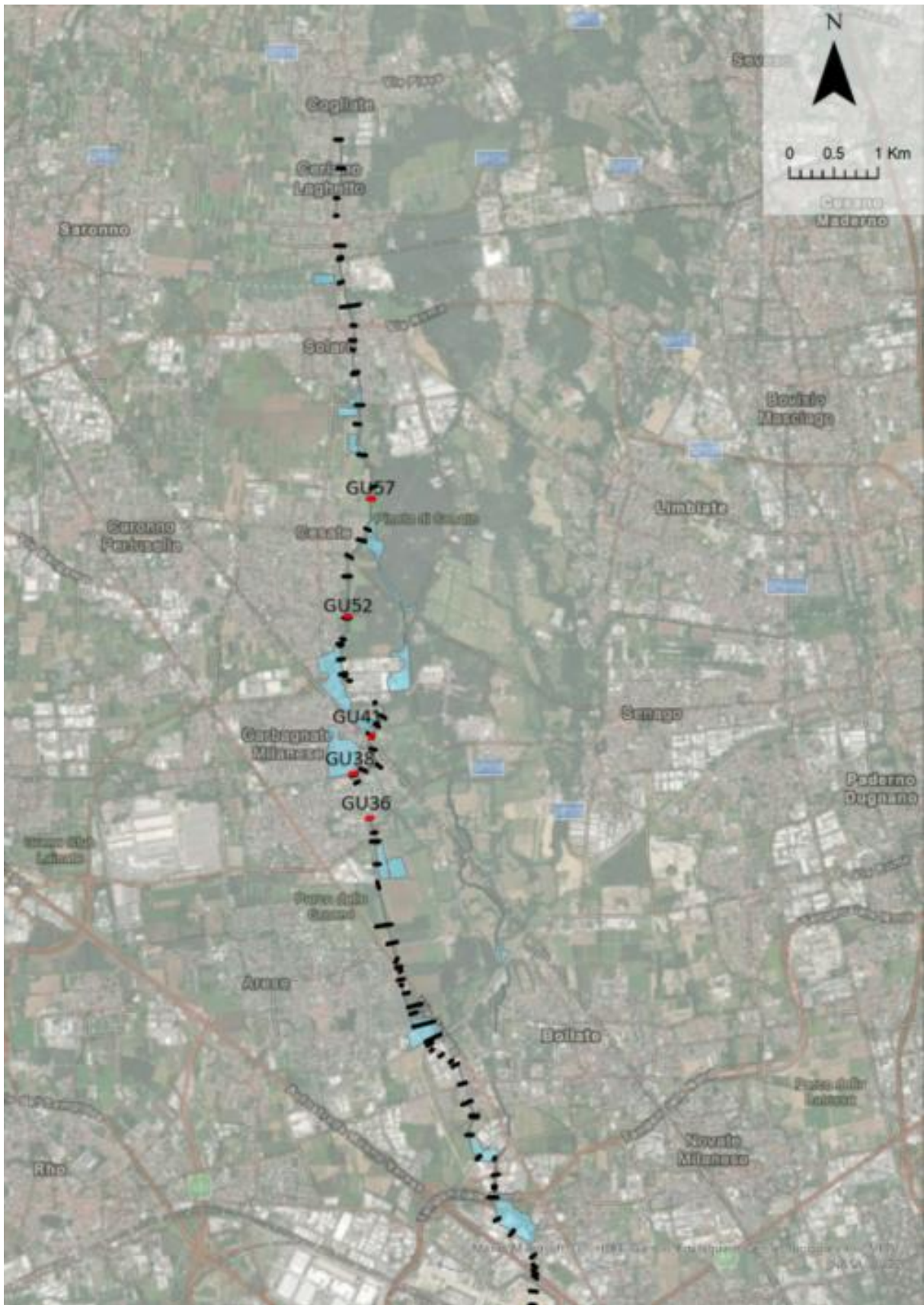
Figure 3.75: Position of the cross-sections where it is performed a comparison between the hydrographs
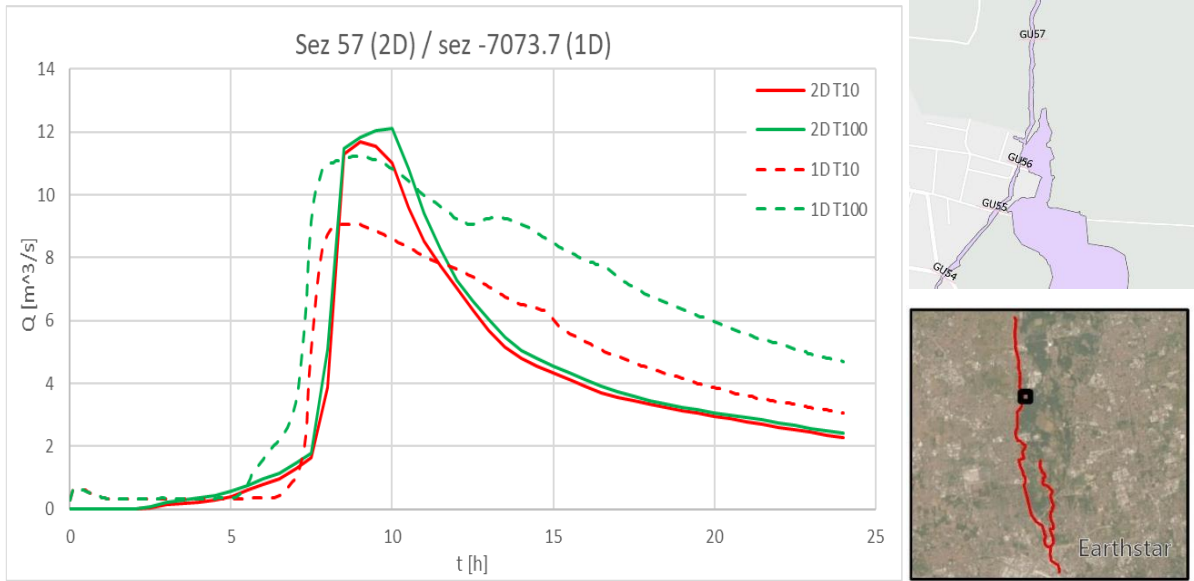
Figure 3.76: Comparison section 57 (1D vs 2D)

In section 57, which is the last section upstream of the first flooded area in the 2D model, the flow rates of the model presented in this thesis are a bit higher than those of the 1D model (particularly for T10). The discharges in both cases are much lower than those given by the sum of the peaks (which are equal to about 15 and about 20 m^3/s for the two return periods).
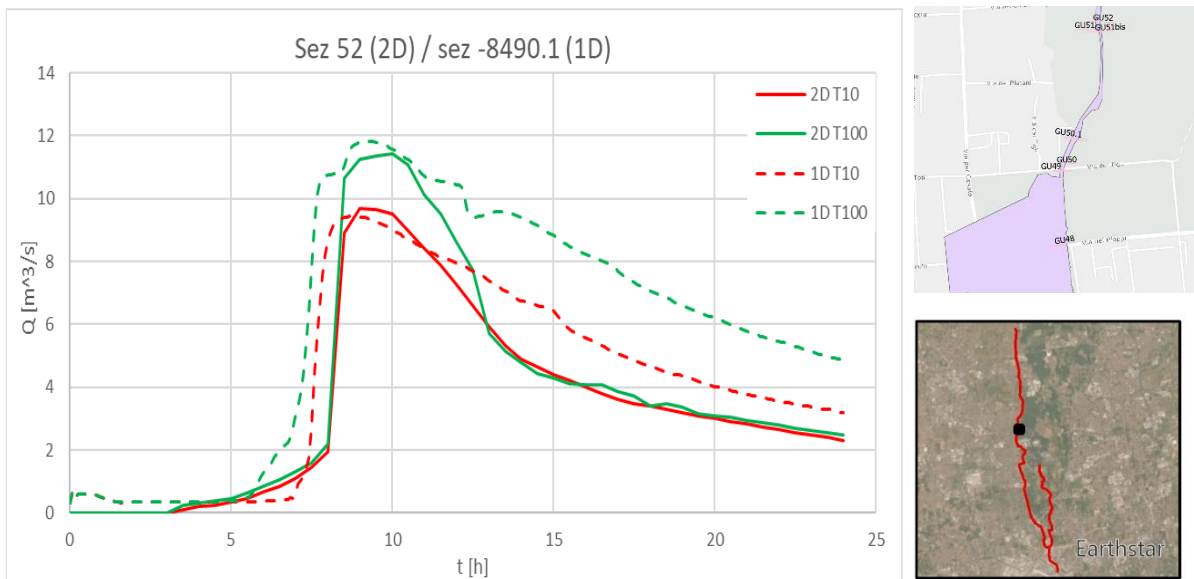
Figure 3.77: Comparison section 52 (1D vs 2D)

In section 52, which is also upstream of a flooded area, the 2D and the 1D model flow rates are very similar and, also in this case, they are in both cases much lower than those given by the peak sum (which are equal to about 25 and about 30 m^3/s for the two return periods).
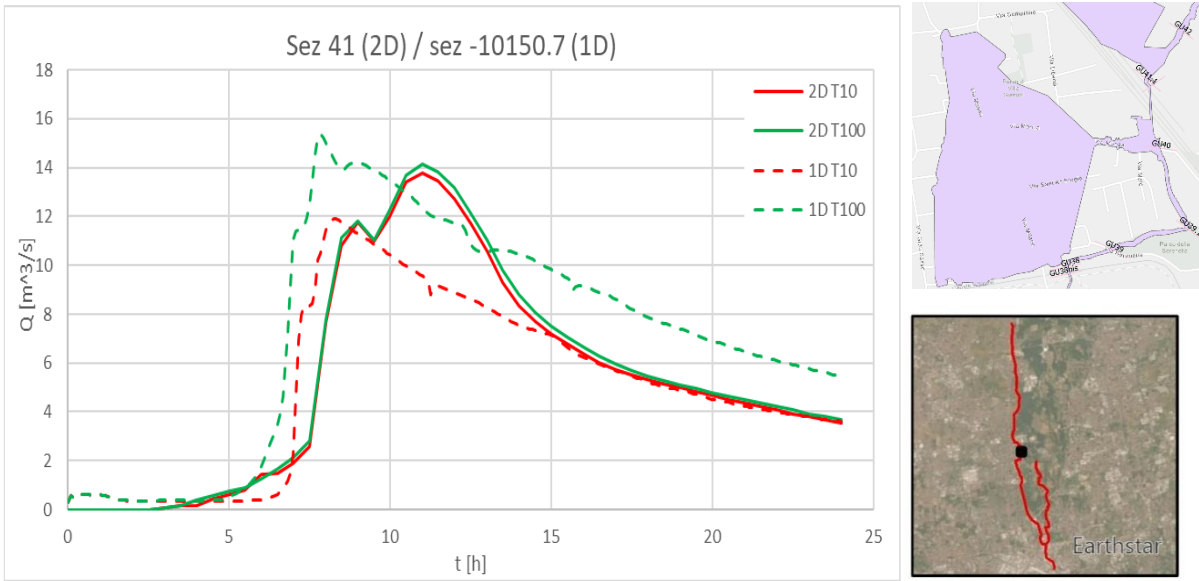
Figure 3.78: Comparison section 41 (1D vs 2D)

In section 41, located upstream of an additional flooded area, the 2D model flow rate is higher than that of the 1D model for T10 and slightly lower for T100. The discharges in both cases are much lower than those given by the sum of the peaks (which are equal to about 25 and about 30 m^3/s for the two return periods).
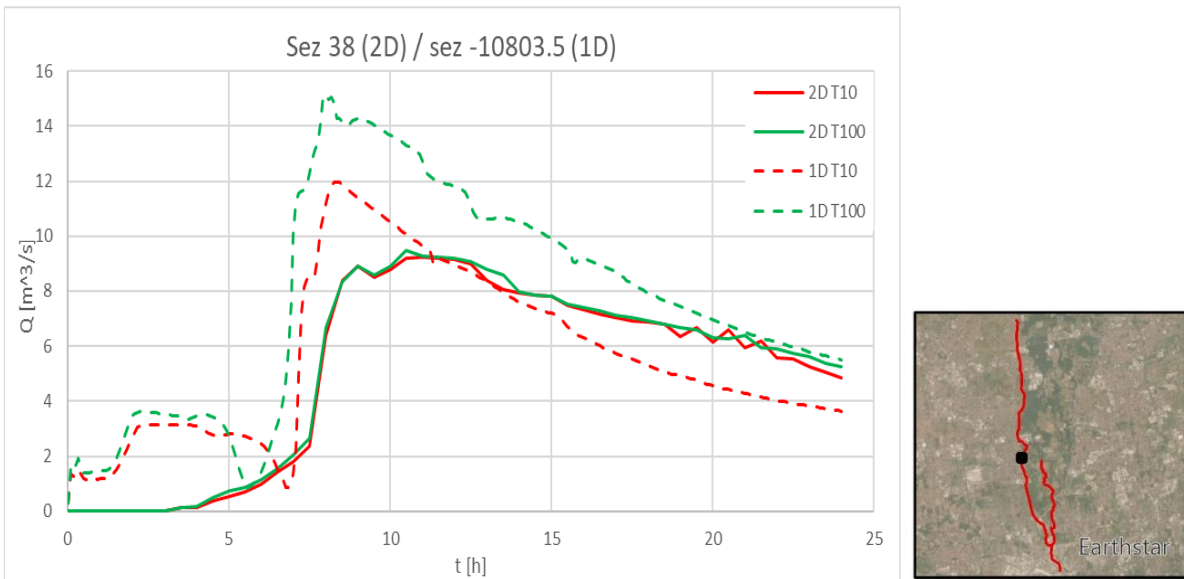
Figure 3.79: Comparison section 38 (1D vs 2D)
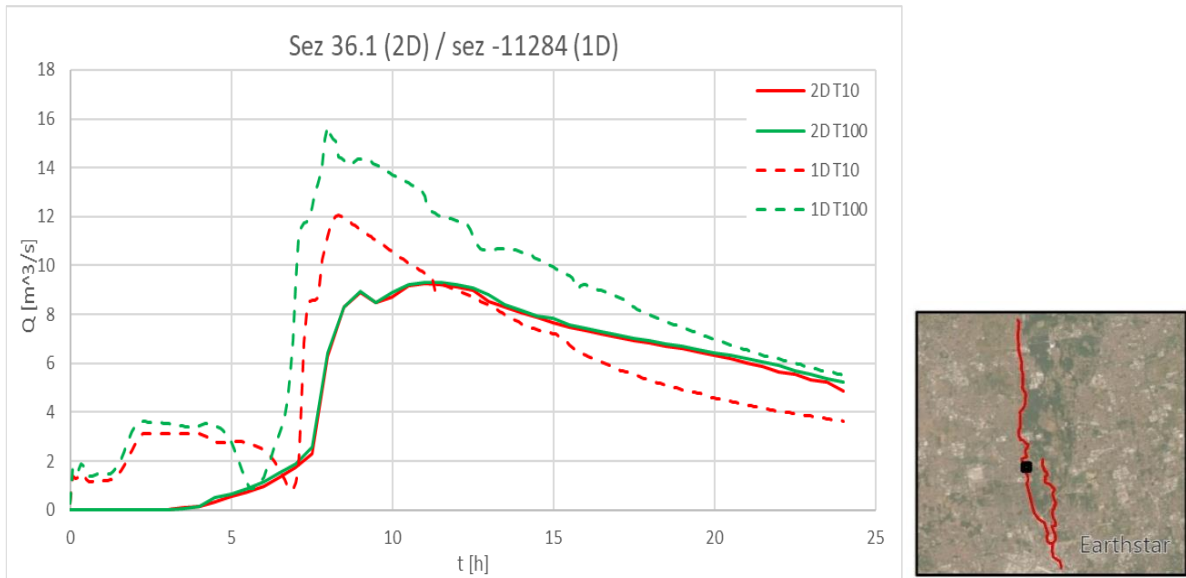
Figure 3.80: Comparison section 36.1 (1D vs 2D)

As far as the last two sections (GU38 and GU36.1) are considered, the difference in the flow rates is greater because of the water outflow occurring in the 2D model (thus the flow rates of the 1D are higher).

From the analysis of the graphs presented above it can be noticed that, considering the scenario H (i.e.: T10) in correspondence of the first and of the third sections used for comparison (GU57 and GU41), the 2D model flow rates are higher than those of the 1D model, leading to an increased level of hazard. The difference between the discharges is presumably due to how the peaks of the lateral inlets have been positioned over time. Instead, in all the other cases, no flow rate difference can explain the greater flooded areas obtained in the 2D model. The only reason which can be suggested for this is that in the model presented in this document there is presumably more backwater at bridges (indeed, as already mentioned, except only for the first water outflow, all the areas in which there is a flooding phenomenon are in correspondence of sections where bridges are located).

4. Critical aspects of the 2D modelling approach

In this chapter some major critical aspects and weak points of the 2D modelling approach are highlighted, in general terms and, more specifically, based on the results obtained using HEC-RAS. Then, for some of these identified aspects, further analysis is made in order to better understand how some characteristics affect the results and, eventually, how models could be improved in follow-up work to obtain more reliable outputs. The main critical aspects identified are:

- Data available, since they are usually old and not recently updated. This is true in terms of both geometry (i.e.: sections and DTM) and hydrological data (i.e.: the shape of the hydrographs and information about the sewage system which contributes to the lateral inlets). In addition, sometimes the problem is that the most recent data cannot be used since they are either incomplete or not available in easily usable formats (e.g.: data from 2018 about the new cross-sections).
- The large size of the models, which in turn determines the number of computational cells (i.e.: grid size definition). Specifically, there is an inverse proportionality between the level of detail of the model and its size, where highly detailed models (i.e.: very small cell size) enable just small areas to be studied, due to the computational performance of any used solver. With respect to this aspect, it is also important to remember that the walls of the model should be put in a place where they do not influence the results (so, the computational domain needs to be large also for a small river, in case the latter inundates a flat area).
- Roughness, due to the intrinsic difficulty in defining its most appropriate values and its coupling to how urban settings are modelled (e.g.: how buildings are considered). This aspect is also related to the previous one, since the highest detail applicable in the roughness definition is limited by the computational cell size.
- Set of equations used in the model, remembering that in HEC-RAS there are three available choices (Chapter 2.3.1).
- Computational time step, which should be carefully defined to obtain an acceptable level of detail of the results with an acceptable simulation time.
- Structures, which can be easily defined in HEC-RAS, but whose influence on the results is still an ambiguous point (also given the fact that in the obtained results most of the outflow regions were located where bridges and culverts are present).

Some of these issues are considered in more detail in the following sections. In particular, issues under consideration are the roughness definition (Chapter 4.1), the joint effect of computational time steps and equations used to model the process (Chapter 4.2), and the computational mesh size (Chapter 4.3). While the analysis on the grid size definition effect has been studied through a fictitious river reach, the sensitivity analyses of the effects of both the roughness parameterization and the computational time step and set of equations used have been performed for one part of the Guisa upstream model (Figure 4.1, where the obtained flooded areas in the original model are also reported). Since this section aims at analysing some critical aspects, the selected area has been chosen because it contains a heterogeneous land cover within a quite widespread urban area, which is very important to study the effects of the roughness, and also because a relatively limited size allows to run several simulations, also when the whole

set of differential equations (SWE) or when very small computational time steps are considered, within a reasonable period of time.
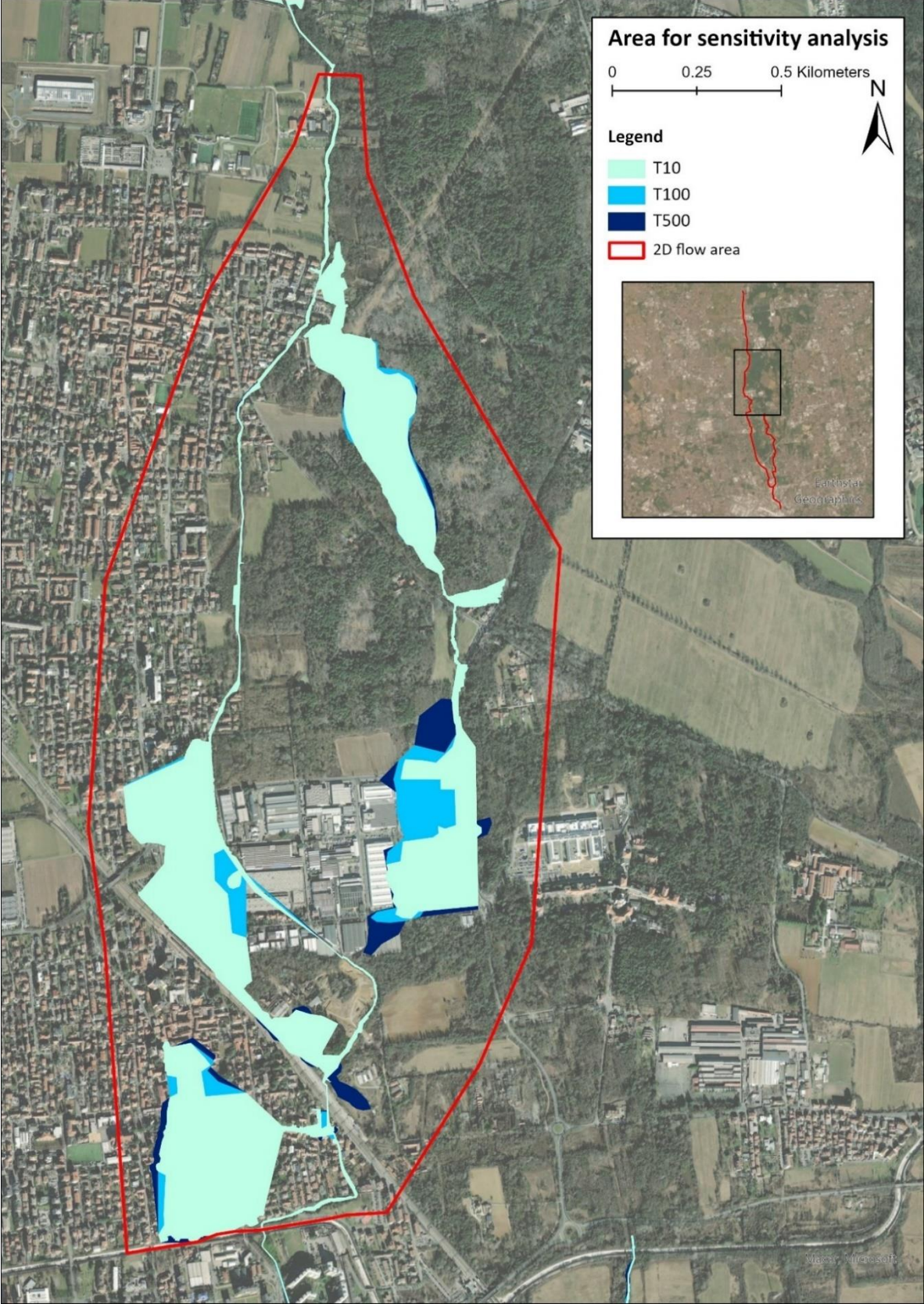
Figure 4.1: Area selected for the sensitivity analysis

Furthermore, all the sensitivity analyses were made for a single return period, the T10. The input hydrograph used for the sensitivity analyses (Figure 4.2) was extracted from the HEC-RAS simulation of the Guisa upstream model in correspondence of the upstream inflow of the new model (which is located between the sections GU59 and GU58). Instead, a rating curve extracted along the Canale Villoresi was used as a downstream BC (Figure 4.3). All the analyses were made with a cell size of 10 m and a refinement region with cells of 3 m.
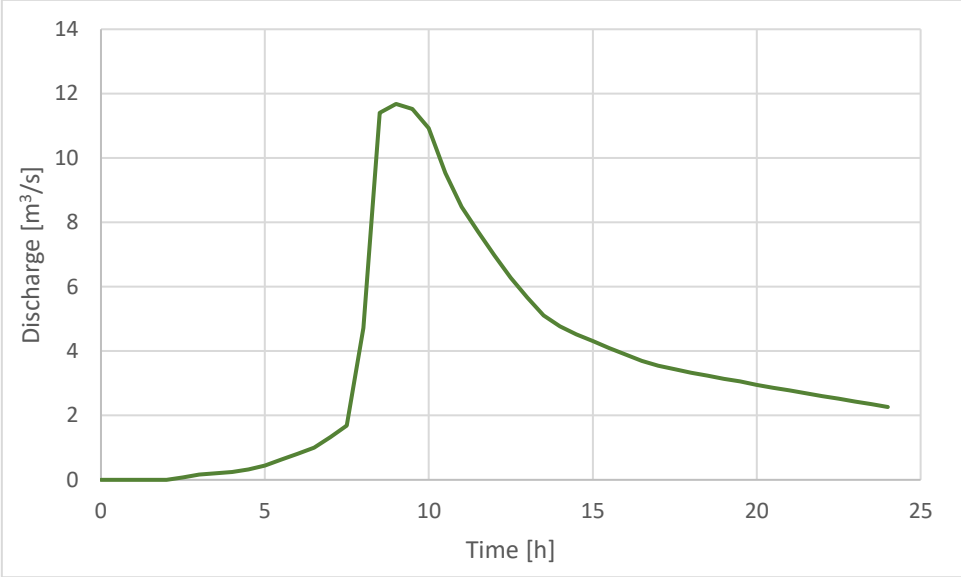
Figure 4.2: Input hydrograph for the sensitivity analyses
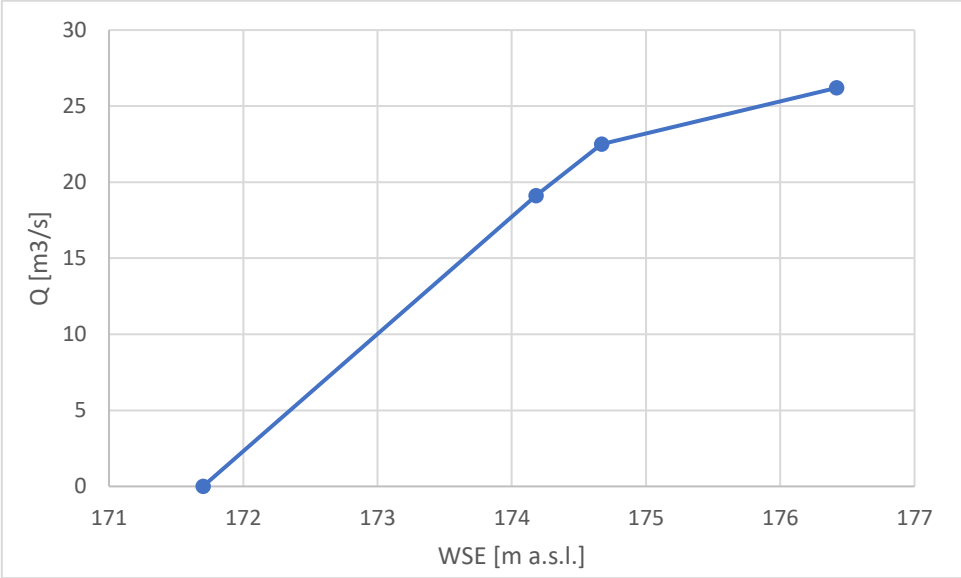
Figure 4.3: Rating curve for the sensitivity analyses

4.1. Sensitivity analysis for the roughness definition

4.1.1. Introduction

This subchapter describes the different models that were defined in order to study the influence of the roughness definition on the results. Specifically, the Manning's coefficient (n) along the riverbed was always considered equal to 0.03 s/m$^{1/3}$, while its definition in the outer part was

considered in four different ways, also depending on how buildings were represented (Figure 4.4).
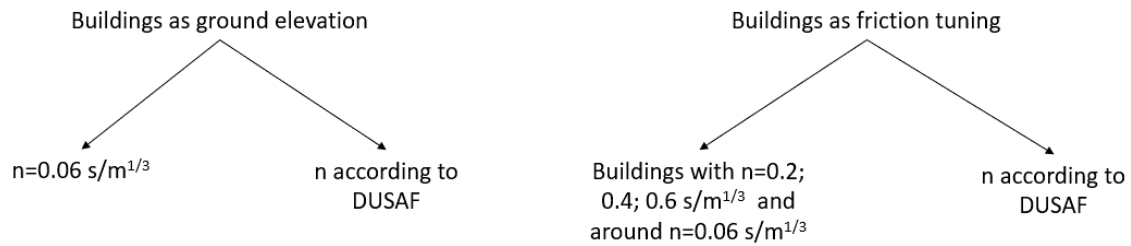
Figure 4.4: Different considered representations of the roughness

Since for one of the two models in which the buildings have been considered as friction tuning three different values of the Manning's coefficient were assigned to them, in total six analyses have been performed. Table 4.1 shows how these simulations have been called, as well as some of their main characteristics, such as the used computational time step and the resulting percentage error.

Simulation	n buildings $[s/m^{1/3}]$	n around $[s/m^{1/3}]$	Δt	Volume error [%]
0	-	0.06	5 sec	5.31
1	-	DUSAF	5 sec	2.78
2	0.2	0.06	5 sec	7.59
3	0.4	0.06	5 sec	7.01
4	0.6	0.06	5 sec	7.69
5	DUSAF		5 sec	3.70

Table 4.1: Characteristics of the different simulations

Simulation 0 corresponds to the base simulation, namely the one described in Chapter 3. In this simulation the buildings are represented with a height of 10 m with respect to the terrain and the Manning's coefficient of the floodplain is equal to 0.06 s/m$^{1/3}$. All the other simulations have been obtained by modifying this one.

In Simulation 1 the buildings are again considered as ground elevation with a height equal to 10 m. Instead, the Manning's coefficient of the model in the floodplain area is defined according to the Land Use [19]. The correspondence between different land uses and the roughness values (Table 4.2) is made within the HEC-RAS table [20]. It is important to highlight that in this simulation the roughness of the urbanized areas has to consider a possible average value without considering the buildings. Therefore, for highly urbanized and industrial areas, the value corresponding to rough asphalt is used (n = 0.016 s/m$^{1/3}$), while for sparsely urbanized areas the value of Manning's coefficient of pasture with no brush and short grass is used (n = 0.03 s/m$^{1/3}$). The resulting Land Cover layer implemented in HEC-RAS is depicted in Figure 4.5.

Code	Name	Manning's [s/m$^{1/3}$]	Classes of Manning
1112 1121 1122	Residential area	0.016	Rough asphalt (B.6.b)
1123	Scattered residential area	0.03	Pasture no brush, short grass (A.2.a.1)
11231	Farmsteads	0.035	Pasture no brush, high grass (A.2.a.2)
12111 12121 12122	Industrial, commercial settlements; Hospital settlements; Public and private service facilities	0.016	Rough asphalt (B.6.b)
12112	Agricultural production settlements	0.04	Field crops (A.2.b.3)
12124	Cemeteries	0.03	Pasture no brush, short grass (A.2.a.1)
1221	Road networks	0.016	Rough asphalt (B.6.b)
133	Yards	0.025	Earth with no vegetation (C.2.a.)
1411	Parks and gardens	0.03	Pasture no brush, short grass (A.2.a.1)
1412	Uncultivated green areas	0.05	Scattered brush, heavy weeds (A.2.c.1)
1421	Sports facilities	0.016	Pasture no brush, short grass (A.2.a.1)
1422	Campsites and tourist accommodation facilities	0.016	Pasture no brush, short grass (A.2.a.1)
2111 21131 21141 2115 2242	Simple arable land, open-field horticultural crops, open-field floricultural crops, family gardens; Other agricultural woodland	0.035	Row crops (A.2.b.2.)
2311 2312	Permanent grassland with pres/absence of tree and shrub species	0.05	Light brush and trees, in winter (A.2.c.3.)
31111 31121 3113 31312	Low/medium/high density coppice-governed broadleaf forests; Riparian formations; Tall shrub forests	0.1	Heavy stand of timber, few down trees, little undergrowth, flow below branches (A.2.d.3.)
314 3241 3242	Recent reforestations, Scrublands with significant presence of tall shrub and tree species, in abandoned areas	0.06	Cleared land with tree stumps heavy sprouts (A.2.d.2)
411	Vegetation of inland wetlands	0.15	Dense willows, summer, straight (A.2.d.5)
511	Riverbeds and artificial watercourses	0.03	Clean, straight, full, no rifts or deep pools (A.1.a.)

Table 4.2: Manning's coefficient values according to land uses (Simulation 1)
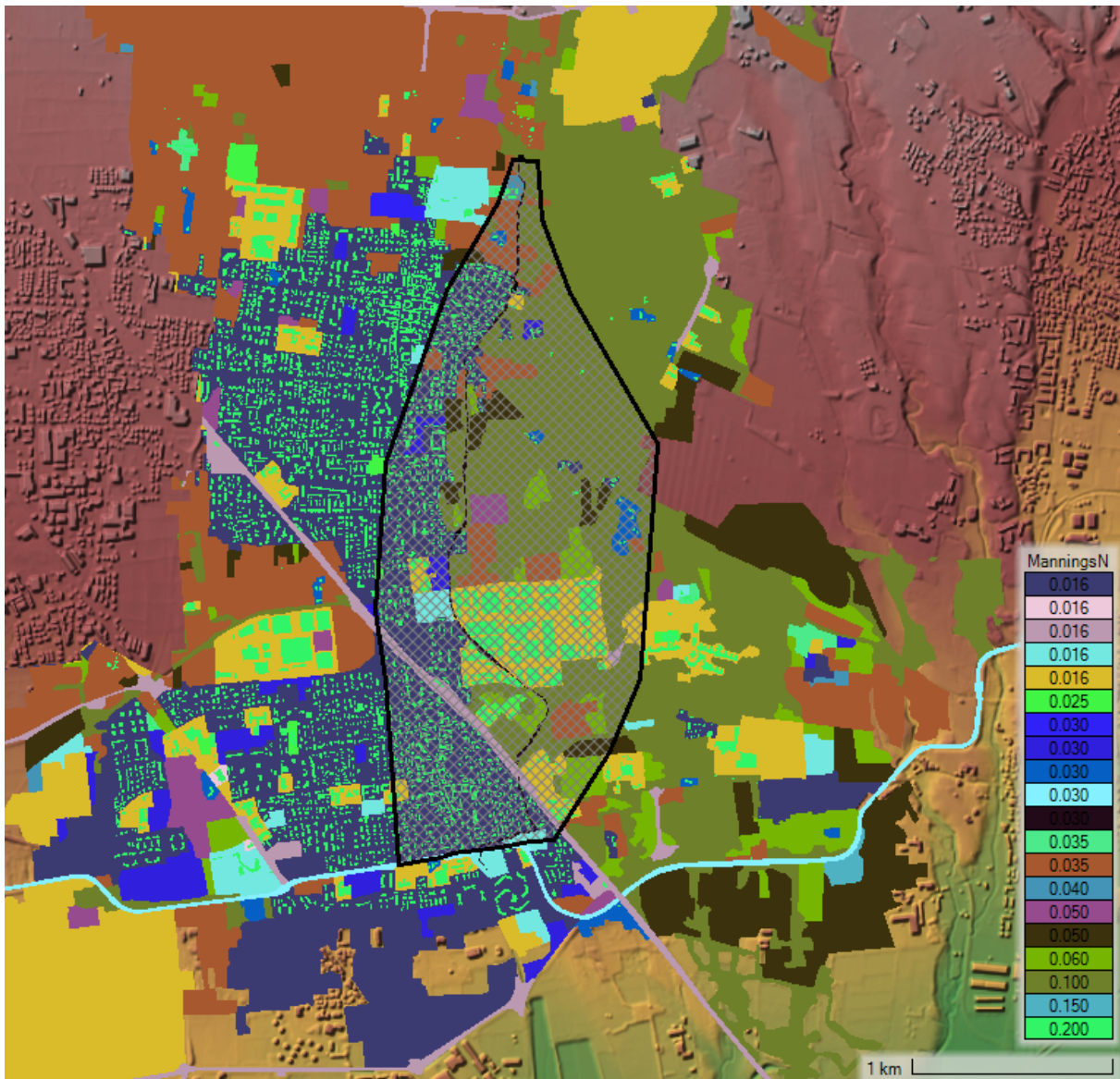
Figure 4.5: Land Cover layer in HEC-RAS with Manning's coefficient values (Simulation 1)

In Simulations 2, 3 and 4 the footprints of the buildings are considered as areas characterized by very high Manning's coefficient values, being respectively equal to 0.2, 0.4 and 0.6 $s/m^{1/3}$. The decision to use three different roughness values for the urban areas stems from the objective of understanding also if this has an important influence on the final results. Instead, the Manning's coefficient value of the floodplains is always considered equal to 0.06 $s/m^{1/3}$.

Finally, Simulation 5 uses again increased roughness for entire urban areas, but the values of the Manning's coefficient are in this case defined according to the Land Use. However, the consideration of entire urban areas leads to Manning's coefficient values much higher than those for Simulation 1 (Table 4.3); again, the *n* values have been identified through another table provided in the HEC-RAS manual [21].

Code	Name	Manning's [s/m$^{1/3}$]	Classes of Manning
1112 1121 1122	Residential area	0.16	Developed, high intensity
1123	Scattered residential area	0.09	Developed, Low intensity
11231	Farmsteads	0.04	Developed, Open Space
12111 12121 12122	Industrial, commercial settlements; Hospital settlements; Public and private service facilities	0.09	Developed, Low intensity
1422	Campsites and tourist accommodation facilities	0.04	Developed, Open Space

Table 4.3: Manning's coefficient values according to land uses (Simulation 5)

4.1.2. Results

Once the results from the simulations are obtained, some important comparisons can be performed. First, the extensions of the different flooded areas are compared (Table 4.4). It is important to highlight that the flooded area has been obtained as shown in equation (4.1):

$$Flooded\ Area = Wet\ Area - Area\ Flooded\ Buildings \qquad (4.1)$$

Simulation	Wet Area [m^2]	Area Flooded Buildings [m^2]	Flooded Area [m^2]
0	308513	-	308513
1	307410	-	307410
2	342127	56609	285518
3	341922	56567	285355
4	343597	56653	286944
5	293030	42329	250701

Table 4.4: Comparison of the values of the flooded areas

To make the comparison more consistent, the flooded areas for the simulations in which the buildings are considered as friction tuning have been determined by subtracting the surface of the flooded buildings from the total wet area returned by a simulation. Some important considerations that can be drawn from Table 4.4 are that when the buildings are considered as ground elevation, apparently there is not a significant influence on how the roughness is defined in the floodplains (since Simulations 0 and 1 return very similar flooded areas). In addition, it can be noticed that the Manning's coefficient value assigned to the buildings does not influence a lot the flooded area (since Simulations 2, 3 and 4 have a very similar extension of the flooded areas). Simulation 5 has a flooded area appreciably smaller than those of other simulations, which is probably because all the residential and industrial zones have a high roughness, thus reducing the velocity of water and therefore its expansion. Figure 4.6, Figure 4.7 and Figure 4.8 provide a visual interpretation of the comparison of the flooded areas for simulations 0, 1, 2 and 5. In these figures it has been decided to put the results of Simulation 0 in the background (also because it is the one with the larger flooded area) and to skip Simulation 3 and 4 since, as previously said, their results are almost identical to the one of Simulation 2.
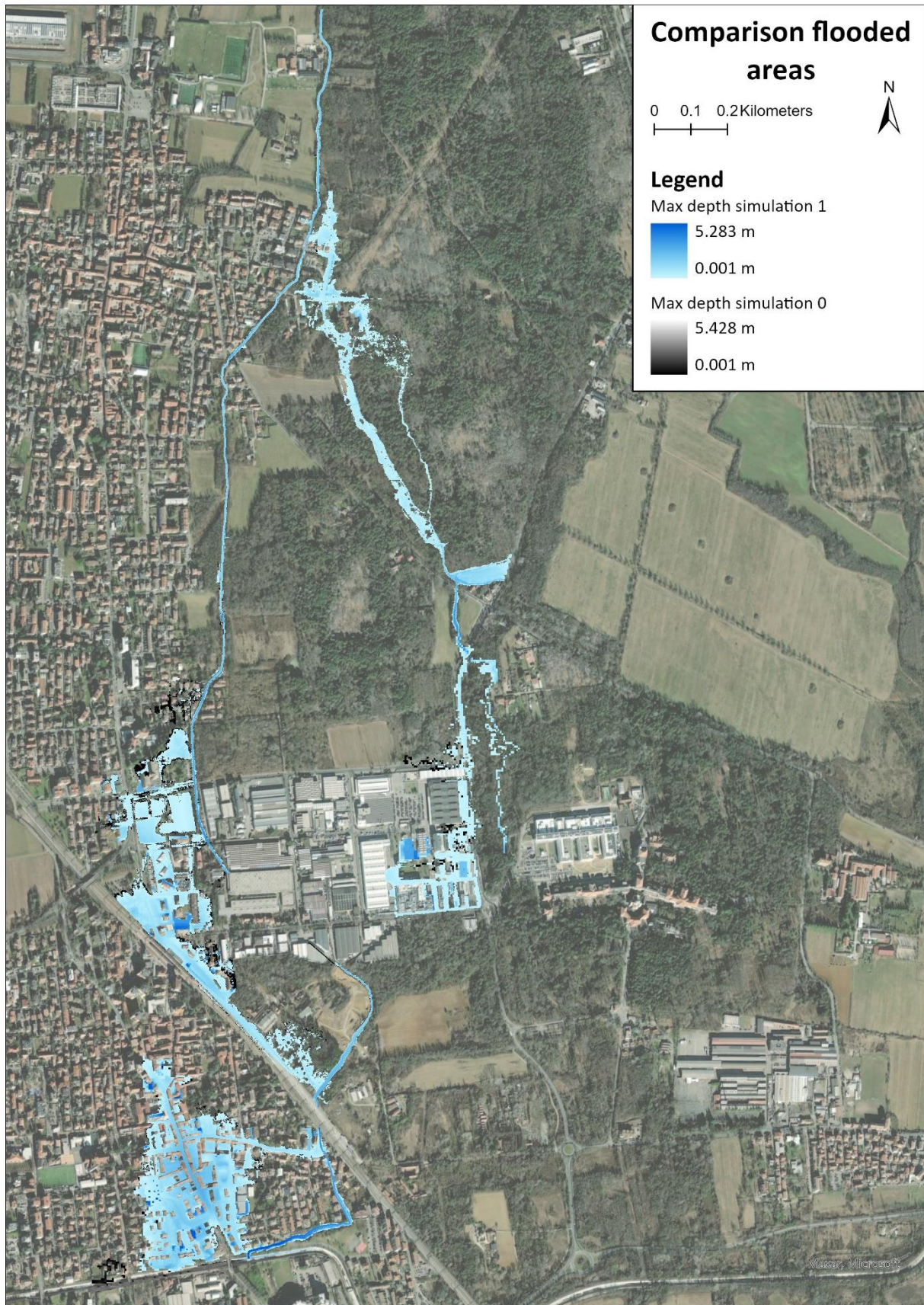
Figure 4.6: Flooded areas Simulation 0 vs Simulation 1
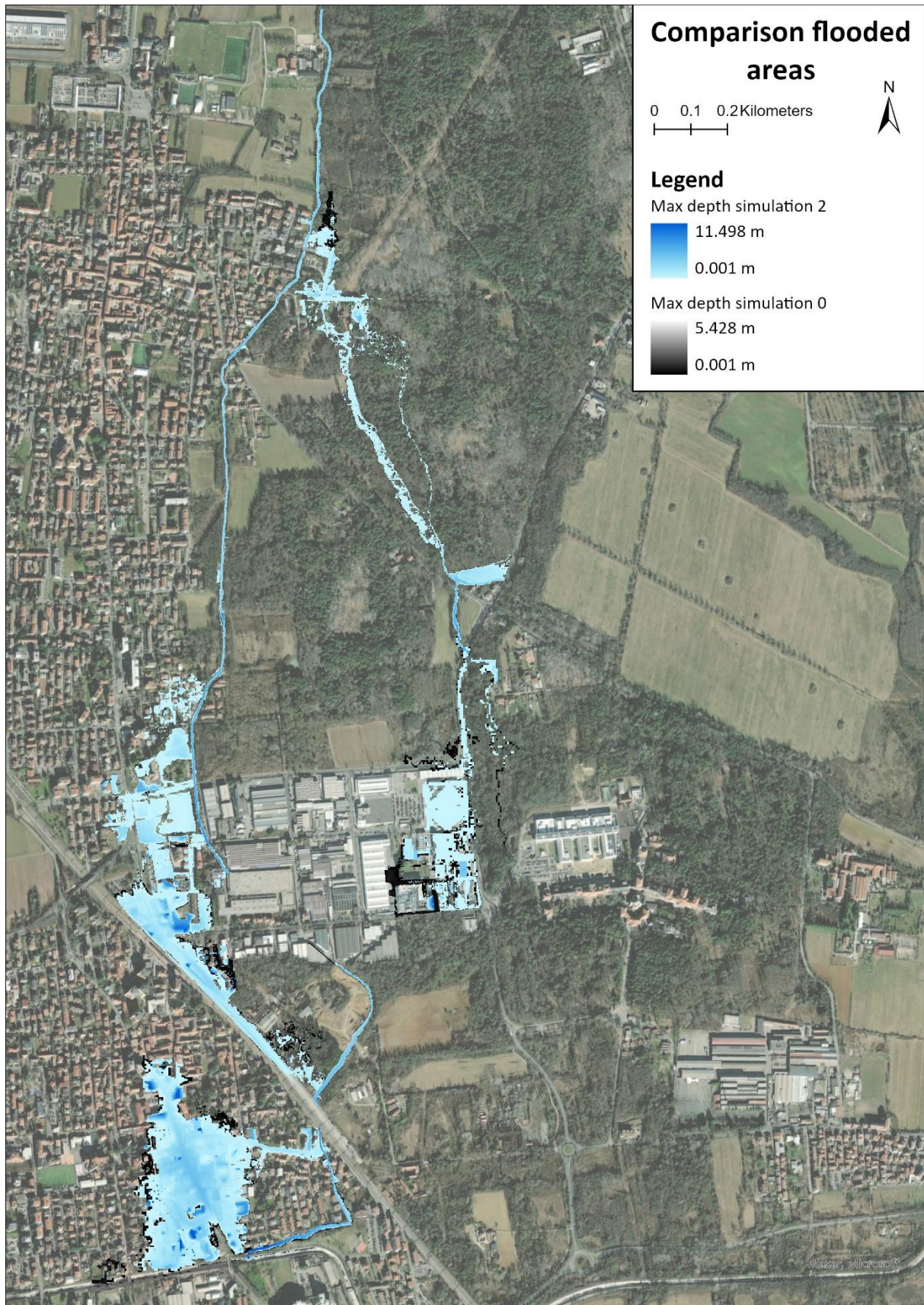
Figure 4.7: Flooded areas Simulation 0 vs Simulation 2
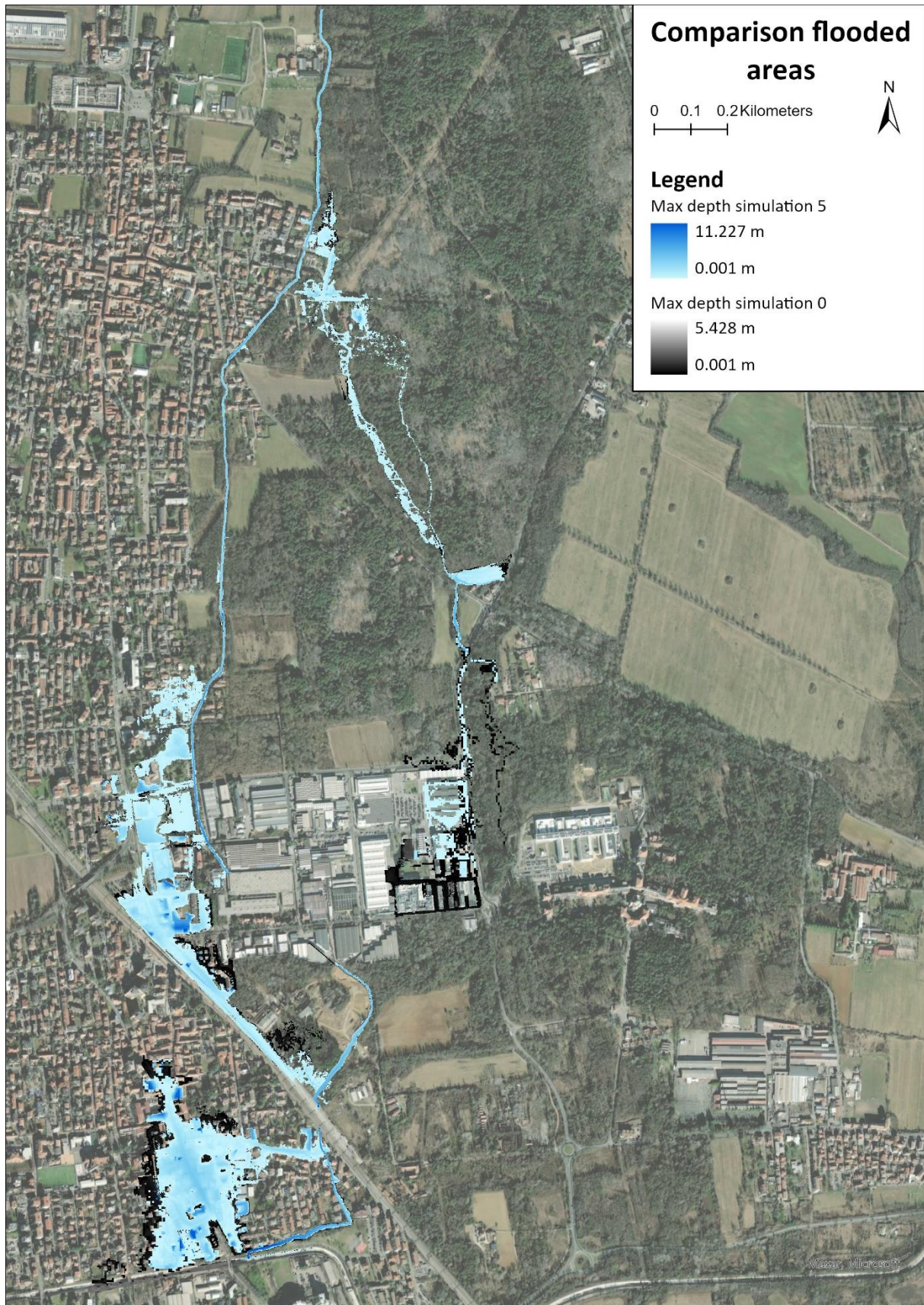
Figure 4.8: Flooded areas Simulation 0 vs Simulation 5

Then, a comparison between the different water depths and velocities obtained has been also performed. In order to do that, the difference has been computed between the values of these two parameters obtained in the raster of Simulation 0 with respect to all the rasters of the other Simulations performed (Table 4.5).

Minus	N° simulation first raster	N° simulation second raster
1	0	1
2	0	2
3	0	3
4	0	4
5	0	5

Table 4.5: Description Minus

In the following pages, the obtained results are reported (from Figure 4.9 to Figure 4.18), as listed in Table 4.6.

Minus	Depth	Velocity
1	Page 103	Page 104
2	Page 105	Page 106
3	Page 107	Page 108
4	Page 109	Page 110
5	Page 111	Page 112

Table 4.6: Organization of the representation of the results

Figure 4.9: Minus depth 1

Figure 4.10: Minus velocity 1

Figure 4.11: Minus depth 2

Figure 4.12: Minus velocity 2

Figure 4.13: Minus depth 3

Figure 4.14: Minus velocity 3

Figure 4.15: Minus depth 4

Figure 4.16: Minus velocity 4
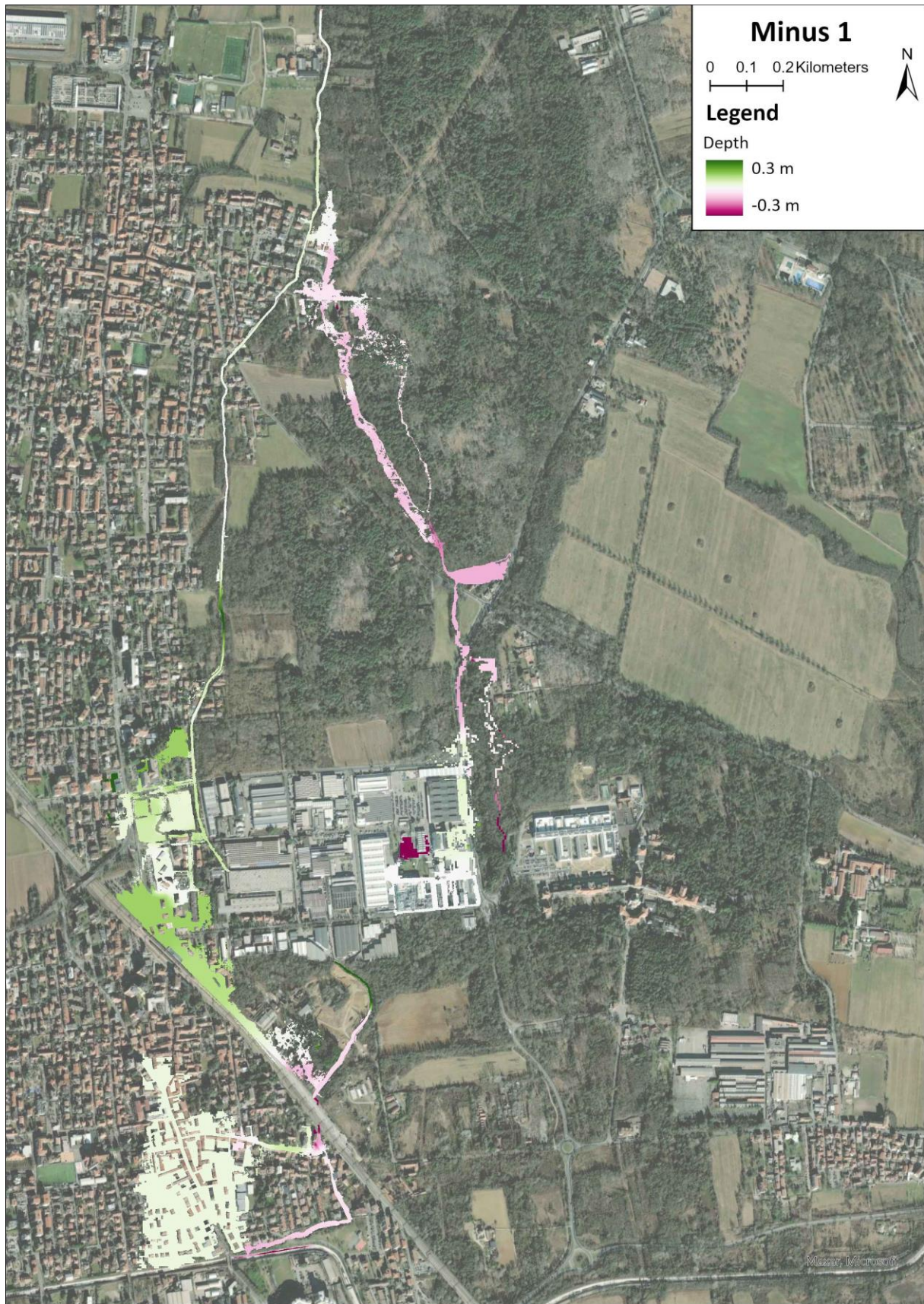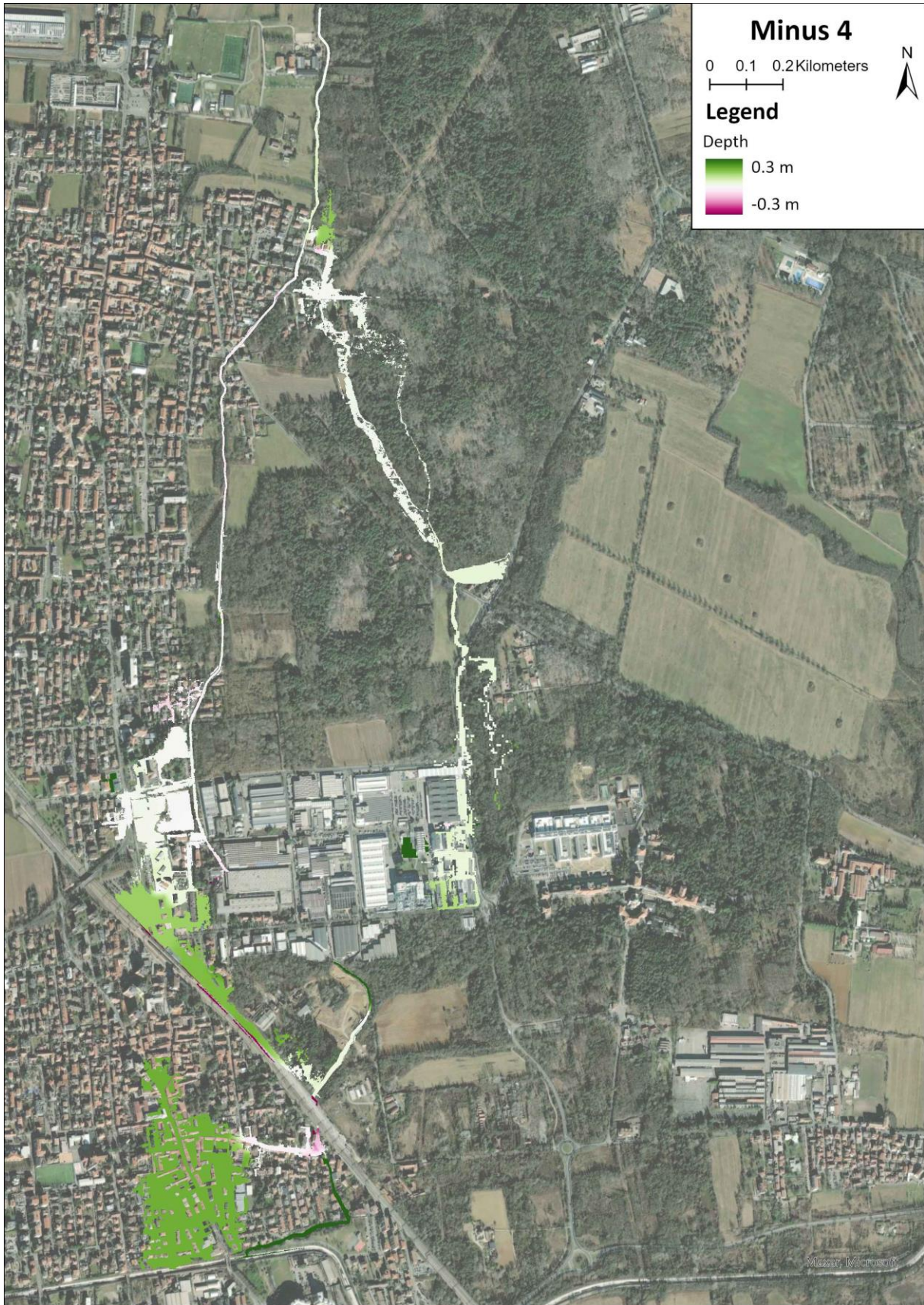
Figure 4.17: Minus depth 5

Figure 4.18: Minus velocity 5

For what concerns the Minus 1 analysis, the results for both the water depth and the velocity follow reasonable expectations. Indeed, in correspondence of regions where the Manning's coefficient has been increased (e.g.: forest) an increase in the water depth and a decrease in the velocity have been detected. Instead, the opposite has been obtained for regions with smaller roughness (e.g.: urban settings). Figure 4.9 and Figure 4.10, indeed, neatly separate the first, leftward outflow and the second, rightward outflow areas.

As far as Minus 2, 3 and 4 analyses are concerned, also in this case it can be noticed that different values of roughness given to the buildings do not lead to particularly different results. Instead, by analysing the maps of the differences, it can be noticed that, as expected, both the water depth and the velocity do not present many differences with respect to Simulation 0 (the biggest differences are in the bottom urban areas, for which a clear explanation cannot be provided). In addition, a very interesting aspect that can be highlighted is that in Simulations 2, 3 and 4, even if they can correctly estimate the amount of water that can be stored in buildings during flood events, the results in terms of flow directions are very different from those for the simulations where the buildings were incorporated into the geometry (example for Simulation 2 in Figure 4.20), since they do not correctly model the fact that in urban contexts water tends to move following the free spaces (as shown in Figure 4.19).
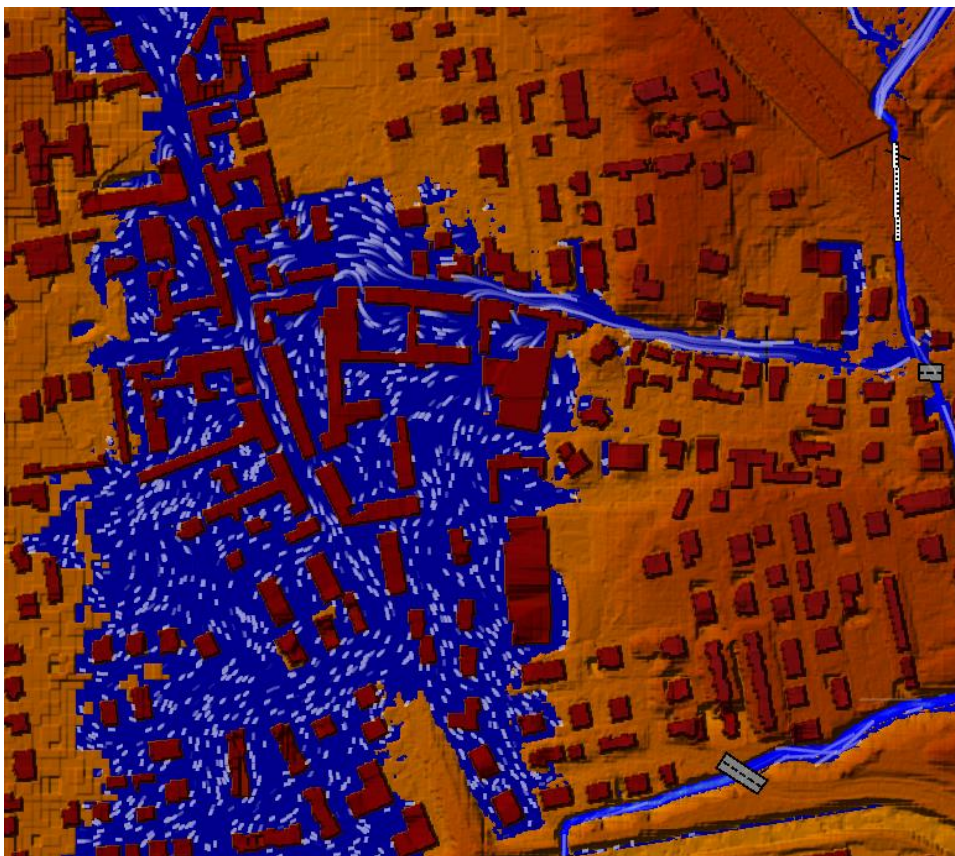

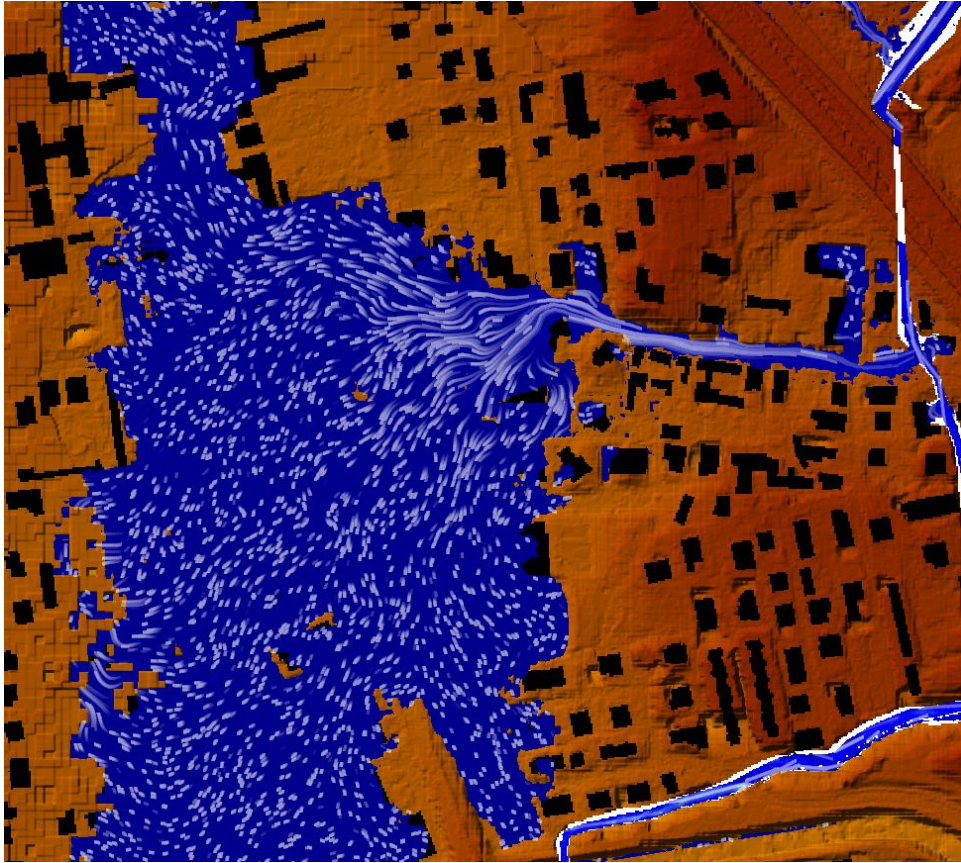*Figure 4.19: Velocity vectors in Simulation 0*

Figure 4.20: Velocity vectors in Simulation 2

Finally, the most significant differences arise from the Minus 5 analysis. In addition, it can be noticed that some unexpected results are detected since there is a decrease in the water depth in regions (e.g.: downstream urban area and where the forest is located) where the Manning's coefficient values have been increased.

However, it is important to highlight the fact that all the data extracted and the corresponding maps represent the maximum values of both the water depth and the velocity for each pixel. Therefore, since the maximum values can be reached at different times, it is also reasonable that sometimes, from the comparisons, some unexpected behaviours can be detected.

Figure 4.21 and Figure 4.22 show the cumulative frequency distributions of the computed differences for depth and velocity, respectively. It is once more confirmed that simulations 2, 3 and 4 gave almost identical results. Water depth differences between Simulations 0 and 1 are generally within ± 0.15 m, demonstrating a weak effect of the roughness parameterization of floodplain areas once the geometric irregularity due to buildings has been accounted for in the terrain model. Simulation 5 returns the largest differences compared to the base one since it suffers from two changes compared to Simulation 0 (building treatment and source for Manning's coefficient values).

114
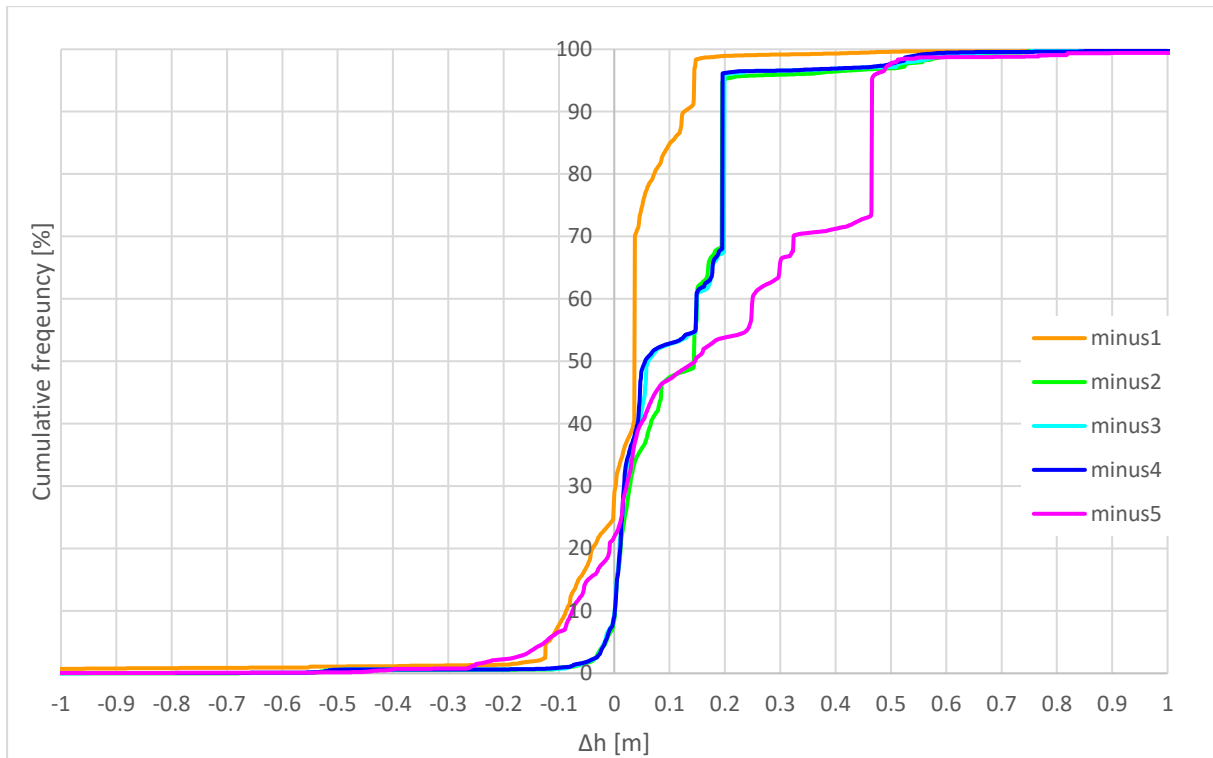
Figure 4.21: Cumulative Minus depth

Figure 4.22: Cumulative Minus velocity
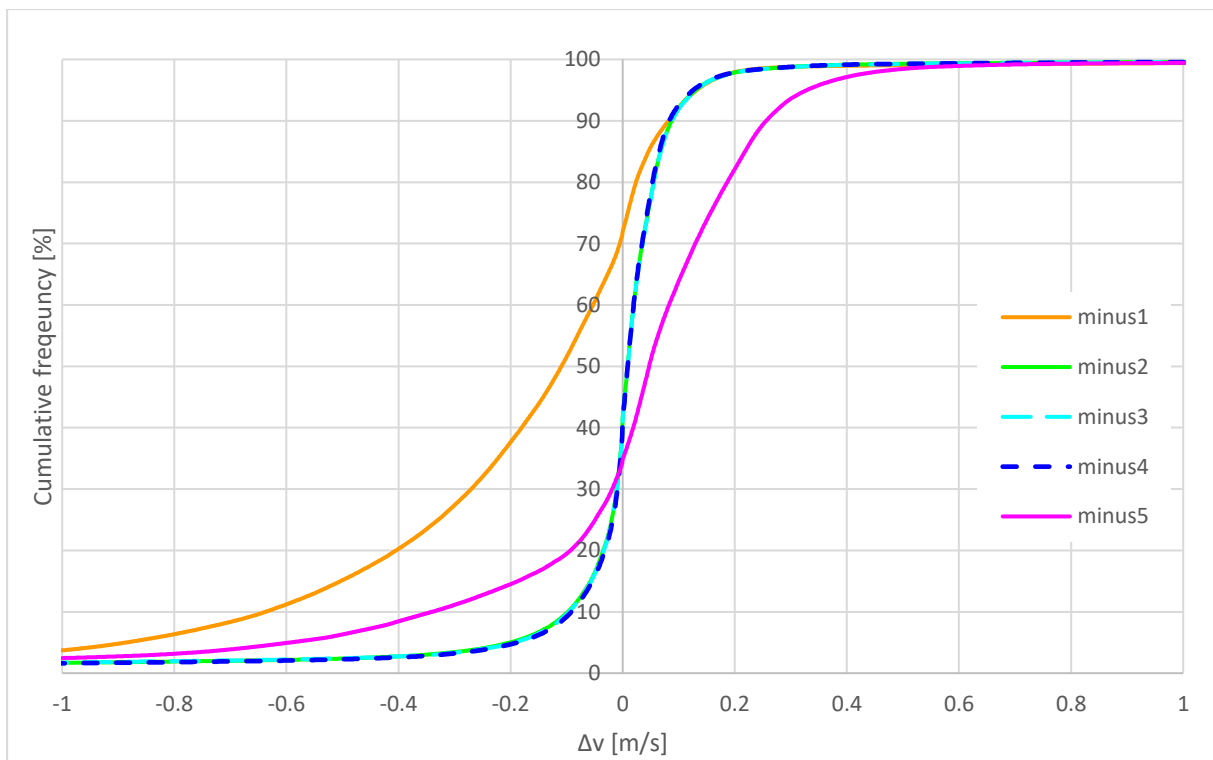
Figure 4.21 points out the fact that the base Simulation tends to return higher values of water depth (with respect to all the other Simulations), since all the cumulative curves of the Minus analyses are mostly on the right-hand (i.e.: positive) part of the graph. Instead, Figure 4.22 shows that for what concerns the velocities the situation is more equilibrated. Specifically,

while in Simulations 2, 3 and 4 the higher and lower velocities with respect to Simulation 0 tends to be the same, it can be noticed the highest velocities have been detected in Simulation 1 while the lowest in Simulation 5. These results seem to be coherent since in Simulation 1 all the urbanized areas are characterized by very low Manning's coefficient values (either 0.016 or 0.03 $s/m^{1/3}$, as shown in Table 4.2), while in Simulation 5, since also the buildings are taken into account, the roughness in urban settings is much higher (mainly 0.16 $s/m^{1/3}$, as shown in Table 4.3).

Finally, an additional analysis has been made by comparing the hydrographs in some interesting cross-sections (usually right downstream or in correspondence to overflow regions, as highlighted in Figure 4.23). The results are reported from Figure 4.24 to Figure 4.28.
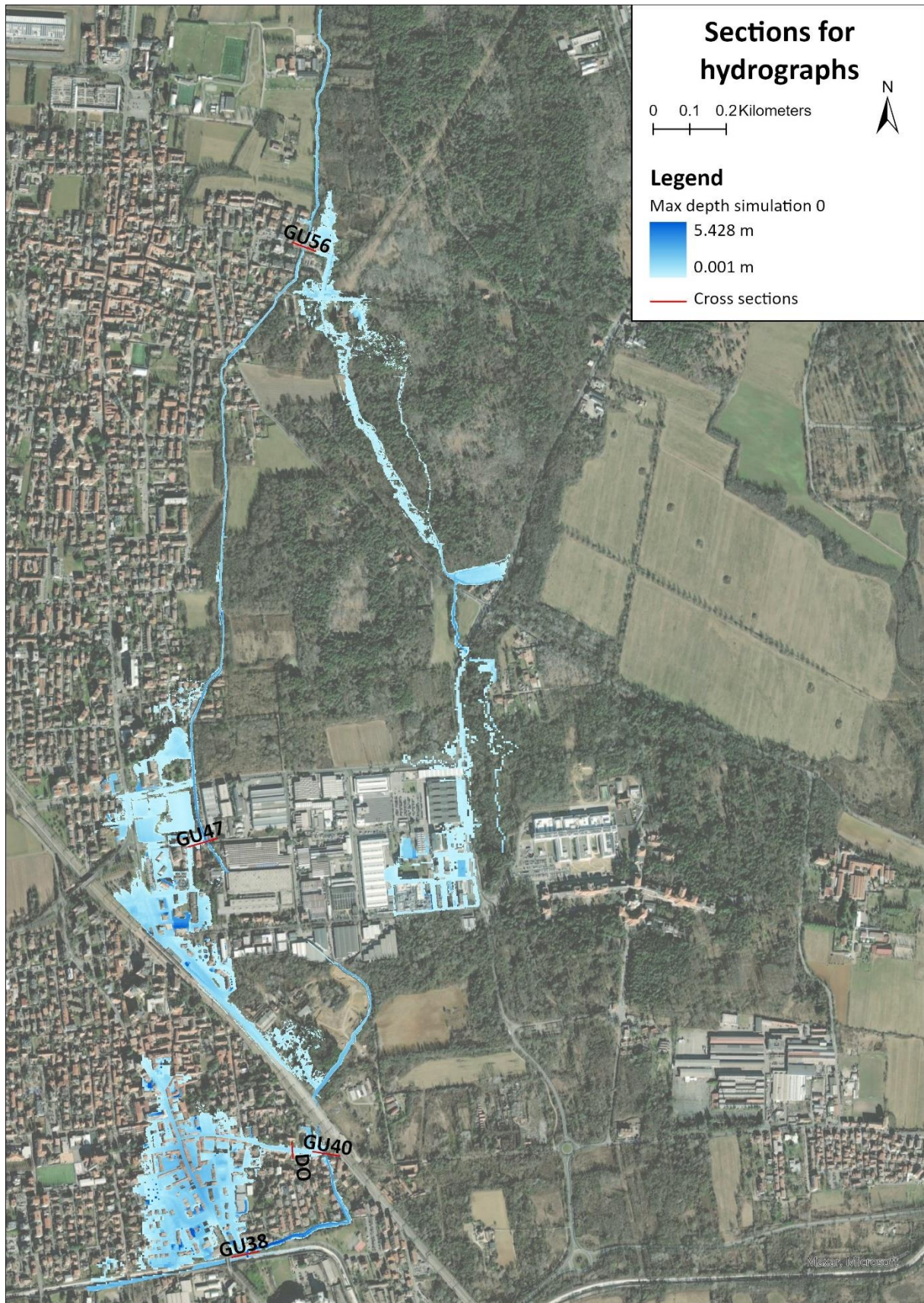
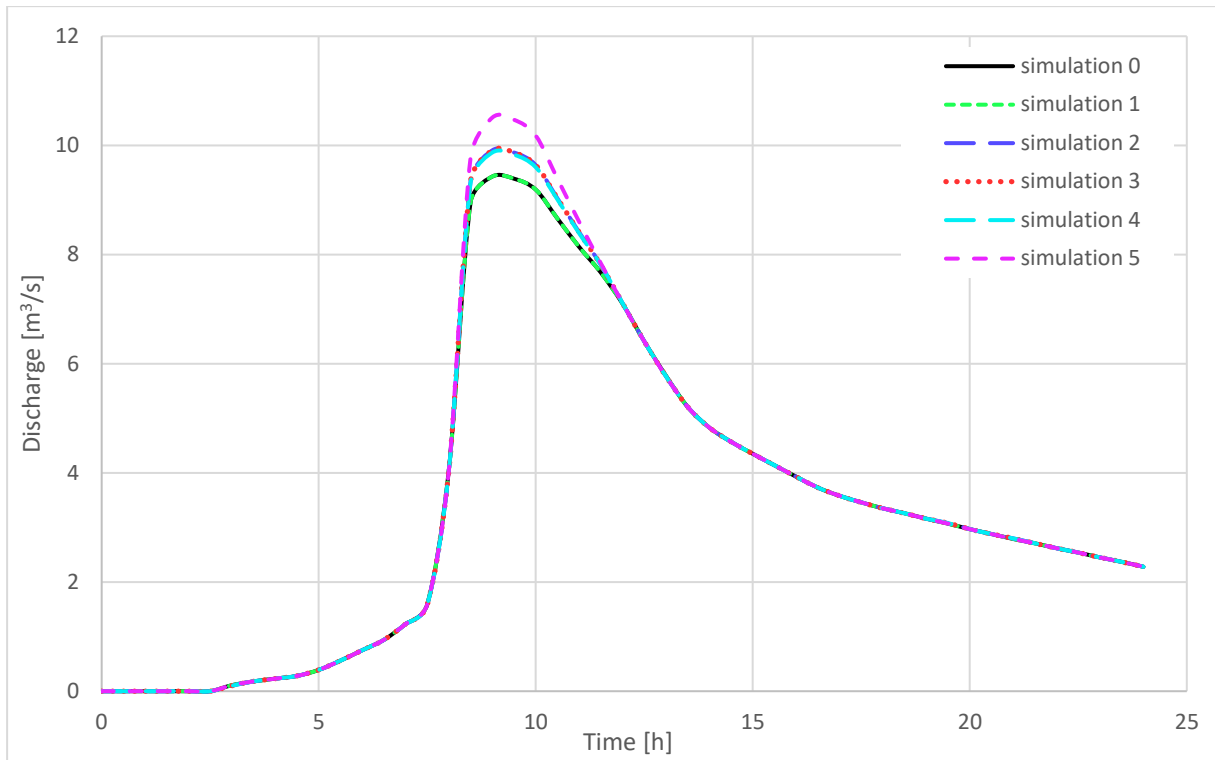*Figure 4.23: Sections for hydrographs*
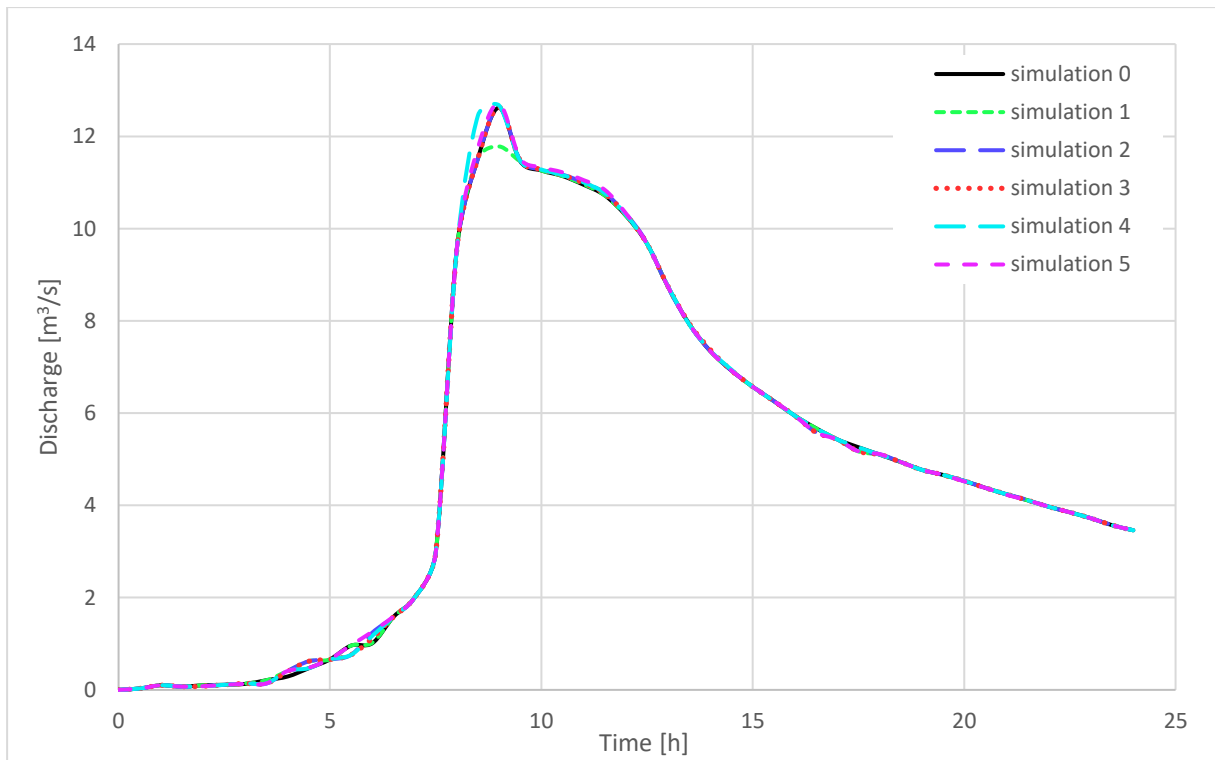
Figure 4.24: Hydrographs - section 56

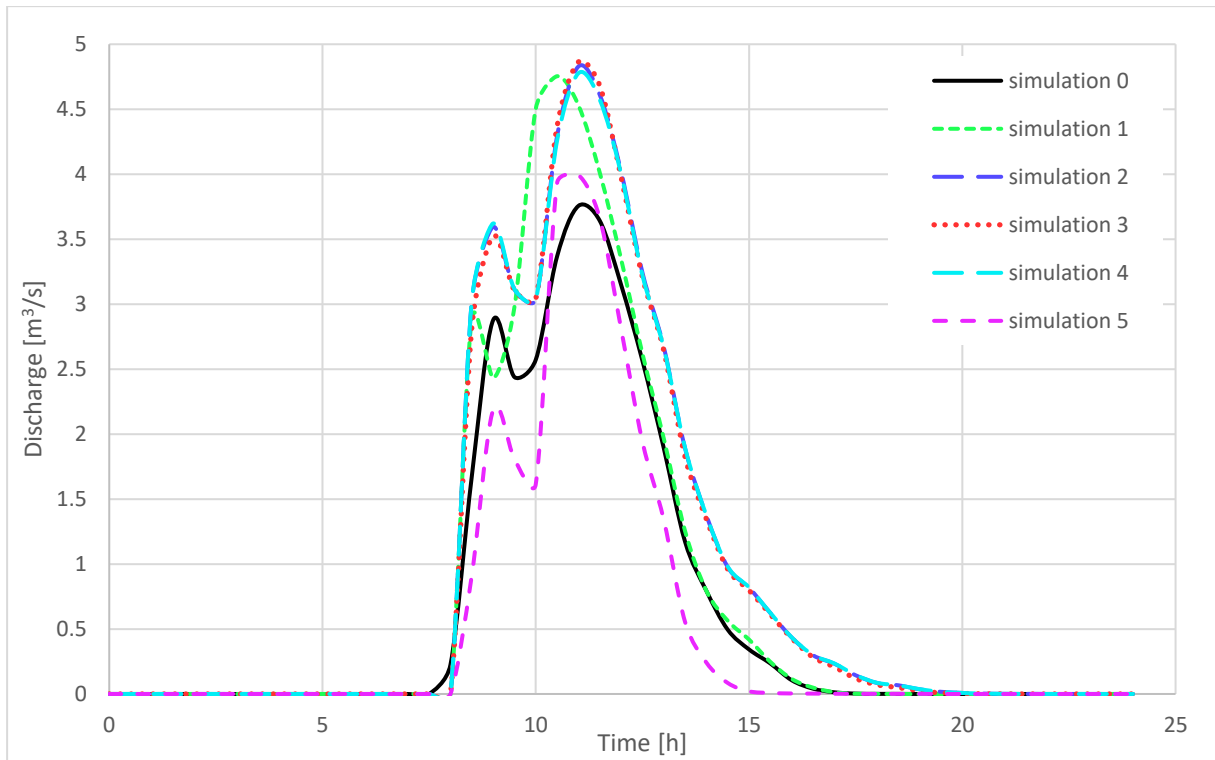*Figure 4.25: Hydrographs - section 47*

Figure 4.26: Hydrographs - Downstream flooded area
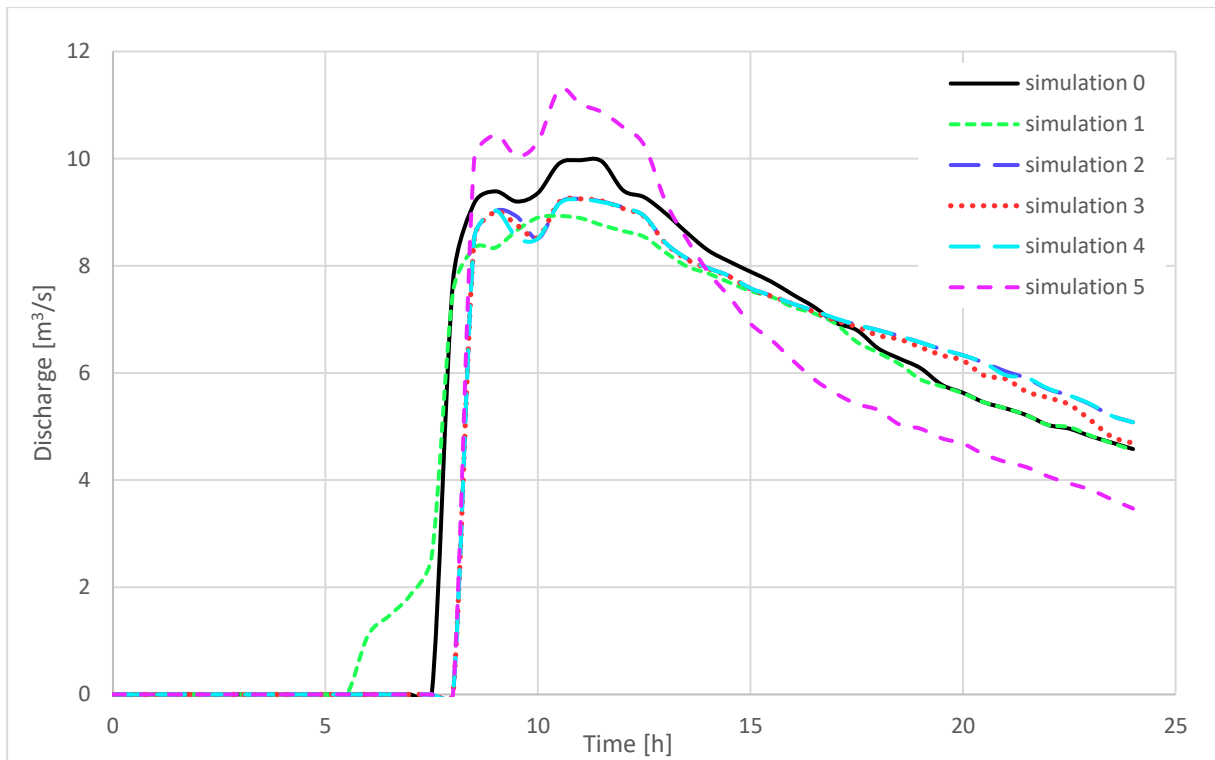

Figure 4.27: Hydrographs - section 40
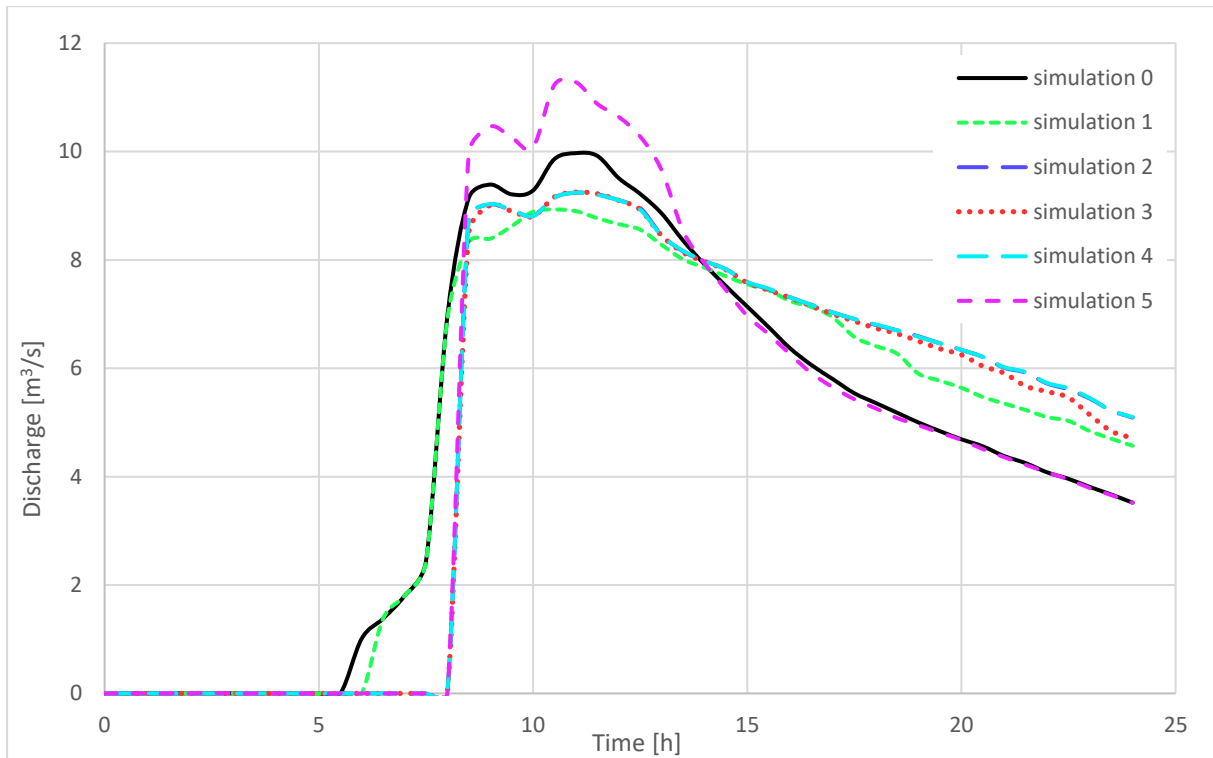
Figure 4.28: Hydrographs - section 38

From the analysis of the hydrographs it can be noticed that the first two out of three water overflows are probably characterized by very similar discharges in all the simulations, since the curves downstream of their locations are very similar between each other (Figure 4.24 and Figure 4.25). Instead, by analysing the hydrographs in correspondence of the third and last overflows (Figure 4.26), it can be noticed that here the discharges are slightly different and the smallest values are reached in Simulation 5, while the highest in Simulations 2, 3 and 4 (which are very similar also to Simulation 1). Finally, from the analysis of both the hydrographs right after this last flooded area and in correspondence of the Downstream BC, which is located in correspondence of the Canale Villoresi (Figure 4.27 and Figure 4.28), it can be noticed that here, as expected, the trend is exactly the opposite of the one detected where the overflow is located, since there is less water available to flow within the river. It can also be noticed that the shape of the hydrographs is always very similar for all the considered simulations.

4.2. Sensitivity analysis of time step and different equations

In this subchapter the influence of both the computational time step and the chosen set of equations is studied. To this aim, simulations were run for all the possible formulations embedded within HEC-RAS and using eight values of the time step, as shown in Table 4.7. The table also reports the running times and the obtained percentages of error on the volume. It is important to highlight that also in this case all the analyses were made with a cell size of 10 m and a refinement region with 3 m cells.

Delta t	DWE		SWE/ELM		SWE/EM	
	Error [%]	Time[h]	Error [%]	Time [h]	Error [%]	Time [h]
10	789537	0.75	Unstable	-	Unstable	-
6	4.189	0.45	Unstable	-	Unstable	-
5	4.473	0.51	Unstable	-	Unstable	-
4	3.181	0.71	Unstable	-	Unstable	-
3	0.252	0.72	Unstable	-	Unstable	-
2	9.195	1.16	1.477	1.89	Unstable	-
1	9.807	1.42	1.212	3.15	Unstable	-
0.5	8.401	5.78	0.795	5.93	Unstable	-

Table 4.7: Percentage of error and running time based on different time steps and equations

From Table 4.7 it can be noticed that the SWE/EM simulations always went unstable, therefore this set of equations would require either smaller computational time steps or a finer computational mesh in order to provide results. Instead, the SWE/ELM simulations provided results only for the three smaller computational time steps used. Since the DWE simulations always provided results (even if, when the time step was equal to 10 s, the error was so high that the simulation was considered meaningless), it can be concluded that SWE, as expected, require smaller time steps to become stable (or smaller grid size), and also that they take longer time to run. In addition, it can be noticed that, in general, the computational time step had an influence on the percentage of error on the volume. Furthermore, looking at the DWE, a time step of 3 s returned the smallest error (while for both the SWE this would be equal to 0.5 s or less). Of course, this optimal time step could be case-dependent and vary when running different models, since it also depends on the grid size, the size of the model, the Land Cover layer definition, and so on. Finally, it can also be noticed that, independently from the set of equations considered, when the computational time steps become very small, the running time starts to become very high (even if this does not necessarily correspond to obtaining a higher accuracy).

Also in this case a comparison between the extensions of the flooded areas has been performed. Table 4.8 highlights that, when the same set of equations is considered, the flooded areas do not change a lot by changing the computational time steps. Instead, the differences measured by considering different sets of equations highlight the fact that this factor influences significantly the obtained flooded areas.

Delta t [sec]	DWE	SWE/ELM
	Flooded Area [m^2]	Flooded Area [m^2]
10	-	-
6	313769	-
5	308513	-
4	308010	-
3	305322	-
2	308684	459187
1	309366	466838
0.5	309331	465570

Table 4.8: Flooded areas with different time steps and equations

Figure 4.29, Figure 4.30 and Figure 4.31. provide a visual interpretation of the comparison of the flooded areas by considering only the three smallest time steps and comparing each time the results obtained from the DWE and the SWE/ELM. In these figures, it has been decided to put the results obtained from the SWE/ELM in the background since they always returned larger

flooded areas. With respect to this, it is important to point out that in the bottom left-hand side of the figures, below the flooded area of the DWE (coloured in black), is almost always present also the flooded area of the SWE/ELM (coloured in blue), as it is demonstrated from Figure 4.32 to Figure 4.37 in which there are highlighted the flooded areas in common between the two sets of equations.
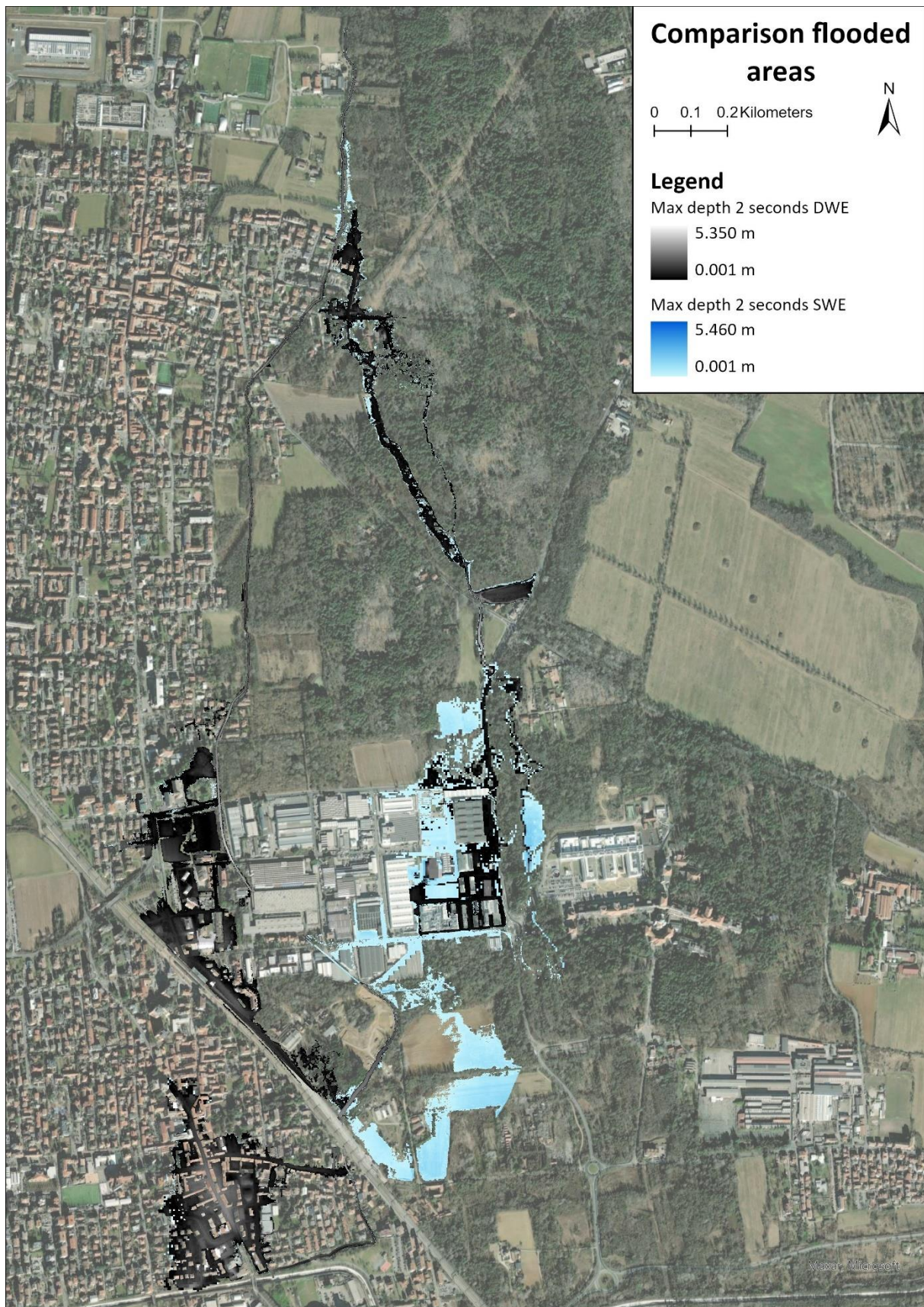
Figure 4.29: Flooded areas - 2 seconds DWE vs SWE/ELM
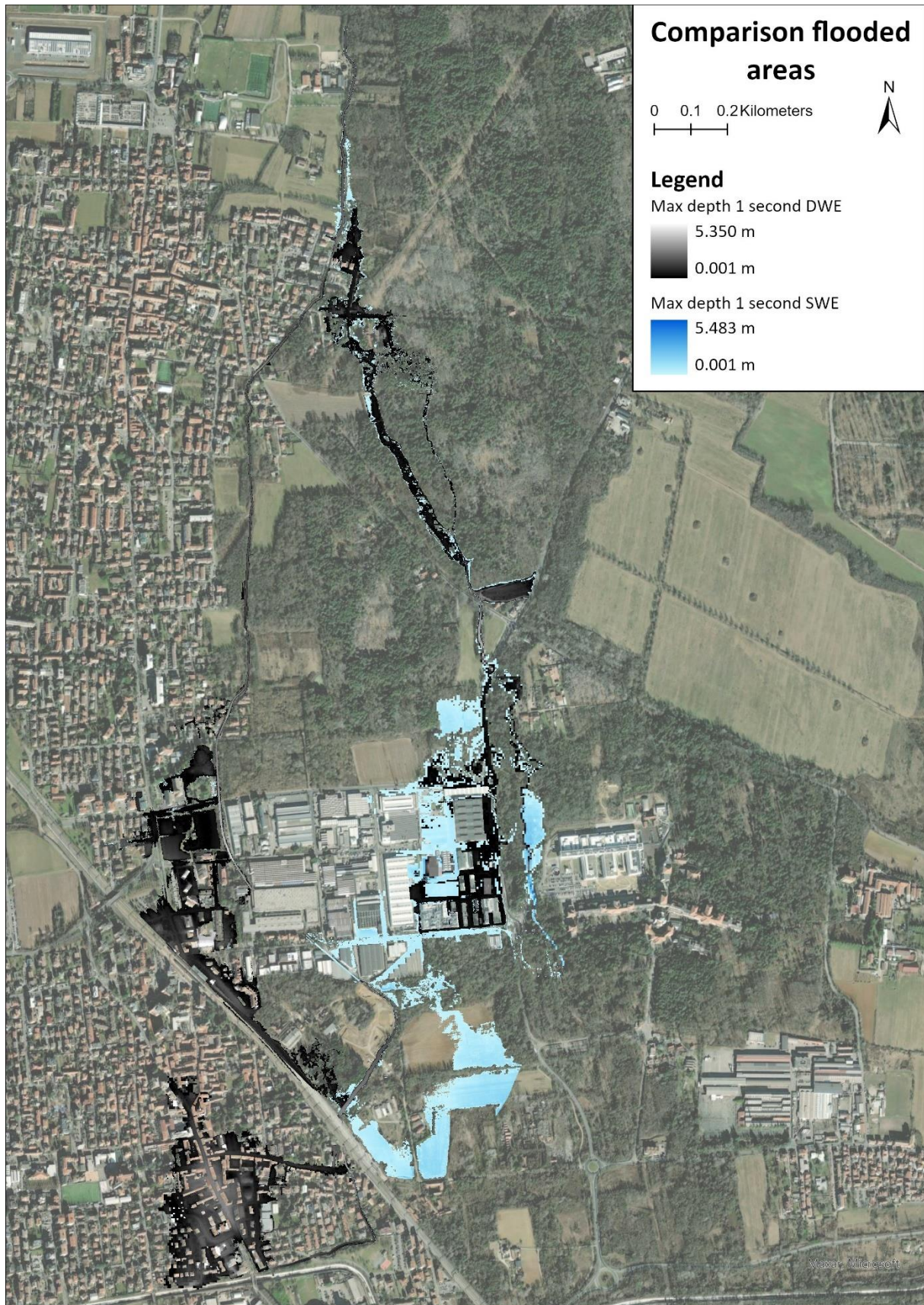
Figure 4.30: Flooded areas - 1 second DWE vs SWE/ELM
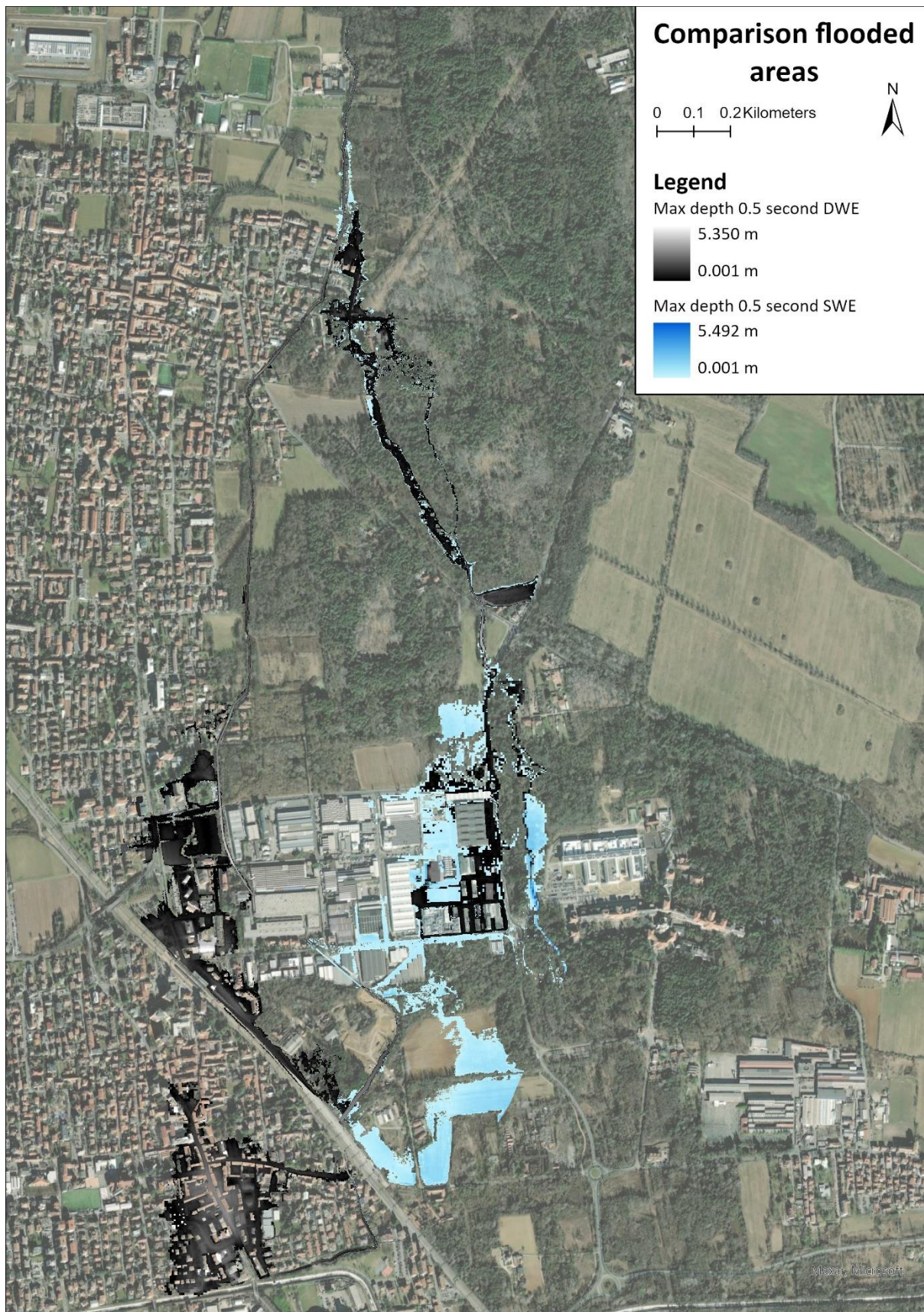
Figure 4.31: Flooded area - 0.5 second DWE vs SWE/ELM

125

Then, also a comparison between the different water depths and velocities obtained has been performed. Again, this analysis has been performed by computing the difference between the values of these two parameters obtained in the raster of the DWE with respect to those obtained in the raster of the SWE/ELM, considering only the three smallest time steps (i.e.: 2, 1 and 0.5 seconds) and the flooded areas which are in commons on the two formulations.

In the following pages, there are reported the obtained results of this analysis (from Figure 4.32 to Figure 4.37), which are presented as listed in Table 4.9.

Minus (DWE – SWE/ELM)	Depth	Velocity
2 seconds	Page 127	Page 128
1 second	Page 129	Page 130
0.5 seconds	Page 131	Page 132

Table 4.9: Organization of the representation of the results

Figure 4.32: Minus depth 2 seconds

Figure 4.33: Minus velocity 2 seconds

Figure 4.34: Minus depth 1 second

Figure 4.35: Minus velocity 1 second

Figure 4.36: Minus depth 0.5 seconds

Figure 4.37: Minus velocity 0.5 seconds

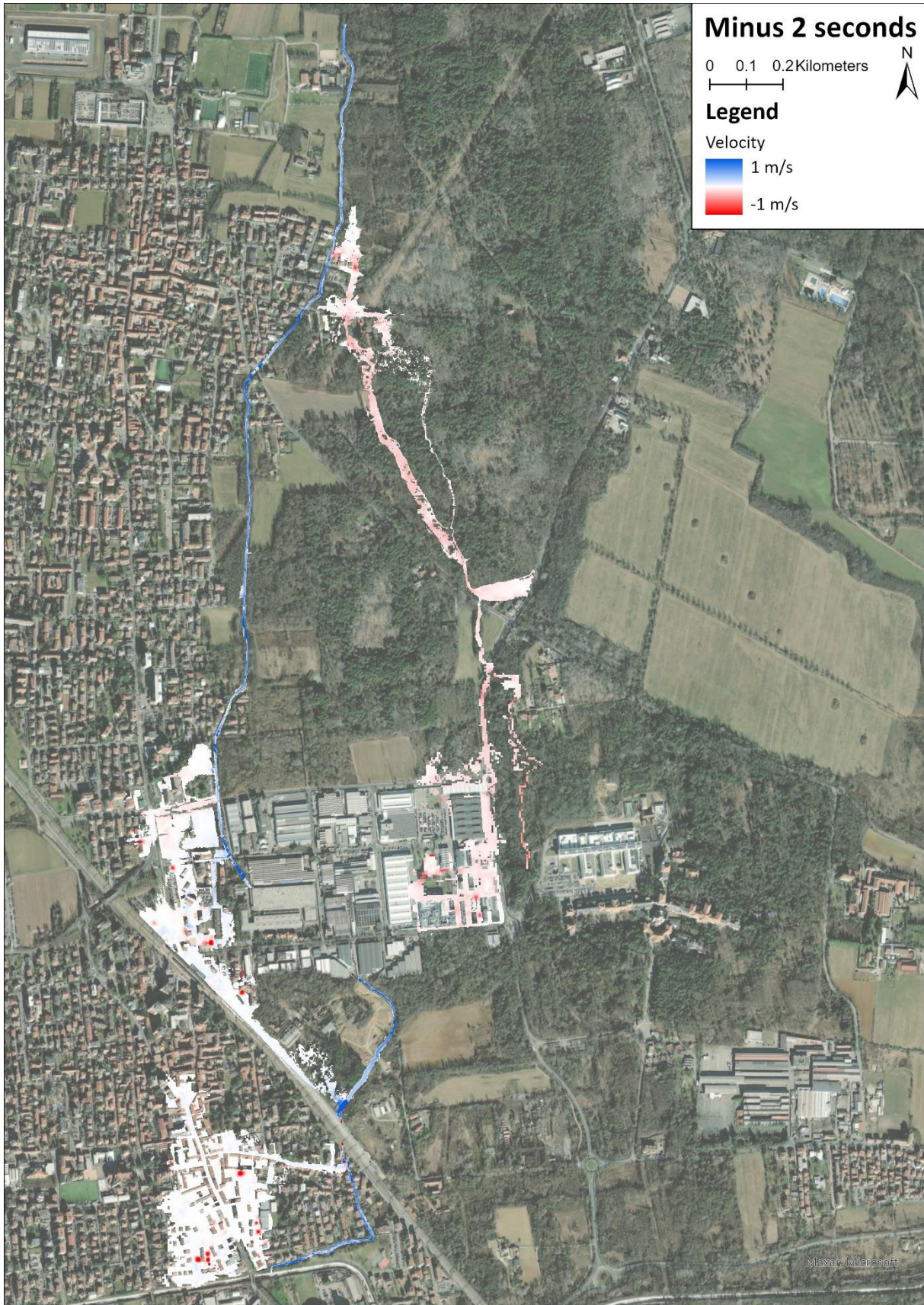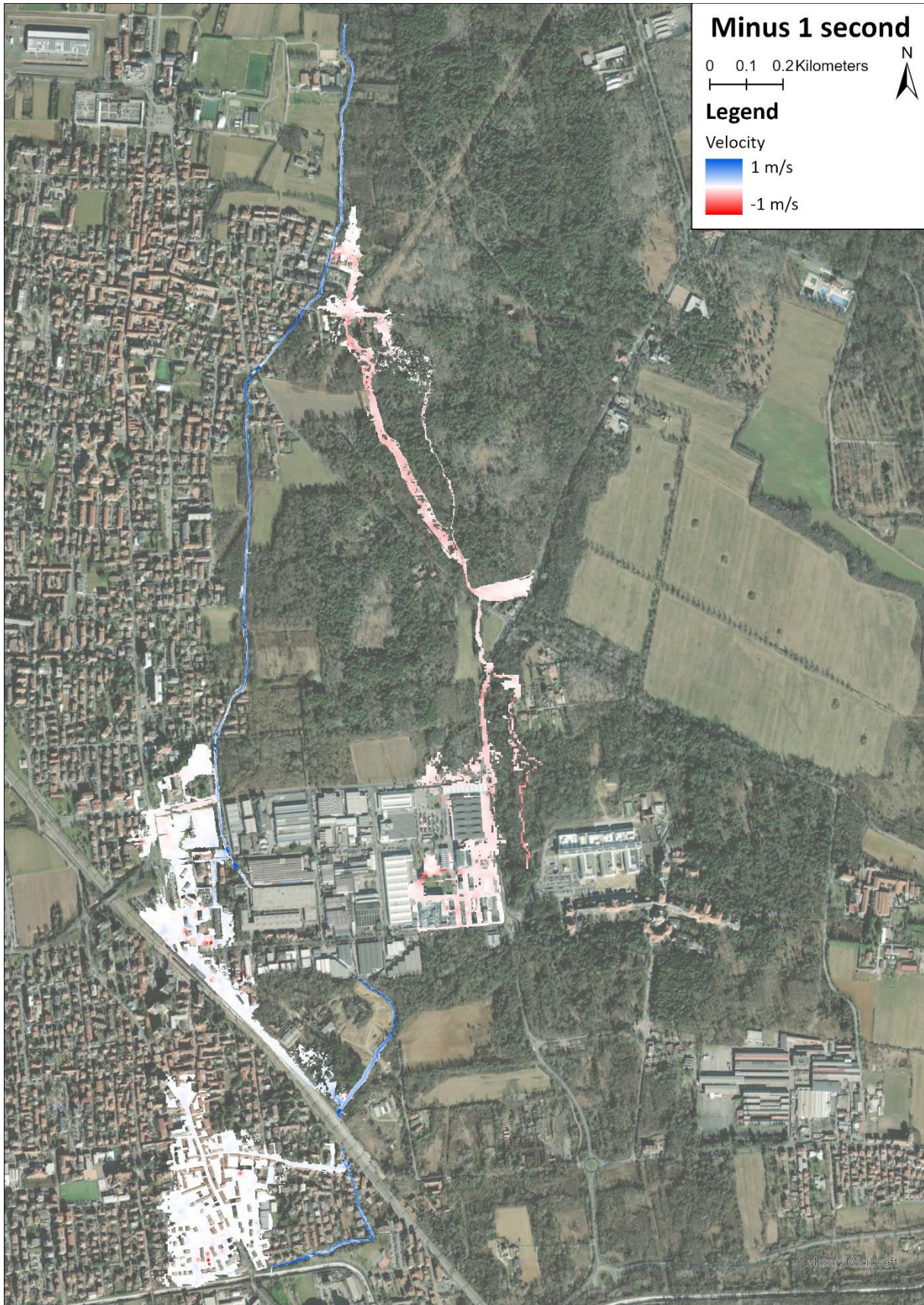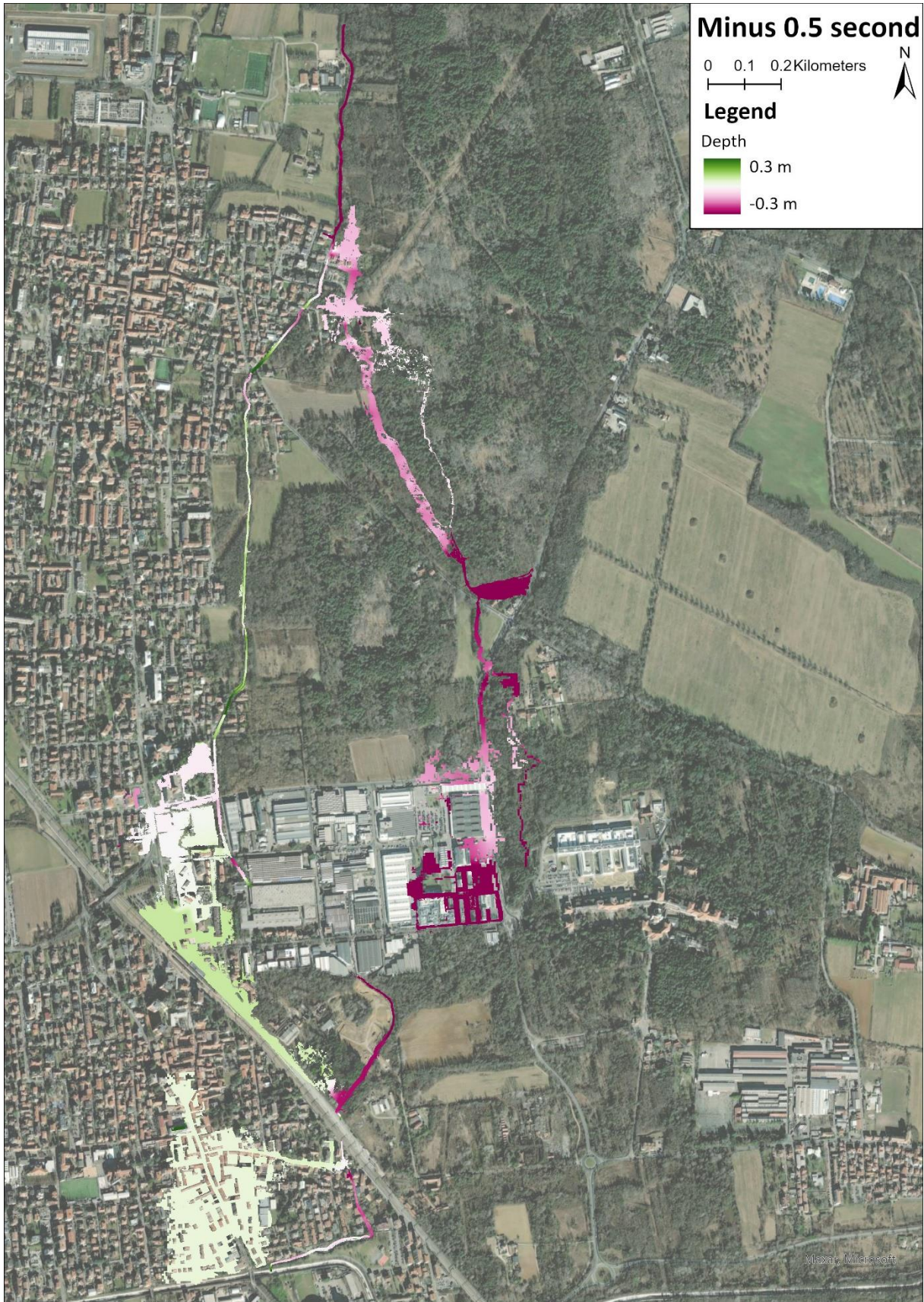From the analysis of the results, it can be noticed the tendency is that the SWE/ELM returns larger water depth with respect to the DWE (even if this trend becomes slightly less pronounced by considering smaller time steps). Instead, for what concerns the velocities there are no clear trends that can be highlighted from this analysis, even if it can be noticed that the differences in this parameter between the two formulations are very small. All these considerations are depicted in Figure 4.38 and Figure 4.39, which show the cumulative frequency distributions of the differences. Indeed, the cumulative curve of the depth difference (Figure 4.38) shows as the negatives values coming from the Minus analysis are larger with respect to the positive ones (even if the percentage of pixels corresponding to positive and negative differences are almost the same), meaning that SWE/ELM formulation tends to return higher water depth values. Generally, approximately 30% of the depth difference values are lower than -0.15 m, while almost no values are larger than 0.15 m. Figure 4.39 shows instead how the velocities of the two models are very similar since almost 90% of the velocity data present a difference which is comprised between -0.2 and 0.2 m/s. These figures also highlight the fact that different time steps lead to very small differences in the comparison between the two sets of equations analysed.
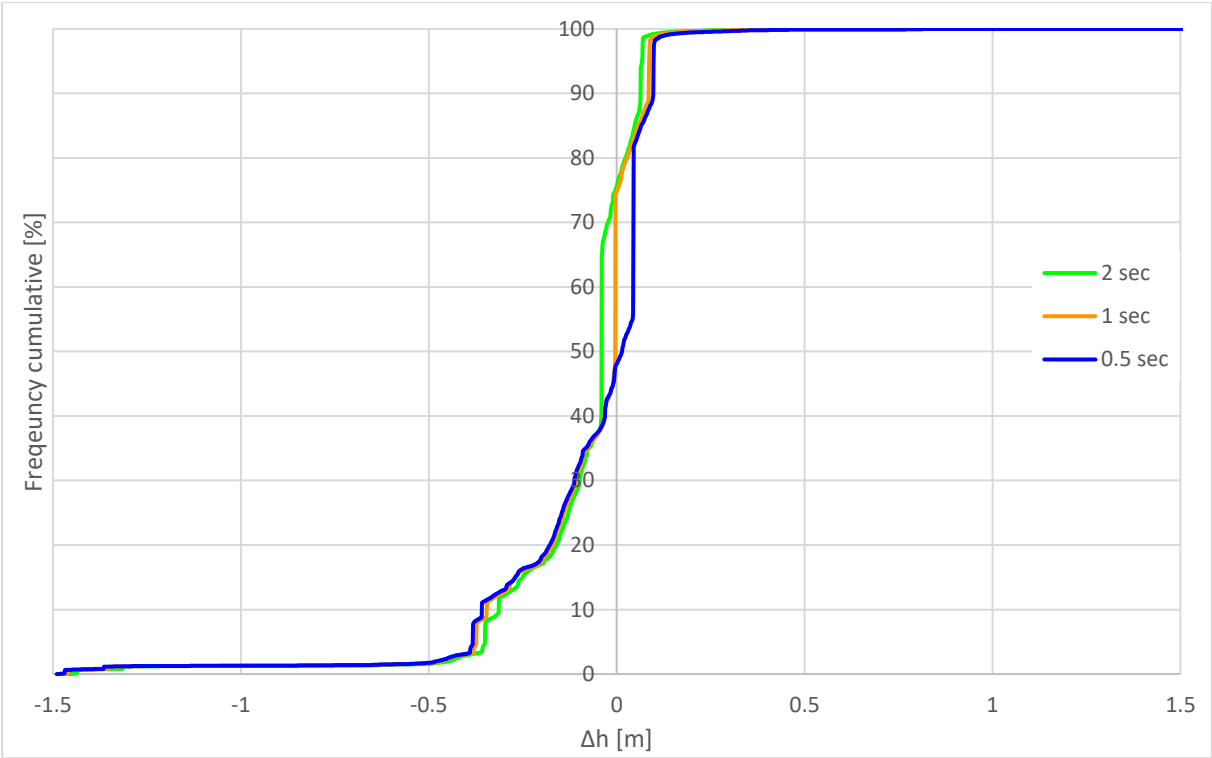

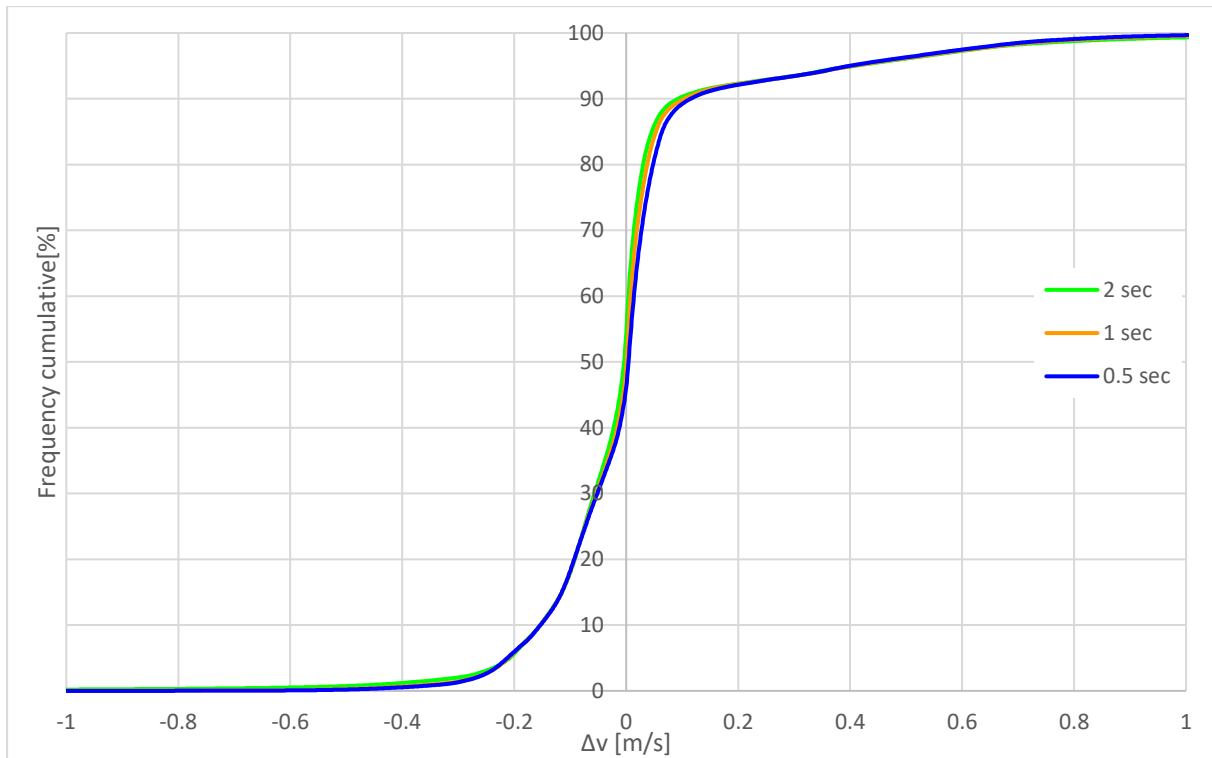*Figure 4.38: Cumulative Minus depth*

Figure 4.39: Cumulative Minus velocity

4.3. Influence of the grid size definition

A characteristic that was detected in the HEC-RAS software is that it traces the water surface elevation within a computational cell horizontally and, sometimes, this feature can lead to an overestimation of the flooded area. Indeed, in case there is a zone with a higher surface elevation (e.g. a levee) that crosses the central part of a cell, the water may be wrongly put outside of the mainstream thus creating also disconnections in the detected flooded area. Since this problem can occur apart from some specific cases, such as when there are sandbars within a river cell, and it may influence a lot the results, it is studied more in detail in this subchapter.

This is done by introducing a trapezoidal synthetic channel, characterized by a lateral expansion in its mid-course. The lateral expansion is separated from the main channel by an internal bank with limited width. In practice, this channel is constructed with the help of six sections. The shape of the first two and the last two sections is trapezoidal and is the same as the one of Section 1, while the two central sections are W-shaped and their profile is the same as the one of Section 3, as shown in Figure 4.40. The final model is characterized by a total length of the main channel equal to 60 m, and a length of the lateral expansion equal to 20 m. In addition, the bottom of the river always has a width of 3 m and its height is equal to 5 m for the external levees and 2.5 m for the internal levee of the W-shaped central region. The internal levee has a width of 1 m. Finally, the slope of the model is equal to 0.0015 and therefore the channel is mild.
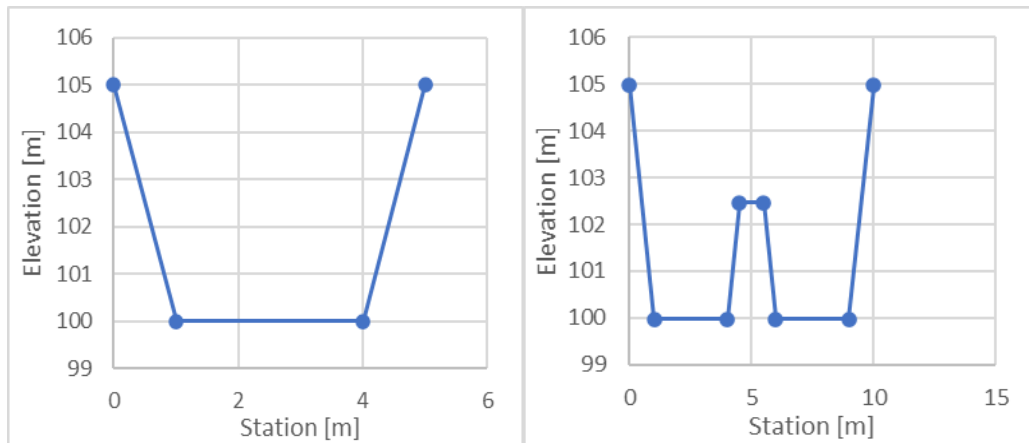
Figure 4.40: Section 1 (left) and Section 3 (right)

Then, the final DTM of the model, which is composed simply by the main channel and the lateral expansion, was created as described in Chapter 3.1.1 and was imported in HEC-RAS, thus defining the geometry of the terrain in the synthetic model (Figure 4.41).
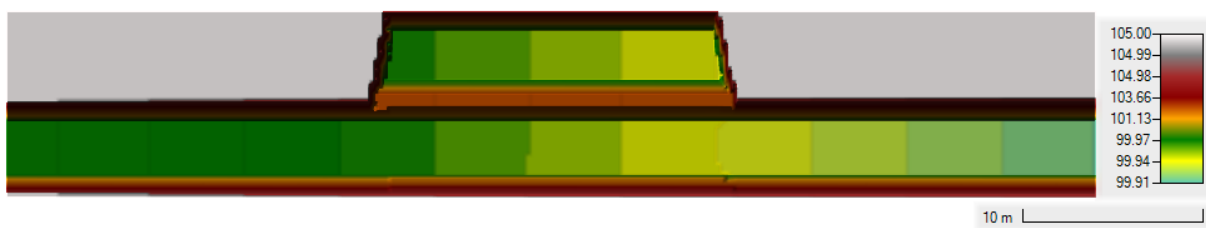
Figure 4.41: Terrain of the synthetic model

The objective of this analysis is to simulate a flow for different computational meshes and assess the conditions in which water enters the lateral expansion. Since the presence of water in the lateral expansion is intended to be wrong, it is necessary to define an upstream BC so that the uniform water elevation in the main channel is below the crest of the internal levee. Therefore, the simulations were run with the inflow hydrograph shown in Figure 4.42, which is characterized by a symmetrical triangular shape and a peak value of the discharge equal to 4.5 m^3/s. Instead, a normal depth was used as a downstream BC. All the simulations lasted 10 h and are characterized by a time step equal to 2 s.
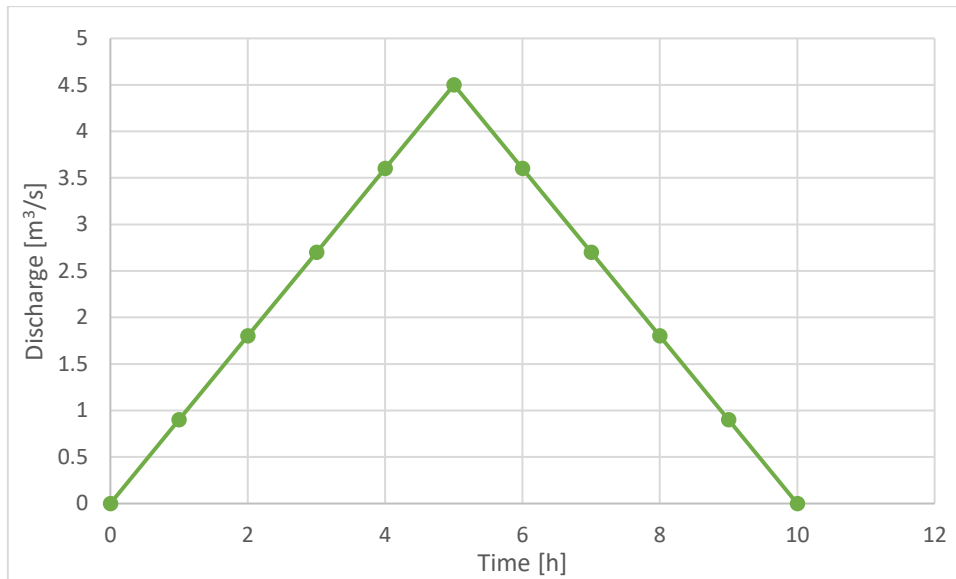
Figure 4.42: Input hydrograph

To validate the chosen input hydrograph, it has been computed its corresponding height of uniform flow (d_0) in the main channel by using the Chezy's formula for a 1D flow (4.2), where Q is the peak discharge, n is the Manning's coefficient, S_0 is the slope of the channel, R_H is the hydraulic radius and A the area of the channel.

$$Q = \frac{1}{n} \cdot \sqrt{S_0} \cdot R_H{}^{2/3} \cdot A \qquad (4.2)$$

By following an iterative procedure, since R_H and A depends on the height of uniform flow, it has been obtained that d_0 should be equal to 2.07 m, which is, being smaller than 2,5 m (i.e.: the height of the internal levee), a coherent result. This result has been further validated by extracting the flow profile from the performed simulations (Figure 4.43), which shows a water depth very similar to the one computed using the Chezy's formula, being almost equal to 2 m. Small discrepancies in the two results can be explained by the fact that the software runs 2D simulations, while the equation (4.2) is for 1D flows.
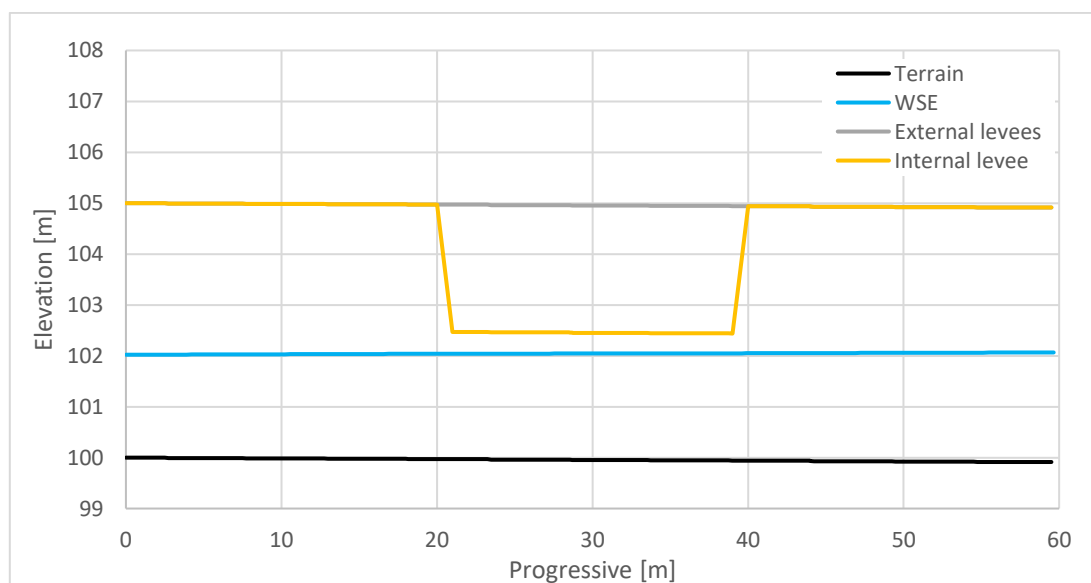
Figure 4.43: Flow profile

From the results it has also been possible to extract the output hydrograph, which, however, due to the reduced length of the defined model, has always been (i.e.: for all the simulations) equal to the one defined as upstream BC, as shown in Figure 4.44.
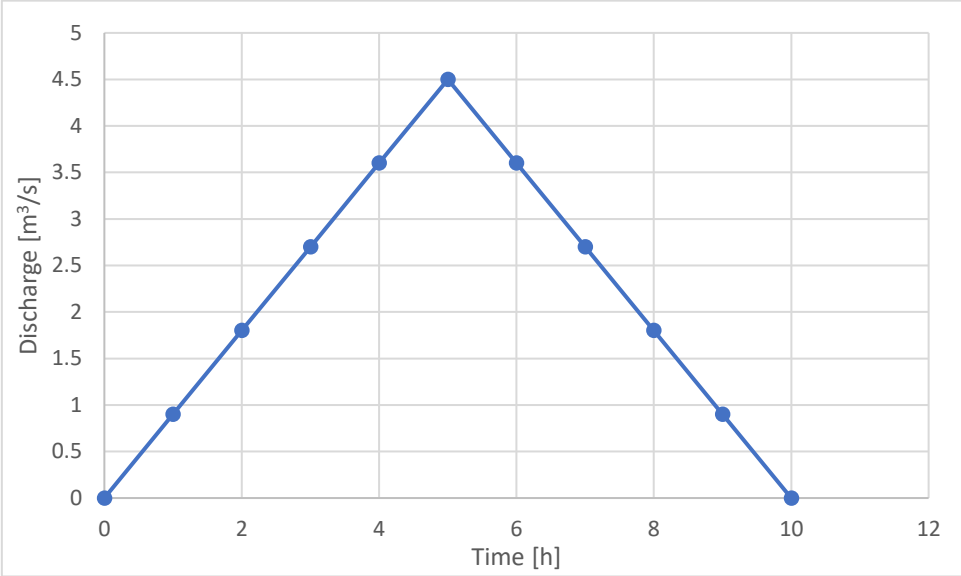
Figure 4.44: Output hydrograph

The flow maps obtained from different simulations, characterized by distinct cell sizes, are depicted in Figure 4.45 to Figure 4.51. Only regular meshes are considered in this first group of results.
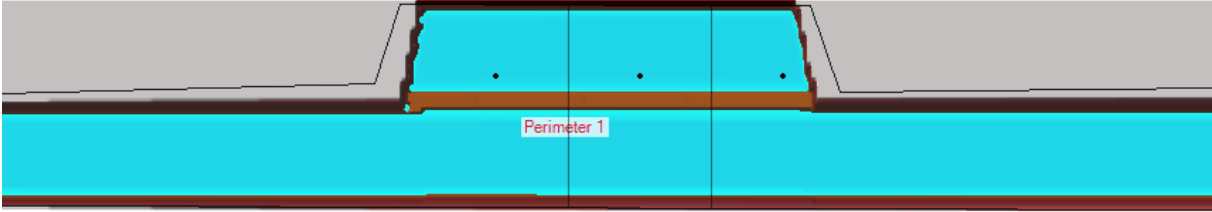
Figure 4.45: Cell size 7 meters
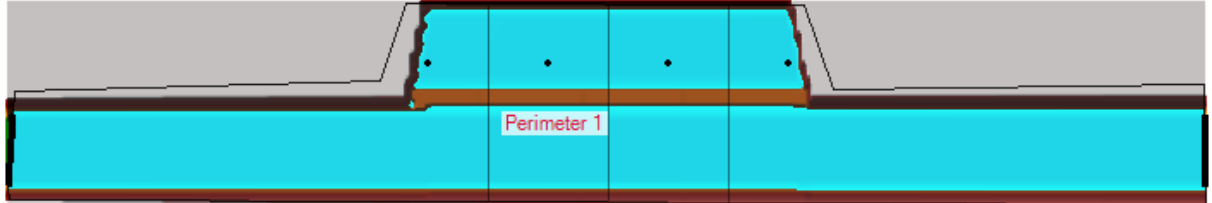
Figure 4.46: Cell size 6 meters
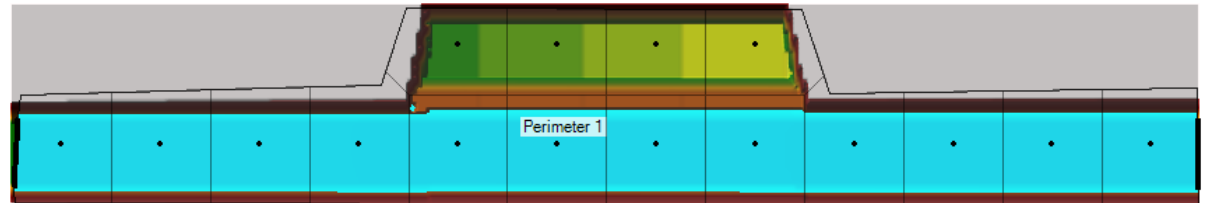
Figure 4.47: Cell size 5 meters

137
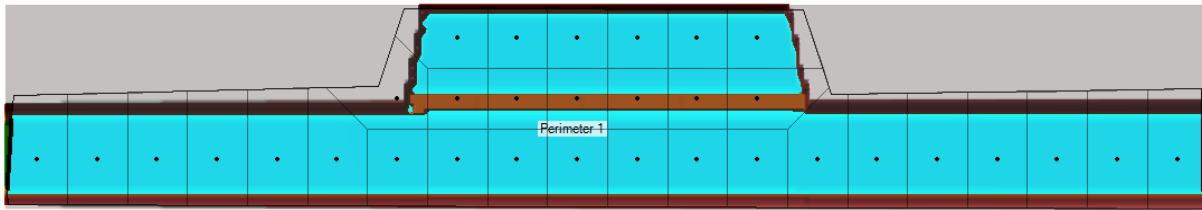
Figure 4.48: Cell size 3 meters
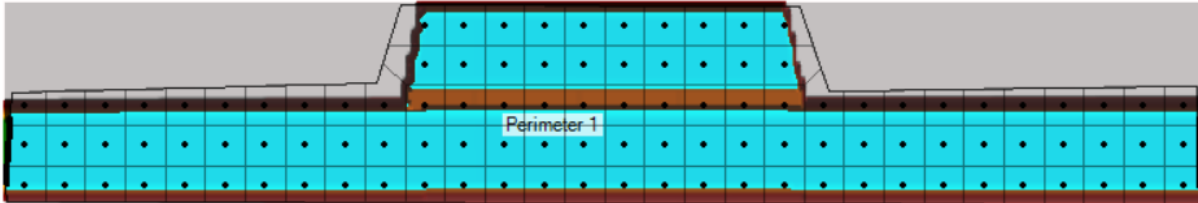
Figure 4.49: Cell size 2 meters
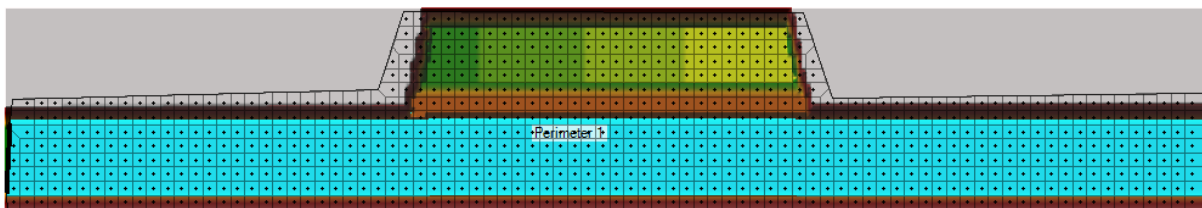
Figure 4.50: Cell size 0.7 meters
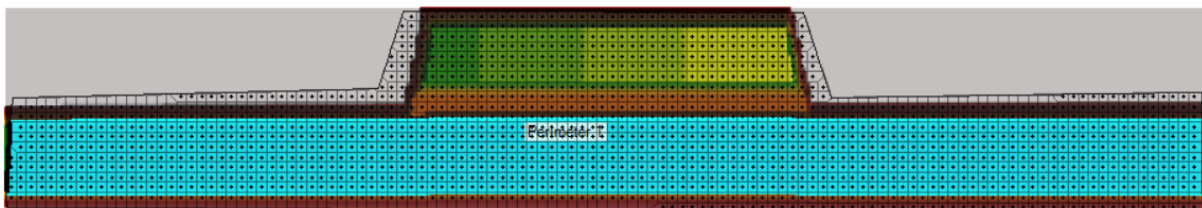
Figure 4.51: Cell size 0.5 meters

With cell sizes larger than 1 meter (thus larger than the top width of the intermediate bank) water was wrongly returned to occupy the lateral expansion (with the exception of the simulation with a cell size equal to the width of the main channel). Figure 4.52 shows an example of a transversal cross-section when the water wrongly occupies the secondary channel. From this, it can be noticed that the water enters the lateral expansion without flowing over the internal levee. As mentioned, with a cell size equal to 5 m the water does not flow into the lateral expansion simply because the borders of two adjacent cells in the central part of the section coincide with the internal levee. Instead, when the cell sizes are smaller than 1 m, it is ensured that the borders of at least two adjacent cells in the central area pass over the internal levee and, therefore, the possibility of having water in the lateral expansion is excluded.
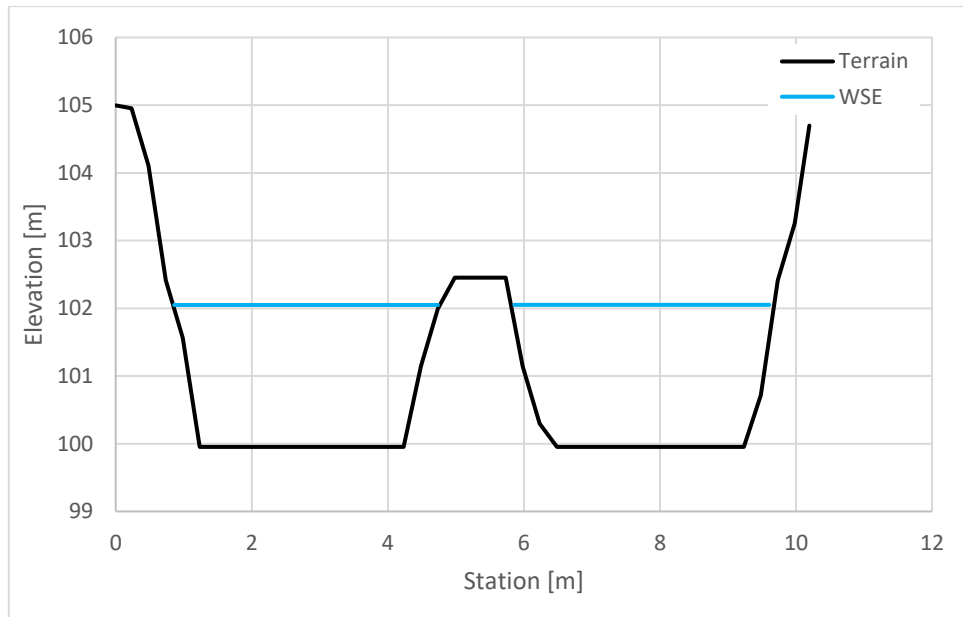
Figure 4.52: Terrain and WSE in a wrongly interpreted result in a W-shaped cross-section

However, it is important to highlight the fact that not only the dimensions of the cells play an important role, but also their shapes. Indeed, this fact is very well demonstrated by analysing two examples of simulations characterized by an irregular mesh (Figure 4.53 and Figure 4.54).
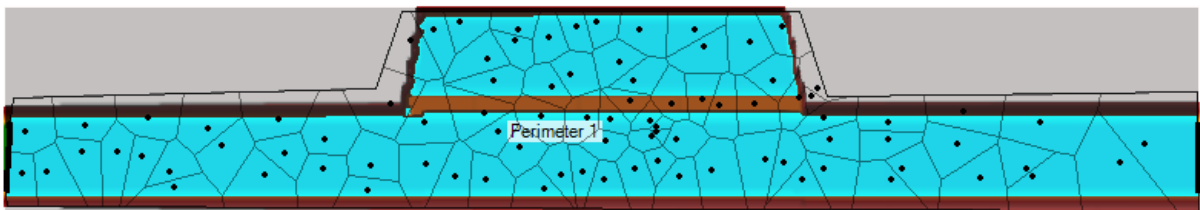
Figure 4.53: Irregular mesh (big)
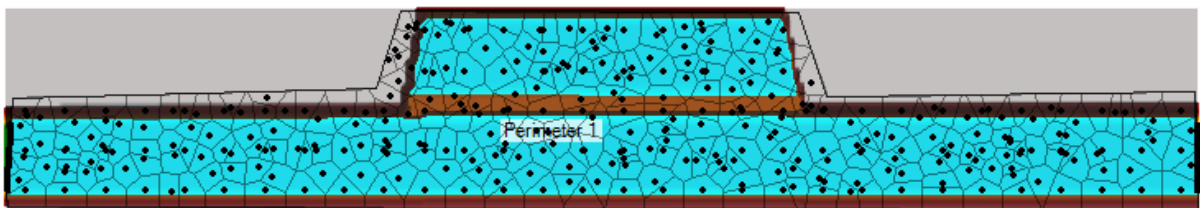
Figure 4.54: Irregular mesh (small)

From these examples it can be noticed that in both cases the water wrongly occupies the lateral expansion, even if the mean dimensions of the cells are very different, being respectively equal to 2.92 m^2 for the example in Figure 4.53 and 0.81 m^2 in Figure 4.54. Figure 4.55 represents very well the problem embedded within HEC-RAS and highlights the fact that it is enough a single cell that is connecting the two channels (i.e.: at least two points of it are not over the internal levee) for turning this issue into reality and therefore having the lateral expansion full of water at the end of the simulation.
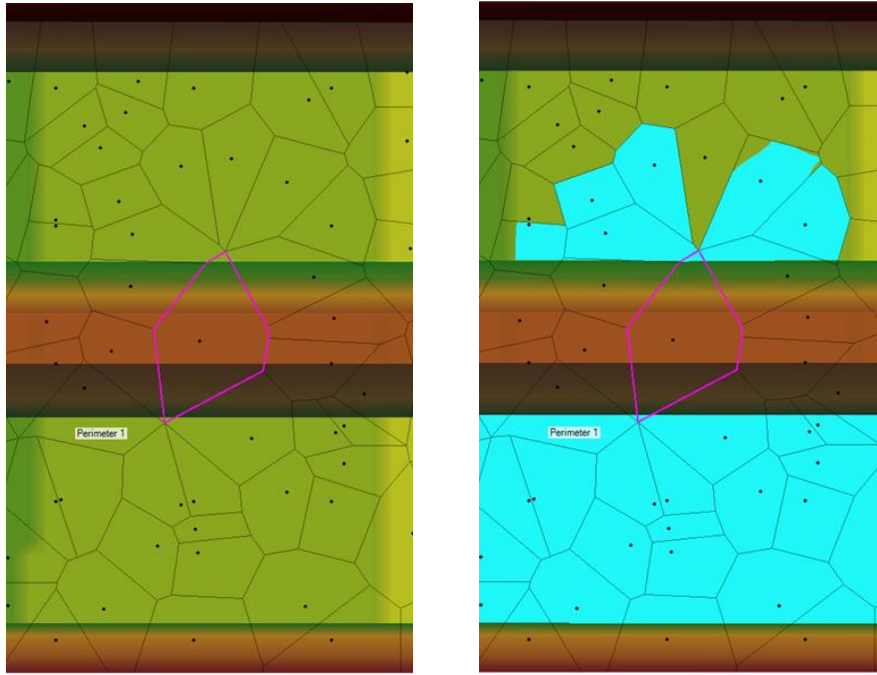
Figure 4.55: Simulation at time 0 (left) and simulation after 4 min and 30 sec (right)

On the other hand, Figure 4.56 shows an example of how this problem can be faced. Specifically, for example for the model represented in Figure 4.54, it is enough to simply add manually a computational point within the problematic cell (i.e.: split this cell into two separate cells) to solve the problem and correctly model the water flow behaviour.
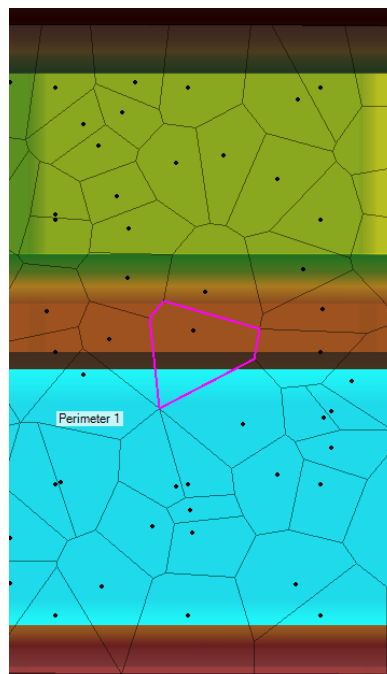
Figure 4.56: Simulation after 4 min and 30 sec with the division of the problematic cell

This solution is possible only when the problem is detected in one or a few cells of a model. For more complex situations, the issue can be overcome by inserting a break line over the width of the internal levee. By doing that, the software will automatically utilize this line for separating two adjacent cells in that area, thus making the shape of the computational mesh

140

potentially less regular, but guaranteeing to avoid incorrectly detected flooded areas in a model. Figure 4.57 and Figure 4.58 show two examples of the application of this solution.

Figure 4.57: Cell size 3 meters with break line
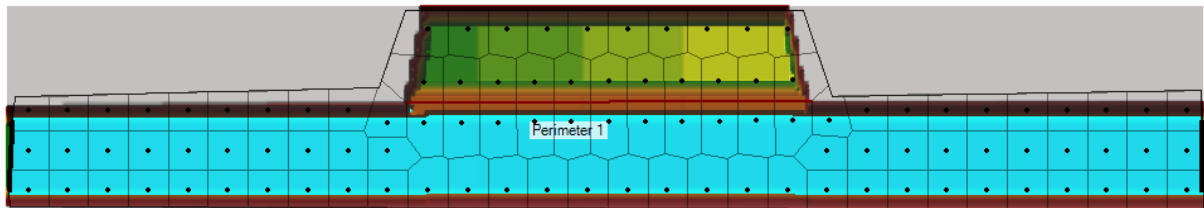
Figure 4.58: Cell size 2 meters with break line

As an alternative, also mesh refinement regions, since their perimeter is automatically considered as a break line, can be used to solve the problem of wrongly detected flooded areas.

4.4. Discussion

The objective of this subchapter is to summarize and discuss the main findings highlighted from the above-described analyses of some of the main critical aspects of the 2D flood modelling approach.

The sensitivity analysis for the roughness highlighted the fact that, in general, once it has been decided how to represent the buildings within a model, there is a weak effect of the roughness parameterization in the floodplain areas. Indeed, Simulations 0 and 1 have shown very similar results in terms of both extension of the flooded area and water depths (generally the differences were within ± 0.15 m). The flooded perimeter has shown slightly larger differences when comparing Simulations 2, 3 and 4 with Simulation 5 (i.e.: when buildings are considered as friction tuning), which could be reasonable since in these simulations the discrepancies in the roughness definition have been larger. In addition, the analysis pointed out that the definition of the roughness of the buildings is not particularly relevant, since Simulations 2, 3 and 4 have returned very similar results.

As far as the sensitivity analysis of both the computational time step and the set of equations used is concerned, the most relevant aspect which has been detected is that, in general, the DWE are more conservative than the SWE, since both the flooded perimeter and (marginally) the water depth tend to be smaller when using the simplified set of equations. However, it has also been observed that reaching numerical stability with the SWE is much more difficult and, usually, it requires either very large cell sizes or very small computational time steps. The analysis of the latter aspect demonstrated that, in general, the time step definition does not have an important role in the extension of the flooded area. Nevertheless, it is of crucial importance that, also to safeguard the stability of the simulations, the computational time step is neither too large, which can correspond to very large error percentages, nor too small, which can correspond to very long running times without introducing any benefit in terms of quality of

the results (when the time step is decreased, this does not necessarily correspond to a decrease in the errors).

Finally, from the analysis of the influence of the grid size definition, it has been highlighted that frequently, also in very simple models, the problem of wrongly detected flooded areas may occur using HEC-RAS (determining an overestimation of the final flooded perimeter). However, an appropriate use of break lines can avoid the wrong assignment of a water depth to a cell that would be external to the flooded area. It can be reasonably supposed that very complex and large models are prone to suffer from this problem; in these situations, the solution may be either to define very small computational cells (but this may be unfeasible most of the time) or to use break lines and mesh refinement in the zones of the model requiring higher detail (e.g: the riverbanks).

5. Conclusions

Every year flood events lead to significant economic, social and environmental negative consequences. However, the impact of such events can be reduced by adopting appropriate measures, whose implementation is favoured if a-priori meticulous assessment of the expected spatial distribution of the hazard and the risk (considering different possible scenarios) is performed. In the European context, the EU Floods Directive (2007/60/EC) requires all the Member States to prepare Flood Risk Management Plans (FRMPs) for identified Areas of Potential Significant Flood Risk (APSFR) and to update these plans every 6 years. The production of flood hazard maps is an important preliminary step in the preparation of a FRMP.

The aim of this thesis has been to contribute to the update of the maps released in 2019 by the Autorità di Bacino Distrettuale del fiume Po (AdBPo). The latter takes care of producing the FRMPs for several APSFRs within the basin of the Po river, including the "North of Milan" area. This APSFR contains a very complex hydrographic network, characterized by the presence of numerous small-medium sized watercourses flowing through a densely urbanized area. Moreover, the area includes several structures and many mitigation measures that have been adopted throughout the years. In this work, the hazard maps have been produced for two rivers included in this APSFR: the Guisa and Nirone. This was done by employing unsteady, two-dimensional hydrodynamic numerical modelling with the solver HEC-RAS, for three different return periods (10, 100 and 500 years; corresponding to three scenarios with a high, medium and low probability of occurrence).

Before running numerical simulations, a very scrupulous data pre-processing work is required. The most demanding step is producing the geometry to be input into the software. Indeed, many transversal cross-sections provided in earlier studies have been individually analysed and eventually modified (possible changes in the width, the position and the shape), also by comparing them with the corresponding sections extracted from the available Digital Terrain Model (DTM) and the base map (satellite imagery) included in ArcGIS Pro. Subsequently, these cross-sections have been interpolated to define the riverbed bathymetry that has been included in the DTM. The latter has been further modified in order to correctly include the culverts, the mitigation measures (four detention ponds situated along the Guisa river) and the buildings, which have been considered as ground elevation (height equal to 10 m). Another challenging step has been to retrieve information about the boundary conditions (BCs) and the lateral inlets. Indeed, hydrographs and rating curves were available only for a limited number of cross-sections and, most of the time, peak discharge values from different sources were not in agreement with each other. Therefore, the information has needed to be completed with a certain degree of arbitrariness, especially regarding the shape of the hydrographs and the timing of the peaks of the lateral inlets (that has been assumed to be always coincident with that of the upstream BC).

The model implementation in HEC-RAS is another very important preliminary step that should be performed carefully in order to obtain reliable results. The most demanding part has been the insertion of all the structures in the model; these structures are quite numerous since, for the Guisa and the Nirone rivers respectively, 11 and 3 culverts (in addition to some culverts added to connect the detention basins to the main channel) and 30 and 7 bridges are present. Furthermore, it has been necessary also to define the computational mesh, the roughness coefficient (that was considered equal to 0.03 s/m$^{1/3}$ in the riverbeds and 0.06 s/m$^{1/3}$ in the

floodplains), the BCs and the computational time step (selected based on a trial-and-error approach, targeting the best trade-off between a satisfactorily small error and a reasonable running time). The numerical simulations were, however, quite computationally demanding, due to the intent of maintaining a high level of detail in the analyses.

The flooded area obtained for the Nirone river was very small for all the scenarios considered. Instead, the analyses on the Guisa river pointed out a significant flooded area, quite similar for the three different return periods; even the simulations of events that a person may experience more than once in a life (i.e.: scenario H) returned inundation of rural and inhabited areas, thus a quite high level of risk is still present for the municipalities situated along this river.

The results obtained in this thesis have been compared to those released in 2019 by the AdBPo. For scenarios H and M it has been noticed that the flooded areas obtained in this document were larger than the previous ones. Contrarily, for scenario L the previous contoured inundation areas were larger than those obtained in this work. The areas of 2019, however, were still produced (for scenario L) without considering the four realized detention ponds along the Guisa river.

A detailed analysis of some of the most critical aspects of the 2D modelling approach has been performed. From a sensitivity analysis of the roughness, it has been possible to detect a weak effect of the roughness parameterization in the floodplain areas once it has been decided how to represent the buildings within a model. In this thesis, also given the size of some of the defined models, a simplified way of representing the roughness has been used (just two values, one for rivers and one for the rest of the domain). However, the sensitivity analysis also highlighted the fact that this approach was leading to the larger flooded areas detected, therefore it can be stated that the results presently obtained were in favour of safety.

By studying more in detail the influence of the chosen time step and set of equations, it has been possible to highlight that, generally, the latter aspect has a larger impact on the extension of the flooded area. Specifically, it turned out that using SWE results in having larger flooded areas (and, tendentially, also slightly larger water depths) and, therefore, it can be stated that the choice of using the DWE in this thesis has not been in favour of safety. However, the analysis also pointed out that SWE went unstable in most of the cases (especially for larger time steps); consequently, the choice of using the DWE is obviously justified. Using the DWE is also legitimated by the fact that the analysis carried out in this document does not match any of the points listed at the end of Chapter 2.1.1 (reporting the situations in which SWE should be used).

HEC-RAS may wrongly return inundated areas when the computational cells enable water to be numerically transported across physical barriers like narrow banks. A specific analysis of the grid size definition revealed that an appropriate use of mesh creation and break line implementation reduces significantly this problem. With respect to this, it is important to highlight that in all the simulations presented in this thesis the risk of having wrong water overflows in correspondence of the river overbanks has been excluded since a mesh refinement region defining the perimeter of the riverbed (which therefore acts as a break line) has always been used. Nevertheless, this problem can also occur in the floodplain of a river (e.g.: when there is a wall anywhere in the model). In those cases, the problem of wrongly detected flooded areas could have potentially happened also in the simulations presented in this thesis.

Is it agreed that, if different modelling strategies are used for a certain river, different results are obtained. From a detailed analysis of the discrepancies between the present models and earlier ones for the Guisa river, it has been possible to conclude that there is presumably not a single cause for the differences one finds. Differences are, instead, probably due to all the many small divergences present in the modelling approaches, such as: geometry, lateral inlets (both in the flow rates and their locations), different models (1D vs 2D), and representation of the structures (bridges and culverts). Model comparison is, however, necessary. Future implementations could be made by trying to consider alternative modelling strategies or numerical solvers. For example, it could be possible to use a coupled model with a 1D component for the main channel and a 2D component for the floodplains. Alternatively, another solver, potentially designed according to different assumptions than HEC-RAS, could be used to obtain an estimation of the hazard and then compare these final results with those obtained in this document. These analyses could allow the user to better understand how the modelling strategies and characteristics could have an impact on the results, as well as try to identify general common rules and recommendations for the parameterization of the previously identified critical aspects (which are also strongly interconnected and influence each other). With respect to this, real case studies or experimental results could be very useful to calibrate the model parameters and/or to validate the obtained results.

Finally, further developments of the work presented in this thesis are obviously to be made by using the obtained results for the hazard in order to produce a complete risk evaluation comprising damage estimations for the municipalities situated along the rivers.

Bibliography

[1] 'Floods'. https://www.who.int/health-topics/floods (accessed Oct. 01, 2022).

[2] 'What are the consequences of floods?', *Office of the Queensland Chief Scientist*, Jun. 12, 2018. https://www.chiefscientist.qld.gov.au/publications/understanding-floods/flood-consequences (accessed Oct. 02, 2022).

[3] Nicklin, Leicher, Dieperink, and Leeuwen, 'Understanding the Costs of Inaction–An Assessment of Pluvial Flood Damages in Two European Cities', *Water*, vol. 11, no. 4, p. 801, Apr. 2019, doi: 10.3390/w11040801.

[4] 'Risks from Natural Hazards at Hazardous Installations (Natech) - OECD'. https://www.oecd.org/chemicalsafety/chemical-accidents/risks-from-natural-hazards-at-hazardous-installations.htm (accessed Oct. 02, 2022).

[5] 'Economic Losses, Poverty & DISASTERS 1998-2017'. Centre for Reasearch on the Epidemiology of Disasters (CRED) & United Nations Office for Disaster Risk Reduction.

[6] 'EM-DAT Public'. https://public.emdat.be/ (accessed Oct. 01, 2022).

[7] 'European past floods — European Environment Agency'. https://www.eea.europa.eu/data-and-maps/data/european-past-floods (accessed Oct. 01, 2022).

[8] 'Dartmouth Flood Observatory'. https://floodobservatory.colorado.edu/Archives/ArchiveNotes.html (accessed Oct. 01, 2022).

[9] 'Flood risk management - Water - Environment - European Commission'. https://ec.europa.eu/environment/water/flood_risk/ (accessed Oct. 01, 2022).

[10] 'Floods Directive', *Geoportale Nazionale*. http://www.pcn.minambiente.it/mattm/en/floods-directive/ (accessed Oct. 01, 2022).

[11] 'WFS SERVICE', *Geoportale Nazionale*. http://www.pcn.minambiente.it/mattm/en/wfs-service/ (accessed Oct. 01, 2022).

[12] 'Studio di fattibilità della sistemazione idraulica dei corsi d'acqua naturali e artificiali all'interno dell'ambito idrografico di pianura Lambro – Olona.' Autorità di bacino del fiume Po, Mar. 2003.

[13] N. F. Silva Muñoz, 'Mapping urban risk: flood hazard assessment methods for long watercourses and their application in rivers of northern Italy'. Apr. 29, 2020.

[14] 'Metodologie per l'aggiornamento delle mappe di pericolosità idraulica nelle APSFR distrettuali – I° piano operativo annuale – (POA 2019)'. Autorità Distrettuale del Fiume Po.

[15] 'Attività per la definizione di soglie di attenzione - allerta - allarme pluviometriche e idrometriche lungo l'asta del torrente Guisa'. Studio Majone Ingegneri Associati, Nov. 2018.

[16] 'Not-Ordinary Plan of Remote Sensing', *Geoportale Nazionale*. http://www.pcn.minambiente.it/mattm/en/not-ordinary-plan-of-remote-sensing/ (accessed Oct. 01, 2022).

[17] 'Servizio di aggiornamento Analisi idrologico-idrauliche del t. Guisa'. Studio Paoletti, May 2017.

[18] 'Database Topografico (DBT) regionale', *Geoportale della Lombardia*. https://www.geoportale.regione.lombardia.it/download-pacchetti (accessed Oct. 20, 2022).

[19] 'Uso e copertura del suolo 2018 (DUSAF 6.0)', *Geoportale della Lombardia*. https://www.geoportale.regione.lombardia.it/download-pacchetti (accessed Oct. 20, 2022).

[20] 'Energy Loss Coefficients'. https://www.hec.usace.army.mil/confluence/rasdocs/ras1dtechref/latest/basic-data-requirements/geometric-data/energy-loss-coefficients (accessed Oct. 20, 2022).

[21] 'Creating Land Cover, Manning's n values, and % Impervious Layers'. https://www.hec.usace.army.mil/confluence/rasdocs/r2dum/latest/developing-a-terrain-model-and-geospatial-layers/creating-land-cover-mannings-n-values-and-impervious-layers (accessed Nov. 02, 2022).

[22] 'HEC-RAS'. https://www.hec.usace.army.mil/software/hec-ras/ (accessed Oct. 01, 2022).

[23] F. Alcrudo, 'Mathematical modelling techniques for flood propagation in urban areas', p. 34.

[24] *Fluid Mechanics*. Berlin, Heidelberg: Springer Berlin Heidelberg, 2008. doi: 10.1007/978-3-540-73537-3.

[25] K. R. Popper and W. W. Bartley III, *The Open Universe: An Argument for Indeterminism*. Routledge, 1988.

[26] 'HEC-RAS 2D User's Manual'. https://www.hec.usace.army.mil/confluence/rasdocs/r2dum/latest (accessed Sep. 30, 2022).